IAEA TECDOC SERIES

IAEA TECDOC 1703

TECDOC No. 1703

Benchmark Analyses on the Natural Circulation Test Performed During the PHENIX End-of-Life Experiments

IAEA
International Atomic Energy Agency

BENCHMARK ANALYSES ON THE NATURAL CIRCULATION TEST PERFORMED DURING THE PHENIX END-OF-LIFE EXPERIMENTS

The following States are Members of the International Atomic Energy Agency:

AFGHANISTAN
ALBANIA
ALGERIA
ANGOLA
ARGENTINA
ARMENIA
AUSTRALIA
AUSTRIA
AZERBAIJAN
BAHRAIN
BANGLADESH
BELARUS
BELGIUM
BELIZE
BENIN
BOLIVIA
BOSNIA AND HERZEGOVINA
BOTSWANA
BRAZIL
BULGARIA
BURKINA FASO
BURUNDI
CAMBODIA
CAMEROON
CANADA
CENTRAL AFRICAN REPUBLIC
CHAD
CHILE
CHINA
COLOMBIA
CONGO
COSTA RICA
CÔTE D'IVOIRE
CROATIA
CUBA
CYPRUS
CZECH REPUBLIC
DEMOCRATIC REPUBLIC OF THE CONGO
DENMARK
DOMINICA
DOMINICAN REPUBLIC
ECUADOR
EGYPT
EL SALVADOR
ERITREA
ESTONIA
ETHIOPIA
FIJI
FINLAND
FRANCE
GABON
GEORGIA
GERMANY
GHANA
GREECE
GUATEMALA
HAITI
HOLY SEE
HONDURAS
HUNGARY
ICELAND
INDIA
INDONESIA
IRAN, ISLAMIC REPUBLIC OF
IRAQ
IRELAND
ISRAEL
ITALY
JAMAICA
JAPAN
JORDAN
KAZAKHSTAN
KENYA
KOREA, REPUBLIC OF
KUWAIT
KYRGYZSTAN
LAO PEOPLE'S DEMOCRATIC REPUBLIC
LATVIA
LEBANON
LESOTHO
LIBERIA
LIBYA
LIECHTENSTEIN
LITHUANIA
LUXEMBOURG
MADAGASCAR
MALAWI
MALAYSIA
MALI
MALTA
MARSHALL ISLANDS
MAURITANIA
MAURITIUS
MEXICO
MONACO
MONGOLIA
MONTENEGRO
MOROCCO
MOZAMBIQUE
MYANMAR
NAMIBIA
NEPAL
NETHERLANDS
NEW ZEALAND
NICARAGUA
NIGER
NIGERIA
NORWAY
OMAN
PAKISTAN
PALAU
PANAMA
PAPUA NEW GUINEA
PARAGUAY
PERU
PHILIPPINES
POLAND
PORTUGAL
QATAR
REPUBLIC OF MOLDOVA
ROMANIA
RUSSIAN FEDERATION
RWANDA
SAUDI ARABIA
SENEGAL
SERBIA
SEYCHELLES
SIERRA LEONE
SINGAPORE
SLOVAKIA
SLOVENIA
SOUTH AFRICA
SPAIN
SRI LANKA
SUDAN
SWAZILAND
SWEDEN
SWITZERLAND
SYRIAN ARAB REPUBLIC
TAJIKISTAN
THAILAND
THE FORMER YUGOSLAV REPUBLIC OF MACEDONIA
TOGO
TRINIDAD AND TOBAGO
TUNISIA
TURKEY
UGANDA
UKRAINE
UNITED ARAB EMIRATES
UNITED KINGDOM OF GREAT BRITAIN AND NORTHERN IRELAND
UNITED REPUBLIC OF TANZANIA
UNITED STATES OF AMERICA
URUGUAY
UZBEKISTAN
VENEZUELA
VIETNAM
YEMEN
ZAMBIA
ZIMBABWE

The Agency's Statute was approved on 23 October 1956 by the Conference on the Statute of the IAEA held at United Nations Headquarters, New York; it entered into force on 29 July 1957. The Headquarters of the Agency are situated in Vienna. Its principal objective is "to accelerate and enlarge the contribution of atomic energy to peace, health and prosperity throughout the world''.

IAEA-TECDOC-1703

BENCHMARK ANALYSES ON THE NATURAL CIRCULATION TEST PERFORMED DURING THE PHENIX END-OF-LIFE EXPERIMENTS

Final report of a co-ordinated research project 2008–2011

Marketing and Sales Unit, Publishing Section
International Atomic Energy Agency
Vienna International Centre
PO Box 100
1400 Vienna, Austria
fax: +43 1 2600 29302
tel.: +43 1 2600 22417
email: sales.publications@iaea.org
http://www.iaea.org/books

For further information on this publication, please contact:

Nuclear Power Technology Development Section
International Atomic Energy Agency
Vienna International Centre
PO Box 100
1400 Vienna, Austria
Email: official.mail@iaea.org

Printed by the IAEA in Austria
July 2013

Benchmark analyses on the natural circulation test performed during the PHENIX end-of-life experiments : final report of a co-ordinated research project 2008-2011. – Vienna : International Atomic Energy Agency, 2013.
p. ; 30 cm. – (IAEA-TECDOC series, ISSN 1011-4289 ; no. 1703)
ISBN 978-92-0-139610-5
Includes bibliographical references.

1. Nuclear reactors – Experiments. 2. Nuclear power plants – Cooling. 3. Liquid metal fast breeder reactors. I. International Atomic Energy Agency. II. Series.

IAEAL 13-00831

FOREWORD

The International Atomic Energy Agency (IAEA) supports Member State activities in the area of advanced fast reactor technology development by providing a forum for information exchange and collaborative research programmes. The Agency's activities in this field are mainly carried out within the framework of the Technical Working Group on Fast Reactors (TWG-FR), which assists in the implementation of corresponding IAEA activities and ensures that all technical activities are in line with the expressed needs of Member States. Among its broad range of activities, the IAEA proposes and establishes coordinated research projects (CRPs) aimed at the improvement of Member State capabilities in the area of fast reactor design and analysis.

An important opportunity to undertake collaborative research was provided by the experimental campaign of the French Alternative Energies and Atomic Energy Commission (CEA) in the prototype sodium fast reactor PHENIX before it was shut down in 2009. The overall purpose of the end of life tests was to gather additional experience on the operation of sodium cooled reactors. As the CEA opened the experiments to international cooperation, in 2007 the IAEA launched a CRP on "Control Rod Withdrawal and Sodium Natural Circulation Tests Performed during the PHENIX End-of-Life Experiments".

The CRP, with the participation of institutes from eight countries, contributed to improving capabilities in sodium cooled reactor simulation through code verification and validation, with particular emphasis on temperature and power distribution calculations and the analysis of sodium natural circulation phenomena.

The objective of this report is to document the results and main achievements of the benchmark analyses on the natural circulation test performed in the framework of the PHENIX end of life experimental campaign. The IAEA expresses its appreciation to all participants in the CRP for their efforts. The IAEA officer responsible for this publication was S. Monti of the Division of Nuclear Power.

EDITORIAL NOTE

This report has been prepared from the original material as submitted for publication and has not been edited by the editorial staff of the IAEA. The views expressed do not necessarily reflect those of the IAEA or the governments of its Member States.

It does not address questions of responsibility, legal or otherwise, for acts or omissions on the part of any person.

The use of particular designations of countries or territories does not imply any judgement by the publisher, the IAEA, as to the legal status of such countries or territories, of their authorities and institutions or of the delimitation of their boundaries.

The mention of names of specific companies or products (whether or not indicated as registered) does not imply any intention to infringe proprietary rights, nor should it be construed as an endorsement or recommendation on the part of the IAEA.

The depiction and use of boundaries, geographical names and related data shown on maps do not necessarily imply official endorsement or acceptance by the IAEA.

The IAEA has no responsibility for the persistence or accuracy of URLs for external or third party Internet web sites referred to in this report and does not guarantee that any content on such web sites is, or will remain, accurate or appropriate.

CONTENTS

1. INTRODUCTION

1.1 OBJECTIVES OF THE CRP

Before the definitive shutdown of the prototype pool-type sodium-cooled fast reactor PHENIX, occurred in the year 2009, the French Commissariat à l'Energie Atomique et aux Energies Alternatives (CEA) decided to carry out a final set of experimental tests, in order to gather data and additional knowledge on relevant aspects of the operation of sodium fast reactors (SFR).

Recognizing the unique opportunity offered by the PHENIX end-of-life tests programme, and thanks to the CEA availability to open it for international collaboration, in 2007 the IAEA, within the framework of the Technical Working Group on Fast Reactors (TWG-FR) activities, decided to establish a Coordinated Research Project (CRP) on 'Control rod withdrawal and sodium natural circulation tests performed during the PHENIX end-of-life experiments'.

The overall objective of the CRP was to improve the participants' analytical capabilities in various fields of research and design of sodium-cooled fast reactors. A necessary condition towards achieving this objective is a wide international verification and validation effort of the analysis methodology and codes currently employed in the fields of fast reactor neutronics, thermal hydraulics and plant dynamics.

More specifically, the CRP aimed at improving SFR simulation methods and design capabilities in the field of temperature and power distribution evaluation, as well as of the analysis of sodium natural circulation phenomena.

Apart from the general outcome of enhanced international team-building and technical cooperation, the CRP was expected to have the following outcomes:

— Improved understanding of fast reactor neutronics and thermal hydraulics;

— Improved understanding of the methodology employed to simulate fast reactors (data and computer codes).

— Improved verification and validation status of this methodology;

Two PHENIX end-of-life tests were analyzed, the 'control rod withdrawal test' and 'Sodium natural circulation test'.

As for 'Sodium natural circulation test', the objective was twofold, including the study of the sodium natural circulation in the primary circuit, as well the determination of the efficiency of natural convection phenomena in the primary circuit, and the qualification of the system codes used to simulate sodium natural convection phenomena.

1.2. IMPORTANCE OF NATURAL CONVECTION FOR SFR DECAY HEAT REMOVAL

Due to the favorable thermophysical properties of liquid metals as coolants, the natural circulation in liquid metal-cooled reactors has been intensely investigated through both analytical and experimental research activities.

The efforts in this field are particularly devoted to the analysis of the potential capabilities of the natural circulation to absolve the decay heat removal function after the reactor shutdown.

Considering that the decay heat removal (DHR) system represents one of the most important safety functions which must be accomplished with a very high reliability level, the possibility of designing natural circulation-based DHR systems, which don't need any external power source, represents an important potential safety feature of sodium-cooled fast reactors, and more broadly of liquid metal-cooled reactors (LMR).

In order to assess the feasibility of sodium natural circulation DHR, both analytical and experimental investigations are needed to verify its real efficiency and characteristics. These investigations are performed in different plant conditions, in particular with and without a relevant heat sink in the secondary sodium circuit. In the second case, it is fundamental to understand if the sole heat losses in the second sodium circuit are enough to maintain the primary sodium temperature, and therefore of the reactor core, under the required safety limits. Then, accurate assessments have to be performed when the DHR function is accomplished rejecting heat to the atmospheric air as an ultimate heat sink.

The natural circulation test performed within the framework of the end-of-life experimental campaign performed in the PHENIX reactor represented a unique opportunity to analyse relevant thermal-hydraulics phenomena related to the sodium natural circulation in a pool-type fast reactor. During the test, important technical aspects concerning the onset of the natural circulation and the long-term plant behaviour after the scram have been deeply analysed.

1.3. INTEREST OF PHENIX NATURAL CIRCULATION TEST FOR CODE VALIDATION

For those Countries with relevant fast reactors programmes, it is essential to develop high-performance and multipurpose simulation tools to be employed in the different areas of reactor physics, thermal hydraulics, structural mechanics, and safety analyses among others.

To this end, broad R&D efforts are focused on the reduction of the calculation uncertainties, on the development of more powerful and reliable codes and methods and on the possibilities of coupling of codes in complete multi-physics and multi-scale simulation tools.

In this process, the activities of verification, validation and qualification of calculation codes are fundamental; from this point of view, the experimental data gathered during the PHENIX end-of-life experimental campaign represented a unique resource to carry out validation analyses and code-to-code comparisons. In particular, the benchmark analyses on the ‘Sodium Natural Circulation’ allowed CRP participants to investigate and verify several system thermal hydraulics calculation codes currently used in the analyses of liquid metal thermal hydraulics phenomena.

The benchmark analyses were carried out comparing the results of the calculation with the large amount of experimental data obtained in PHENIX. Moreover, the evaluation of a large set of plant parameters allowed performing accurate code-to-code comparisons, with the overall purpose to understand the critical open issues and recognize gaps which will require further investigations.

1.4. CRP BENCHMARK OBJECTIVES AND PROCEDURES

The main scope of the benchmark analyses was to simulate the PHENIX plant behavior during the natural circulation test. More in details, the objectives of the calculations can be summarized as follow:

— Study the onset of sodium natural circulation in the primary circuit, as well as determine the efficiency of natural convection phenomena in the primary circuit;

— Qualify the system codes used to simulate natural convection phenomena in classical 1D approach, as well as in coupled 1D/3D approach.

With the overall purpose of improving the participants’ capabilities in thermal-hydraulic simulation and analysis, the following three-step process was defined.

— Blind calculations prior to the tests with assumed experimental conditions;

— Blind calculations subsequent to the test with real experimental conditions;

— Post-experiment calculations with experimental data available.

The first step of the analyses was aimed at the simulation of the test performed in PHENIX without the knowledge of the real conditions of the plant during the test. For the calculations, the CEA provided the reactor design parameters, as well as the detailed procedure of the test.

A second step of calculations was performed after CEA provided the real conditions of the plant observed during the test. The aim of this second step was to perform more accurate codes validation analyses, directly comparing the predicted behaviour of the reactor with the experimental data.

Finally, a final set of post-test calculations and sensitivity analyses was performed with the overall purpose to compare the calculation codes and methods used in the calculations.

2. THE PHENIX REACTOR

Phenix is a sodium cooled pool-type fast reactor of 563 MW(th) (250MW(e)). It started in operation in 1973 and it was stopped in 2009. From 1993, it was operated at a reduced power of 350 MW(th) (140 MW(e)).

The reactor block is of the suspended type (see Fig.1) [1].

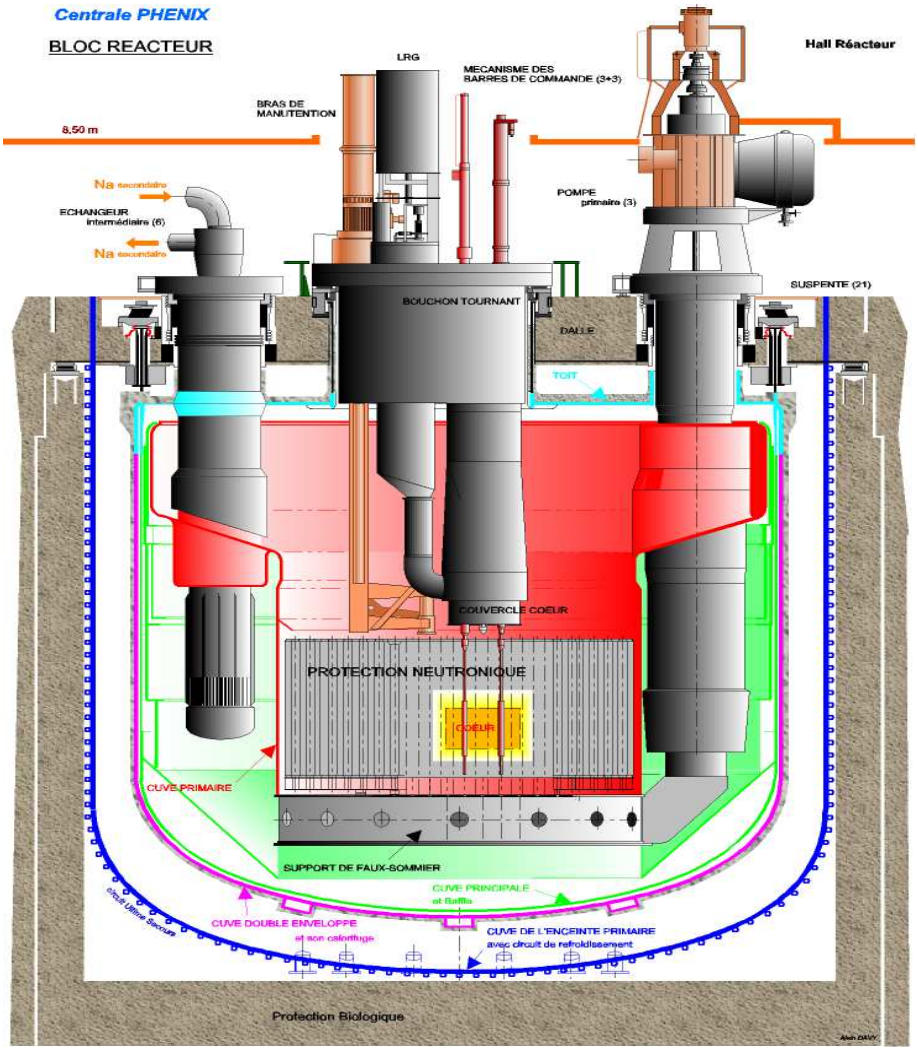

FIG. 1. Schematic of the reactor block.

The upper cover slab supports all the vessels, ensures biological protection, and allows the passage of components.

The main vessel, 11.8 m in diameter and holding about 800 tons of primary sodium, is attached to the upper slab by 21 suspension hangers. Closure is by means of a flat roof, featuring penetrations for the components. A double-envelope vessel, welded to the upper region of the main vessel, has the purpose of containing any possible sodium leaks. The roof and the double envelope vessel are fitted with thermal insulation. A third vessel, the primary containment vessel, is welded to the slab's underside, and attached to the reactor pit. This vessel's role is to contain radioactive products, in the event of a severe accident. It carries the final emergency cooling system, welded onto its outside, this having the purpose of keeping reactor pit concrete at ambient temperature, and ensuring decay heat removal, in the event of a loss of normal cooling systems.

Inside the main vessel, core support structures include a conical shell, welded to the vessel, the strongback, bearing the diagrid feeding the core assemblies, along with the dummy diagrid holding the lateral neutron shielding. The hot pool and the cold pool are separated by the primary vessel, which features a conical baffle.

Two hydraulic baffles, supported by the conical shell, are fed with cold sodium, from the diagrid, for the purpose of main vessel temperature control. Three vertical-axis primary pumps ensure sodium circulation, sodium being drawn into the cold pool, and discharged into the diagrid by way of three connector pipes.

A rotating plug, fitted with a fusible metallic seal, holds the core cover plug, this in turn supporting the control rod drive mechanisms and core instrumentation.

The core consists of an array of hexagonal assemblies, with a width across flats of 127 mm, for an overall length of 4.3 m. Each assembly contains 217 pins. The fuel is mixed uranium–plutonium oxide. Within the core, a central fissile zone, comprising two regions, involving different enrichment values, is surrounded by annular fertile zones, and further out by steel reflectors, and lateral neutron shielding rods.

Reactor control was ensured, initially, by means of 6 control rods, involving two distinct drive mechanisms. A further rod, positioned at the core centerline, was added in 1996.

Six intermediate heat exchangers, connected in pairs to the three secondary loops, remove the heat generated by the core. These are straight-tube heat exchangers. Primary sodium is circulated along the outside of the tubes.

Auxiliary systems, located outside the vessel, ensure primary sodium storage, filling, draining, and purification functions.

Three secondary loops serve to transfer heat from the intermediate heat exchangers to the steam generators (see Fig. 2).

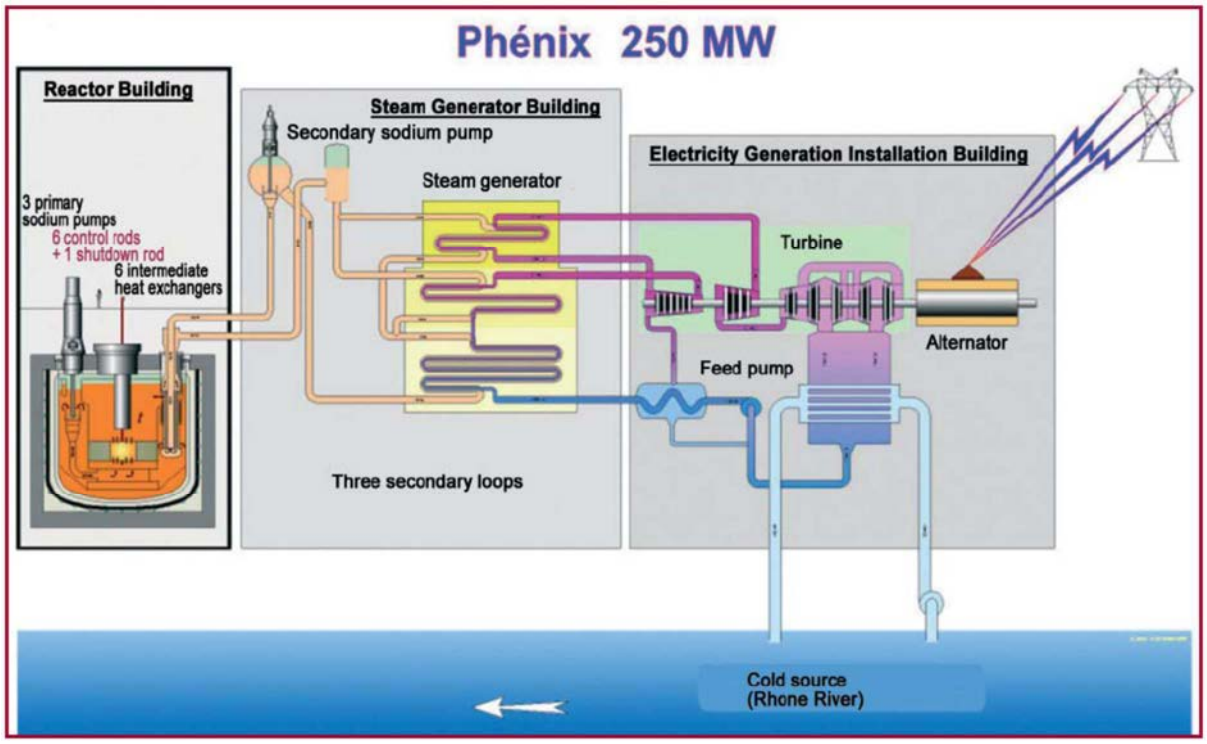

FIG. 2. Schematic of the whole power plant [1].

Each secondary loop holds about 140 tons of sodium and comprises one mechanical pump located inside the expansion tank, main pipes (500 mm in diameter), a buffer tank, and auxiliary systems ensuring sodium storage, filling, and purification.

Each secondary loop feeds a steam generator, comprising three stages: evaporator, super-heater, and re-heater, each of them in turn comprising 12 S-shaped modules (double-S-shaped modules, for the evaporators). Each module comprises 7 tubes, held inside a shell, water circulating inside the tubes and sodium outside the tubes in counter current.

The steam generators are each one held inside a casing, strong enough to withstand a sodium leak incident, involving a sodium–water reaction. Stacks, in the upper region, and hatches in the lower region, make it possible to ensure air circulation inside the casing, this providing the means normally used for reactor decay heat removal, during outage periods, when the feed water plant is not operating.

Refuelling is carried out with the reactor shut down, primary sodium temperature standing at 250°C (see Fig. 3).

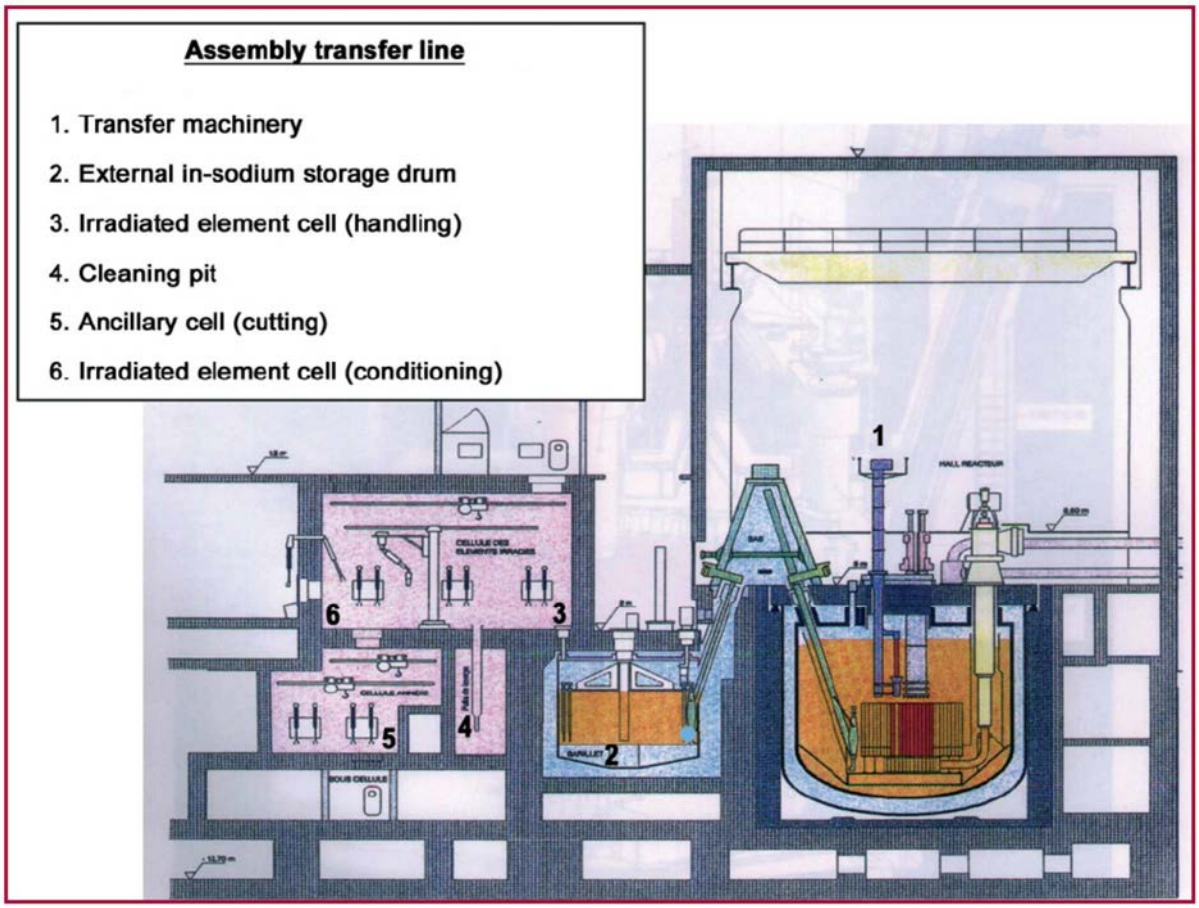

FIG. 3. Schematic of the fuel handling [1].

Elements in the core are transferred to internal storage positions, to allow for initial decay, and subsequently removed inside a sodium-filled pot, using a transfer ramp, to the external storage drum. Internal handling of core elements is effected through combined rotations of the rotating plug and transfer arm.

Once assembly decay heat has fallen off sufficiently, assemblies are transferred to the irradiated element cell, for the purposes of washing off residual sodium, cutting away assembly structural components and placing the pins in containers.

These hot cells are also used to carry out post-irradiation examinations and operations to assemble experimental irradiation devices. These cells are fitted with a neutronography reactor.

Fresh assemblies are stored on site, in air, in a storage facility. After inspection, they are loaded into the external storage drum, and subsequently into the reactor, taking the reverse route to irradiated assemblies.

Some technical characteristics are set out in Table 1.

TABLE 1. PHENIX REACTOR - TECHNICAL CHARACTERISTICS

Parameter	563 MW regime 1974–1993	350 MW regime 1993–2009
Thermal power (MW)	563	345
Gross electrical power (MW)	250	142
Net electrical power (MW)	233	129
Neutron flux at core centerline (n/cm2·s)	$7\ 10^{15}$	$4.5 \cdot 10^{15}$
Primary sodium core outlet temperature (°C)	560	530
Primary sodium core inlet temperature (°C)	400	385
Secondary sodium SG inlet temperature (°C)	550	525
Superheated steam temperature (°C)	512	490
Turbine HP cylinder steam pressure (bar)	163	140

More details about the operation of Phenix reactor are available [1].

The standard instrumentation available in the reactor and a special instrumentation for the final tests were used simultaneously.

The standard instrumentation consists in:

- Primary and secondary pumps speed which can be used to estimate the flow rate via the pumps characteristics;
- Secondary mass flow rate on each secondary loop;
- Core inlet temperature based on the measurement of the temperature at the outlet of the primary pumps;
- Specific pole of thermocouple giving the temperature at the primary pump inlet elevation;
- Fissile subassemblies outlet temperature measured a few centimetres above each fuel subassembly;
- Intermediate heat exchangers inlet and outlet temperatures on the primary side and on the secondary side;
- Steam generator inlet and outlet temperatures on the secondary side and on the tertiary side;
- Wall temperatures on the reactor vessel, on the baffle, on the counter-baffle and on the primary vessel;

A special instrumentation is also used for the final tests. Four poles of thermocouples are installed, two in the cold pool and two in the hot pool.

3. DESCRIPTION OF THE TEST

The natural convection test in Phenix reactor was performed on June 22 – 23, 2009, during the end of life tests campaign [2].

3.1. TEST SCENARIO

Before the beginning of the test, the reactor was operating at full power (350 MW(th)) during six days from June 12 to June 18 and then during approximately one day from June 21 to June 22. The reactor power was manually decreased from 350 MW(th) to 120 MW(th) on June 22 at 15:00 and the test started at 19:15 (local time).

The test scenario is described hereafter:

- the reactor is stabilized at a power of 120 MW(th) with the three primary pumps in operation at 350 rpm and two secondary pumps at 390 rpm (one secondary circuit is not operating). The core inlet temperature is 360°C and core outlet temperature is 432°C;
- the test begins (reference time t_0) by a manual dry out of the two steam generators to reduce the temperature difference in the IHX between the primary and secondary sides inlet;
- manual scram is done 458 seconds later when the previous criteria concerning the ΔT of IHX (15 °C) is reached;
- manual trip is done on the three primary pumps 8 seconds after the scram, with pumps speed decreasing to zero on their own mechanical inertia;
- secondary pumps speed decreases automatically to 110 rpm in about one minute, due to the scram;
- onset and development of natural convection in the primary circuit.

The natural convection test in the primary circuit is divided into two phases:

- phase 1 with no significant heat sink in the secondary circuits, except the heat losses along the piping and through the casing of the steam generator;
- phase 2 with significant heat sink in the secondary circuits, by opening the casing of SG at the bottom and at the top which involves efficient air natural circulation in the SG casing.

The duration of phase 1 is about 3 hours and the duration of phase 2 is about 4 hours. The benchmark case ends when the casing of SG is closed after the phase 2. Details of the test phases are reported in Table 2.

TABLE 2. MAIN ACTIONS OF THE PHENIX NATURAL CONVECTION TEST

Time	Action
0 s	Dry out of steam generators 1 and 3. No change in pumps speed.
458 s	Scram Secondary pumps 1 and 3 automatically reduced to 110 rpm in 1 min
466 s	Stop of the 3 primary pumps, beginning of the 1st phase
4080 s	Secondary pumps speed reduced to 100 rpm (back-up motors)
10320 s	Steam generators cooled by air, beginning of the 2nd phase
24000 s	Closing of SG casings and end of the benchmark

3.2. REACTOR BEHAVIOR AND GLOBAL RESULTS

3.2.1. Before the scram

After the dry out of the steam generators, the IHX secondary inlet temperature increases from 307°C to 420°C in about 300s as shown in Fig. 4.

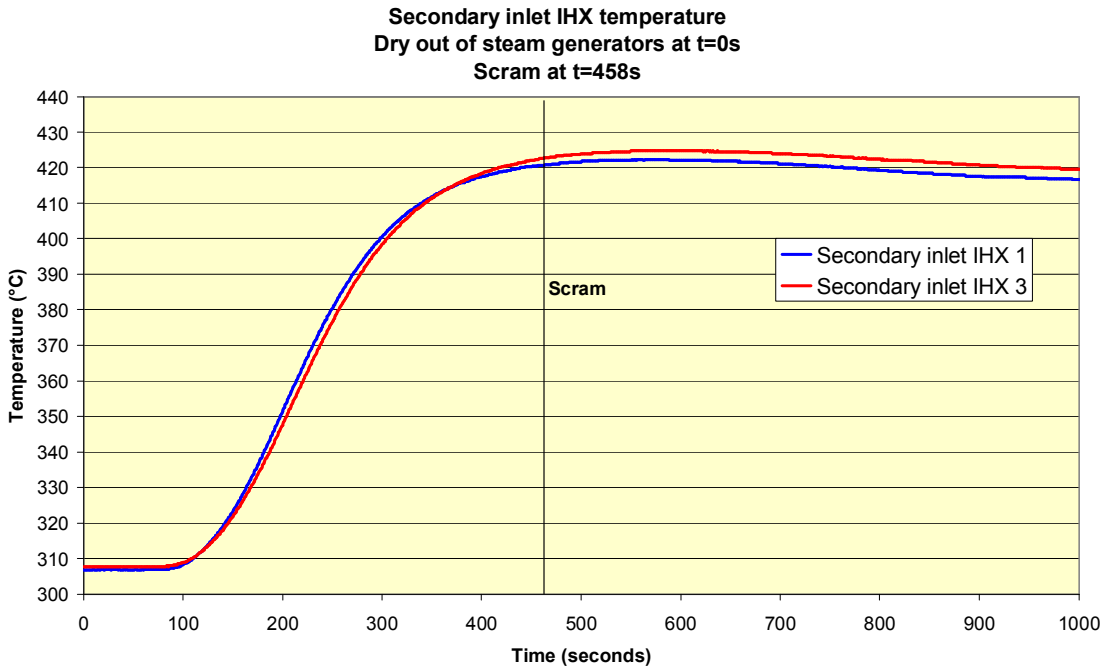

FIG.4. IHX secondary inlet temperature.

Consequently, the core inlet temperature increases from 360°C to 400°C in about 280s as shown in Fig. 5.

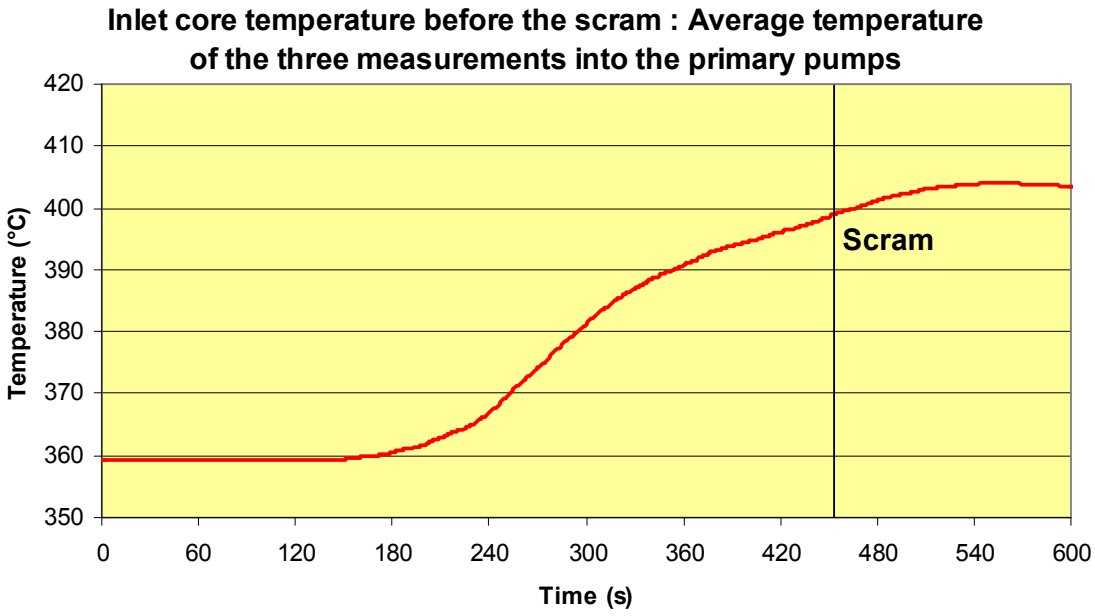

FIG. 5. Core inlet temperature.

The core power decreases from 120 MW(th) to about 50 MW(th) before the scram as shown in Fig. 6.

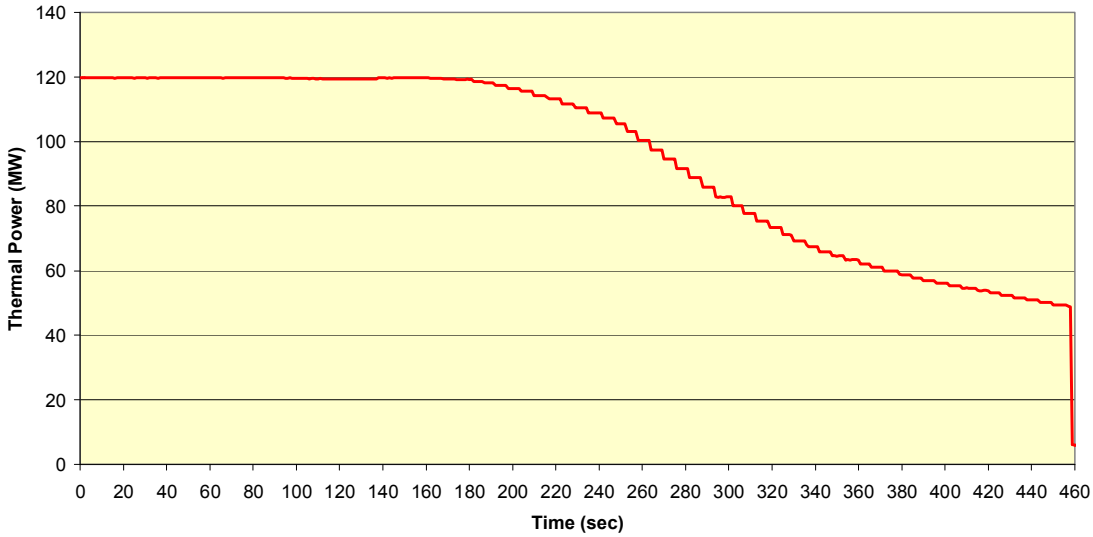

FIG. 6. Core thermal power before the scram.

This significant decrease of power is induced by the temperature increase at the core inlet after the steam generators dry out (transient close to the LOHS, Loss of Heat Sink).

Several reactivity feedback effects are concerned with the temperature increase, such as the Doppler effect, the expansion of the diagrid, the relative expansion of the control rods. In that case, the main effect is the expansion of the diagrid which involves a significant negative reactivity.

This well-known negative reactivity effect induced by the increase of temperature at the core inlet is clearly confirmed by this Phenix test. This is an important safety feature of sodium cooled fast reactors. The reactivity feedback concerning the relative expansion of control rods is also effective in this transient. At the beginning of the transient, the diagrid expansion effect is the most significant effect, but after the temperatures homogenization of the cold pool, it appears that the expansion of the main vessel acts like a relative extraction of the control rods. This positive reactivity effect is marked by the inflexion of the evolution of power at 300s. The global reactivity is still negative but it increases since the vessel expansion reactivity effect appears, as shown in Fig. 7.

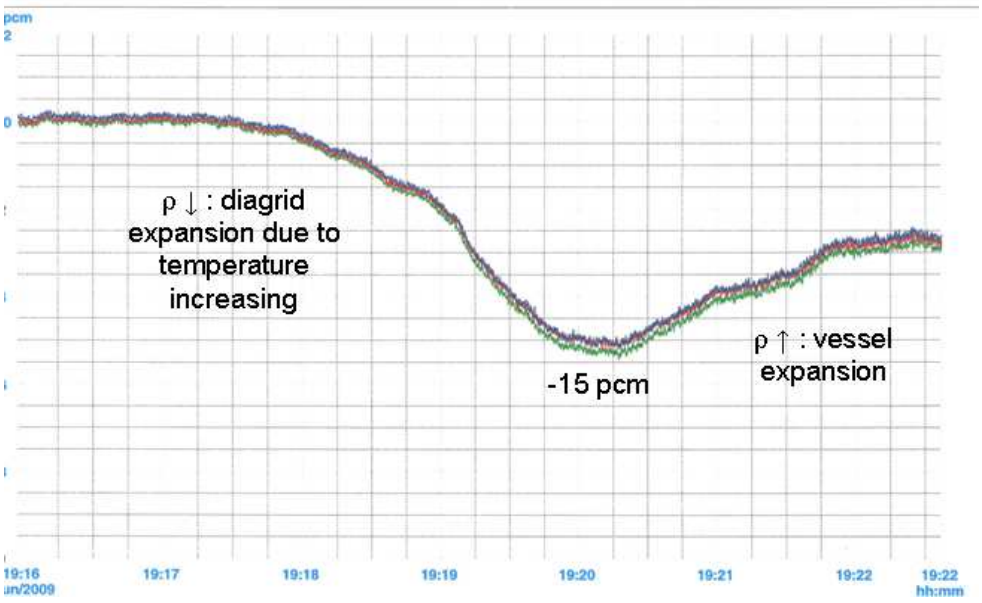

FIG. 7. Reactivity before the scram.

Just before the scram, the inner core outlet temperature has decreased from 450 °C to 440 °C due to the power decrease. After the scram, the core power is lower than 5 MW(th) after 30 seconds. The decay heat, which is calculated, is shown in Fig. 8.

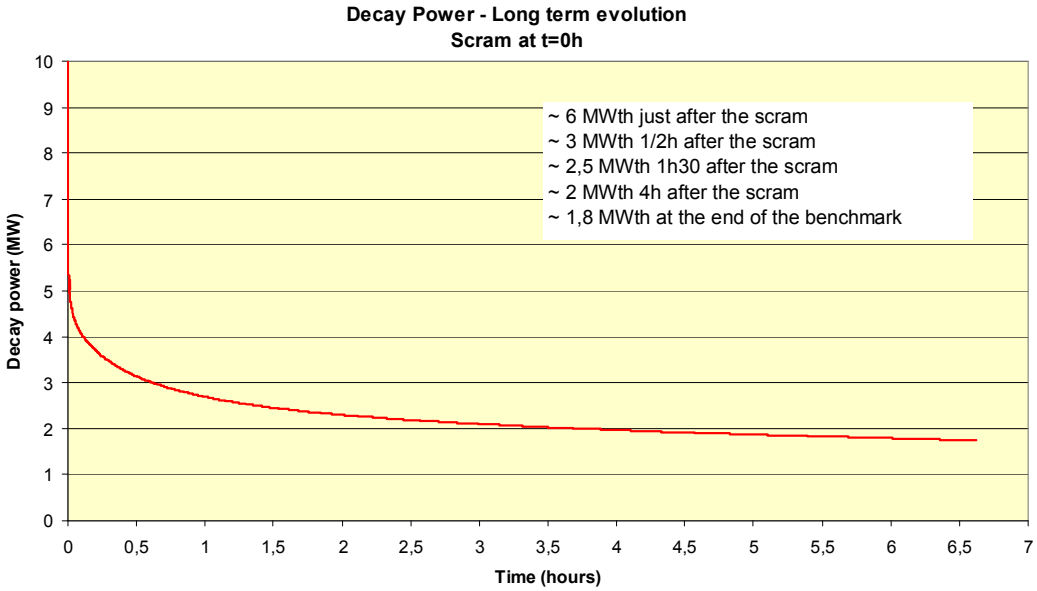

FIG 8. Decay heat after the scram.

3.2.2. After the scram

The manual scram is done at 458s when the criteria concerning the criteria on the IHX inlet temperature difference (15 °C) is reached.

The three primary pumps are tripped 8 seconds after the scram and the pump speed decreases to half-speed in 30 seconds and reaches zero within two minutes. The secondary pumps speed decreased to 110 rpm automatically, due to the scram (see Fig. 9).

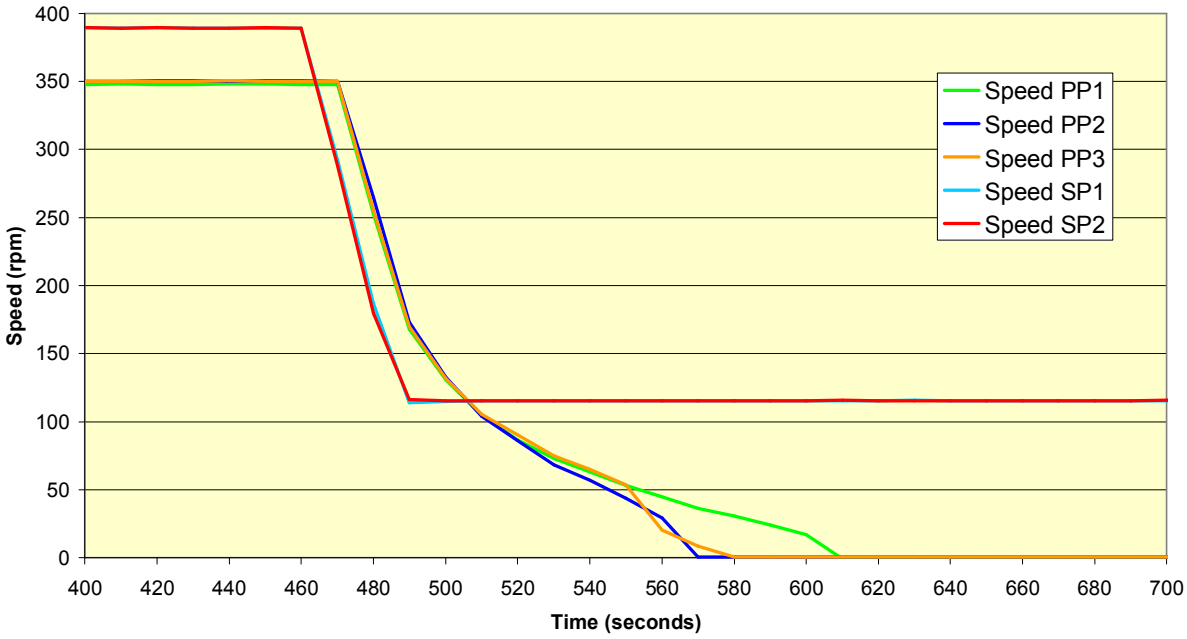

FIG. 9. Primary and secondary pumps speeds.

Some other curves are given in Section IV corresponding to those used as boundary conditions of the calculations, specially the secondary IHX inlet temperature and the flow rate of both secondary circuits.

3.2.3. Core outlet temperature

Core outlet temperature is measured by thermocouples located 10 centimetres above each fuel sub-assembly. For natural circulation conditions, it is difficult to deduce the global core outlet temperature because each sub-assembly flow rate is unknown and the thermal-hydraulics of the above core area is very complicated. For the comparison with computed temperatures, it is chosen to compare with several data estimated on the basis of measured core outlet temperatures:

— Outlet temperature of the hottest subassembly;

— Average outlet temperature of the 1st row;

— Average outlet temperature of the inner core;

— Average outlet temperature of the whole core (including blanket zone).

Average temperatures are simple arithmetically averaged values, without taking into account flow rate of each SA which is unknown in natural convection. This is a major difficulty of the interpretation of core outlet measurements in natural convection.

The inner core (core 1) outlet temperature decreases from 438 °C at the scram to 410 °C in about one minute. Then, the inner core outlet temperature increases to 448 °C in about three minutes corresponding to the onset of natural convection. About five minutes after the scram, the increase of the core outlet temperature stops, due to the establishment of natural convection.

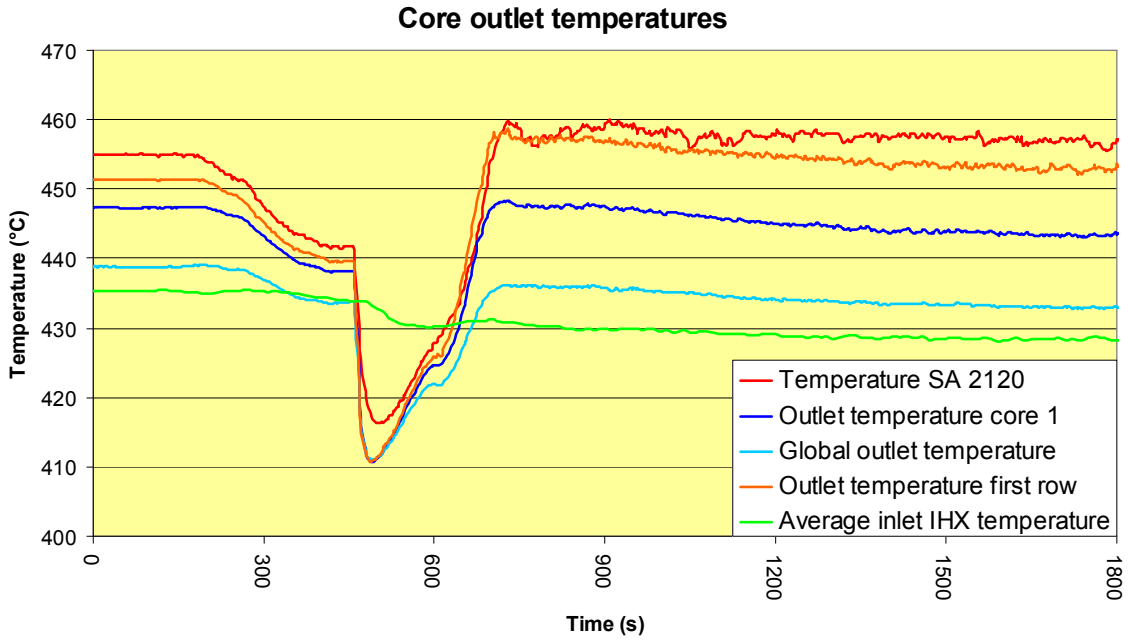

FIG. 10. Core outlet temperatures – beginning of the test.

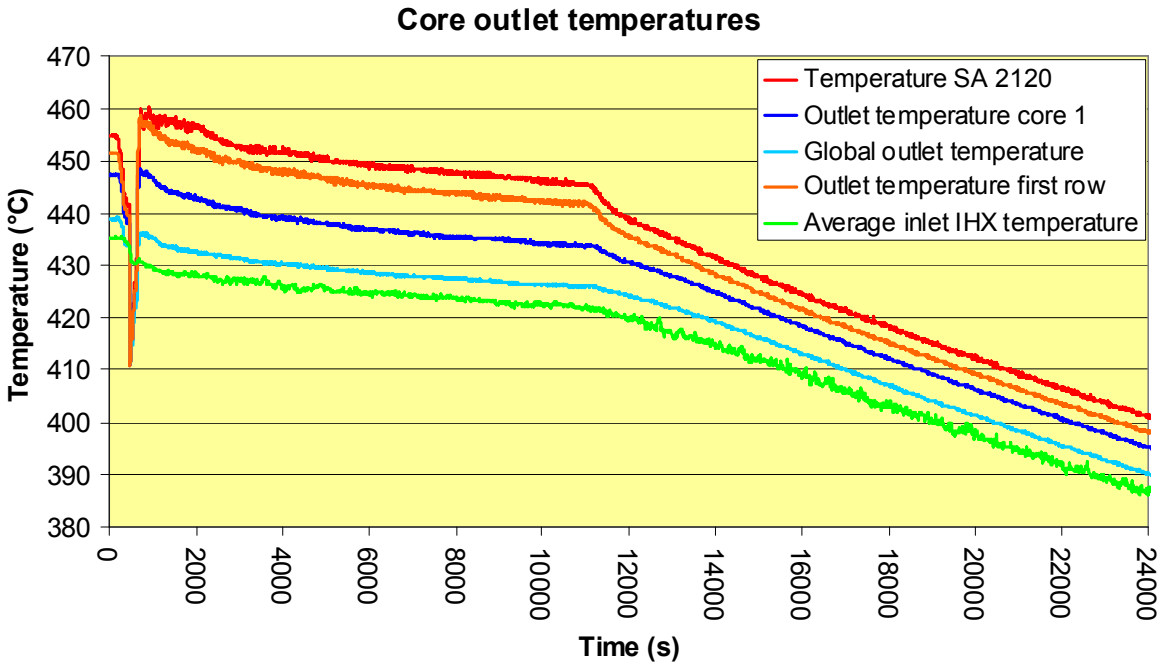

FIG. 11. Core outlet temperatures – whole test.

The core outlet temperatures decrease more quickly after the opening of steam generators casings. Moreover, the differences between each sub-assemblies area tightens, which means that natural convection flow rate is increasing during this phase of the test. It confirms that natural convection in the primary circuit is more efficient with a more efficient cooling of the secondary circuits.

The outlet temperatures of the first row of sub-assemblies are quite homogeneous during the transient. The natural convection is characterized by the stabilisation of temperatures after 5 minutes but also by the disturbed signal measured by the thermocouples, due to the mixing of rather low speed sodium jets from different subassemblies outlets.

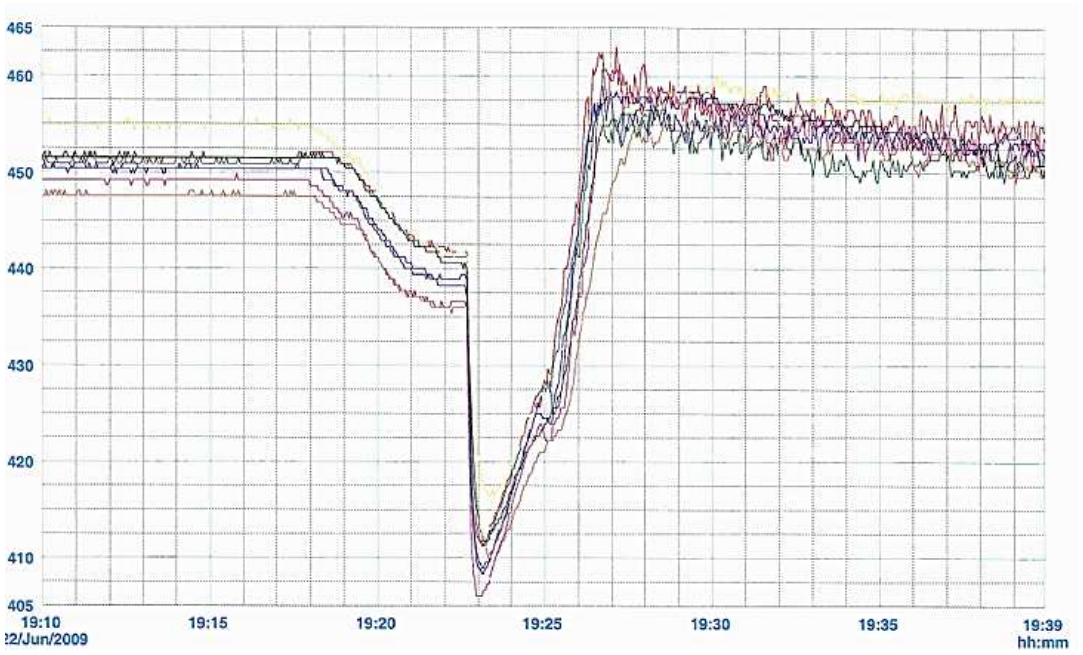

FIG. 12. Core outlet temperatures – beginning of the test.

The measurements made by the subassemblies outlet thermocouples are more difficult to analyse in natural convection due to these thermal-hydraulic perturbations, as shown in Fig. 13:

- Under-estimation of the temperatures due to the inter-wrapper cooling effect, especially at the establishment of natural convection when the inter-wrapper region is colder than the core outlet flow;
- Complicated mixing of different sodium jets from subassemblies outlet because of the low sodium velocity in this area.

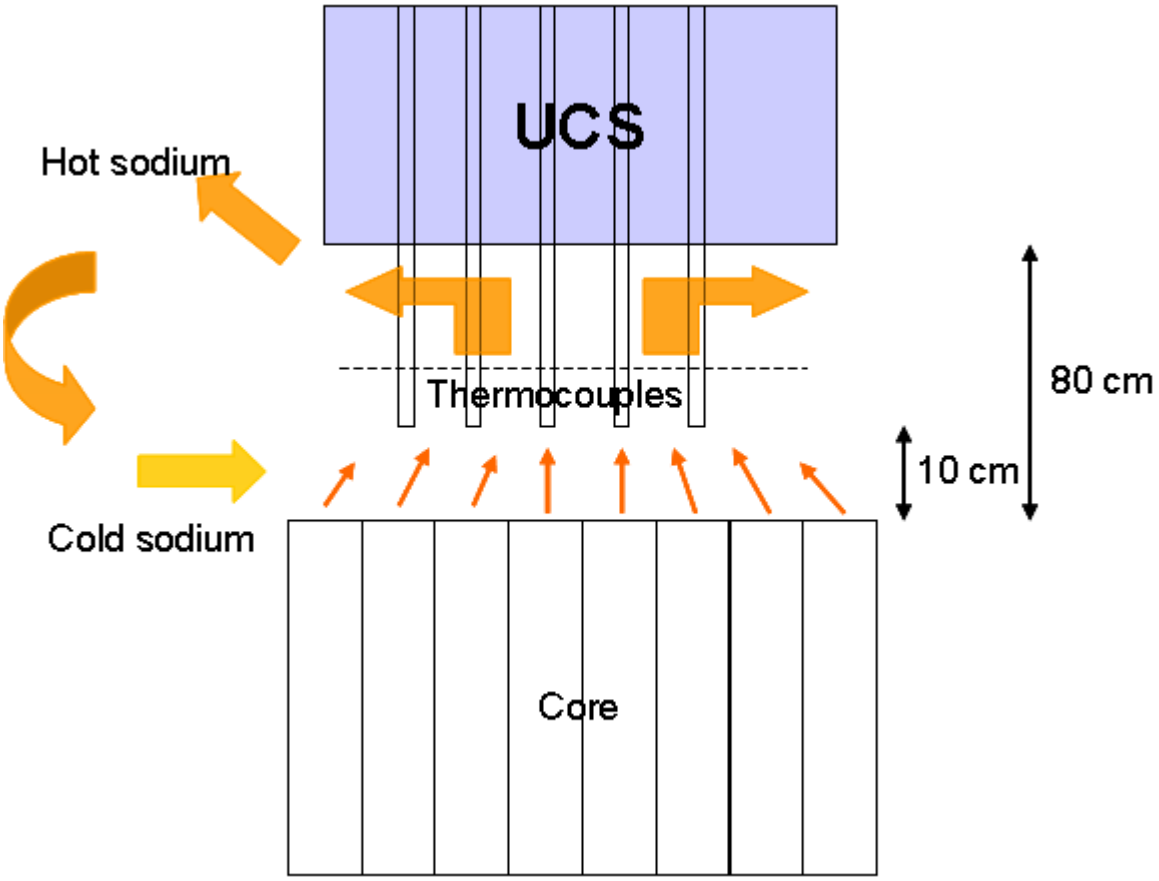

FIG. 13. Thermalhydraulics of the core outlet area.

Previous tests in Phenix with some primary pump restarting during natural convection shows that the maximum difference could be up to 30°C during the first minutes of natural convection between the measured temperature by these thermocouples in natural convection and the temperatures at the exit of the fissile zone.

3.2.4. Core inlet temperature

Some difficulty also appears for the core inlet temperature measurement in natural convection. Thermocouples are located in a derivation pipe inside each primary pump, which allows knowing the core inlet temperature for normal operation in forced convection.

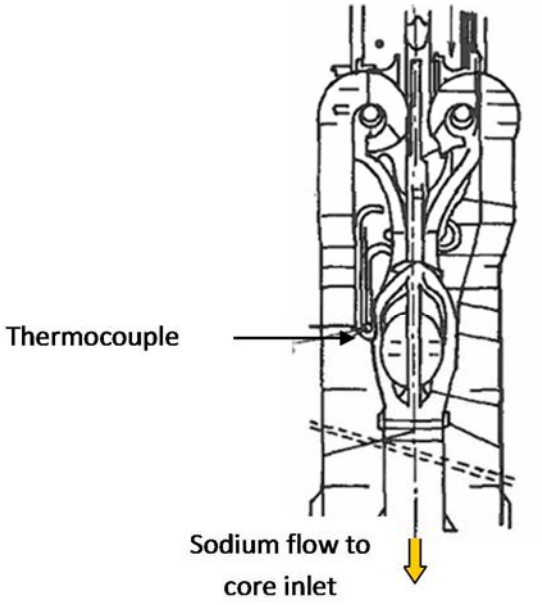

FIG. 14. Core inlet temperature measurement.

Flow in this derivation is sufficient in forced convection, but drastically reduced in natural convection. So thermocouple in the derivation may be influenced by the surrounding stratified hot sodium, which is confirmed by other measurements made by the DOTE pole in the cold pool. We notice that after the primary pumps trip, this temperature is very close to the DOTE temperatures at the same level in the cold pool.

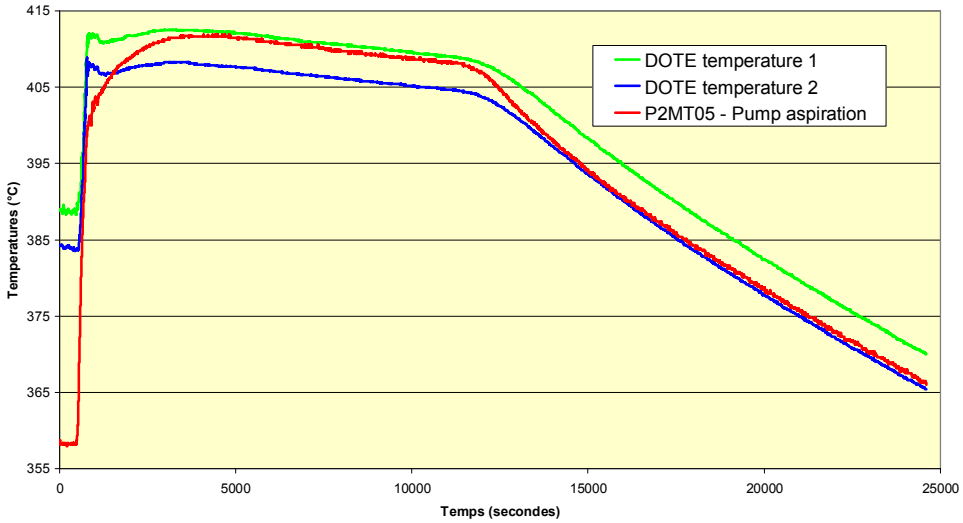

FIG.15. Core inlet temperature measurement and DOTE measurements.

A relevant thermocouple which could be used to represent the pump inlet temperature is one of the DOTE pole located at the level of the pump skirt suction (z = -5400mm).

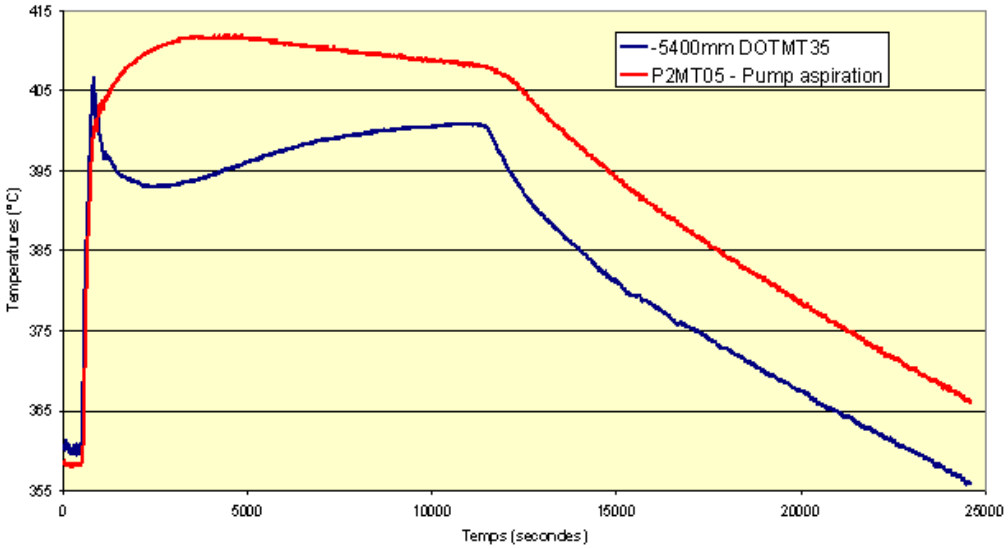

FIG. 16. Comparison between the usual core inlet temperature measurement and the DOTE thermocouple located at -5400mm.

The DOTE temperature evolution is more realistic: first a hot shock due to the dry out of steam generators, then a cold shock due to the scram, then a slow increase as there is no real heat sink, except the reactor thermal inertia and the heat losses in the secondary circuits, and then a regular decrease in the next phase of the test, with cooling of steam generators casings.

3.2.5. IHX inlet temperature

Thermocouples are located at the top of each IHX inlet window. These measurements are considered relevant even if there is some stratification above the IHX inlet window.

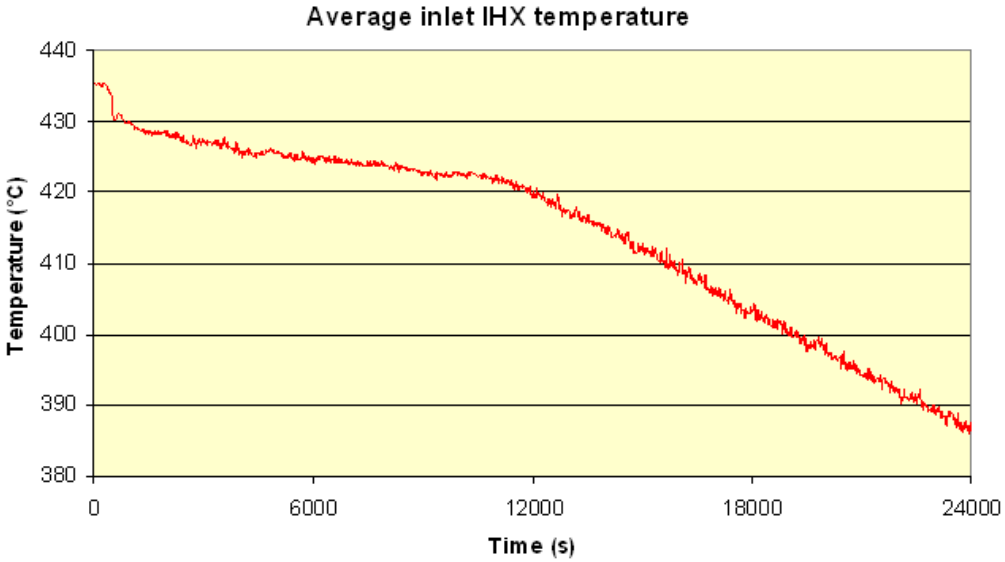

FIG.17. Average IHX inlet temperature.

The temperature at the IHX inlet is logically similar to the core outlet temperature.

3.2.6. IHX outlet temperature

Thermocouple is located at the top of the outlet window, very close to the tube bundle (see Fig. 18).

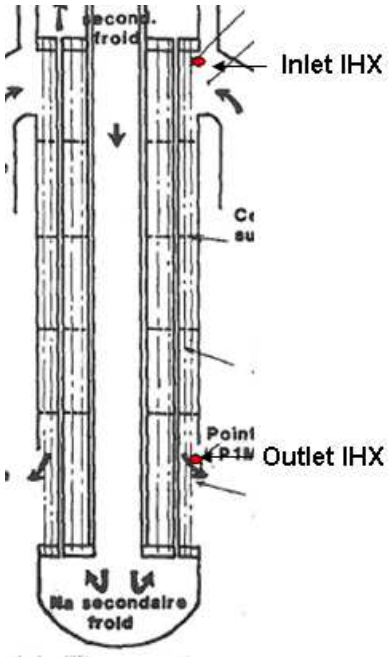

FIG.18. IHX outlet thermocouples.

The measurement is not considered relevant because of the stratification in the outlet window of IHX. Nevertheless, previous thermal hydraulic studies have shown that most of the IHX flow is located at the bottom of the IHX window. One thermocouple of the IHX-M pole located at the level of the bottom of the IHX window (elevation z=-4200m) can be used as an estimation of 'IHX primary outlet temperature'.

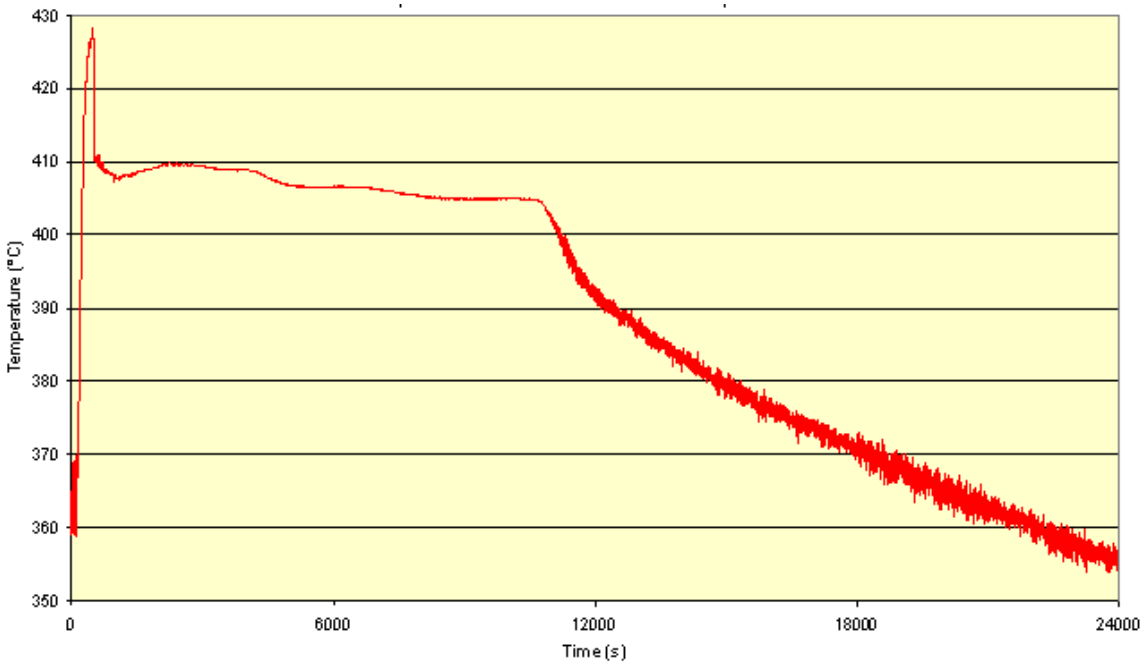

FIG.19. IHX outlet temperature (IHX-M at -4200mm).

Two precautions have to be taken:

— The real mean temperature depends on the velocity profile in the outlet window, which is not measured of course;

— This measurement is limited to IHX-M and one has to assume that the three other IHX have the same behavior to compare with the calculations.

The temperature evolution is similar to the pump inlet temperature one, as shown in Fig. 20. During the first phase, the difference is due to the important stratification in the cold pool. After opening the steam generators casing, the two measurements are very close, meaning that the homogenization of the cold pool occurs because of the increase of natural convection flow rate. Moreover, we can notice the measurement noise at the IHX outlet during this test phase, as a consequence of mixing of fluid at different temperatures.

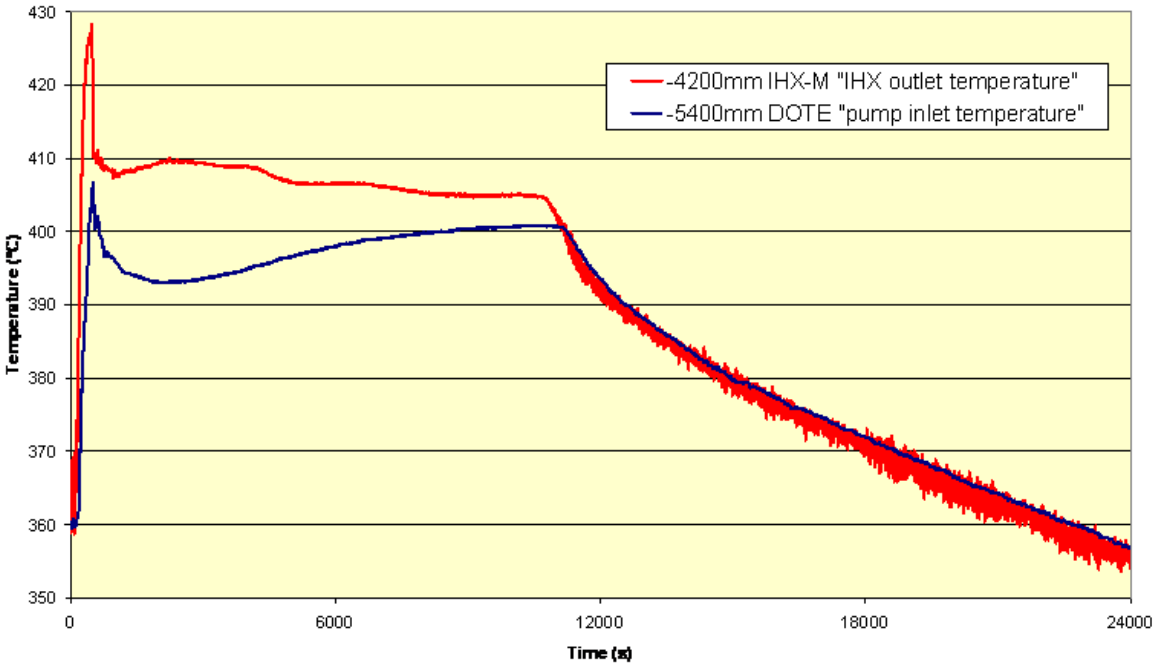

FIG. 20. Comparison between the two proposed measurements for IHX outlet and pump inlet.

3.2.7. Some conclusions on the test

The test was performed without difficulty, quite as predicted. A lot of thermal hydraulics data are now available for system codes comparison.

The negative reactivity effect induced by the increase of temperature at the core inlet is clearly confirmed by this Phenix test. This is an important safety feature of sodium cooled fast reactors.

Natural convection is efficient to cool the reactor core after the scram without any other significant heat sink than thermal inertia and heat losses, as shown by the first phase. Then, with a significant secondary heat sink, natural convection is very efficient, as shown by the second phase. The global cooling gradient is about 10°C/h during this second phase.

The global core flow rate in natural convection is not measured. It is estimated by post-calculations between 30kg/s and 60 kg/s, meaning 2 to 3 % of the nominal flow rate.

Instrumentation for forced convection is not always adapted for natural convection. For both core inlet and core outlet, and also for IHX outlet, comparison of measurements and calculations has to be done with caution, because of the unsuited instrumentation for natural convection regimes in the primary circuit and the heterogeneous thermal-hydraulics situation.

We should compare what is comparable and have in mind the differences between the measurement, the real values and the calculations.

Besides the valuable features of this test for system code validation, other thermal hydraulics phenomena are specifically interesting:

- Natural behavior after the hot shock at the beginning of the test for understanding of neutronic feedback coefficients;
- Thermal stratification in the hot and cold pools;
- Stratification and recirculation in the lower part of the hot pool and under the UCS which disturbs the core outlet temperature measurements in natural convection;
- Instrumentation issues in natural convection with stratified plenums.

4. BENCHMARK SPECIFICATION

The aim of this Section is to present the list of data supplied by the CEA to all participants of this CRP in order to perform calculations. The natural convection test specifications are classified as follows: core, primary circuit, primary pumps, IHX, shutdown system, operating parameters, test scenario and real test conditions.

However uncertainties are associated to each plant operational data:

- ± 5 MW(th) on thermal power before scram;
- 10% after scram for decay heat;
- Less than ± 5 °C on temperatures;
- ± 5 % on flow rates.

4.1. PLANTS PARAMETERS

The following ties give the main plant parameters:

- Total thermal power generated in the core : 350 MW(th);
- 3 primary pumps;
- 2 IHX per primary pump
- 2 secondary loops in service : n°1 and n°3;
- 4 IHX in service;
- 2 DOTE (replacement of IHX corresponding to secondary circuit n°2);

General overview and top view of the reactor is given in Fig. 21 and Fig. 22.

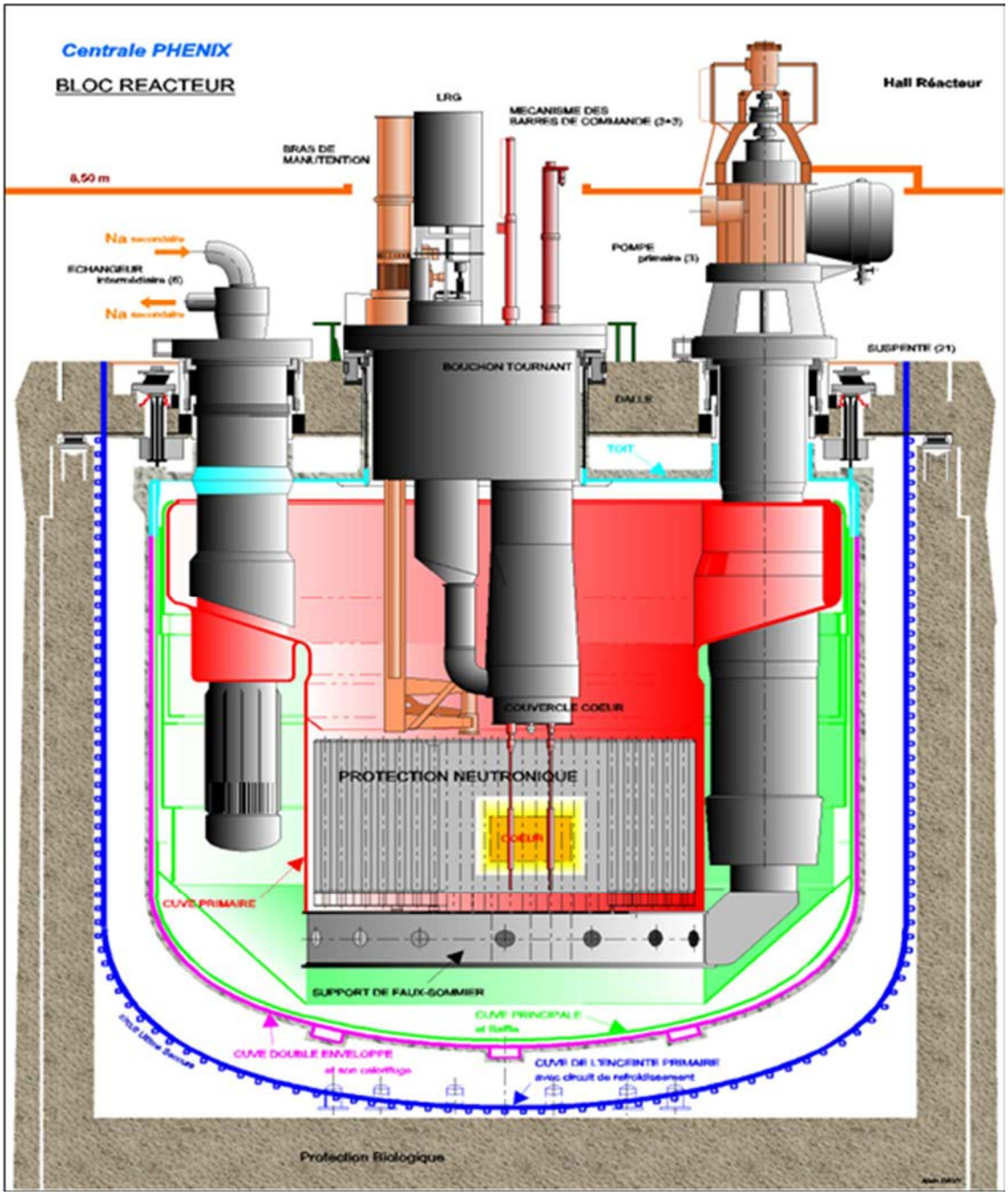

FIG. 21. Phenix reactor - General view of the reactor [1].

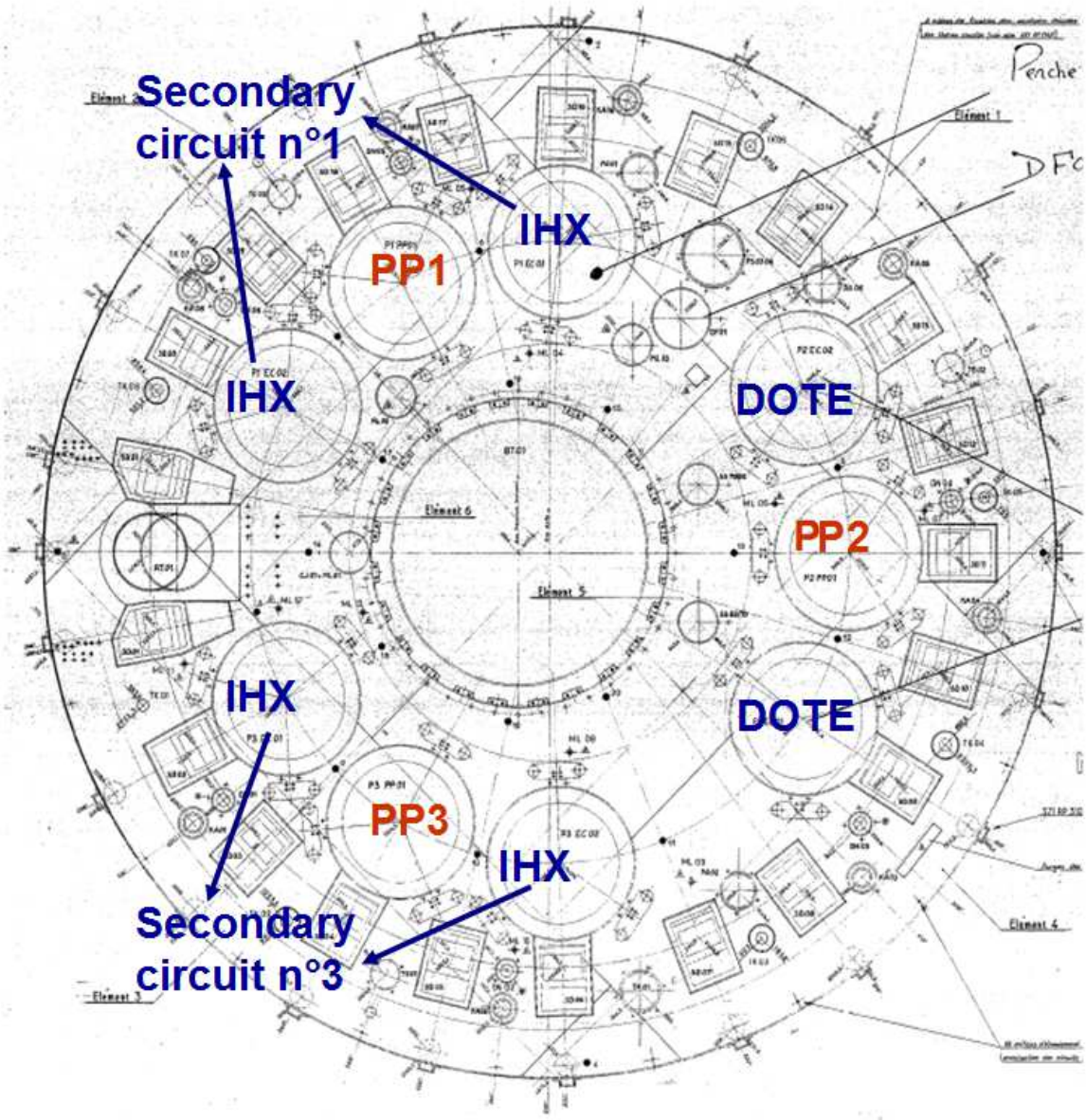

FIG. 22. Phenix reactor - Top view of the reactor vessel [1].

4.2. CORE

4.2.1. Core configuration

Top view of the core loading is in Fig. 23.

- Number of fuel SA in the inner core: 54;
- Number of fuel SA in the outer core: 56;
- Number of fertile SA: 86;
- Number of control rod SA: 6;
- Number of safety rod SA: 1;
- Number of steel reflector SA: 212;

– Number of B4C shielding SA: 765;
– Number of steel shielding SA: 297;

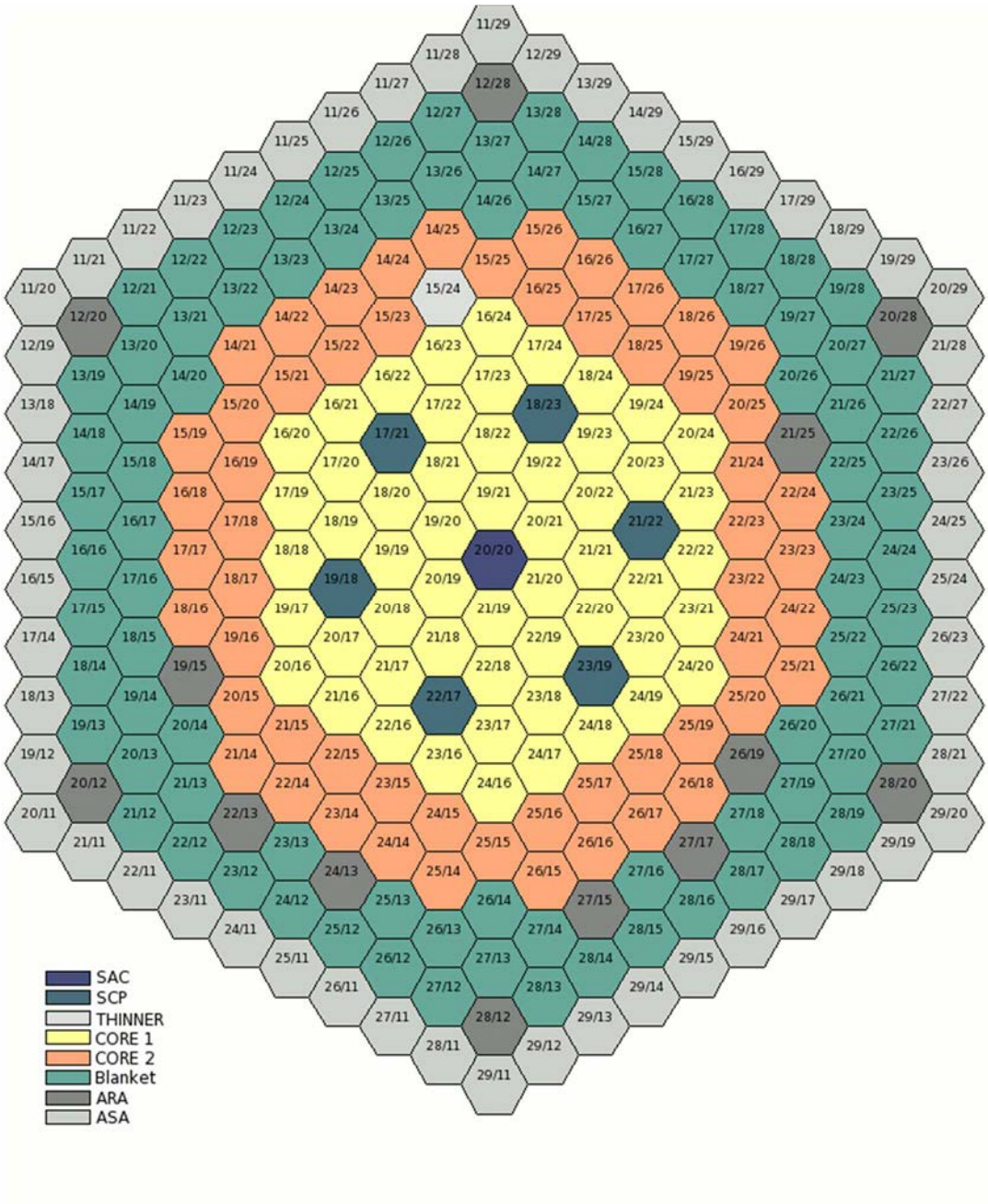

FIG. 23. Phenix reactor - Top view of the core loading [1].

4.2.2. Power and flow zoning

— Power of the inner core: 180,9 MW(th)
— Power of the outer core: 143,1 MW(th)
— Power of fertile SA: 24,1 MW(th)
— Power of steel SA: 1,2 MW(th)

— Power of control rods : 0,7 MW(th)
— Power of in-containment fuel storage SA: 1,7MW(th)
— Sodium flow rate of the inner core: 861 kg/s
— Sodium flow rate of the outer core: 779 kg/s
— Sodium flow rate of fertile zone: 226 kg/s
— Sodium flow rate of steel zone: 62 kg/s
— Sodium flow rate of control rods: 14 kg/s
— Sodium flow rate of in-containment fuel storage zone: 46 kg/s

See Fig. 24 for the primary hydraulic scheme.

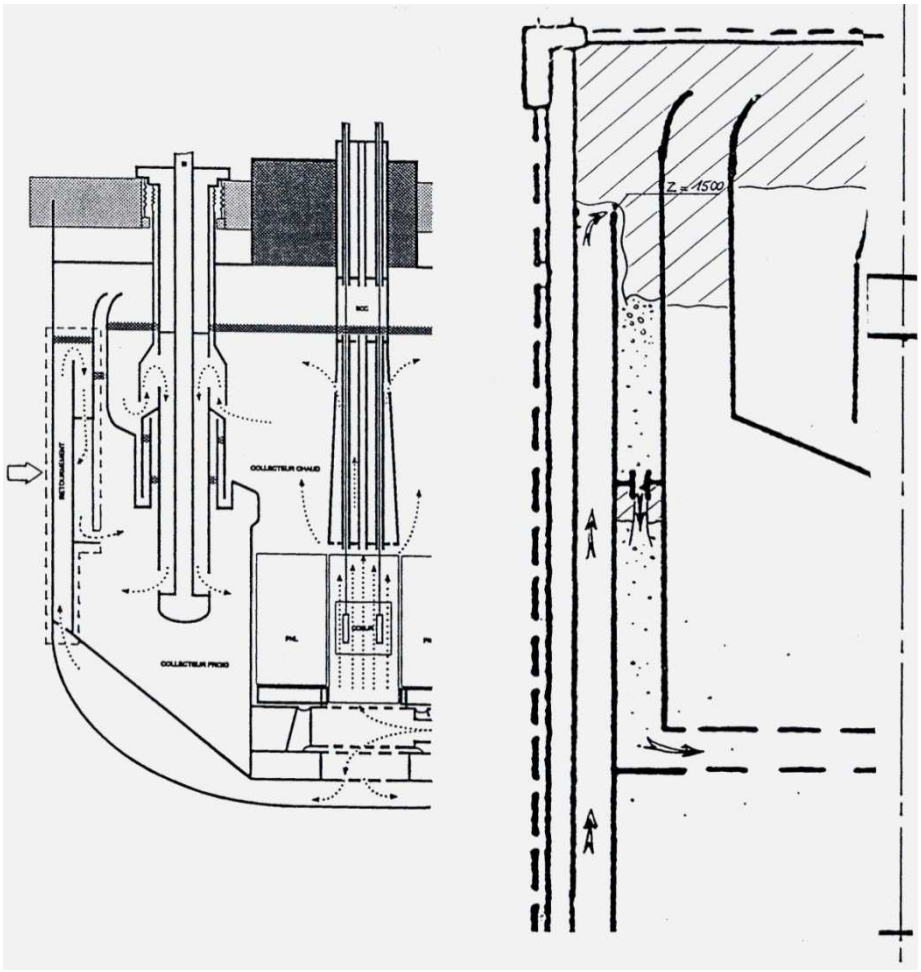

FIG. 24. Phenix reactor - Scheme of vessel cooling flow path [1].

4.2.3. Geometrical data for fuel SA

See Fig. 25 for a scheme of sub-assemblies.

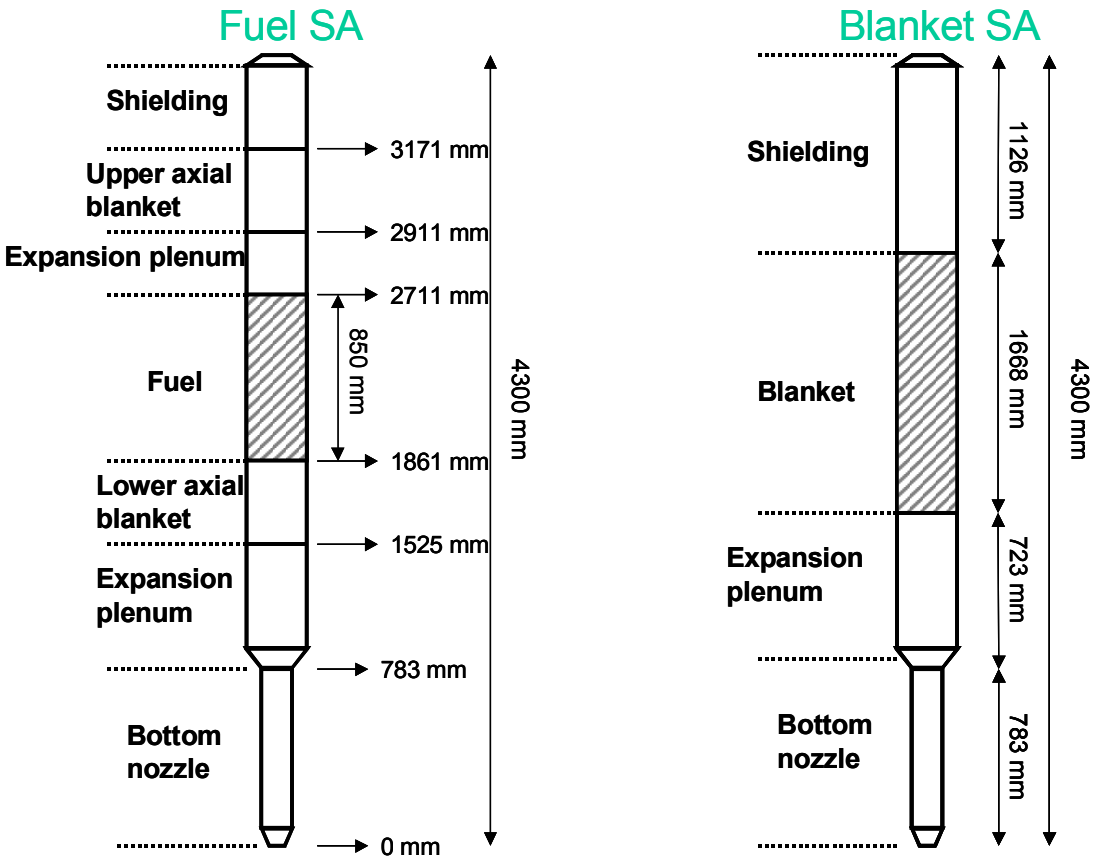

FIG. 25. Phenix reactor - Scheme of fuel and blanket SA [1].

— Number of pins in SA: 217
— Pitch of pins: 7,773 mm
— Inner diameter of fuel clad: 5,65 mm
— Outer diameter of fuel clad : 6,55 mm
— Pitch of wire wrap: 150 mm
— Diameter of wire wrap: 1,15 mm
— Diameter of fuel pellet: 5,42 mm
— Width across flat of SA: 116,9 mm
— Lattice pitch: 127 mm
— SA length: 4300 mm
— Active core portion length: 850 mm
— Length of control rods: 1 270 mm
— Length of control rod drive shaft: 1 418 mm
— Recommendation for modeling: 90% linked fuel, 10% free fuel.
— Thermal exchange coefficient between fuel and clad :
  - 1500 W/m^2°C with free fuel (beginning of life)
  - 5000 W/m^2°C with no gap between fuel and clad (end of life)

- 2500 W/m^2°C with blanket pins

4.2.4. Geometrical data for blanket SA

See Fig. 25 for a scheme of sub-assemblies.

— Number of pins in SA: 61;
— Inner diameter of fuel clad: 12,45 mm;
— Outer diameter of fuel clad: 13,4 mm;
— Pitch of wire wrap: 200 mm;
— Diameter of wire wrap: 1,08 mm;
— Diameter of fuel pellet: 12,15 mm;
— Fertile portion length: 1 668 mm.

4.2.5. Neutron kinetics data

The neutron kinetics parameters are listed below:

— Isothermal temperature coefficient k: -2,2 pcm/°C;
— ΔT core coefficient g: -1,9 pcm/°C ;
— Power coefficient h: -1 pcm/MW;
— Doppler worth in fissile core: -510 pcm;
— Doppler worth in fertile core: -170 pcm;
— Sodium void worth: -0,018362 pcm/°C;
— Grid plate expansion: -1,2075 pcm/°C;
— Radial expansion of clads: -0,009465 pcm/°C;
— Axial expansion of clads: 0,0057604 pcm/°C;
— Radial expansion of hexagonal sheaths: -0,0014106 pcm/°C;
— Axial expansion of hexagonal sheaths: 0,012919 pcm/°C;
— Axial expansion of fuel: -0,31396 pcm/°C;
— Strap effect: 0 pcm/°C;
— Sodium void in the control rods zones: -0,022525 pcm/°C;
— Neutron life time: 0,38 μs;
— Decay constants for six groups of delayed neutron precursors (sec-1):

3,703 1,376 0,3439 0,1346 0,0313 0,01295

— Delayed neutron fractions for these six groups :

1,6E-4 5,198E-4 1,168 E-3 6,154E-4 7,046E-4 8,22E-5

— Temperature of fuel in fissile SA: 1 227 °C
— Temperature of fuel in fertile SA: 628 °C

See Fig. 26 and Fig. 27 for radial and axial power distribution in the core.

See Fig. 28 for the six control rods worth.

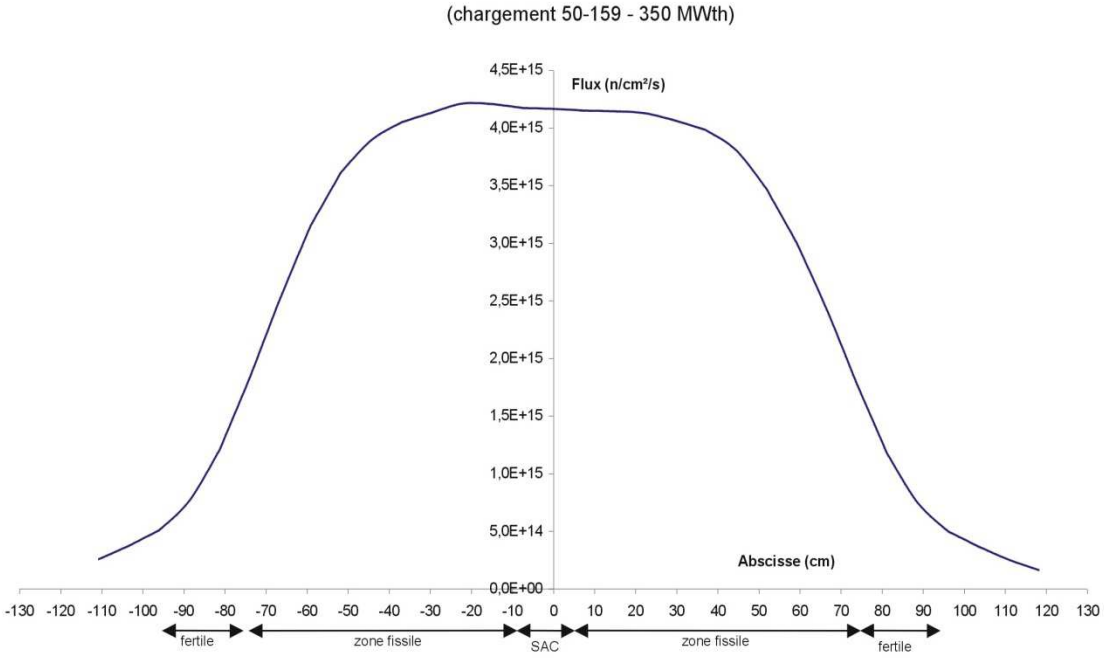

FIG. 26. Phenix reactor - Radial distribution of neutronic flux.

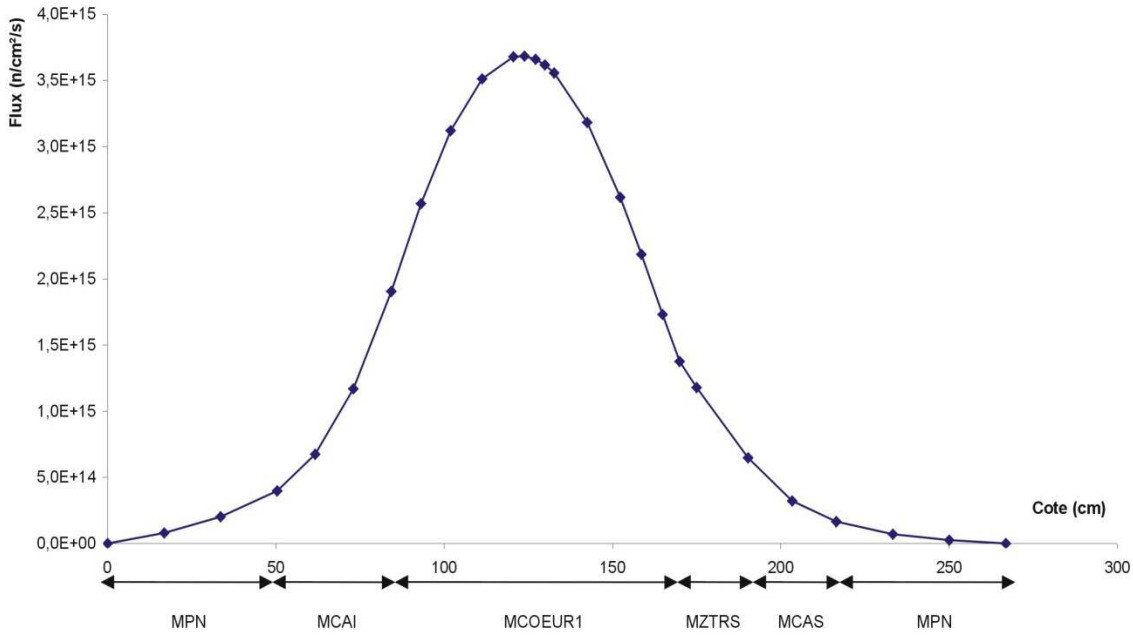

FIG. 27. Phenix reactor - Axial distribution of neutronic flux.

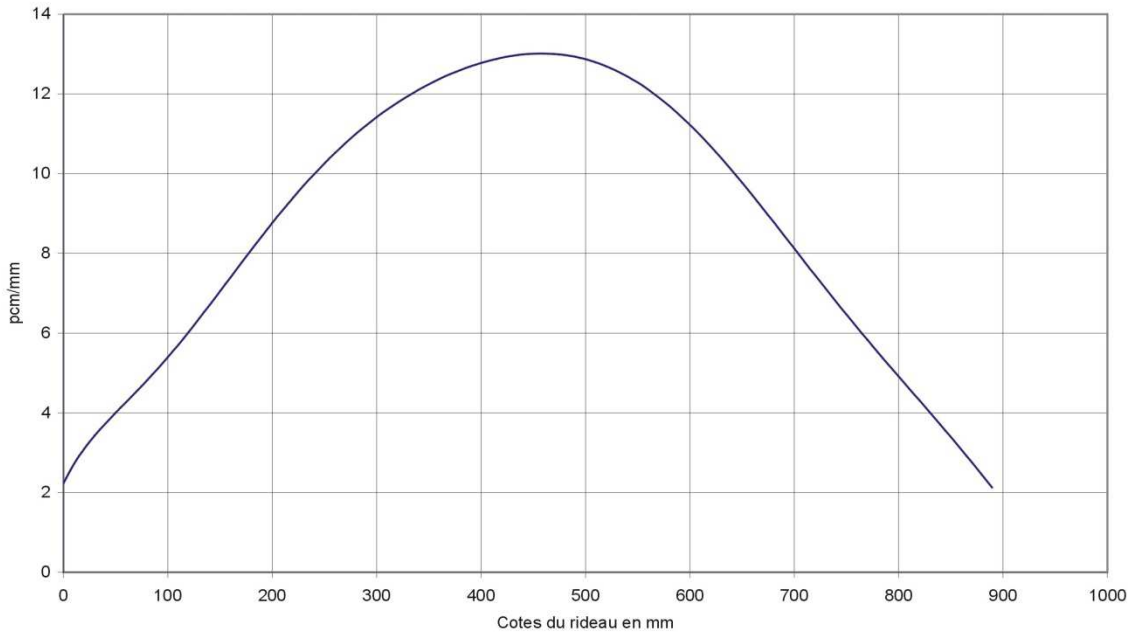

FIG. 28. Phenix reactor - Six control rods worth.

4.2.6. Core materials

- Fuel volume fraction over whole core: 37%;
- Sodium volume fraction over whole core: 35%;
- Steel volume fraction over whole core: 25%;
- Void volume fraction over whole core: 3%;
- Inner core Pu enrichment: 18%;
- Outer core Pu enrichment: 23%;
- Total Pu content of core: 931 kg;
- Average power density: 1200 kW/L of fuel;
- Cladding material of core: Cr17 Ni13 Mo2,5 Mn1,5 TiSi;
- Thermal conductivity of steel: 21,4 W/(m.°C).

4.3. PRIMARY CIRCUIT

A scheme of primary circuit with elevations of the different components is given in Fig. 29. The plans are also given in Figs 30 – 32.

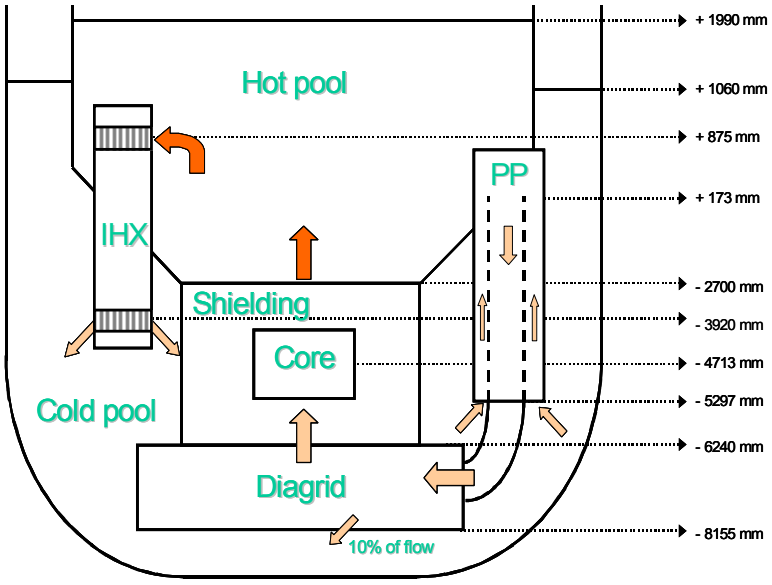

FIG. 29. Phenix reactor - Scheme of primary circuit [1].

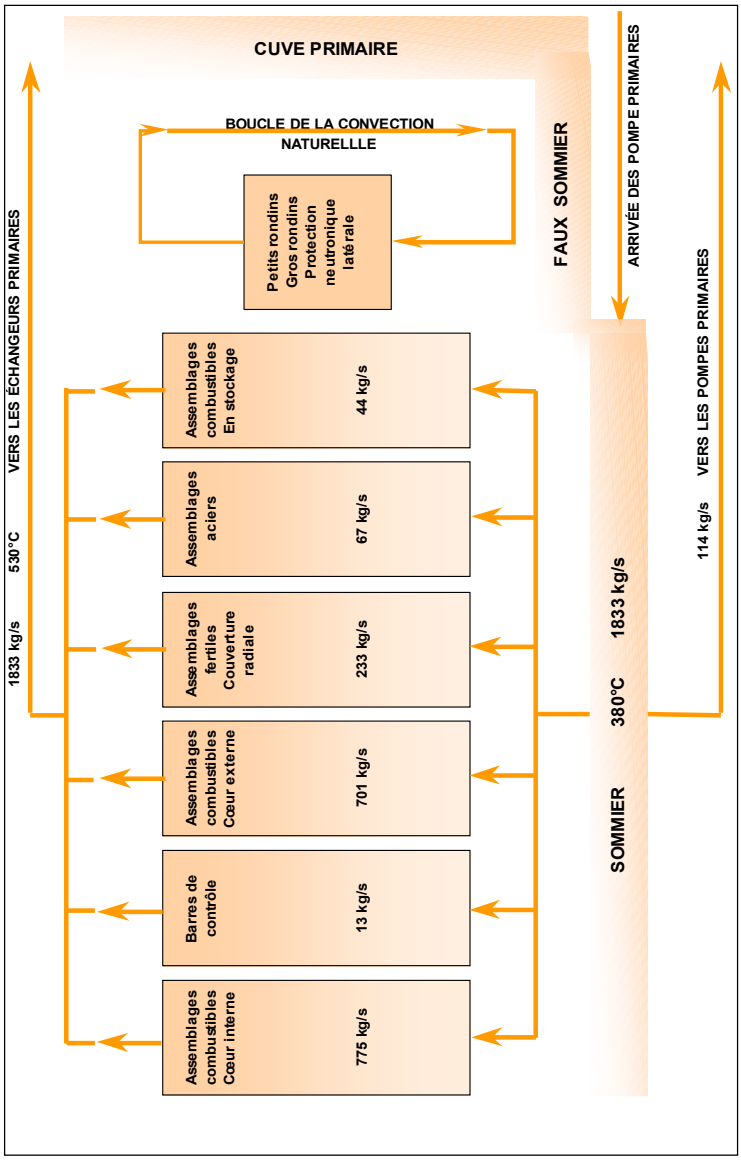

FIG. 30. Phenix reactor - Primary hydraulics [1].

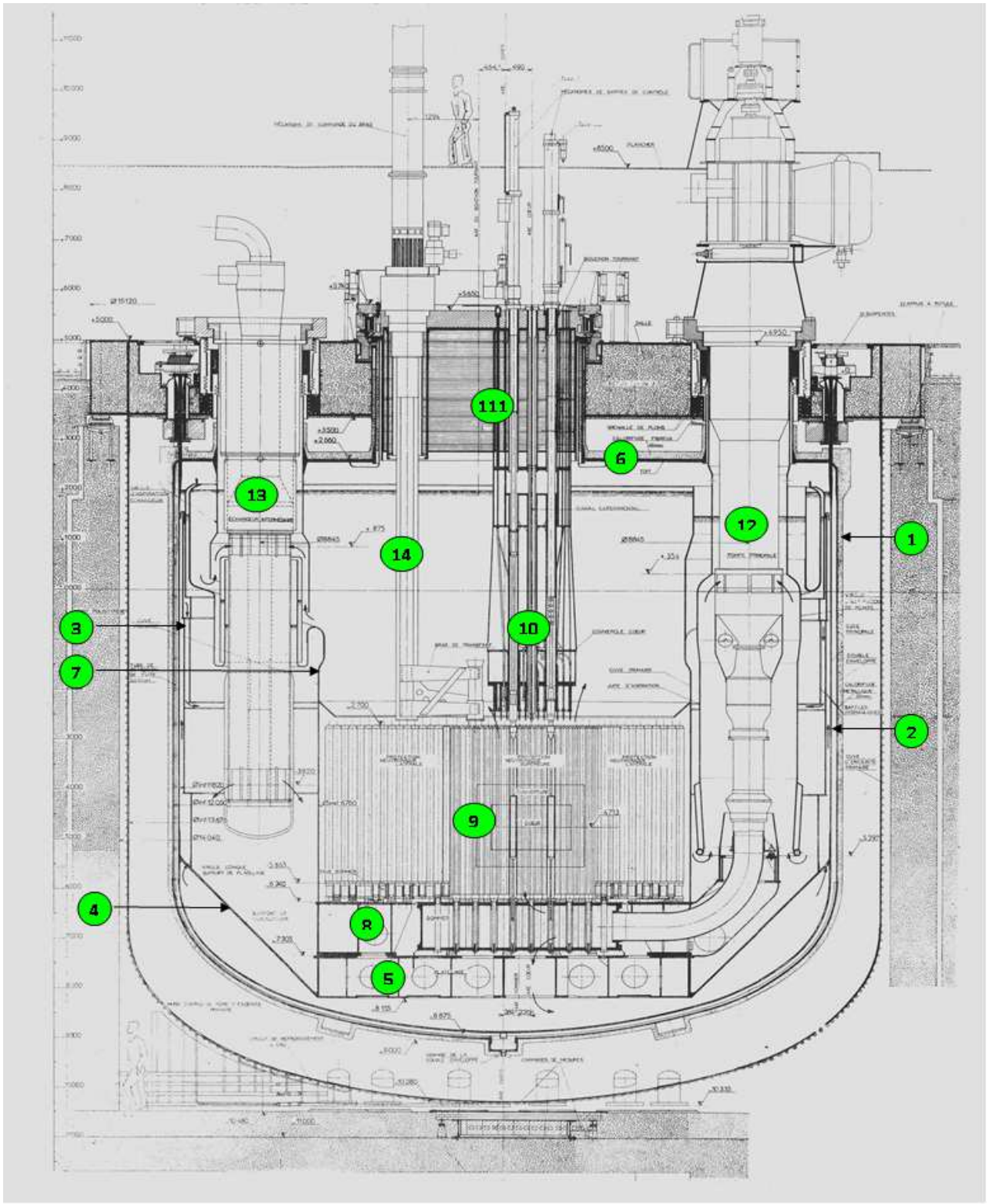

FIG. 31. Phenix reactor - Reactor sectional drawing primary pump-IHX [1].

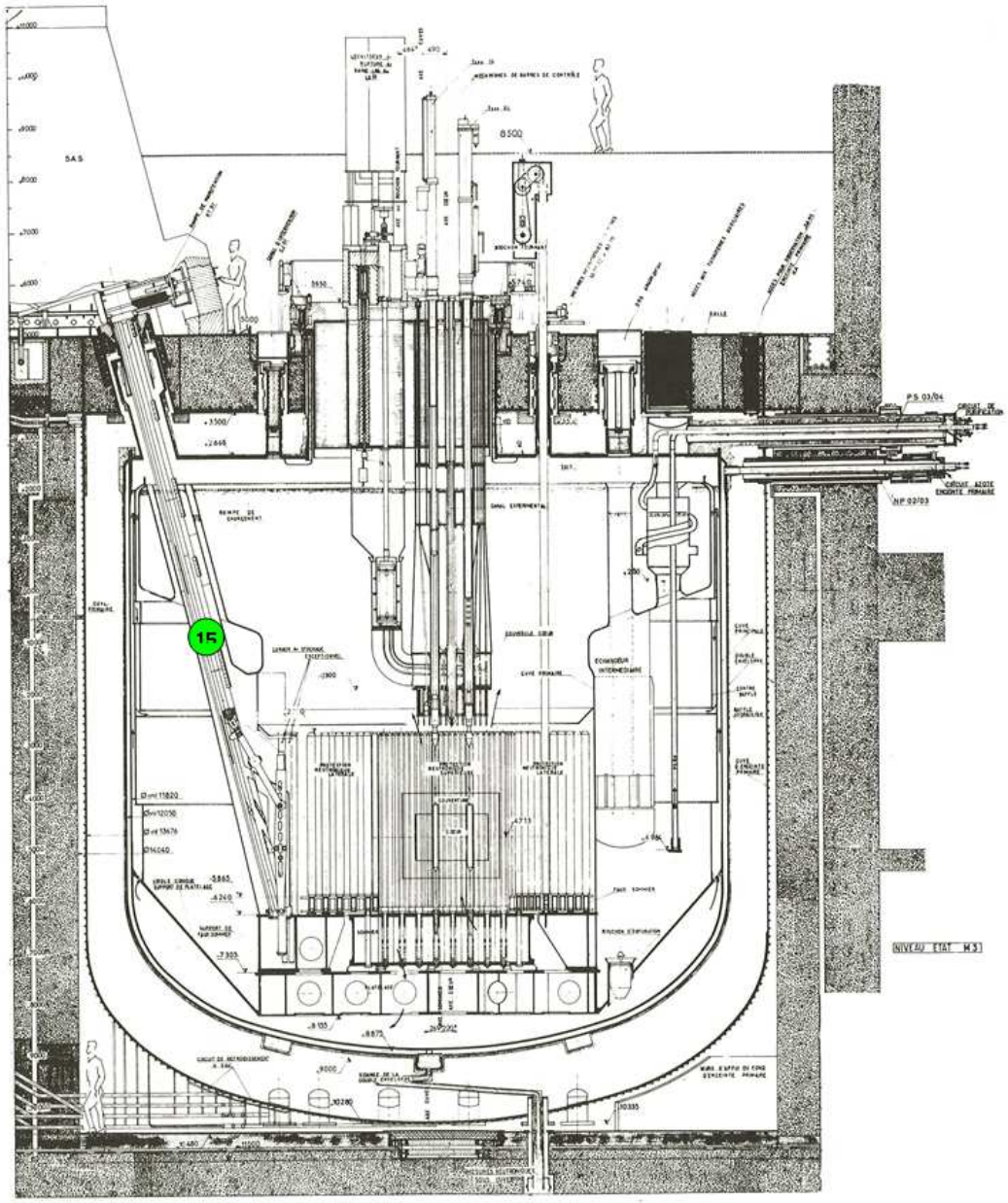

FIG. 32. Phenix reactor - Reactor sectional drawing handling ramp-IHX [1].

Double envelope vessel	1
Main vessel	2
Hydraulic wrappers	3
Conical shell	4
Strong back	5
Roof	6
Primary vessel	7
Diagrid	8
Core	9
Control plug	10
Rotating plug	11
Primary pumps	12
IHX and DOTE	13
Transfer arm	14
Handling ramp	15

4.3.1. Primary circuit geometry

The main primary circuit parameters are given below:

— Thickness of shell between hot and cold pool: 20 mm ;
— Area of primary pump (PP) discharge pipe: 0,229 m2;
— Sodium area in the IHX: 0,585 m2;
— Cold pool area: 9,12 m2;
— Hot pool area: 84 m2;
— Length of PP discharge pipe: 7,4 m;
— Length of IHX: 4,09 m;
— Length of core: 4,07 m;
— Equilibrium level at 400°C: 1,783 m;
— Leakage rate to cool the inner vessel: ~ 10% of nominal flow rate;
— Flow rate in the control plug: ~ 1,5% of nominal flow rate;

A scheme of the weir for vessel cooling is given in Fig. 24.

4.3.2. Pressure drops of primary circuit (for 350 MW(th))

The main pressure drops of the primary circuit for the nominal state of 350 MW(th) are given below:

— Pressure drop in core SA for nominal flow: 1,955 bar;
— Pressure drop in diagrid for nominal flow: 0,0304 bar;
— Pressure drop in IHX tube bundle for nominal flow: 0,0565 bar;
— Pressure drop between PP and diagrid: 0,0494 bar;
— Pressure drop in PP for nominal flow: 2,0901 bar.
— Pressure drop in reversal for vessel cooling: 0,0219 bar.

4.3.3. Cold pool and hot pool

The separation between hot and cold pool is shown in Fig. 21: the red area for hot pool and the green one for cold pool.

— Vessel surface: 452 m2;
— Power evacuated by emergency cooling circuit in W per m2 of surface vessel (T is the average temperature of cold pool in °C);

$$P = 3{,}229E\text{-}9\ T^4 + 1{,}028E\text{-}5\ T^3 - 5{,}552E\text{-}3\ T^2 + 2{,}912\ T - 246.9;$$

— Power evacuated by the roof in W (T is the average temperature of hot pool in °C):

$$P = 390\ T - 4000;$$

— Sodium mass in the cold pool: 536 t;

— Sodium mass in the hot pool: 265 t;
— Fuel mass of core: 17 t;
— Graphite mass of core (shielding): 74 t;
— Steel mass of double envelope vessel: 64 t
— Steel mass of main vessel: 65,5 t;
— Steel mass of hydraulic wrappers: 44,5 t;
— Steel mass of conical shell: 21 t;
— Steel mass of strongback: 26 t;
— Steel mass of roof: 73 t;
— Steel mass of primary vessel: 47 t;
— Steel mass of diagrid: 74,6 t;
— Steel mass of core: 241 t;
— Steel mass of control plug: 10 t;
— Steel mass of rotating plug: 27,5 t;
— Steel mass of three primary pumps: 82,5 t;
— Steel mass of four IHX and two DOTE: 115,4 t;
— Steel mass of transfer arm: 6 t;
— Steel mass of handling ramp: 5 t;

Precisions on geometry are given in Fig. 30.

4.4. PRIMARY PUMPS

A scheme of a primary pump is given in Fig. 33.

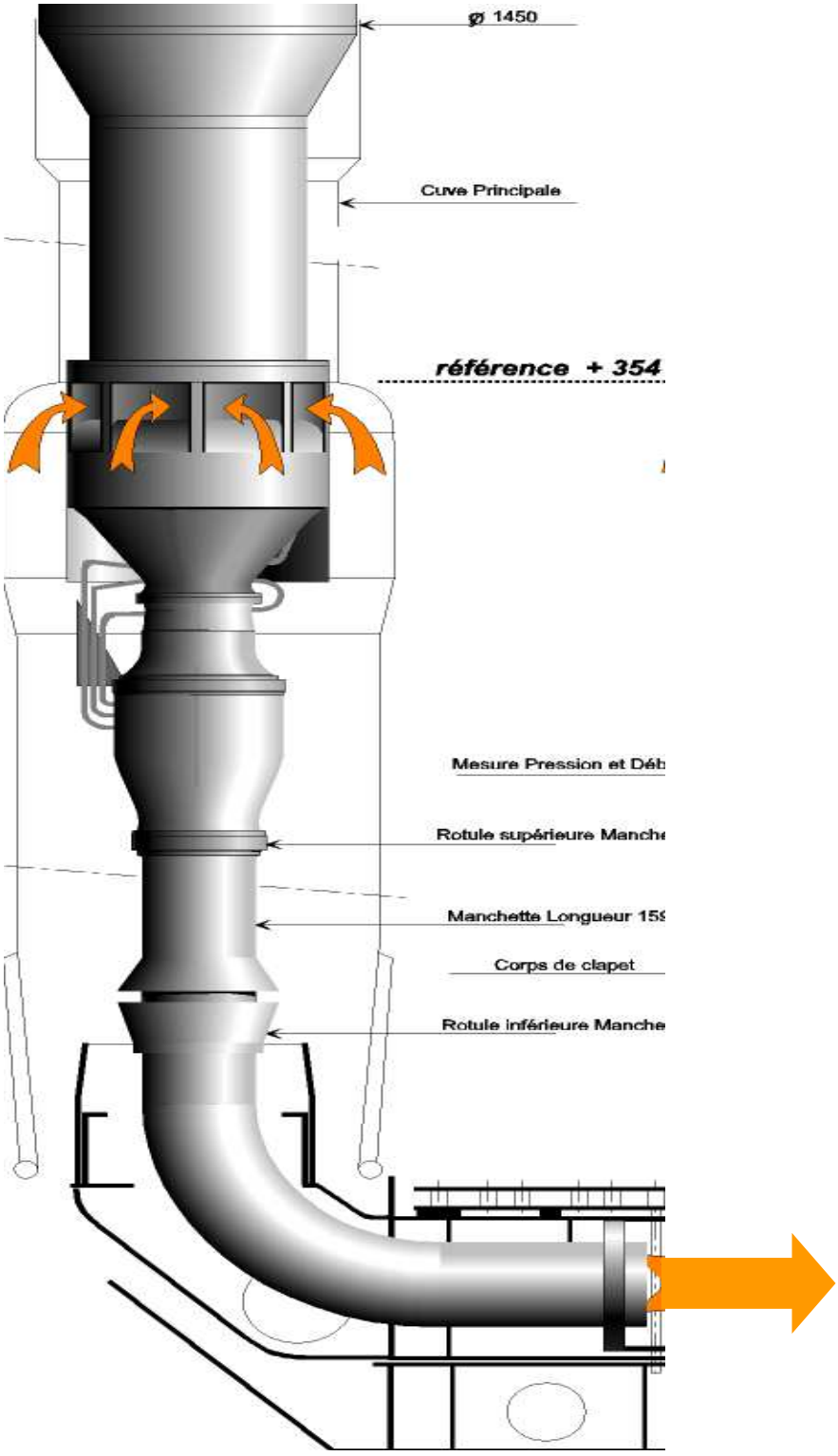

FIG. 33. Phenix reactor – Scheme of primary pump [1].

- Speed of PP: 540 rpm ;
- Back-up motor speed: 100 rpm;
- Rated speed of PP: 800 rpm;
- Rated head of PP: 63,2 m;
- Rated flow of PP: 1,0312 m^3/s;

— Rated torque of PP: 8,795 $m^5/s^{2;}$

— Rated NPSH of PP: 13,25m ;

— Power due to PP in W: $0,00131*(V_{PP})^3$, V_{PP} in rpm;

— Resisting torque of PP in N.m: $100exp(-0,44V_{PP})$, V_{PP} in rad/s;

— Inertia of PP: 765 $kg.m^{2;}$

Further data and characteristics are reported below (Fig. 34, Table 3, Table 4, Table 5). The traditional pump description with homologous representation by octants was used. Such description is often used by system codes. An alternative description (not recommended) is also provided.

Reference data

The values are the following:

– Angular rotation speed: ω_{ref}= 800 rpm ± 1%

– Volumetric flowrate: Q_{ref}= 1,0312 m^3/s ± 5%

– Head: H_{ref}= 62,3 m ± 2%

– Specific hydraulic torque: T_{ref}= 8,795 m^5/s^2 ± 2.5%

Homologous representation

Pump operation can be divided in 8 octants. Data for octants 1 and 2 are available.

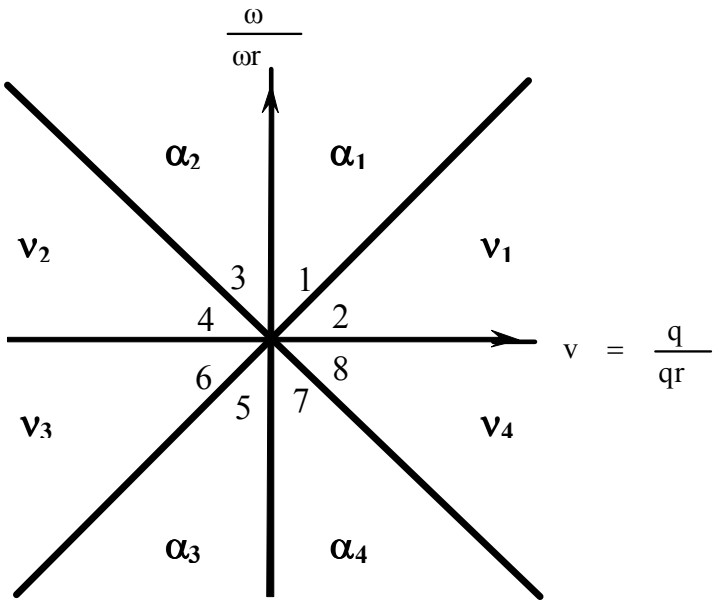

FIG. 34. Quadrants and octants of a pump.

The reduced variables and functions are defined:

— Reduced rotation speed: $\alpha_N=\omega/\omega_{ref}$

— Reduced volumetric flow rate: $\nu=Q/Q_{ref}$

— Reduced head: $h=H/H_{ref}$

— Reduced specific hydraulic torque: $\beta=T/T_{ref}$

TABLE 3. PHENIX DATA PACKAGE - HOMOLOGOUS HEAD AND TORQUE DATA (OCTANT 1)

ν/α_N	0.00	0.08	0.23	0.31	0.48	0.55	0.65	0.73	0.82	0.91	1.00
h/α_N^2	1.33	1.31	1.30	1.30	1.24	1.23	1.20	1.17	1.12	1.06	1.00
β/α_N^2	0.51	0.55	0.64	0.70	0.77	0.81	0.89	0.92	0.96	0.98	1.00

TABLE 4. PHENIX DATA PACKAGE - HOMOLOGOUS HEAD AND TORQUE DATA (OCTANT 2)

α_N/ν	1.00	0.92	0.85	0.79	0.73	0.70	0.64	0.57	0.52	0.43	0.34
h/ν^2	1.00	0.78	0.61	0.47	0.35	0.27	0.17	0.04	-0.06	-0.18	-0.29
β/ν^2	1.00	0.85	0.72	0.62	0.53	0.47	0.38	0.26	0.17	0.04	-0.09

Alternative description

TABLE 5. PHENIX DATA PACKAGE - HEAD AND POWER AT DIFFERENT FLOWS FOR AN ANGULAR SPEED OF 800 RPM

Flow (l/s)	0.	80.0	240.0	320.0	500.0	571.4	674.9	750.0	843.8	937.5	1031.2
Head (m)	82.7	81.9	80.8	80.8	77.3	76.6	74.6	72.7	69.8	66.3	62.3
Power (kW)	320.0	348.7	407.7	440.3	484.5	514.1	562.0	584.1	606.3	621.7	632.2

Flow (l/s)	1125.0	1218.7	1312.5	1406.2	1482.1	1600.0	1800.0	2000.0	2400.0	3000.0
Head (m)	58.0	53.0	47.4	40.7	35.2	25.7	7.7	-12.9	-61.9	-154.6
Power (kW)	638.9	639.5	634.6	624.2	610.0	579.0	506.6	406.8	124.6	-503.9

4.5. INTERMEDIATE HEAT EXCHANGER

The main parameters for the IHX are listed below: A scheme is reported in Fig. 35.

- Total number of tubes: 2279;
- Inner diameter of tubes: 12 mm;
- Outer diameter of tubes: 14 mm ;
- Outer diameter of down comer: 392 mm;
- Inner diameter of outer shell: 1128 mm;
- Outer diameter of outer shell: 1136 mm;
- Outer diameter of central tube: 325 mm;
- Pitch: 20 mm;
- Total heat transfer length: 5365 mm;
- Total heat transfer area: 450 m2 ;

— Size of inlet window: 350 mm;

— Size of outlet window: 598 mm;

— Specific heat of tubes: 562,28 J/(kg °C);

— Density of steel of tubes: 7775 kg/m3.

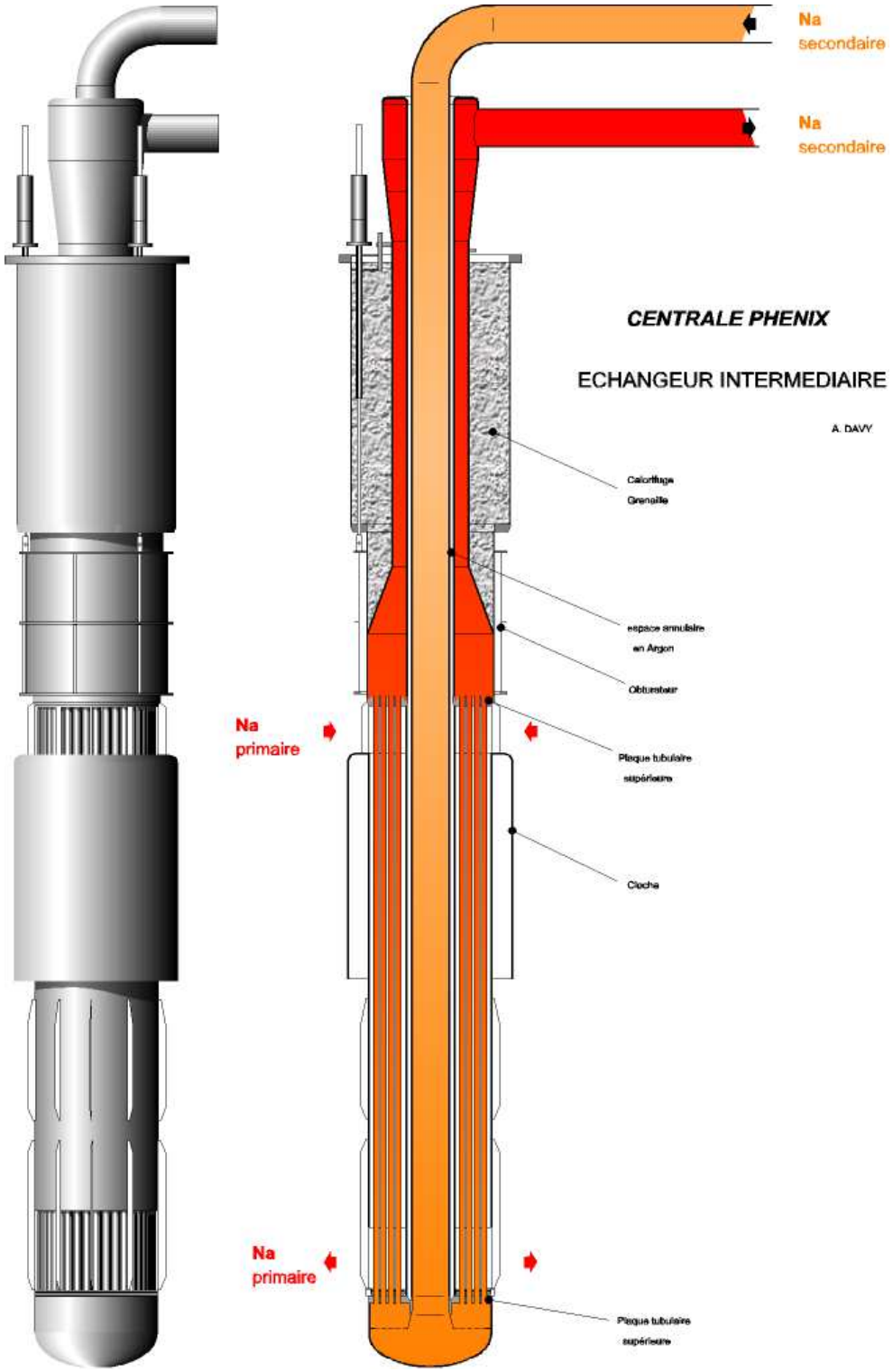

FIG. 35. Phenix reactor – Scheme of IHX [1].

4.6. SHUTDOWN SYSTEMS

The main parameters for the shutdown systems are listed below:

— Number of safety shutdown rods: 1;
— Number of regulating rods: 6;
— Speed of rods during a scram: 1,5 m/s;
— Speed of rods during a fast stop: 1,4 mm/s;
— Whole reactivity of rods: - 8 830 pcm.

4.7. OPERATING CONDITIONS AT NOMINAL POWER

The main parameters for operating conditions at nominal power are listed below:

— Core inlet : 385°C
— Core outlet: 525°C;
— IHX primary inlet: 525°C;
— IHX primary outlet: 385°C;
— IHX secondary inlet: 320°C;
— IHX secondary outlet: 525°C;
— Core flow rate: 1988 kg/s;
— Primary flow rate in IHX: 497 kg/s;
— Secondary flow rate: 690 kg/s;
— Secondary flow rate in IHX: 345 kg/s;
— Speed of primary pumps: 540 rpm;
— Speed of secondary pumps: 700 rpm;
— Level of hot pool: 2061 mm;
— Level of cold pool: 1325 mm;
— Level of vessel cooling flow path: 1540 mm.

4.8. NATURAL CONVECTION TEST CONDITIONS

4.8.1. Initial state at 120 MW(th)

The main parameters for the initial state at 120 MW(th) are listed below:

— Core inlet: 358°C;
— Core outlet: 432°C;
— IHX primary inlet: 432°C;
— IHX primary outlet: 360°C;
— IHX secondary inlet: 308°C;

— IHX secondary outlet: 432°C;
— Core flow rate: 1284 kg/s;
— Flow rate of the fissile zone: 1055 kg/s;
— Flow rate of fertile zone: 149 kg/s;
— Flow rate of steel zone: 41 kg/s;
— Flow rate of control rods: 9 kg/s;
— Flow rate of in-containment fuel storage zone: 30 kg/s;
— Primary flow rate in IHX: 321 kg/s;
— Secondary flow rate: 380 kg/s;
— Secondary flow rate in IHX: 190 kg/s;
— Speed of primary pump: 350 rpm;
— Speed of secondary pump: 390 rpm;
— Level of hot pool: 1876 mm;
— Level of cold pool: 1569 mm;
— Level of vessel cooling flow path: 1652 mm;
— Pressure drop in core SA: 0,839 bar;
— Pressure drop in diagrid: 0,0127 bar;
— Pressure drop in IHX tube bundle: 0,0236 bar;
— Pressure drop between PP and diagrid: 0,0205 bar;
— Pressure drop in PP: 0,8956 bar;
— Pressure drop in reversal for vessel cooling: 0,009 bar.

4.8.2. Test description

See Section 3 for a detailed description of the test.

4.8.3. Data provided for blind calculations

An Excel file was joined with these specifications, containing all useful data for blind calculations:

— Power evolution (MW(th));
— Primary pumps speed (rpm);
— Secondary pumps speed (rpm);
— Secondary inlet temperature for both circuits (°C);
— Secondary flow rate for both circuits (kg/s);

These data are also plotted in the following Figs 36 – 44;

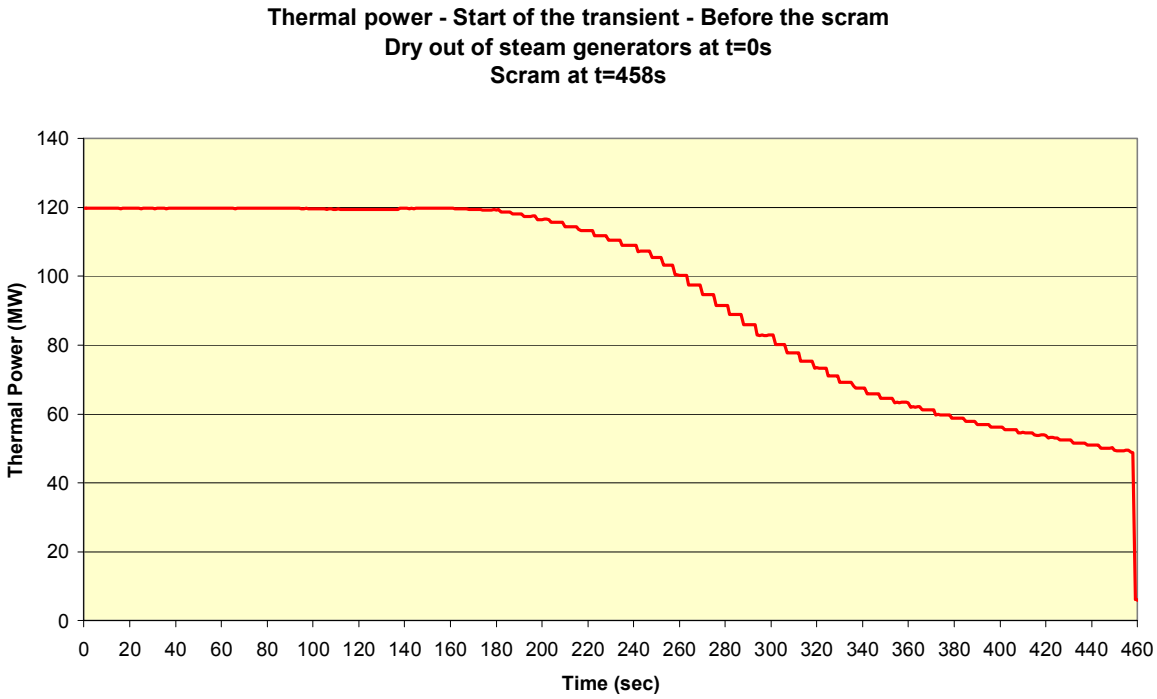

FIG. 36. Data for blind calculations - Core thermal power – beginning of the transient before the scram.

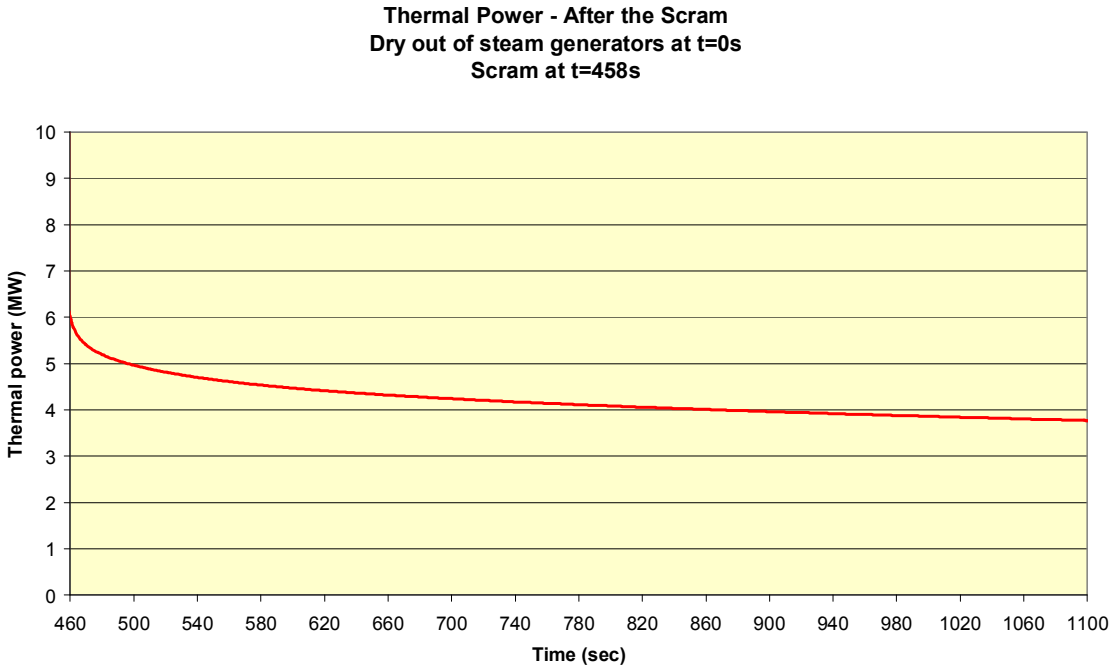

FIG. 37. Data for blind calculations - Core thermal power – after the scram to 1100s.

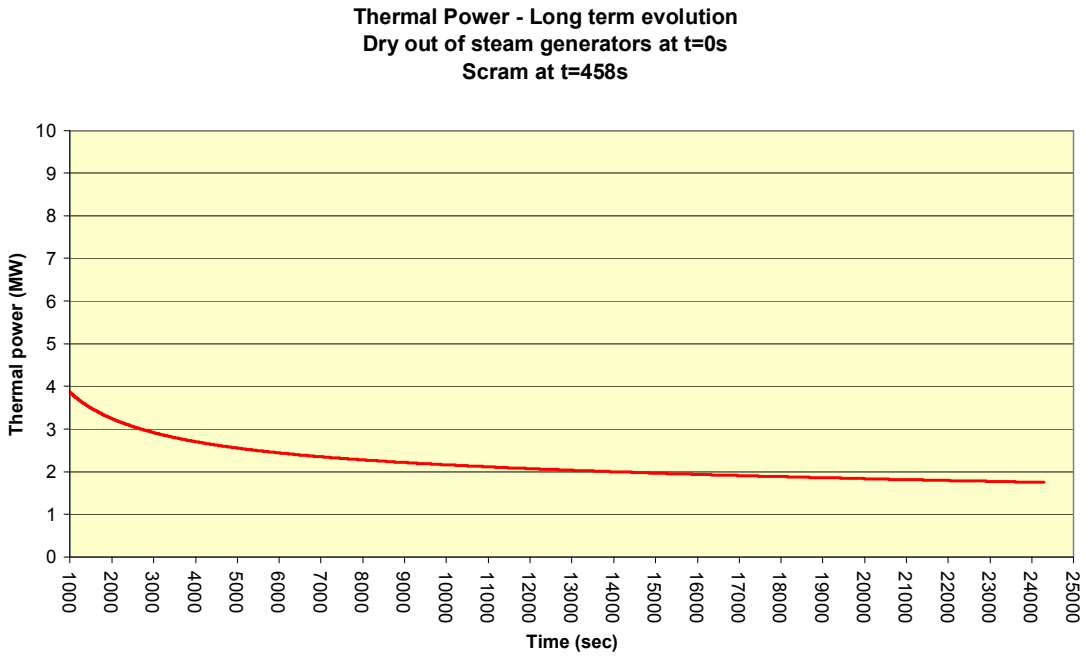

FIG. 38. Data for blind calculations - Core thermal power – after the scram from 1000s to 24000s.

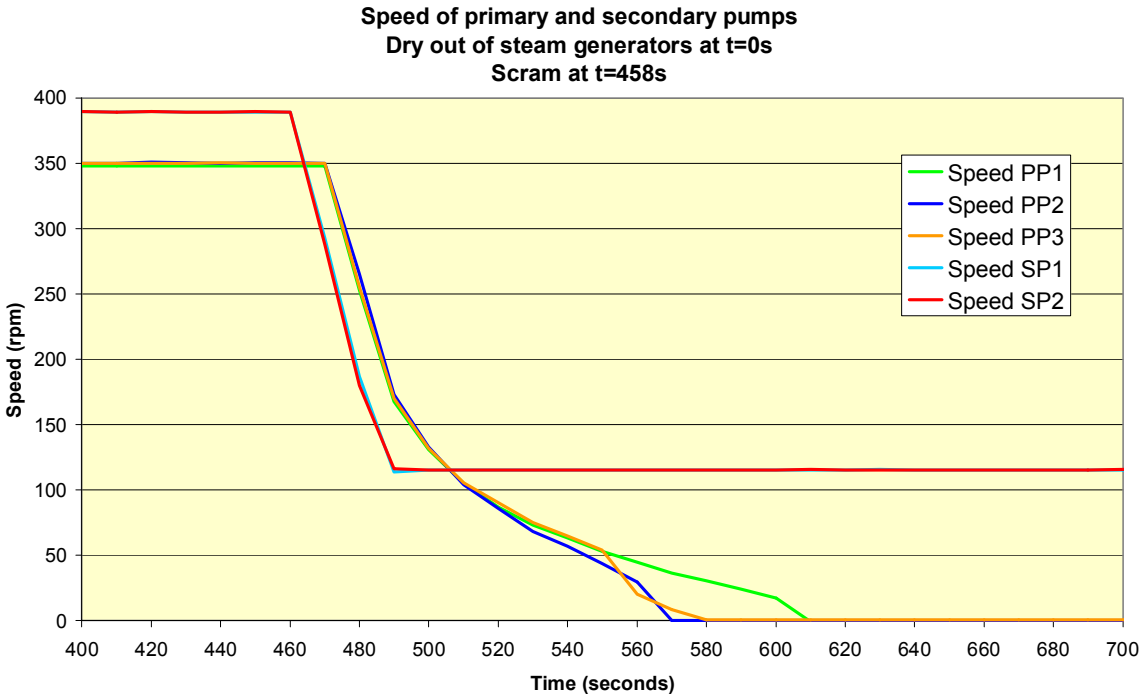

FIG. 39. Data for blind calculations - Primary and secondary pumps speeds – short term.

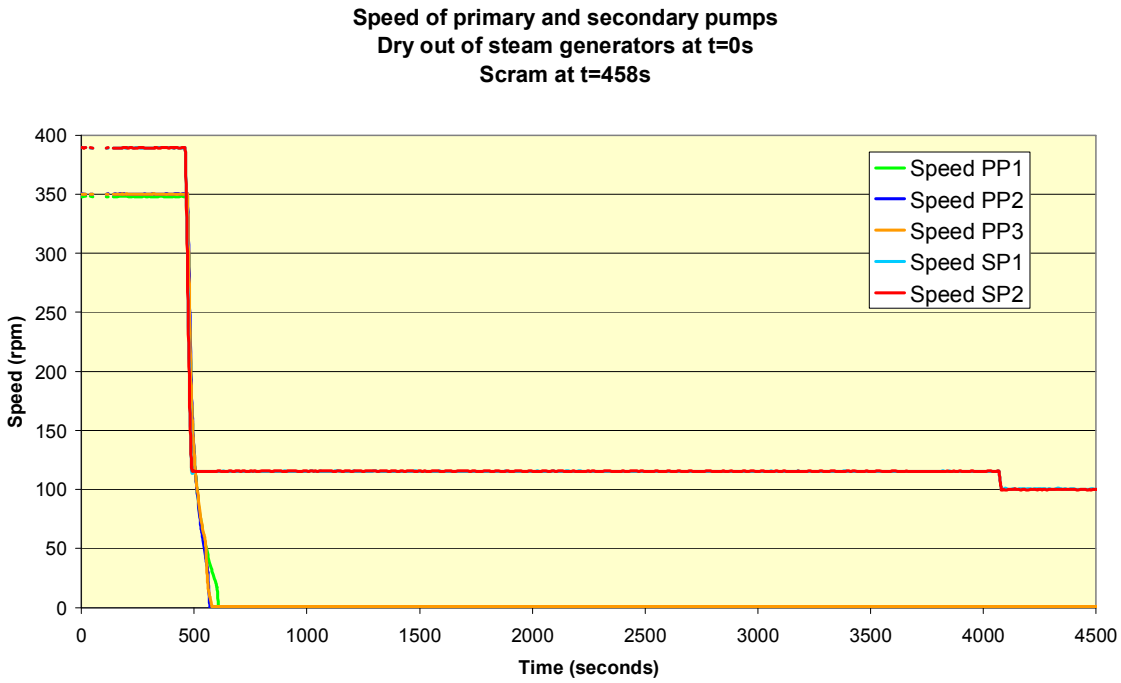

FIG. 40. Data for blind calculations - Primary and secondary pumps speeds – long term.

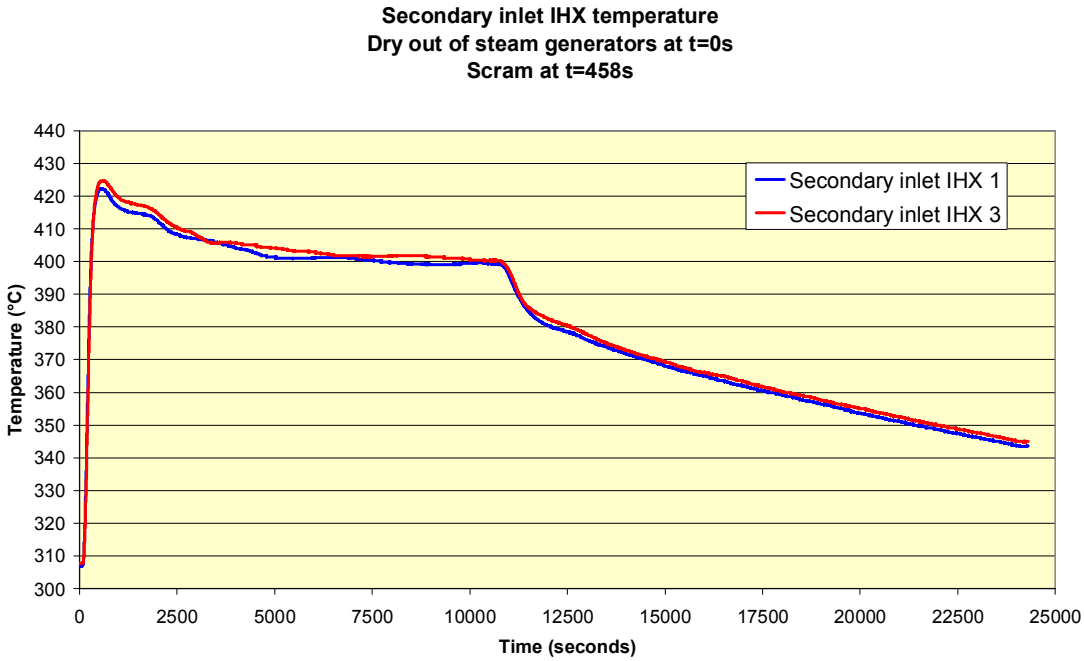

FIG. 41. Data for blind calculations - Secondary inlet IHX temperature.

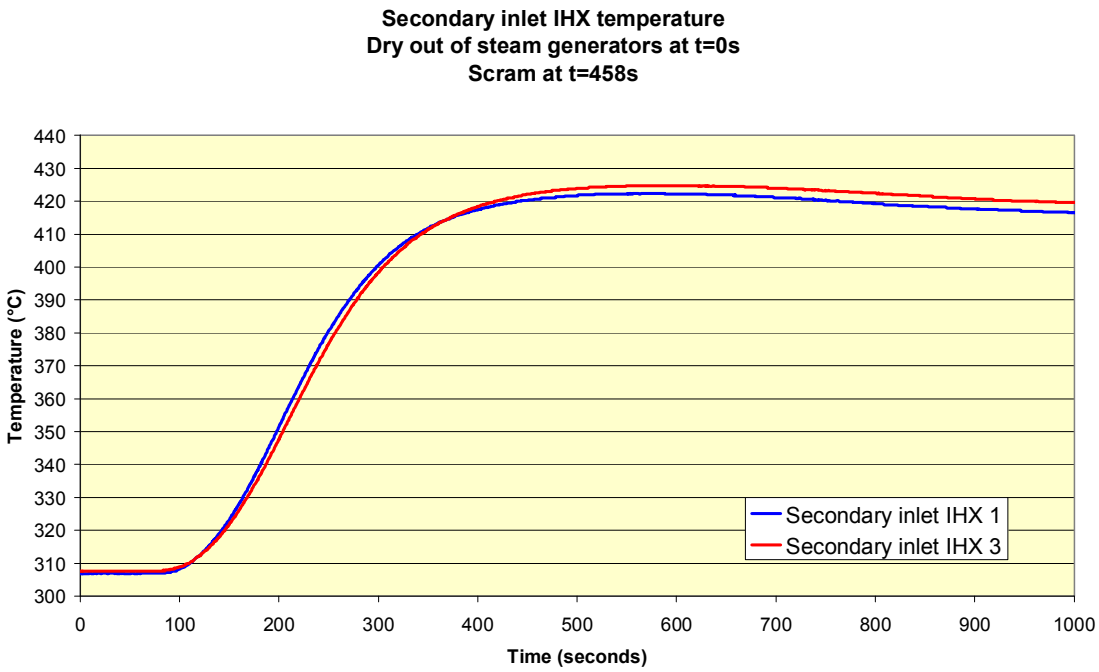

FIG. 42. Data for blind calculations - Secondary inlet IHX temperature after the SG dry-out.

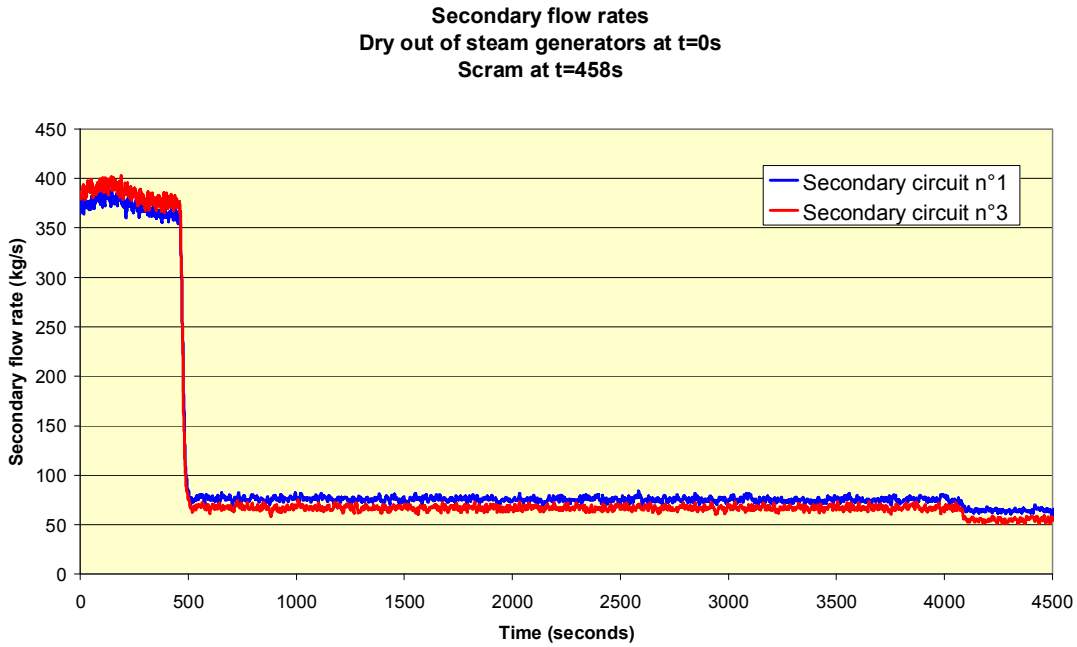

FIG. 43. Data for blind calculations - Secondary flow rates – long term.

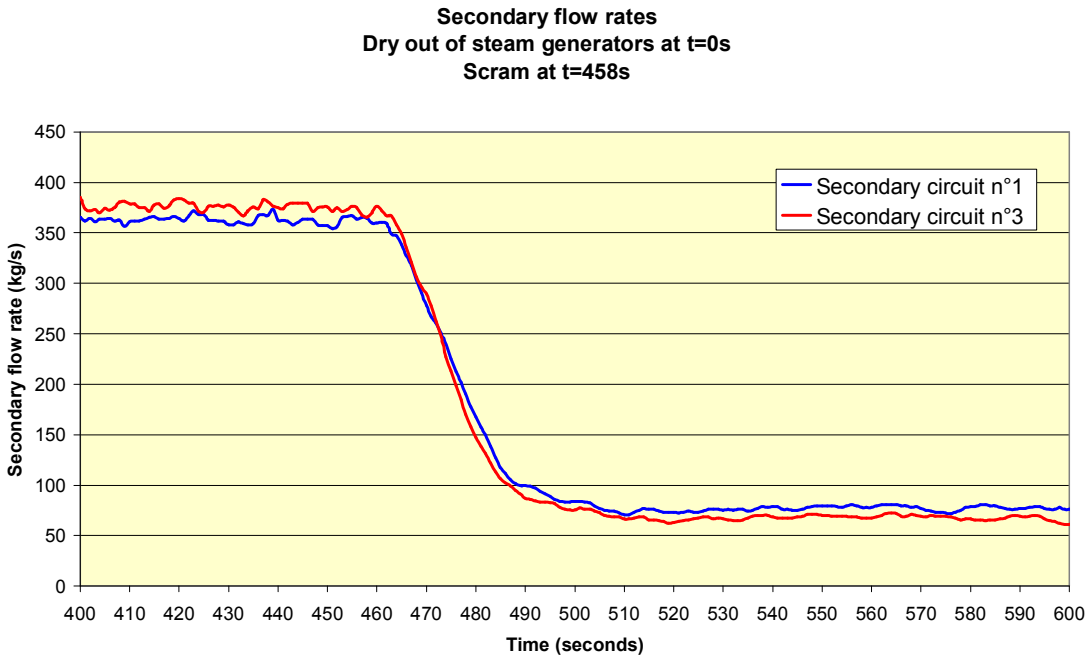

FIG 44. Data for blind calculations - Secondary flow rates after the scram – short term.

5. PARTICIPANTS AND CODES

5.1. PARTICIPANTS: BACKGROUND, HISTORY

5.1.1. ANL

Argonne National Laboratory (ANL) is one of the United States Department of Energy's oldest and largest national laboratories for science and engineering research, and is the lead American institute for fast reactor research and design. Argonne researchers were responsible for designing both the Experimental Breeder Reactor-I, the first nuclear reactor to produce electricity, and the Experimental Breeder Reactor-II, which demonstrated passive safety even under complete loss of flow without scram from full power. Argonne also designed the Transient Reactor Test (TREAT) facility, which performed a variety of transient tests on reactor fuels to test their performance under extreme conditions. Argonne developed the liquid-metal fast reactor safety code SAS4A/SASSYS-1, which predicts the transient response of the reactor system in posited scenarios for anticipated off-normal events, design basis events, and severe accidents. SAS4A/SASSYS-1 analysts currently support industry efforts to design sodium-cooled fast reactors, and participate in international efforts to validate safety codes.

5.1.2. CEA

CEA (Commissariat à l'Energie Atomique et aux Energies Alternatives) is the French state research institute dedicated to nuclear and alternative energies. In this frame, CEA has a long background and history in sodium fast reactor including:

— Reactor design, reactor construction and reactor operation (Rapsodie, Phenix and Superphenix);

— Technology: developments of new technology for sodium applications;

— Safety: analysis of specific safety issues of sodium fast reactor;

— Code development (neutronics, mechanics, thermal-hydraulics) and validation;

— International cooperation with other countries interested in sodium fast reactors.

In the framework of Generation IV, CEA is in charge of the ASTRID project (Advanced Sodium Technological Reactor for Industrial Demonstration), to develop an industrial prototype, which should be in operation around 2020.

CEA is developing ASTRID in cooperation with AREVA and EDF companies.

CEA was responsible of Phenix end of life tests performed in 2009. The natural convection test used for the present IAEA/CRP benchmark is part of these tests.

5.1.3. IGCAR

Indira Gandhi Centre for Atomic Research (IGCAR), the second largest establishment of the Department of Atomic Energy in India, was setup in 1971 with the main objective of conducting broad based multidisciplinary programmed of scientific research and advanced Engineering, directed towards the development of sodium cooled fast breeder reactor (FBR) technology, in India. Towards meeting the objectives, the sodium cooled Fast Breeder Test Reactor (FBTR), with a nominal power of 40 MW(th), has been built in 1985 and is presently in operation. The centre has designed the 500 MW(e) Prototype Fast Breeder Reactor (PFBR) which is presently in an advanced stage of construction. In the area of fast reactor safety, the centre has developed 1-D plant dynamics codes

(DYANA-P and DHDYN) to study the plant behaviour under various design basis events and also developed CFD codes (THYC-2D and THYC-3D) to study multi-dimensional effects in local areas of interest. Presently the centre is concentrating on new designs for future fast reactors. The centre also participates in various IAEA collaborative projects and shares its knowledge with researchers working in the similar areas.

5.1.4. IPPE

The State Scientific Center of the Russian Federation – the Institute of Physics and Power Engineering (SSC RF IPPE) is a leading research center involved in the development of the reactors for diversified nuclear power systems (NPS). A considerable number of NPS`s have been created under the scientific supervision of the IPPE ranging from the World`s First Nuclear Power Plant (Obninsk) and the Bilibino thermal neutron cogeneration plant to fast neutron power reactors BN-350 (Aktau) and BN-600 (Beloyarsk), to lead-bismuth cooled reactors for nuclear-powered submarines, to BOUK and TOPAZ space nuclear reactors.

The Institute carries out fundamental and applied research in the area of nuclear and reactor physics, reactor core and shielding physics of low temperature and recombination-non-equilibrium plasma, lasers physics, solid state physics, radiation material science, physical chemistry of coolants, thermal physics, and hydrodynamics of nuclear power facilities. There are skilled staff and up-to-date experimental facilities to conduct these studies.

The IPPE is the initiator and scientific leader in the development of:

— Sodium cooled fast neutron reactors;

— Lead-bismuth cooled reactor designed for marine and ground nuclear power installations;

— High temperature small-size alkali metal cooled reactors with direct power conversion for space application.

All these developments have been already implemented and are considered to be very promising.

5.1.5. IRSN

The Institute for Radiological Protection and Nuclear Safety (IRSN) is the technical support to French public authorities. As such, IRSN is in charge of safety assessment of operating and under construction reactors, as well as future projects. SFR is the reference Generation IV concept for France and a prototype is scheduled around 2020 (ASTRID). After the shutdown of Superphénix in 1998, there was a strong reduction of R&D efforts related to safety issues of sodium reactors. In this context, IRSN develops new skills in order to be able to assess the design studies that will be performed in the framework of the safety demonstration. IRSN especially focuses on numerical tools, with the objective of assessing their ability to predict the behavior of the reactor in normal and accidental conditions.

5.1.6. University of Fukui

University of Fukui is one of the national universities in Japan. The graduate school of Nuclear Engineering has been established in 2004. In April 2009, the Research Institute of the Nuclear Engineering has been newly established in order to emphasize the research in the core of the nuclear engineering. Professors in the institute cover the following fields:

— Fast reactor engineering;

— Advanced reactor engineering;

— Fuel and material engineering;

— Medical physics and chemistry.

The most active field is the Fast Reactor Engineering in the area of neutronics, thermal-hydraulics, structure analysis, and plant system. In order to carry forward the development of the fast reactor system, most professors in the institute are participating the project, i.e., 'R&D Core Program for Practical Realization of Fast Breeder Reactor by using MONJU' entrusted to University of Fukui by the Ministry of Education, Culture, Sports, Science and Technology of Japan (MEXT). After the severe accidents at the Fukushima-daiichi NPP site, we are going to focus on the study of the accident management.

5.1.7. KAERI

Korea Atomic Energy Research Institute (KAERI) is the sole national laboratory specializing in nuclear related research in the Republic of Korea. Since its establishment in 1959, KAERI has made significant contributions to the nation's nuclear technology development and has been developing LMR design technologies with the goal of competitive economics and enhanced safety. With the development of LMR designs, computer codes are being developed and basic sodium thermal hydraulics experiments are being performed as well. Recently, the KAERI is concentrating on the development of advanced SFR design technologies to fulfil the national goal of the construction of demonstration SFR by 2028, which has been approved by the Atomic Energy Commission (AEC) of the Republic of Korea.

5.1.8. PSI

The Paul Scherrer Institute, PSI, is the largest research centre for natural and engineering sciences within Switzerland. The three main research areas are Matter and Material; Energy and the Environment; and Human Health. The FAST (Fast-spectrum Advanced Systems for Power Production and Resource ManagemenT) project is an activity performed in the Laboratory for Reactor Physics and Systems Behaviour in the area of fast-spectrum reactor behaviour with an emphasis on the comparative analysis of Generation IV systems. We are building a centre of competence in carefully chosen research areas to conduct studies within international frameworks aimed at safety enhancement of the fast-spectrum systems considered for construction in Europe. In more specific terms, the goal of the project is to develop and maintain the ability to provide expert analysis in the three main areas, namely neutronics, thermal hydraulics and fuel behaviour, with the use of the three main measures, namely: use of a unique computational tool, integration into international programs, and organization of an efficient team, for the three Gen-IV fast-spectrum reactor systems, namely sodium-, gas- and lead-cooled reactors.

One of the main objectives of the project is to build and maintain a code system for neutronic, thermal-hydraulic and mechanic analysis of the static and dynamic behaviour of the fast-spectrum cores, and the whole reactor systems, for different coolants, fuel types, cooling system designs, etc . A code system of this complexity is particularly important in the context of transmutation and safety related studies aimed at establishing and comparing the basic parameters of the Generation IV fast reactors. This code system allows us to systematically analyse:

— Multi-batch equilibrium cycle;

— Fuel base-irradiation behaviour;

— A wide variety of transients.

One of the important R&D directions of the project is validation of our code system. In this context, we participate in the two IAEA CRPs on analysing the selected PHENIX-EOL tests.

5.2. BRIEF DESCRIPTION OF CODES

5.2.1. Brief description of the SAS4A/SASSYS-1 code (ANL)

The SAS4A/SASSYS-1 code was developed at Argonne to perform safety analysis for liquid-metal cooled reactors. SAS4A/SASSYS-1 contains extensive modelling capabilities that represent several hundred person-years of code development effort supported by experimental validation [3]. These capabilities include:

- Multiple channel and subchannel modelling of core thermal-hydraulics;
- Point kinetics and spatial kinetics capabilities including decay heat and reactivity feedback models for fuel Doppler; fuel, cladding, and coolant density variations; coolant voiding; core radial expansion; control-rod driveline expansion; and primary vessel expansion;
- Detailed mechanistic models for oxide fuel and cladding that characterize porosity migration, grain growth, fission gas release, fuel cracking with crack healing, fission-gas-induced swelling, irradiation-induced steel swelling, gas plenum pressurization, fuel-cladding gap conductance changes, fuel and cladding mechanical behaviour, thermal expansion, and cladding failure;
- Detailed models of metallic fuel cladding transient behaviour, metal fuel pre-transient thermophysical properties characterization, and pre-failure transient behaviour models for fuel element mechanics, central cavity formation, extrusion, fission-gas-induced swelling, plastic flow, fuel-cladding eutectic formation, and fuel element failure detection;
- Two-phase coolant thermal hydraulics model to characterize low-pressure sodium boiling with the ability to track the formation and collapse of multiple bubbles and the ejection of liquid slugs from coolant channels;
- Intra-pin oxide fuel melting and relocation; cladding failure; molten cladding dynamics including melting, relocation, and freezing; fuel-coolant interactions in flooded channels including fission gas release, cladding perforation, molten fuel flow, and fuel freezing and plating; and fuel, fission gas, cladding, and coolant vapour dynamics in voided coolant channels;
- Primary and intermediate loop reactor coolant systems models for compressible volumes (with or without cover gas), pipes, intermediate heat exchangers, centrifugal pumps, electromagnetic pumps, valves, bypass channels, annular flow elements, reactor vessel auxiliary cooling systems (RVACS), air-dump heat exchangers, and steam generators;
- Balance of plant thermal hydraulics modelling capabilities including component models for deaerators, steam drums, condensers, reheaters, turbines, and several other components.
- Reactor control system models that are driven by user-defined mathematical operators controlled by simulation variables.

SAS4A/SASSYS-1 version 3 has been exported to domestic industrial partners and to research organizations in foreign countries. The SAS4A/SASSYS-1 code package continues to undergo development in response to advanced fast reactor simulation needs.

5.2.2. Brief description of the CATHARE code and specific model for SFR calculations (CEA and IRSN)

The system code CATHARE has been developed and validated in collaboration between CEA, EDF (electricity supplier), IRSN (French safety authority), and AREVA-NP (plant manufacturer) for the French Pressurized Water Reactors. The CATHARE code is the reference code in France for the PWR safety analysis. It has also been used for other light water reactor concepts (VVER, BWR, RBMK) and for experimental reactors applications.

It is a 6-equations code for two-phase flows (2 equations of mass balance, 2 equations of energy balance and 2 equations of momentum balance).The main variables are the pressure, the liquid and gas enthalpies, the liquid and gas velocities, the void fraction (and possibly mass fraction of incondensable gases). The aim of the code is to represent mechanical non-equilibrium and thermal non-equilibrium, at all flow regimes and all heat transfer regimes within the range of design and safety analysis. The code uses an oriented-object structure permitting the representation of any kind of hydraulic circuit, from the analytical experimental facilities to the whole reactor power plant. There are five main modules, with specific correlations and closure laws (1D: axial; 0D: volume, THREED or 3D: PWR reactor vessel, BC: boundary condition and RG: double ended break). The code numerical scheme is fully implicit (1D and 0D) or semi-implicit (3D), with an implicit thermal coupling between the walls and the fluid. The non-linear system is solved by a Newton-Raphson iterative method.

In the Generation IV framework, the standard version of the code (CATHARE_2v2.5_2) has already integrated new developments in order to calculate gas cooled reactors and super critical light water reactors. The development of CATHARE code for sodium-cooled reactors has followed this trend [4].

The main developments in CATHARE code to address sodium cooled reactor calculations deal with:

— Sodium fluid properties (the thermodynamic and transport properties of liquid and vapour are issued from former CEA system codes);

— Specific heat exchange correlations (Skupinski and Boriihanski heat exchange correlations);

— Specific friction loss coefficient in the fuel pins zone (Pontier's law);

— Update of the neutronics points kinetics model taking into account neutronics feedback effects due to diagrid expansion, wrapper axial and radial expansion, fuel clad axial and radial expansion Specific electro-magnetic pump models.

The CATHARE code is ready for use for sodium cooled reactor calculations and new concept evaluations. CATHARE is the thermal hydraulics system code used in the frame of the ASTRID project, the Generation IV French prototype project. Its validation for these applications is underway [5], [6].

5.2.3. Brief description of the STAR-CD and DYANA-P system codes (IGCAR)

STAR-CD is a commercial CFD code which solves the governing differential equations of flow physics by numerical means on a computational mesh [7]. It has the capability of solving steady, transient, laminar, turbulent, compressible, incompressible flow phenomena along with heat transfer (convection, conduction and radiation) even in porous medium. It has in-built pre-processor and post processor known as PROSTAR. It has the basic mesh generation capability. Complex mesh can be imported from any standard mesh generating tools. User defined program modules can be added to the code to modify the material properties as well as pressure drop and heat transfer characteristics dynamically during transient. The code has been validated extensively against bench-mark data.

DYANA-P is a system dynamics code developed by IGCAR for performing plant dynamics studies for pool type fast breeder reactor systems [8]. This is the design tool used for the safety analysis of Prototype Fast Breeder Reactor (PFBR). DYANA-P has models for reactor core, primary sodium circuit, secondary circuit, sodium pumps, heat exchangers and sodium pools. Steam water system is not modelled in the code. However, steam generator is modelled with appropriate boundary conditions for the water side.

Mathematical models in the DYANA-P code are based on those used for most of the fast reactors. Thermal models are based on heat balance between various sections exchanging the heat such as fuel and sodium through the clad in SA, primary sodium and secondary sodium through the tube wall in IHX, sodium and ambient air through the pipe wall and insulation in sodium piping, secondary sodium and water through the tube wall in steam generators (SG) etc. Hydraulic model is based on

momentum balance between various flow segments in the primary and secondary sodium circuits. Torque balance is adopted for the modelling of pump with the characteristics derived from generalized homologous characteristics. Fluid levels in the tanks are modeled through dynamic mass balance. Neutronic model for the core is based on point kinetics approximation. Transient solution is obtained by prompt jump approximation. Detailed models are also incorporated for the calculation of various reactivity feed back effects due to radial expansion of grid plate where SA are supported, control rod expansion, volumetric expansion of sodium inside the fuel and blanket portion of core, axial clad steel expansion, axial fuel expansion, Doppler effect due to changes in fuel temperature. Major assumptions made in the mathematical models of the various reactor and heat transport components are:

— Liquid sodium flow is assumed to be incompressible and single phase throughout.

— Flow of sodium is treated as one dimensional through the pipe lines, fuel rod bundles, heat exchanger tubes etc.

— In all the places where mixing and recirculating flow patterns exist, a perfect mixing assumption is made for the thermal model and incoming kinetic energy head due to flow is assumed to be fully converted into static pressure head for hydraulic calculation.

— Axial conduction heat transfer in coolant pipe material, heat exchanger tubes and fuel pin, clad walls are neglected in comparison to radial heat transfer.

Initial steady state conditions are calculated in the code through the solution of steady state balance equations. For the transient solution, numerical integration of hydraulic models is obtained by utilizing a standard ordinary differential equation solver based on the Hamming's Predictor-Corrector method. Semi-implicit formulation has been adopted for the integration of thermal balance equations. A similar methodology is adopted in the formulation of computer codes such as DYNAM and SIFDYN developed for performing the dynamic calculations in Fast Breeder Test Reactor (FBTR). These codes have been validated through various tests carried out in Fast Breeder Test Reactor.

5.2.4. Brief description of GRIF code and modeling approach for Phenix reactor

GRIF is Russian computational tool for single-phase thermal hydraulics analysis of the transients in the reactor as a whole and in its parts [9]. The code can characterized as a system code with extended capabilities for the simulation of spatial distributions of most important parameters in reactor bulk volumes and in structural elements. One of important objectives of the GRIF code is the simulation of long-term processes in the reactor including the secondary and auxiliary circuits *(decay heat removal problem and etc.)*.

The code includes in itself the following modules:

— 3D thermal hydraulic model for calculation of sodium velocity, pressure and temperature in the primary circuit;

— 3D model for simulation of inter-wrapper sodium thermal hydraulics;

— Primary pump model (analytical correlation);

— Module «Wrapper» for calculation of temperature distributions in the SA wrappers;

— Module «IHX» for simulation of flow and temperature in the IHXs;

— Module «DHX» for simulation of flow and temperature in the DHXs *(module is not activated in Phenix test simulation)*;

— Module «PIN» consists of the set of Option of 1D-3D models that optionally can be used for calculation of temperature in fuel pins, absorber pins, shielding elements simulation and etc;

— Module «REACTIVITY», analytical correlations with recalculated reactivity coefficients *(module is not activated in Phenix test simulation);*

— Module «KINETICS» 'Point' kinetics with 6 groups of delayed neutrons *(module is not activated in Phenix test simulation).*

For simulation of heat and mass transfer in the reactor the set of 3D heat and mass transfer equations in approximation by the model of viscous non-compressible liquid flowing in the porous body is solving in GRIF code. Non-isothermal conditions effect is taking into account using Business approximation.

Porosity of the coolant medium is varies spatially and the porous medium resistance coefficients may depend on flow parameters. The thermal hydraulic properties - effective kinematics viscosity, coolant density and specific heat capacity are the functions of sodium temperature. Effective conductivity coefficients of porous medium can be different for different directions.

The similar set of equations is solved for simulation of sodium behavior in the inter-wrapper space, the only difference being that mass and heat flux sources in the equations have opposite signs. Mass source value is different from zero only on the outer circuit of sub-area modeling reactor core, since two sodium flows (the main flow in the subassemblies and that in inter wrapper space) are sewed together only on the boundaries. Heat transfer between these sodium flows occurs in the entire core volume.

The above two sets of equations have been solved numerically, and the solutions are sewed together explisitly by iteration method.

5.2.5. Brief description of NETFLOW++ code (University of Fukui)

The system analysis 1D code NETFLOW++ has been developed by Mochizuki [10], [11]. The code can calculate single-phase and two-phase flows of water. One-dimensional flow with no compressibility is assumed in the single-phase flows of water or liquid sodium. Piping is divided into some segments called main links by main joints. The main link can be divided into smaller segments called sub-links by sub-joints. When the sub-joint is provided, one can change diameter of piping between sub-links. The main joint can connect several main links, but sub-joint cannot. Other than these joints, two kinds of joints for setting pressure boundary conditions and flow rates are prepared. Simultaneous mixing is assumed at the joint.

The one-dimensional momentum and continuity equations are applied to the flow segment together with the energy equation. In the temperature calculation of piping and heat transfer tubes of a heat exchanger, the material is divided into inside and outside at a half thickness in order to have symmetrical equations for both sides. Temperature is calculated based on the heat transfer between fluid and pipe wall, and also pipe wall to environment or the flow outside the heat transfer tube. Heat transfer coefficient is given to the code as a function of the Reynolds number and the Prandtl number. Several types of heat exchangers are modelled, e.g. a usual shell-and-tube type, a shell-and-tube type with boundary conditions on one side, an air cooler with finned heat transfer tubes, and steam generators. In the case of a steam generator, a heat transfer coefficient for a helically coiled heat transfer tube is prepared other than a straight type. When a pump is provided on the sublink, pressure increase occurs. The pump characteristic is expressed as a Q-H curve, and the pressure head is approximated as a function of quadratic volumetric flow rate. In the pump characteristics evaluation for steady state and transients such as pump start-up and coast-down, the kinetic equation with pump efficiency is solved. In regard to a valve, two kinds of inputs are prepared. One is a time table of local loss coefficients. The other one is a combination of a valve characteristic Cv as a function of throttling and a time table of the valve throttling. A check valve characteristic is also modelled.

Models in the code are verified using test results of mock-ups of a boiling water reactor. Thermal-hydraulics and neutronics of the coupled system of the core, heat transport systems and the turbine system can be calculated by this code. The models in the code have been developed further in order to

simulate some characteristics specific to liquid metal cooled fast reactors. These are the model of inter-subassembly heat transfer that becomes obvious under the natural circulation condition, the heat transfer and heat transfer models for air cooler, the heat transfer model for IHX, the model of the upper plenum, etc…The code have been validated using the sodium-cooled experimental fast reactor 'Joyo' and the prototype fast breeder reactor 'Monju, i.e., the natural circulation test with Mark-II core of 'Joyo', the intentional scram test at 'Joyo' with Mark-III core, the natural circulation test in 'Monju' using pump heat input and the turbine trip test at 'Monju'. One of the characteristics of the code is fast running using PC. A one week event of 3-loop 'Monju' can be calculated within 30 minutes. This code is used for the education of students in the University of Fukui.

5.2.6. Brief description of MARS-LMR code (KAERI)

The MARS-LMR code has been developed by the KAERI for the design and analysis of a liquid-metal cooled system based on the MARS (Multi-dimensional Analysis for Reactor Safety), which has been widely used for the analysis of transients of water cooled reactor systems in the Republic of Korea.

MARS is an multi-D, transient, two-fluid, 6-equation model for flow of a two-phase steam-water mixture that can contain non-condensable components in the steam phase and/or a soluble component in the water phase. The two-fluid equations are formulated in terms of volume and time-averaged parameters of the flow. The primary variables are the single pressure, two phase internal energies, and the void fraction at the scalar control volume and two phase velocities at the momentum control volume. The code employs semi-implicit numerical scheme to solve a non-equilibrium and non-homogeneous thermal hydraulic problem. The heat structure can be coupled either implicitly or explicitly with the fluid and the code contains the point kinetic module.

The code continued to evolve by adding new features such as multi-dimensional module, CANDU specific models, HTGR specific models, and LMR models. In the Gen-IV framework, to extend the applicability of the code to the analysis of transients for a sodium-cooled fast reactor system, it is required to reinforce some models which represent the inherent characteristics of liquid sodium cooled fast reactors. First, liquid sodium has quite different characteristics from water. Therefore, it is necessary to add several new models, such as, a liquid metal coolant property table, wall heat transfer coefficients related to liquid metal, and the friction factor correlations associated with wire spacers of fuel rod were implemented to the code. The material properties tables are implemented using the equation of state (EOS) based on the semi-empirical soft-sphere model. Other dynamic properties such as viscosity, conductivity and surface tension are provided by the relevant correlations. For a description of the pressure drop in a wire-wrapped rod bundle the correlation by S.C. Cheng and N. E. Todreas has been implemented in the MARS-LMR code. The heat transfer by a liquid metal flow in nuclear fuel bundles is described by the modified Schad's correlation. For the liquid metal heat transfer in a heat exchanger tube the correlation by Aoki is selected and it is found that the Graber-Rieger model is best for a shell side heat transfer

5.2.7 Brief description of TRACE code (PSI)

TRACE [14] is a thermal-hydraulics code developed by the U.S. Nuclear Regulatory Commission (NRC). Formerly called TRAC-M, TRAC/RELAP Advanced Computation Engine is the latest in a series of advanced, best-estimate reactor system codes. It combines the capabilities of the NRC's four main systems codes (TRAC-P, TRAC-B, RELAP5 and RAMONA) into a single modernized computational tool. TRACE has been originally designed to perform best-estimate analyses of loss-of-coolant accidents (LOCAs), operational transients, and other accident scenarios in PWRs and BWRs. Also, its versatility allows one to model a wide variety of thermal-hydraulics experiments in reduced-scale facilities. Models used include multidimensional two-phase flow, non-equilibrium thermodynamics, generalized heat transfer, reflood, level tracking, and reactor kinetics. The programming language is standard Fortran 90.

The partial differential equations that describe two-phase flow and heat transfer are solved using finite-volume numerical methods. The heat transfer equations are evaluated using a semi-implicit time-differencing technique. The fluid-dynamic equations in the spatial 1D, 2D and 3D components use a multistep procedure (SETS numerics). The finite-difference equations for hydrodynamic phenomena form a system of coupled, nonlinear equations that are solved by the Newton-Raphson iteration method. The resulting linearized equations are solved by direct matrix inversion.

The modeling of a reactor system is based on a component approach. Each physical piece of equipment in a flow loop can be represented as some type of component, and each component can be further nodalized into some number of physical volumes (cells) over which the fluid, conduction, and kinetics equations are averaged. The number of reactor components in a problem and the manner in which they are coupled, are arbitrary. The only limit on the problem size is the amount of computer memory. The hydraulic components available in TRACE for the reactor description include, among others, PIPEs (1D), VESSELs (3D), PLENUMs (0D), PUMPs, VALVEs and TEEs. The fuel elements and heated walls in the reactor system can be modeled with HTSTRs (heat structures), that compute 2D conduction and surface-convection heat transfer in X-Y or R-Z geometries. The energy delivered to the fluid via the HTSTRs is specified in the POWER components. The power generation in the reactor core can be specified in different ways: either constant or via a time-dependent table, calculated from the point-reactor kinetics with reactivity feedbacks, or calculated from 3D kinetics (when TRACE is used in coupled mode with PARCS that provides the reactor power and power distribution at each time-step). The boundary conditions in the hydraulic components are applied from the FILL and BREAK components, used to apply the desired coolant-flow and pressure boundary conditions, respectively.

The TRACE code is currently being extended at PSI to sodium two-phase flow models in order to allow the simulation of boiling event in SFRs. Extensive validation of the implemented model has been performed on the basis of past out-of-pile experiments [15], [16]. The analysis of the Phenix NC test constitutes a step towards the further validation of the TRACE code for SFR transient simulation.

5.3. BRIEF DESCRIPTION OF CODE MODEL FOR PHENIX

5.3.1. Brief description of the SAS4A/SASSYS-1 model for Phenix (ANL)

The SAS4A/SASSYS-1 model of the core features separate channel models for each of the five flow zones in the core. The channel geometry in the fuel pin section is taken from the detailed specifications in the CRP package. In the reflector regions above and below the fuel pin section, some reasonable estimates were made for the geometric parameters based on schematics and the specifications for the total steel and sodium mass.

A schematic of the primary and secondary coolant systems model is provided in Fig. 45, with detailed descriptions of the components provided in table 6 and table 7. Flow enters the core from the inlet plenum in the diagrid (CV_1), is heated in the core and enters the hot pool (CV_2). Because of the difference in sodium elevation in the hot and cold pools, the hot sodium is driven into the shell side of the intermediate heat exchanger (E_2) and cooled sodium returns to the cold pool (CV_4). The cold pool is divided into two parts: The upper volume (CV_3) contains the cover gas and is considered to have an annular shape, and the lower volume (CV_4) contains most of the sodium mass. A special flow segment (S_4) represents the flow between these to volumes inside the cold pool. In normal operating conditions, the primary pump (E_4) forces sodium to return from the cold pool to the inlet plenum.

The boundary conditions specified in the CRP include tabulations of the time-dependent evolutions of power, primary pump speed, secondary-side flow rate, and secondary-side temperature. In most cases, these tables were provided as input to SAS4A/SASSYS-1. However, there are strict limits on the size of these tables in the input deck, for instance the power evolution can contain no more than 20 points in time. Therefore, 20 points (out of several thousand in the specification) were carefully selected to

represent the transient. Because the power evolution was specified, there is no need to employ the point kinetics or the decay heat model.

By default, compressible volumes in SAS4A/SASSYS-1 employ a perfect mixing model to determine the temperature. Thus there is only one temperature value to represent the entire volume. In the case of the hot pool in particular, this is an inadequate representation because it ignores the effect of thermal stratification during low flow conditions when estimating the primary-side IHX inlet temperature. The thermal stratification model was employed for the hot pool, which provides three temperature layers to represent mixing. In this way, the model has some capability to distinguish between the mean pool temperature and IHX inlet temperature. Moreover, it provides a better representation of the natural circulation head. The maximum error in the data reduction was estimated to be 4% for the power data and 7°C for the steam generator temperature data.

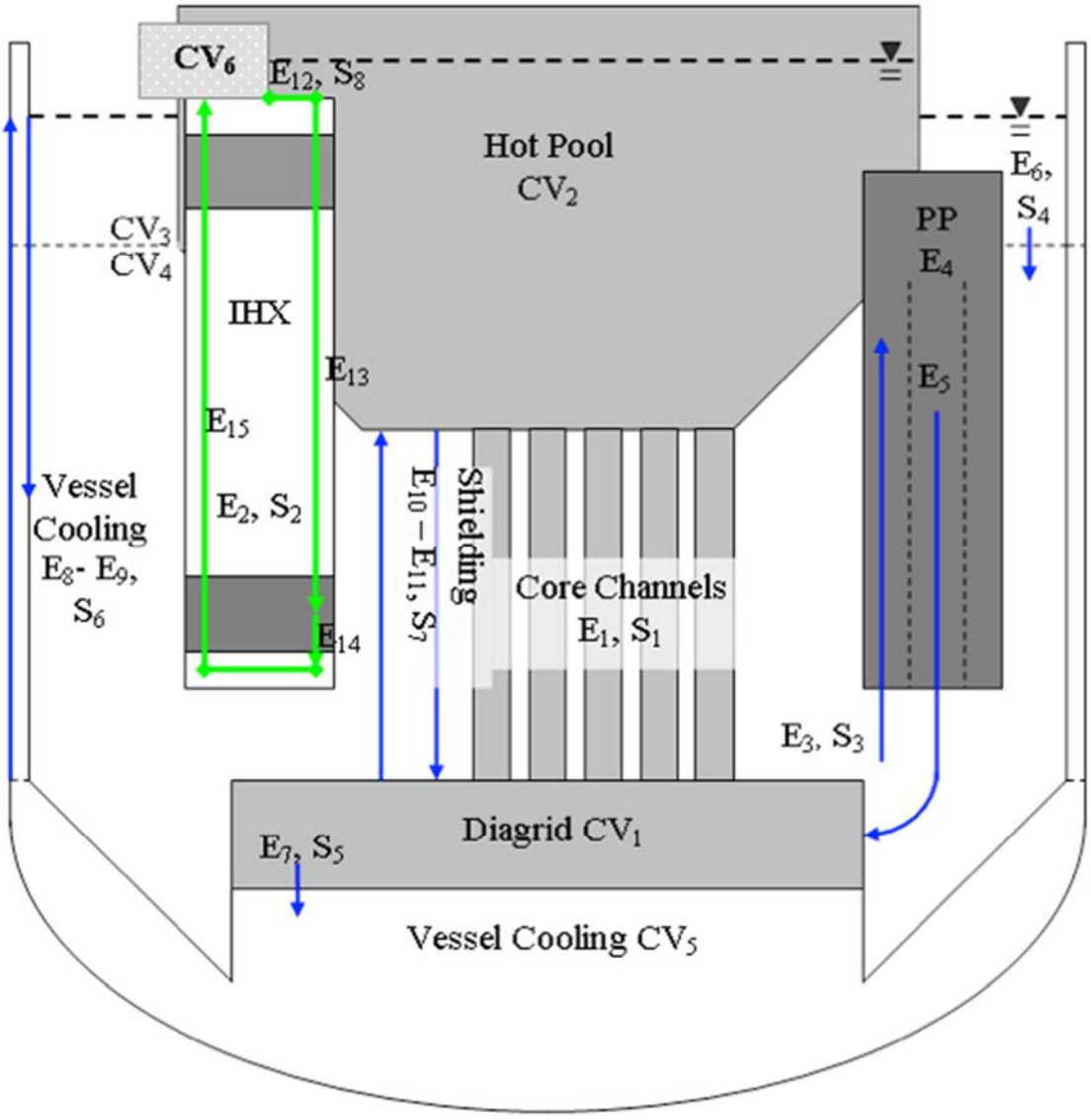

FIG. 45. Schematic of the ANL SAS4A/SASSYS-1 model.

TABLE 6. COMPRESSIBLE VOLUMES IN ANL SAS4A/SASSYS-1 MODEL

Compressible volume	Description
1	Diagrid (or inlet plenum)
2	Hot pool
3	Cold pool annulus
4	Cold pool bulk
5	Vessel cooling
6	Intermediate loop expansion volume

TABLE 7. ELEMENTS IN THE ANL SAS4A/SASSYS-1 MODEL

Element	Usage	Nodes	Inlet elevation (mm)	Outlet elevation (mm)
1	Core & shielding flow	-	-6240	-2700
2	IHX Shell Side	41	1160	-4205
3	PP Inlet	23	-5297	354
4	Primary Pump (PP)	-	354	354
5	PP Outlet	30	354	-6772.5
6	Internal Flow in CP	3	0	0
7	Diagrid Leakage	3	-7305	-7305
8	Vessel Cooling #1	28	-5500	1500
9	Vessel Cooling #2	15	1500	-2312.5
10	Radial Shielding #1	16	-2200	-6240
11	Radial Shielding #2	14	-6240	-2700
12	Intermediate Pump	-	1160	1160
13	Pipe to SG Inlet	21	1160	-4105
14	Steam Generator	2	-4105	-4205
15	IHX Tube Side	41	-4205	1160

The vessel-cooling system is modelled with annular flow elements that may transfer heat from the cold pool volumes. Elements must contain flowing gas or liquid; only compressible volumes are permitted to include both phases. Thus, this model does not treat the open nature of the vessel-cooling circuit, and the elevation of the sodium-gas interface in the cold pool cannot be predicted for comparisons with measured test data.

For this exercise, the CEA provided estimates of the pressure drop in several flow segments at the test conditions in the CRP package. The pressure drop specifications were matched in the SAS4A/SASSYS-1 model by adjusting the orifice coefficients at select locations.

A simplified secondary system model has been developed in order to accommodate the IHX tube-side inlet temperature boundary condition data that CEA provided for the boundary condition of the secondary system. SAS4A/SASSYS-1 permits the user to directly specify the steam generator outlet temperature evolution. Therefore, an ad-hoc steam generator was placed immediately upstream of the IHX and the specified IHX inlet temperatures were applied at the steam generator outlet. The

remainder of the secondary system model consists of a pump that draws sodium from an expansion volume and simple connecting pipes with no bends, constrictions, or heat losses.

Heat removal from the hot pool to the ambient environment above is modelled using a constant temperature heat sink attached to the hot pool. To model the heat removal from the emergency cooling around the cold pool vessel, another constant temperature heat sink is attached to the two annular elements in the vessel-cooling segment. The heat transfer coefficients and bulk heat sink temperature required for these models were determined by performing a linear regression against polynomials provided by the CRP package.

5.3.2. Brief description of the CATHARE model for Phenix (CEA)

According to the CRP data-package, the modeling scope of CATHARE input deck includes the primary circuit, which is contained by the reactor vessel. The main reactor vessel components are the core, the hot and cold pools, the primary pumps, the reactor vessel lower plenum, the strong arm, the diagrid and the shell side of the Intermediate Heat eXchanger (IHX). Due to the uncertainties in the heat losses along the secondary loop, the field of simulation is restricted to the secondary side of the IHX (tubes), the secondary IHX inlet and outlet plenum, short hot and cold pipes and boundary conditions. The flow rate evolution is assigned as the inlet boundary condition, while the pressure is assigned at the outlet boundary.

In CATHARE, the reactor vessel is modeled by a set of 0D modules (VOLUME) and 1D modules (AXIAL). The details of the reactor vessel model, with the main assumptions and hypothesis, are given below:

- Diagrid, strong arm and reactor vessel plenum:;
  - 3 × 0D modules;
- Reactor Vessel Cooling system;
  - 1D module;
  - 0D module;
  - 1D module.
- Primary pump (× 3);
  - 1D module with definition of a volumetric pump;
  - Assumptions on primary pump homologous curves;
  - Assumptions on metal mass;
- Core;
  - 1D modules;
  - 4 channels;
    - Inner core: fissile sub-assemblies;
    - Outer core: fissile sub-assemblies;
    - Blanket: fertile sub-assemblies;
    - Nearly stagnant zone around the core;
  - Fuel assemblies connected to neutronics point kinetics model;
- Hot pool;
  - Several 0D modules;

- Sodium mass respected;

— Cold pool;
  - Several 0D modules;
  - Sodium Mass respected;
  - Azimuthal sectorization:;
    - 2 × 2 IHX;
    - 3 primary pumps;

— IHX primary side (connected to 2 secondary loops);
  - 1D module;
  - Inlet and outlet elevations;

— IHX secondary side (connected to 2 secondary loop);
  - IHX pipe 1D module;
  - Plenum 0D module;
  - Secondary inlet and outlet pipes: 1D modules;
  - Inlet and outlet boundary conditions: imposed;

— Heat losses;
  - Heat losses from hot pool to roof and reactor vessel drawn from the data package (function of the sodium temperature);
  - Explicit computing of heat losses from the hot pool to the cold pool;

— Non-condensable gas;
  - Argon gas is defined in the computation;
  - Junction between hot and cold pools: there is the same pressure in the upper sub-volumes of the modules at the top of the pools.

Regarding to the specific design of the IHX inlet wrapper tube and physical phenomena involved in Phenix reactor, specific attention has been given:

— To model the reactor vessel cooling system, in order to get the proper heat stratification in the cold pool at nominal state;

— To model the inlet wrapper IHX primary side (the elevation of the inlet wrapper tube is not constant);

— And to model the radial heat exchanges between hot pool / cold pool and cold pool / reactor cooling vessel system (these heat exchanges terms play a key role during long term transient).

For the volume with a free level (upper part of the reactor vessel), the code computes the evolution of the free level due to the density effect in the lower sub-volume and hydraulics conditions below. As long as the upper part of the reactor vessel is modeled by 3 different VOLUME modules (one for the reactor cooling vessel system, one for the cold pool and one for the hot pool), the code computes the evolution of 3 free levels.

The following table gives an overview of the numerical scheme.

TABLE 8. CEA MODEL: MESHES NUMBER

Module	Meshes
Primary circuit	
Number of 0D modules	23
Number of 1D modules	16
Number of boundary condition modules	1
Total number of meshes	614
Secondary circuit	
Number of 0D modules	4
Number of 1d modules	6
Number of BC modules	4
Number of meshes	274
Total of meshes	888

Fig. 46 shows the CATHARE model of the PHENIX reactor with the main components.

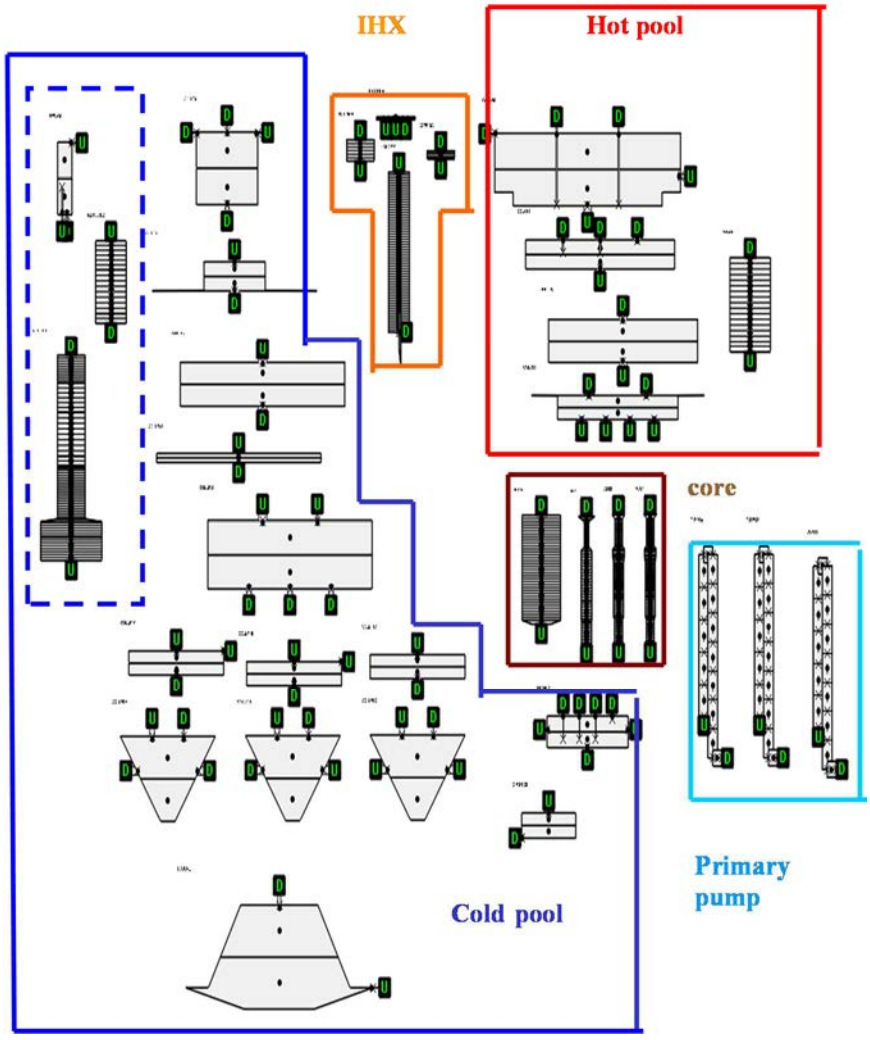

FIG. 46. Schematic of the CEA CATHARE model.

5.3.3. Brief description of STAR-CD and DYANA-P models for Phenix (IGCAR)

5.3.3.1. STAR-CD model

Details of 3D model of the primary circuit are given below. Total number of computational cells in the model is ~ 60,000.

Overall Structure: the core, hot pool, cold pool, primary side of IHX, pump and main vessel cooling circuit are modeled as an integrated CFD model, without any external coupling.

In view of the geometrical locations of various components and thermal hydraulics conditions that follows a primary sodium pumps trip event, a 180° sector model of hot and cold pools has been considered for the analysis. Primary sodium pumps are located 120° apart. IHX are located 60° apart.

The vertical section of CFD model used for the study is shown in Fig. 47.

Core

The core is divided into convenient number of radial zones and each zone is represented as a ring in the core location. The power and flow in each zone are given as per the supplied data. Each radial zone is further divided into two rings representing solid and fluid volumes separately (Fig. 47). Further, these zones are divided axially into three zones to represent active fuel region separately (Fig. 48). Whole core region is then discretized into convenient number of volumes.

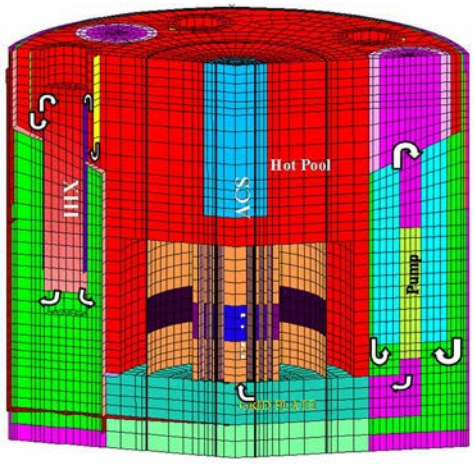

FIG. 47. IGCAR STAR-CD model - vertical section without solid materials.

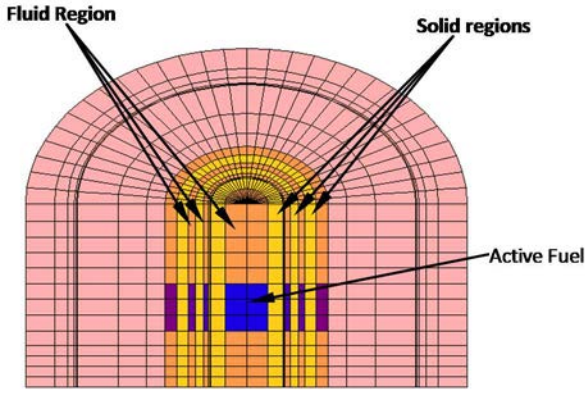

FIG. 48. IGCAR STAR-CD model - Core model.

The solid portion of the core takes care of the thermal capacities of fuel and steel. Pressure drop in the core region is modeled using baffles at the inlet to SA from grid plate. The baffle resistance coefficients are calculated using the given steady state flow rate and pressure drop conditions. Heat generated in the core is defined as a uniform heat source in the active fuel region as a function of time.

Control Plug

Control plug is modeled as porous region with a resistance such that it permits 1.5 % of the core flow to pass through it. The lattice plate, core monitoring thermocouples and control rod drive mechanisms are modeled as porous bodies.

Inner Vessel

Inner vessel is modeled as an impermeable baffle, which permits heat exchange between hot and cold pools by thermal conduction. The conduction resistance of inner vessel is provided as input data to CFD calculations.

Pump

Pump is modeled as a momentum source calculated as a function of time using a user subroutine. The transient momentum source is estimated using Homologous characteristics of the pump.

Grid plate

Grid plate is modeled as a porous body with distributed momentum sink. The pressure loss coefficient is obtained from the initial steady state value of pressure drop across the grid plate. The loss coefficient for radial and circumferential momentum sinks can also be estimated using correlations for 'Cross flow over tube banks'.

IHX

IHX is modeled as a porous body with distributed pressure drop in momentum equations and heat sink in energy equation. The heat sink in IHX is calculated using an external program in a staggered manner (i.e. sink value at time step / iteration 'n' is determined from the primary temperature conditions at time step / iteration 'n-1'). The steps followed in the program are (Fig. 49):

— The average primary sodium temperature at each axial location is extracted from the CFD calculations.

— With the given (i) secondary sodium flow rate, (ii) secondary inlet temperature and (iii) the extracted primary sodium temperature, the secondary sodium temperature and heat transferred from primary to secondary side are calculated.

— The heat sink calculated by this procedure is used as heat sink in IHX for CFD calculation in the next iteration / time step.

Heat transferred to main vessel and roof slab

Average sodium temperature of the cold pool and the hot pool free surface are calculated from CFD predictions. These temperatures are used to calculate the amount of heat transferred through Main Vessel and roof slab using the given relationships of the form, Heat transfer = function of temperature. The calculated heat transfer rates are used as heat sinks in cold pool and hot pool respectively.

Core Support Structure

The internals of core support structure are not modelled.

Main vessel cooling system

The main vessel cooling flow is taken from core support structure plenum and it is allowed to flow along the main vessel through a channel representing main vessel cooling circuit. This flow joins the cold pool at a level above IHX primary outlet. The outer surface of the main vessel is treated as adiabatic.

Turbulence in the flow is simulated by standard high Reynolds number k-ε model. First order upwind scheme is used for convective terms. Pressure velocity coupling is done by SIMPLE algorithm.

Fig. 49 shows the flow chart for CFD analysis. The flow coast-down in primary pumps is calculated using one-dimensional code using homologous characteristics of the pump. The momentum source is calculated based on the pump speed and is given as input to the code.

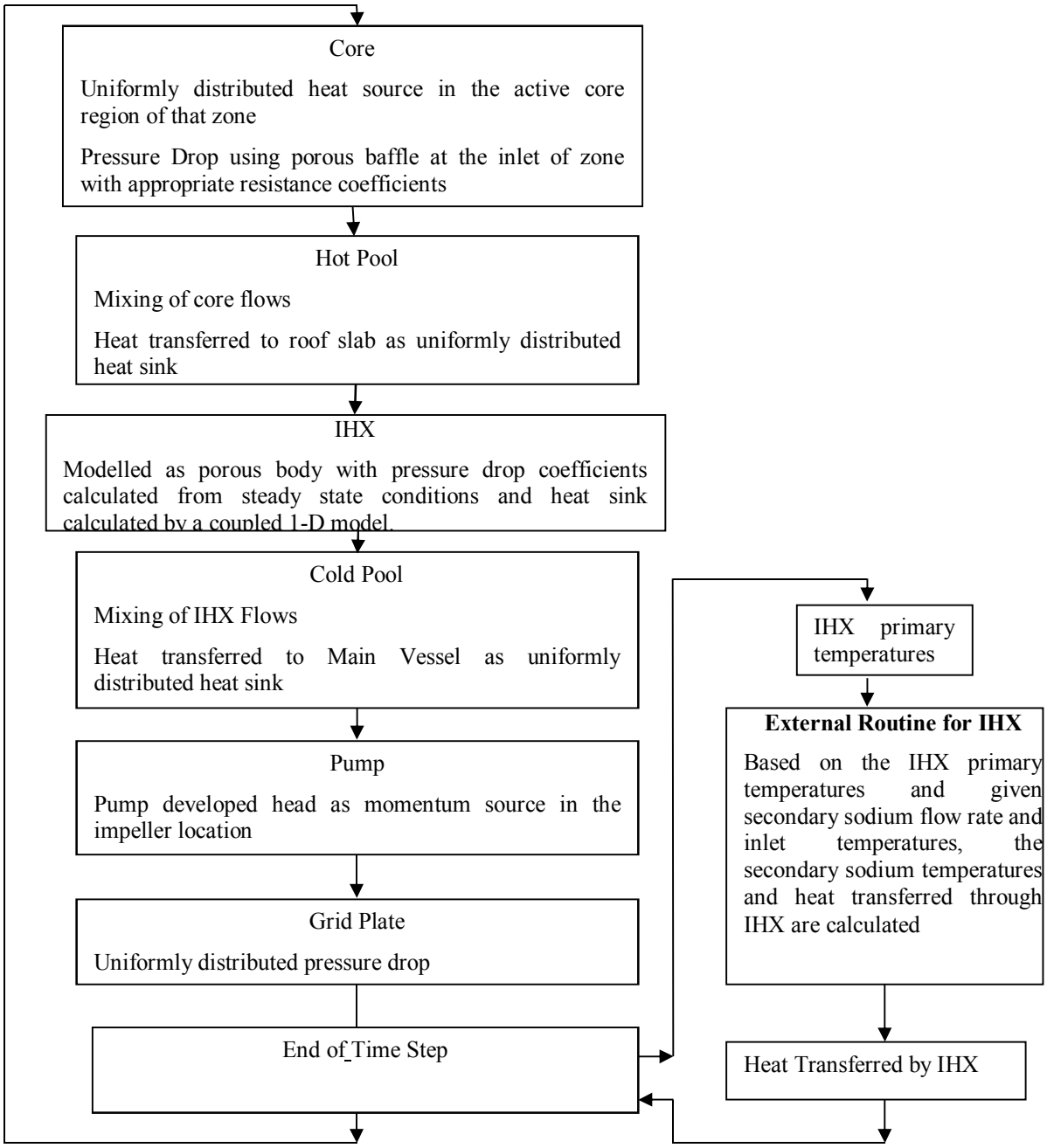

FIG. 49. IGCAR STAR-CD model – Flow chart of CFD model for natural convection studies Flow chart of CFD model for natural convection studies.

5.3.3.2. DYANA-P model

DYANA-P code which is developed for plant dynamics studies in PFBR has been modified to model primary circuit of Phenix. Nodalization scheme used is shown in Fig. 50. Reactor core is modeled as 10 radial channels. Inner core, outer core, fertile zone and reflector regions have been modeled through 3, 2, 3 and 2 channels respectively. 18 control volumes are considered in the axial direction of subassemblies. Radial power distribution in various zones is considered as per the supplied data. Axial power distribution is considered according to flux distribution supplied. Hydraulic inertias of various segments are modeled as per the length and area data provided. Hydraulic resistances of various paths are modeled as per the flow and pressure drop data supplied. IHX is subdivided into 19 control volumes. Pump characteristics has been modeled using homologous characteristics corresponding to the given rated conditions. Pump coast down characteristics is modeled through

inertia and drive resistance. Main vessel cooling circuit is not considered in the model. Thermal inertia of cold pool region in the annulus between main vessel and inner vessel is considered as a part of the hot pool. Thermal inertia of diagrid is considered along with that of hot pool. Thermal inertia of shielding subassemblies is not considered. Secondary sodium circuit is not modeled in the code. IHX is modeled with secondary sodium flow and inlet temperature as input conditions corresponding to the experimental data. This simulates the heat sink from primary sodium circuit. Due to the unavailability of kinetics data, core power evolution is also used as input corresponding to the CRP data set.

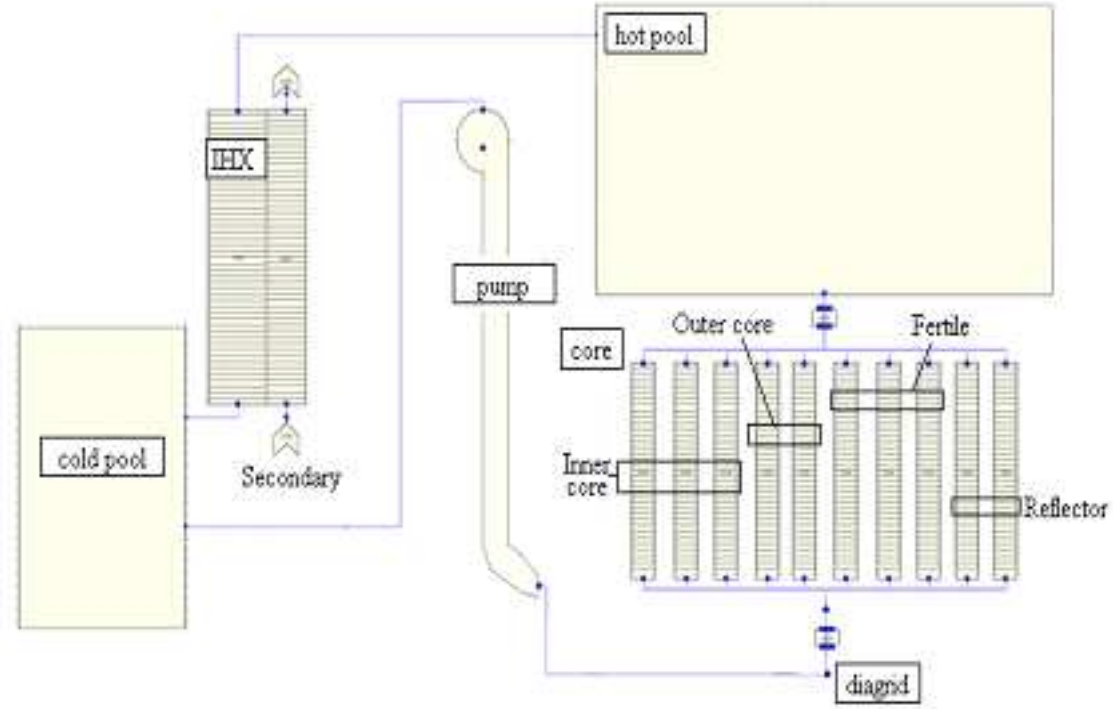

FIG. 50. IGCAR DYANA-P model – Nodalization diagram in DYANA-P code.

5.3.4. Brief description of GRIF model for Phenix (IPPE)

5.3.4.1. Modelling approach for Phenix

— The GRIF model of the Phenix reactor system during the natural convection test includes the following major features:

— A porous body formulation is used to calculate the distributions of flow and temperature in the sub-regions where the internal geometry is complex, such as the tube bundles in the IHXs.

— Mass exchange between inter-wrapper flow and ‘main’ flow occurs through the top and lateral surface of the core sub-region. Sodium leakage through the bottom (SA seals) is specified neglected.

— Turbulent viscosity and conductivity is considered as a constant that doesn’t depend on space coordinates are spatially uniform.

— Variation of the sodium level in the reactor pools is not modeled.

— Evacuation of power by the emergency cooling system and by reactor roof are taken into account by specifying the proper boundary conditions at top, bottom and lateral surfaces of computational domain.

— Leakages through control plug (1.5%) are not modeled.

5.3.4.2. Nodalization scheme

It is assumed that LOOP1 and LOOP3 of the reactor are identical and the reactor has symmetrical design. Therefore only half of reactor is simulated in the model. The computational domain is covered with the following non-uniform (r×z×φ)-mesh – (27×47×39). Mesh indexes are accordingly (i, k, j).

Vertical cross-sections of the reactor model for two selected angle positions are presented in Fig. 51. The horizontal cross-sections of reactor model are shown in Fig. 52.

More detailed pictures of vertical and horizontal cross-sections of the core are presented on Fig 53 and Fig. 54. Fissile part of core is represented with 7 rings (i=2÷8). Control rods are modeled as separate channels in the core. Power is specified as a function of time in accordance with data provided by CEA. IWS flow and SA Wrappers parameters were calculated in the sub-region (i=2÷15, k=5÷27, j=2÷39) only. It was assumed that the bottom of IWS is isolated (no leakage) and mass and heat exchange with 'main' flow is allowed only through top and lateral sides. Table 9 gives the distribution of subassemblies among the rings of core model.

TABLE 9. IPPE GRIF MODEL – DISTRIBUTION OF SUBASSEMBLIES AMONG THE RINGS OF CORE MODEL

SA types	Channel number "I"	Number of SA in channel
Control rods	2	1
Fuel Inner SA	3	6
Fuel Inner SA	4	12
Fuel Inner SA+Control rods	5	12+6
Fuel Inner SA	6	24
Fuel Outer SA	7	24
Fuel Outer SA	8	24
Breeder	9	30
Breeder	10	30
Breeder	11	30
Reflector	12	100
Reflector	13	116
Storage	14	45
Storage	15	45

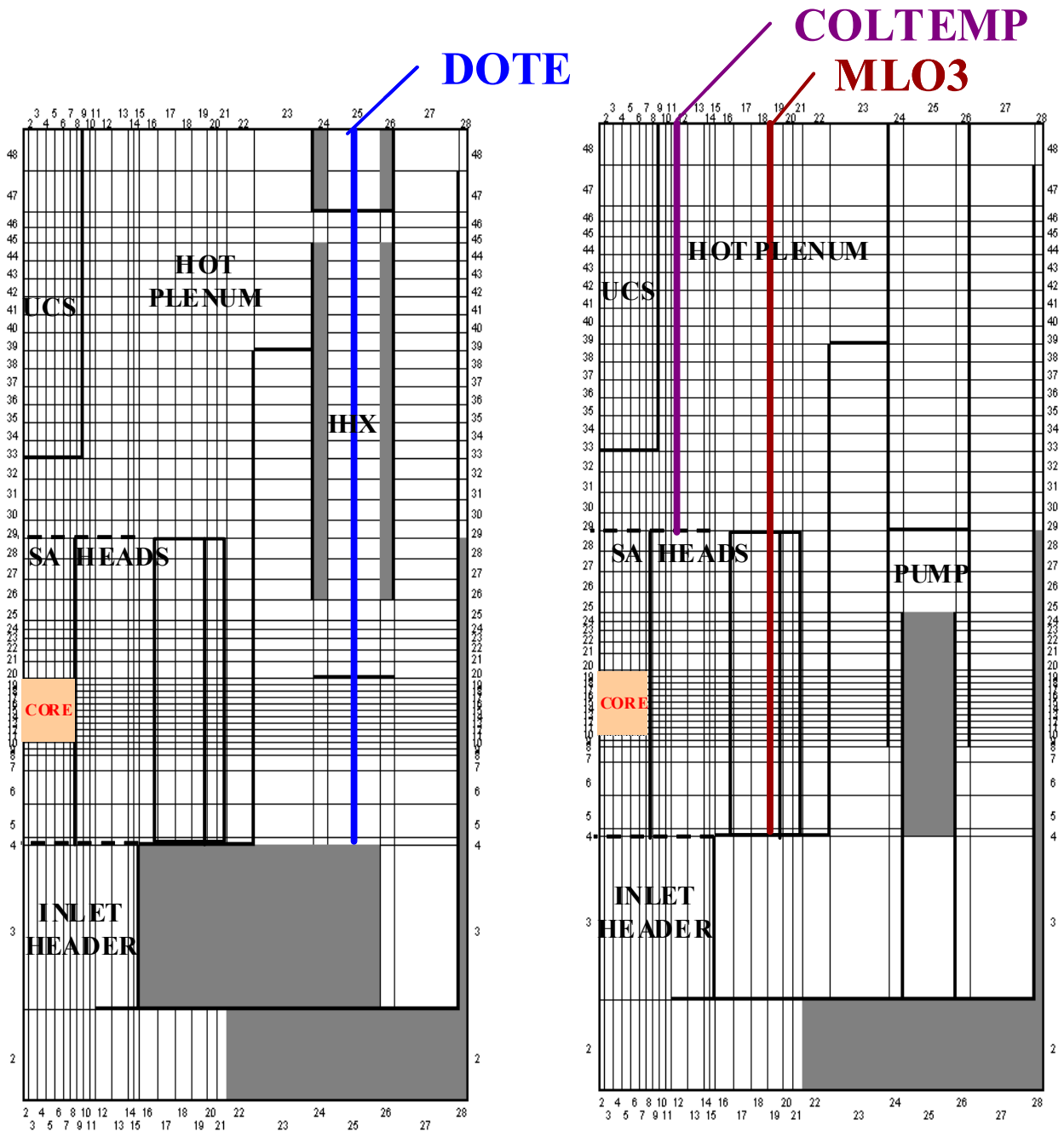

a) J=9 b) J=15

FIG. 51. IPPE GRIF model – Vertical cross-sections of calculation domain.

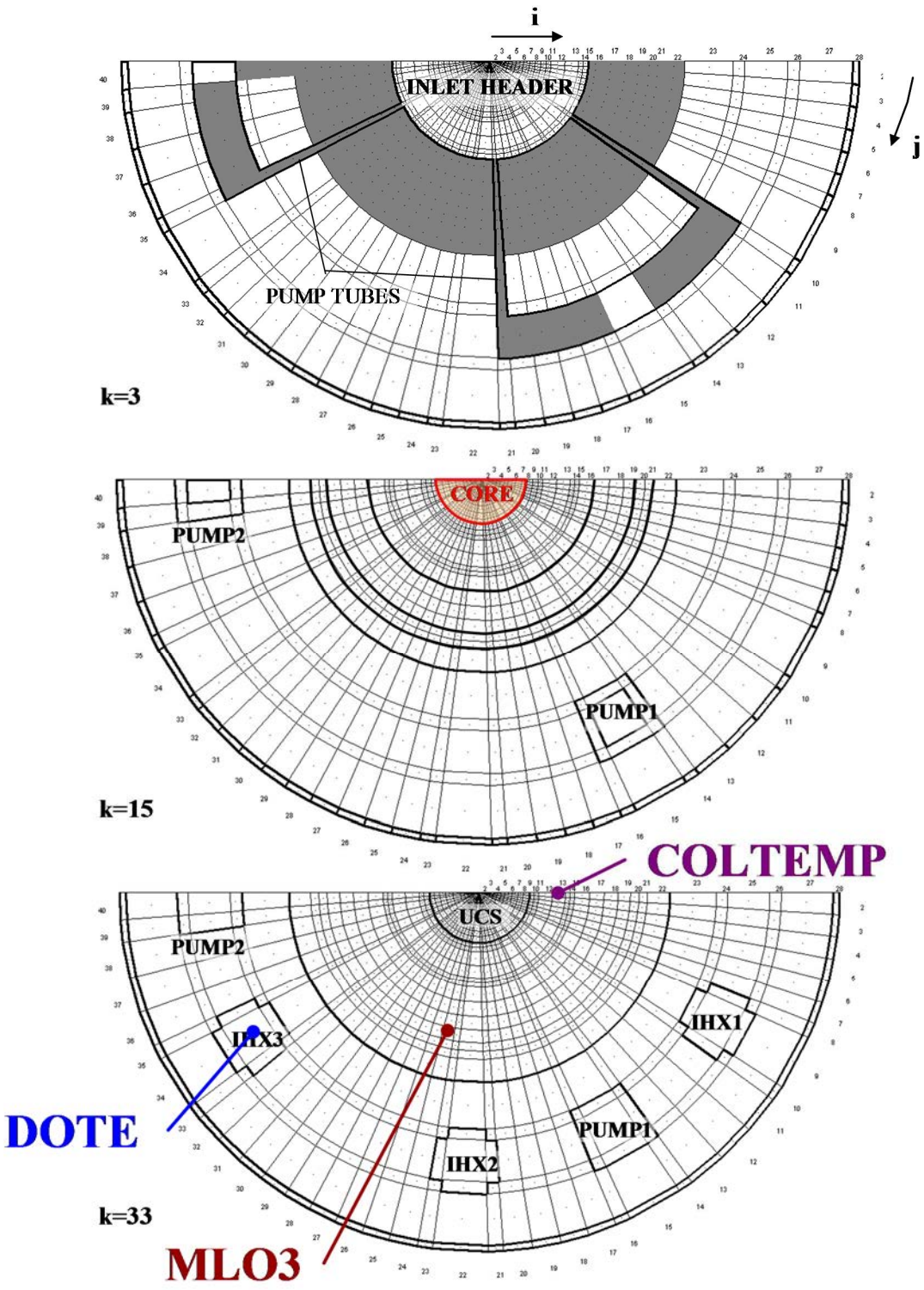

FIG. 52. IPPE GRIF model – Horizontal cross-sections of calculative domain.

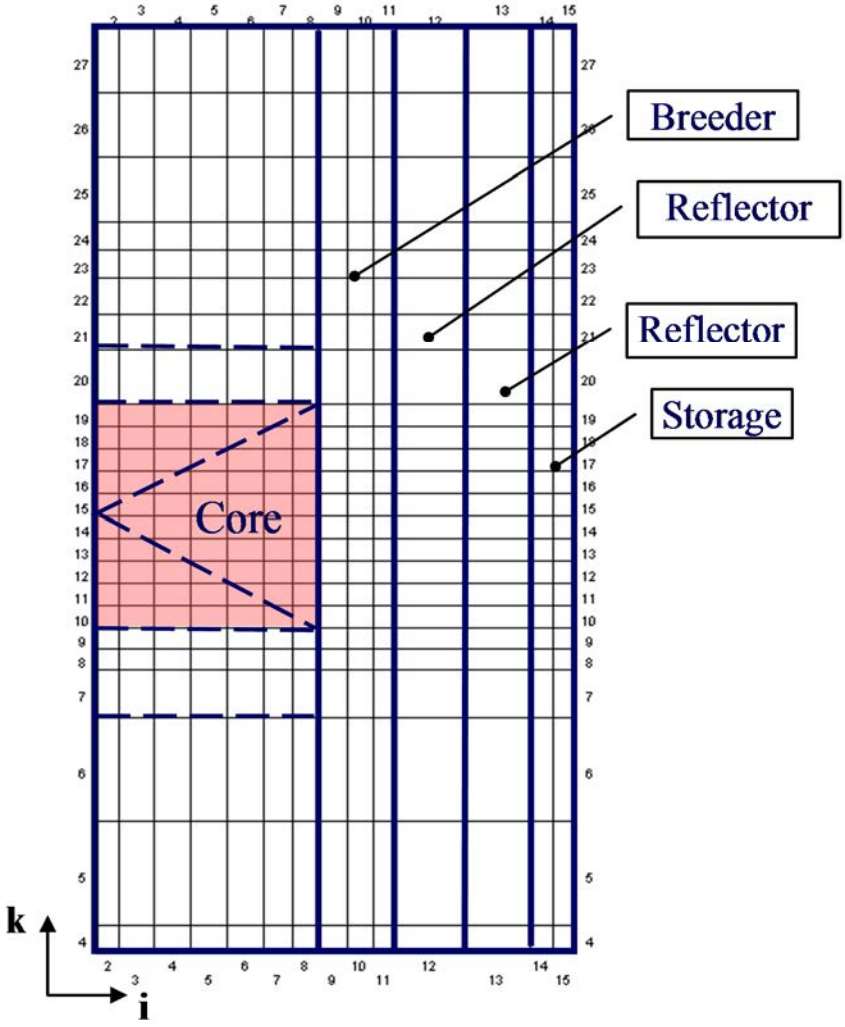

FIG. 53. IPPE GRIF model – Vertical cross-sections of core domain.

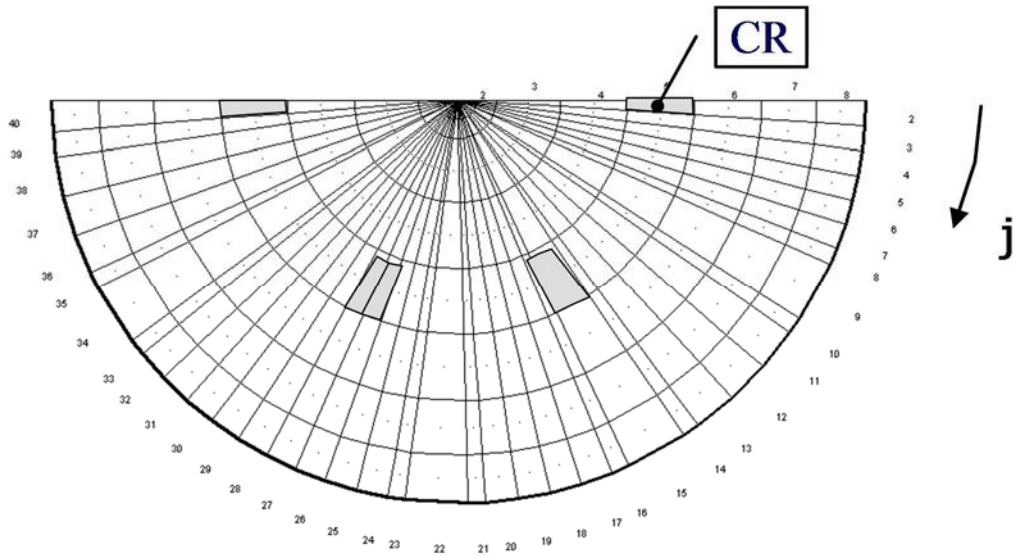

FIG. 54. IPPE GRIF model – Horizontal cross-sections of core domain.

5.3.5. Brief description of the CATHARE model for Phenix (IRSN)

The primary circuit of the Phénix reactor was modeled using 0D and 1D elements. The CATHARE nodalization is shown in Fig. 55. The secondary circuit is simulated with boundary conditions: experimental results for temperature and mass flow rate at IHX secondary inlet are directly imposed.

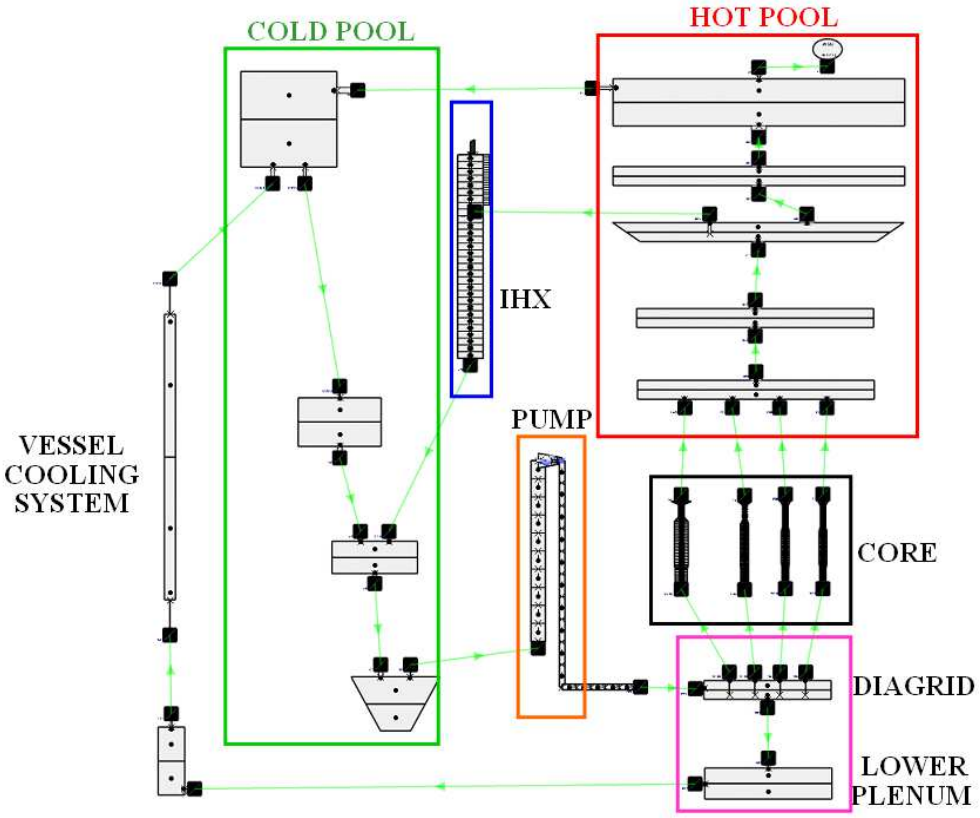

FIG. 55. IRSN model – CATHARE nodalization of the Phenix primary circuit.

The components of the primary circuit are described below:

— Core (Fig. 56):

- 4 parallel 1D pipes (see figure below);
  - inner core (fissile assemblies);
  - outer core (fissile assemblies);
  - blanket zone (fertile assemblies);
  - steel reflector zone;
- Singular head losses at channels inlet tuned in order to match the steady-state core mass flow rate distribution given in the data package;
- Specific friction law for fuel pins (Pontier's correlation with a correction for low Reynolds number);
- Experimental power evolution directly used as a boundary condition (data package).

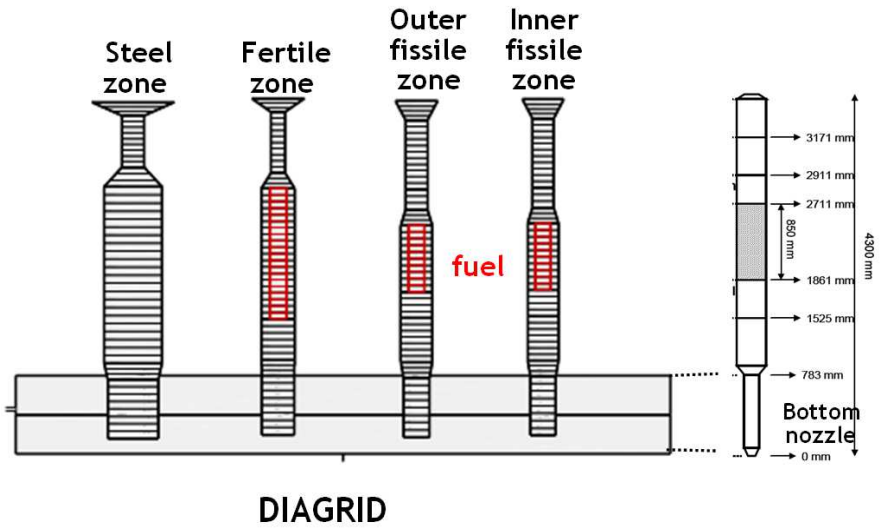

FIG. 56. IRSN model – CATHARE nodalization of the core.

— Hot pool;
  - Five 0D volumes (5 layers);
  - Sodium mass respected;
  - Free level modeled;
  - Argon cover;
  - Heat losses from hot pool to roof (law issued from the data package);
  - Heat exchanges between hot pool and cold pool ;

— Intermediate heat exchanger (IHX);
  - Two counter-current 1D pipes with a weight of 4;
  - Inlet boundary conditions imposed at the secondary side (data package);

— Cold pool;
  - Four 0D volumes (4 layers);
  - Sodium mass respected;
  - Free level modeled;
  - Argon cover (junction between hot and cold pools);
  - Heat exchanges between hot pool and cold pool;

— Primary pumps (weight of 3);
  - 1D pipes with of a CATHARE pump gadget;
  - Characteristics of the pump described by homologous curves (data package);
  - Assumptions on the steel mass distribution;

— Diagrid and lower plenum;
  - Two 0D volumes;
  - Singular head losses imposed at the lower plenum inlet and tuned to match the steady-state mass flow rate of the reactor vessel cooling system (about 10% of the nominal flow rate);

— Reactor vessel cooling system;

- Two 0D volumes;
- Heat losses from vessel cooling system (law issued from the data package);
- Free level not modeled (lack of information concerning this part of the primary circuit);

5.3.6. Brief description of the NETFLOW++ model for Phenix (University of Fukui)

The calculation model of the Phenix is shown in Fig. 57. The core is separated into 10 channels and one bypass channel. The channel geometry of the fuel subassembly is taken from the specifications in the CRP document. The heat transfer between the hot pool and the cold pool is taken into account using two heat exchanger models which has equivalent heat transfer and flow areas of the flow pass from the outlet of the core to the inlet of IHXs. Four active IHXs are modelled using two IHXs. In order to enhance the mixing in the hot pool, the upper part of the hot pool is linked to the inlet of the two IHXs. The cold pool is modelled with a simple pipe. The vessel cooling system is modeled with two shell-and-tube type heat exchangers. The radioactive heat transfer between the two walls is simulated equivalent thermal resistance on the heat transfer tubes. Three primary pumps are modelled with two pumps. Since boundary conditions for two loops are different, two kinds of boundary conditions are given to the loop-1 and loop-2 independently.

TABLE 10. FUKUI NETFLOW++ MODEL - ARRANGEMENT OF THE FUEL SUBASSEMBLIES IN THE MODEL

Channel number	SA types	Number of SAs in channel
1	Center and 1st layer (Inner driver)	7
2	2nd layer (Inner driver)	12
3	3rd layer (Inner driver)	12
4	4th layer (Inner driver)	24
5	5th layer (Outer driver)	29
6	6th Layer (Outer driver)	27
7	7th and 8th layers (Blanket)	86
8	Control rods	7
9	Reflectors	212
10	Shieldings	1062
11	Bypass	1

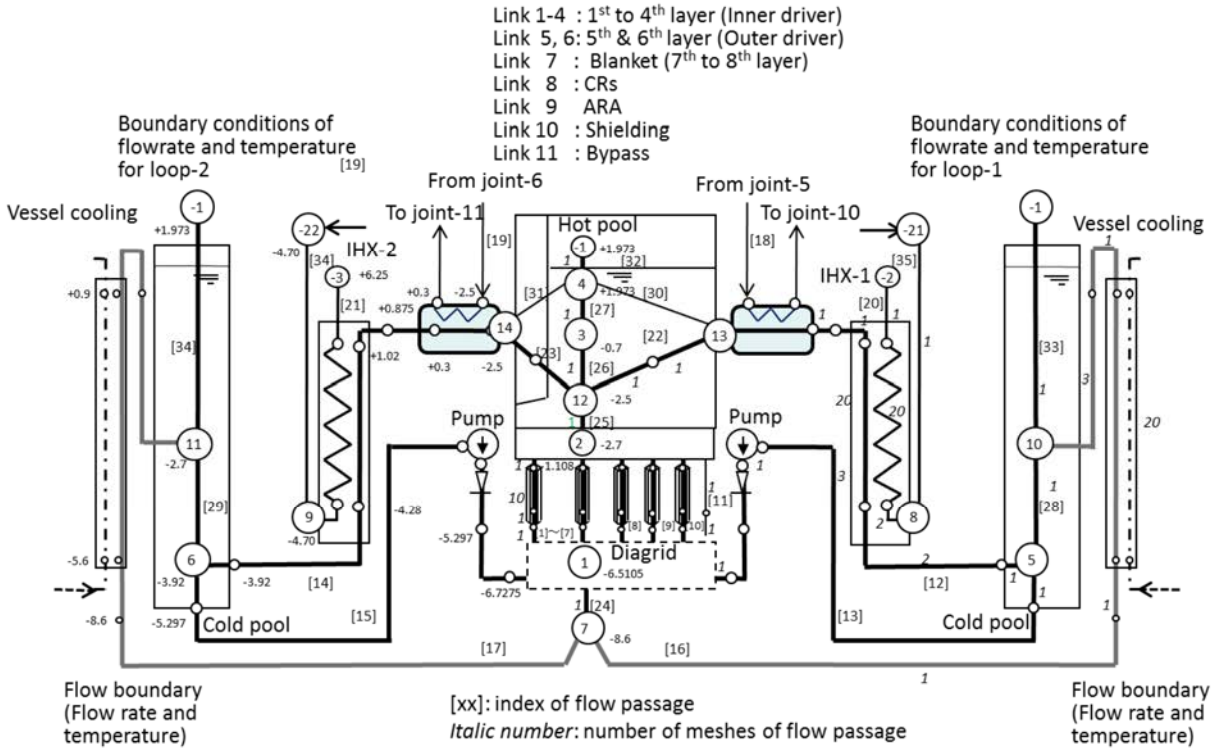

FIG. 57. Fukui university model – Calculations model of Phenix using the NETFLOW++ code.

5.3.7. Brief description of the MARS-LMR model for Phenix (KAERI)

The fluid systems are basically described with 1D components (pipes) with flow junctions in MARS-LMR modelling (Fig. 58). The structure and heat transfer between the fluidic volume and heat structure are modeled with a heat structure input which describes the structure material, volume of structure and heat transfer area. As an option, a pool volume can be modeled as a 3D component with which the momentum changes in x-, y-, and z-directions are conserved.

For the description of the Phenix primary system and IHXs the thermal-hydraulic systems are nodalized into several volumes. Total 981 subassemblies in the core are modeled into 7 flow channels. The active 4 IHXs are modeled independently to describe an asymmetric flow condition through the IHXs. The cold pool is modeled by the two axial nodes, 100 and 110 having 7 and 12 sub-volumes, respectively. The reactor vessel cooling system is modeled to match the flow balance in the primary system. The secondary circuit is simulated with the boundary conditions: time history for IHX inlet temperature and flow rate.

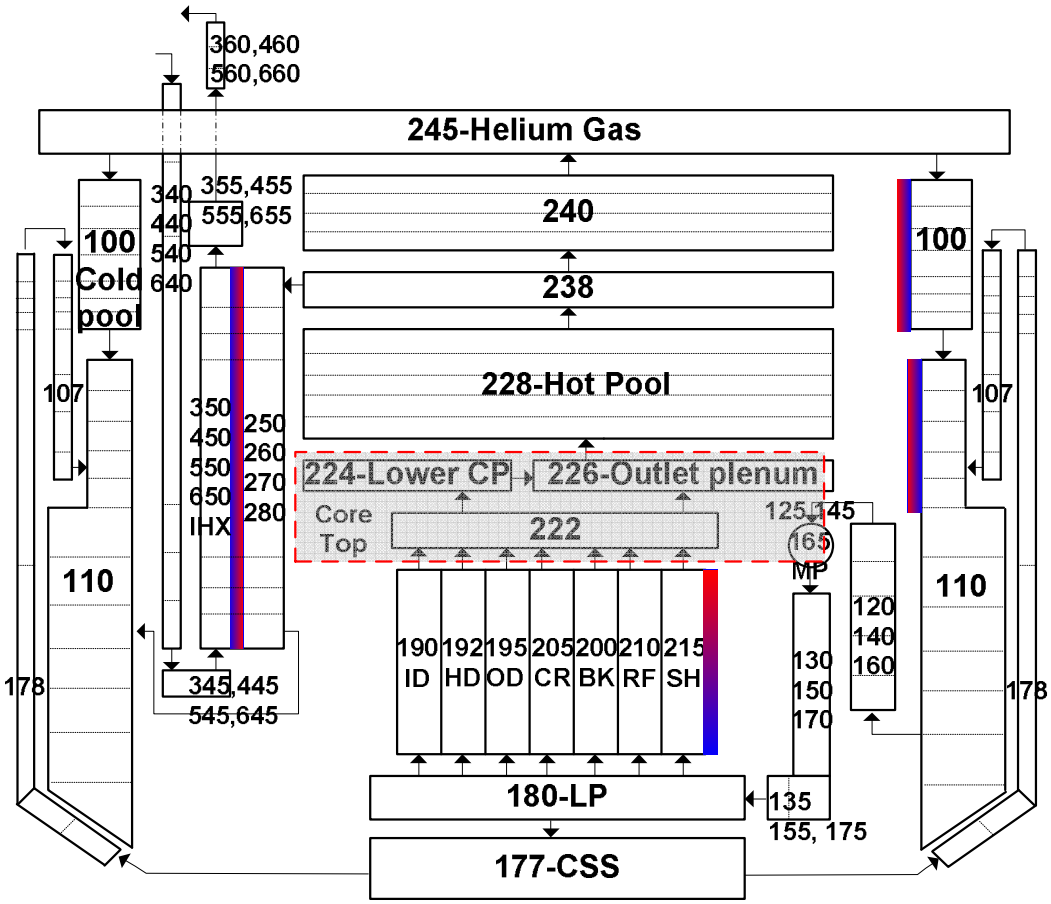

FIG. 58. KAERI Model – MARS nodalization diagram.

5.3.8. Brief description of the TRACE model for Phenix (PSI)

For the analysis of the natural convection test, the entire primary circuit was modeled in TRACE. The modeling of the intermediate circuit was limited to the heat exchangers (IHXs) with appropriate boundary conditions on the inlet temperature, flow rate and outlet pressure. The experimental power evolution was used as boundary condition.

Fig. 59 presents the nodalization scheme developed in TRACE to model the Phenix reactor. Main reactor components' thermal-hydraulics characteristics are reported in table 11. Special attention has been focused on the accurate simulation of the component elevations, the pool free surfaces and the heat-structure description. Various heat structures have been used to represent:

- The wall between the hot and cold pool;
- The power evacuated through the roof;
- The power evacuated by the emergency cooling circuit (heat structure connected to the vessel cooling system);
- The steel in the pump and diagrid.

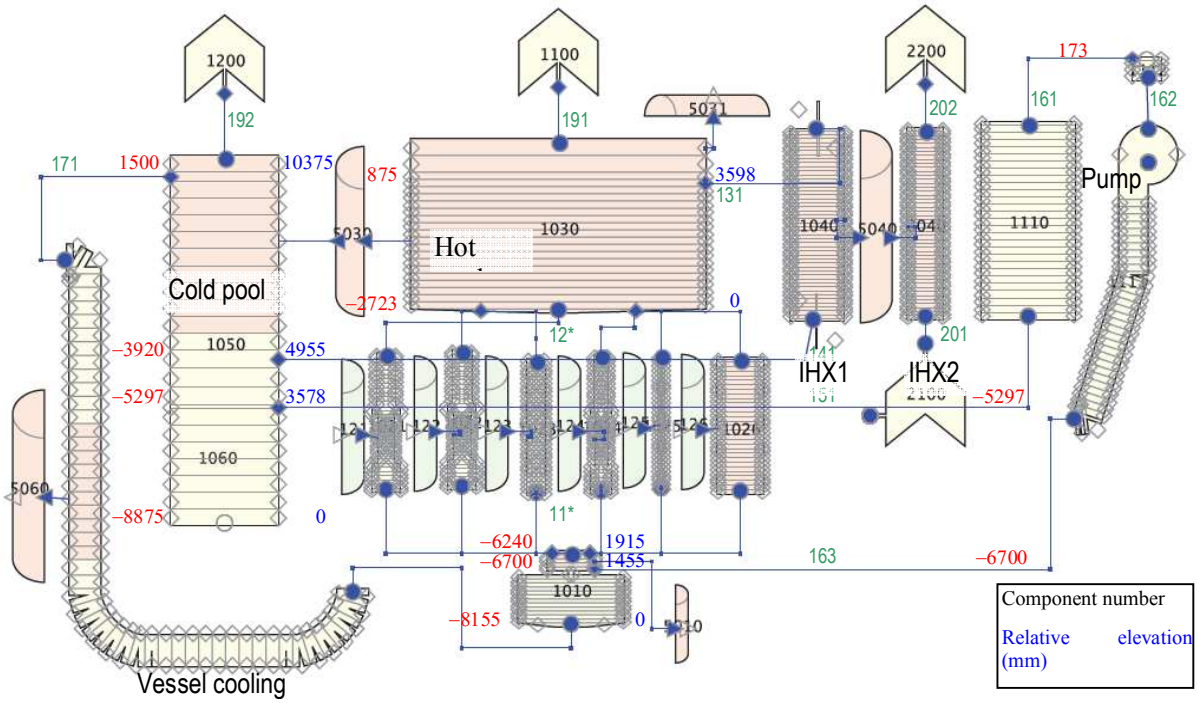

Diagrid

FIG. 59. PSI model – TRACE nodalization diagram.

Described below are the geometry and nodalization scheme for the core, the pools, the IHXs, the pumps and the diagrid.

The core

The TRACE model considers the following six core regions: inner core (54 SAs), outer core (56 SAs), blanket (86 SAs), fuel stored in the core, control rods and steel reflector.

In order to reproduce the correct pressure drop in the core, a simplified model of the inner vessel (diagrid, core and hot pool) was developed. The latter allowed one to adjust the gagging of each core region in an independent way. For this purpose, each region was simulated with the corresponding nominal conditions, the inlet temperature and flow rate being imposed by a FILL. The hot pool was simulated with a free surface. A BREAK was used to simulate the IHX flow discharge. Having the appropriate core outlet pressure imposed, together with the corresponding flow rate and power, the friction coefficient could easily be adjusted to reproduce the core pressure drop as specified by the CEA. This procedure was repeated for each core region, taken separately, and thus enabled one to reproduce the correct core friction losses in the complete model.

Hot and cold pools

The hot and cold pools are represented with a pipe connected to a BREAK component. The use of side junctions allowed one to connect the different components at the correct elevation. The outlet plenum has been simulated with side junctions (instead of the PLENUM component), as recommended in the TRACE user manual. The hot pool is connected to the IHX at an elevation of +875 mm. The IHX outlet is connected to the cold pool at -3920 mm. The pump is connected via a side junction linked to the cold pool at -5297 mm. Furthermore, the vessel cooling component is linked to the cold pool at +1500 mm. The free surface in the latter has not been considered in the model and the component was directly linked to the cold pool.

In order to reproduce the correct levels, the free surfaces of both pools have been initialized at 1783 mm, which corresponds to the specified level at 400°C. The volume of the bottom cells have been adjusted to obtain the sodium mass of 265 t and 536 t in the hot and cold pool, respectively, the specification being assumed to be at 400°C.

IHX and secondary circuit

The four intermediate heat exchangers (IHXs) have been simulated with two counter-current pipes, a down-flow pipe in the primary side and an up-flow pipe in the intermediate circuit. In order to represent the correct elevation, the primary side pipe was connected to the pools via perpendicular junctions and horizontal cells. This ensured that the IHXs were effectively connected to the middle of the corresponding pool cells. The hydraulic diameter, which could not be calculated from the specified design characteristics, was adjusted such as to allow one to reproduce the correct pressure losses between the hot and cold pools. This could be done knowing the pool levels under nominal conditions.

Since the modeling of the intermediate circuit has been limited to the IHXs, appropriate boundary conditions specified by the CEA have been used, viz. the inlet temperature and mass flow rate evolutions.

Pump and diagrid

The three pumps have been simulated together, using a three-fold rated flow and keeping the other rated characteristics at their nominal values. The built-in TRACE pump has been used, yielding satisfactory results. The specified steel mass of 82.5 tones was accurately modeled, but an assumption was made on the heat-exchange area since the latter has not been provided by the CEA.

In the diagrid component, the total pump flow divides between the core (~90 %) and the vessel cooling system (~10 %), as specified by the CEA. Since the geometry of the diagrid is complex and not detailed in the CRP specifications, the area and friction losses have been adjusted to reproduce the correct flow distribution. This was done using the specifications at nominal power presented in the following section. The specified steel mass of 74.6 tones was correctly modeled. The heat-exchange area was assumed to be ~250 m^2.

The following table describes the thermal-hydraulics components used for the representation of the Phenix reactor with TRACE.

TABLE 11. PSI MODEL - THERMAL-HYDRAULIC COMPONENTS CHARACTERISTICS

Element	Usage	Multi-plicity	Inlet elevation (m)	Outlet elevation (m)	Length (m)	# of nodes	Area (m^2)	Hydraulic diameter (m)
Primary circuit								
1010	diagrid	1	0	1905	1905	19	1.85	1.5 / 3.5e-3
1001	inlet plenum	1	1905	1915	10	1	-	-
1021	inner core	54	1915	5432	3517	36	4.30E-03	3.04E-03
1022	outer core	54	1915	5432	3517	36	4.30E-03	3.04E-03
1023	fertile core	90	1915	5432	3517	28	3.18E-03	4.00E-03
1024	storage core	40	1915	5432	3517	36	4.30E-03	3.04E-03
1025	core by-pass	216	1915	5432	3517	36	4.30E-03	1.00E-03
1002	outlet plenum	1	5432	5455	23	1	-	-
1030	hot pool	1	5455	11380	5925	59	68.5	10.34
1040	IHX1	4	9030	4235	-4795	48	0.585	0.0075
1050	cold pool	1	-770	10285	11055	55	9.12	3.41
1110	pump upflow	3	2858	8328	5470	28	2.316	1.28
1112	connection pump	3	8328	7770	-558	4	0.229	0.54
1111	pump	1	7770	1455	-6315	1	3*0.229	0.54
Secondary circuit								
2100	FILL	1	4235	4235	0	1		
2040	IHX2	4*2279	9030	4235	-4795	48	1.13E-04	0.012
2200	BREAK	1	9030	9030	0	1		

6. CALCULATIONS

This section presents successively the blind calculations and the post-test calculations.

The calculations are based on Phenix test boundary conditions described in Section 3:

— The core power evolution versus time;

— The primary pumps speed evolution versus time;

— The IHX secondary coolant mass flow rate per loop versus time;

— The IHX secondary coolant inlet temperature per loop versus time.

The calculation results are compared with the following reactor measurements:

— The temperature at fuel outlet assemblies (hottest fuel assembly, average inner core and average entire core);

— The primary pump inlet temperature (compared to core inlet temperature predictions for blind calculations (*) as there is no core inlet temperature measurement);

— The primary coolant temperature at IHX inlet and outlet;

— The sodium level in hot pool, cold pool and vessel cooling circuit.

(*) After analysis, it turns out that the Phenix primary pump inlet temperature presents important bias in natural convection regime. As long as the DOTE thermocouple sensor at pump inlet elevation (elevation z=-5400mm) gives a more reliable indication, this sensor has been selected for comparison between Phenix and code prediction at the pump inlet.

6.1. INTRODUCTION

In order to improve the participants' capabilities in the field of fast reactor thermal-hydraulic simulation and analysis of sodium natural circulation phenomena, the different steps defined by the CRP have been followed:

— Blind calculations prior to the tests with assumed experimental conditions;

— Blind calculations posterior to the test with real experimental conditions;

— Post-experiment calculations with experimental data available.

The first set of blind calculations was carried out by the different participants on the basis of the CEA specifications of the Phenix reactor. Code-to-code comparisons were presented and discussed. However, these results could not be directly compared to the experimental data, since the real test conditions significantly differed from the boundary conditions initially specified. In particular, the core power had been considered constant up to the reactor scram, without consideration of the core response to the increasing core inlet temperature – which leads to a 40% reduction of the core power during the first 450 s of the test before the scram.

Considering the large discrepancies between the specified boundary conditions and the real test conditions, it was decided to perform a second set of blind calculations before providing the participants with the test results. It was decided to use the experimental power evolution as boundary conditions in order to reduce the possible source of errors and facilitate the comparison of the thermal-hydraulic results. Furthermore, a calculation scheme was established, i.e. the participants agreed to do the necessary adjustments of their model on the basis of the normal operating condition (at 350 MW(th)) and used the developed model as is for the analysis of the NC test (starting from a reduced

power of 120 MW(th)). This procedure should limit the number of adjustments as well as enable further validation of the models at steady-state.

Since the first set of blind calculations significantly differed from the experimental results due to the above-mentioned reasons, only the second set of blind calculation, performed with the real test conditions, are presented here. In the first section, each participant presents his own analysis of the test, based on the blind results. Then, the second section presents the post-test calculations, including the improvements performed with use of the experimental results. Finally, the code-to-code comparisons are presented at the end of this Section.

6.2. BLIND CALCULATIONS USING PHENIX TEST CONDITIONS

6.2.1. ANL

6.2.1.1. Boundary conditions

The CEA provided a table with their estimate of the core power during the transient, derived from measured data prior to scram and their own decay heat model afterwards. They also provided the measured steam generator outlet temperature at a 1 Hz frequency during the test. Because SAS4A/SASSYS-1 limits the number of entries in the power table to 20 and the steam generator temperature table to 14, the data in the two tables was reduced. The maximum error in the data reduction was estimated to be 4% for the power data and 7°C for the steam generator temperature data. Note that the mass flow rate weighted average of the two steam generator temperatures was used at each time step.

For the flow boundary condition, the CEA provided the evolution of the pump impeller speed (rev/min) of each primary and secondary pump. They also provided the flow rate evolution for the secondary pumps. The SAS4A/SASSYS-1 primary and secondary pumps are represented using the homologous pump model. When employing this model, the pump torque is specified as a function of time. The key is to match the pumps' flow and head to the specifications at the steady-state condition, and then provide the appropriate tables of relative pump torque vs. time. Although the SAS4A/SASSYS-1 results will not correctly predict the pump torque and speed accurately, the predictions of the pump flow are expected to be accurate as long as the flow and head are correct during steady state. In the case of the primary pump, the transition is relatively straightforward since the motor is shut off completely. Thus, the relative torque goes from 1.0 to 0.0 in one second. The secondary pump speed decreases approximately linearly over the course of a minute while the flow rate is diminished by a factor of 5. These pump coast downs were represented by a simple table of torque vs. time with only 4 points. The resulting primary pump speed was found to reach zero 10 seconds later than the CEA specifications. The secondary circuit flow rate was found to agree well early in the transient, but the SAS4A/SASSYS-1 predictions exceed the measurements by 10 kg/s late in the transient, from 5000s to 12000s.

6.2.1.2. Results of code predictions

The CEA provided three different measured estimates of the core outlet temperature: the temperature measured at the outlet of the peak subassembly, the mean temperature for the entire core outlet, and the mean temperature of the inner core zone. Unfortunately, the discrepancy between these three measured evolutions is typically smaller than the discrepancy between the measured and predicted evolutions. Immediately following the scram, the core subassembly outlet temperature drops dramatically, and then rises dramatically in response to the shutoff of the primary pumps. The SAS4A/SASSYS-1 predictions seem to exaggerate both the drop in temperature in response to the scram and the rise in temperature in response to the pump coast down. The peak core outlet

temperature occurs just prior to 800 sec, in both the measured and predicted evolution, at which point the predicted temperature is approximately 485°C, but is only 460°C even for the peak subassembly outlet. The discrepancy in outlet temperature may be due to inadequate modeling data for the intra-assembly above-core structures, or heat transfer from the hot pool. According to the measured evolutions, the core outlet temperature levels off or slowly declines following this sharp rise, but the predictions show a more rapid decline in temperature. Thus at 1800 sec, the discrepancy between the predicted core outlet temperature and measured peak subassembly outlet is reduced somewhat. Again, late in the transient, the agreement between the predicted and measured evolutions improves.

The IHX primary inlet temperature evolution tends to agree within 5°C early in the transient. The apparently rapid rise near t=1700 sec is actually caused by a shift in the thermal stratification model—the thermal layer adjacent to the IHX inlet shifted at one time step, causing a sudden increase in temperature. With only three temperatures representing the entire hot pool, such sudden changes in the local temperature are expected. Following this change at 1700 sec, the SAS4A/SASSYS-1 predictions tend to over predict the inlet temperature by approximately 10°C. Because of the 40°C difference in the initial temperature at the IHX outlet the agreement is poor early in the transient. At the time of the scram, the predictions are within 10°C of the provided measured values. Later in the transient, the discrepancy in the temperature exceeds 20°C.

The measurements for the hot pool sodium level are rather noisy but the mean elevation appears to be slightly higher than the SAS4A/SASSYS-1 predictions. Note that the density effect associated with the over prediction of the hot pool temperature (as can be inferred from the IHX primary-side inlet and core outlet temperatures) would tend to raise the hot pool level. Thus, it is anticipated that the under prediction of the sodium level in the hot pool is actually a hydraulic effect. The difference in hot pool and cold pool elevations are a function of pressure drops in the primary coolant system, in particular the pressure drop across the IHX tube bundle. It is expected that the under prediction of the sodium level in the hot pool corresponds to an over prediction of the cold pool level and under prediction of the IHX pressure drop. Pressure drops in the hydraulic circuit will be investigated for the final post-test analysis.

The predicted secondary-side outlet temperature agrees fairly well with the measured data. Because this provides the boundary condition for the primary coolant system, good agreement should be required to prevent error propagation. The predicted values tend to be higher than the measurement, which implies under-prediction of the heat removal rate from the IHX.

6.2.2. CEA

We compare the CATHARE code prediction and the Phenix data for the following parameters:

- Core inlet temperature assumed to be the pump inlet temperature (*);
- Average core outlet temperature;
- Primary coolant temperature at IHX inlet;
- Primary coolant temperature at IHX outlet;
- Secondary coolant temperature at IHX outlet;
- Hot pool, cold pool, reactor vessel cooling system levels;

The evolution of other parameters - not measured in Phenix reactor - seems interesting in order to understand the physical phenomena and the code prediction:

- Total core mass flow rate
- Mass flow rates in the different regions of the core
- Reactor cooling vessel flow rate
- IHX heat removal

— Hot/cold pools heat exchanges

— Heat removal by vessel cooling system and by the roof.

(*) After analysis, it turned out that the value given by the core inlet sensor is not consistent when the primary pumps are stopped. In fac

t, the core inlet sensor is located in a small bypass line at a relative higher elevation than the physical elevation of the core inlet. When the primary pump are stopped:

— There is no flow in this sensor bypass line: the fluid becomes stagnant;

— The sensor is disturbed by the external conditions.

Therefore, for the post-analysis test, the comparison between code and experimental data will be made with the 'primary pump inlet' temperature (sensor of the DOTE pole of thermocouples at the elevation z=-5400mm, which is the elevation of the primary pump inlet tube).

6.2.2.1. Short term (t = 0s – 1800s)

Core inlet temperature

The CATHARE code predicts the increase of temperature due to the loss of heat sink. But the thermal inertia seems slightly overestimated and the maximum temperature is 15°C lower than in Phenix (a part of this underestimation is due to the thermal inertia of the lower plenum below the core). After the scram, the cold shock occurs with a delay: the code prediction is consistent with the Phenix experimental data.

Core outlet temperature

The initial core outlet average temperature calculated by CATHARE is about 10°C lower than the reactor one. The Phenix core average temperature is higher because it is based on the monitored fuel assemblies, as the CATHARE one is calculated for the whole core. The cold shock induced by the decrease of the core power after the steam generator dry-out is over-predicted by CATHARE code. So, the temperature before the scram is about 20°C lower than in Phenix. The cold shock induced by the scram is well predicted. Then, the primary pump trip and the onset of natural convection produce an increase of temperature. With the assumption of a full mixing at whole core outlet in the CATHARE calculation, the hot shock is delayed: the maximum temperature is reached at 1000s, whereas it is reached at 700s in Phenix. Afterwards, the slow decrease of temperature is correctly predicted by the code.

Primary coolant temperature at IHX inlet

The initial IHX primary inlet temperature calculated by CATHARE is about 6°C lower than the reactor one. This could be linked to the initial under-estimation of the core outlet average temperature in CATHARE calculation. The cold shock induced by the decrease of the core power after the steam generator dry-out is over-predicted by CATHARE code, as for the core outlet average temperature. Then, the slope of the temperature decrease measured in Phenix is well predicted.

Primary coolant temperature at IHX outlet

The initial IHX primary outlet temperature calculated by CATHARE is a few degrees lower than the reactor one. The rapid increase of temperature due to the steam generator dry out is well predicted, with a small under-estimation of the maximum temperature. The cold shock produced by the scram is under-estimated in the calculation. This is due to the large temperature gradient at the IHX outlet window as CATHARE calculates an average temperature. Then, the stabilization of the temperature is correctly estimated by the code.

Secondary coolant temperature at IHX outlet

The secondary coolant flow rate in one IHX and temperature at IHX inlet are inlet boundary conditions for the calculation. The initial secondary coolant temperature at IHX outlet is well predicted by CATHARE. Before the scram, the decrease of temperature is overestimated by the code (-5°C). During the transition between forced convection and natural convection, the CATHARE code gives the right global trends. When the natural convection is well established (t>800s), the CATHARE results are quite good.

Hot pool, cold pool, reactor vessel cooling system levels

At nominal state, due to the CATHARE modeling choices (volume module), the code computes three free levels:

- The hot pool level;
- The cold pool level;
- The reactor cooling vessel system level.

The CATHARE calculations are consistent with the Phenix data, taking into account the sensors uncertainties. Before the scram, due to the heating of the lowest part of the reactor vessel, there is a slight increase of all the levels in the reactor (+3cm for the hot pool level, +8cm for the cold pool level and +4cm for the reactor vessel cooling system level). When the scram and the primary pump trip occur, as long as the mass flow rates in the hydraulics paths of the reactor vessel are shrinking:

— The hot pool level decreases.

— The cold pool and reactor vessel system levels increase.

CATHARE predicts these trends, but we can notice that the fall of hot level is slightly under-predicted by CATHARE code (-2 cm for CATHARE code and -6 cm for Phenix data).

Total core flow rate

In the CATHARE calculation, the primary coolant flow rate follows the trend of the primary pump speed: nearly a constant value before the scram and a drastic fall at the primary pump trip with a minimum value of 20kg/s. Then, with the development of natural convection, the core flow rate increases slowly up to 30 kg/s at 1800s. Unfortunately, there is no flow rate measurement in the primary circuit of Phenix reactor to be compared with the calculation.

Mass flow rates in CATHARE fissile and fertile zones

In the fissile zone, CATHARE calculates an upward flow during the whole first phase. In the fertile and blanket zones, CATHARE code predicts a reverse flow at the onset of the natural convection regime, until t=800s where the flow becomes upwards again.

Reactor vessel cooling flow rate

At nominal condition, the reactor cooling vessel flow rate is supposed to be 10% of the primary pumps mass flow rate. When the primary pumps are stopped:

— The reactor vessel cooling system flow rate decreases;

— The reactor cooling system level increases.

Due to the reactor design, CATHARE predicts a reverse flow in the reactor vessel cooling system. This reverses flow remains during the whole transient.

IHX heat removal

At the initial state, the IHX heat exchanges are estimated to 28 MW per IHX. Due to the steam generator dry-out, the secondary IHX coolant inlet temperature increases. Therefore, the IHX heat

removal decreases to nearly zero. When the scram and the primary pumps trip occur, the heat removal remains very low. When the natural convection is established and the total core mass flow rate increases slightly, the IHX heat removal follows this trend.

Due to the stratification at IHX windows in Phenix plant during the transition between forced convection and natural convection, heat balance estimation based on IHX inlet and outlet temperatures could lead to wrong values.

Hot/cold pools heat exchange

The heat exchange between the hot and cold pools at the initial state induces stratification in the cold pool: CATHARE predicts nearly 50°C of stratification in the cold pool.

During the first step (steam generator dry-out phase), there is a drastic decrease of the hot/cold pool heat exchange (from 3MW to 1.6MW) due to the heating of the lowest region of the reactor. At the primary pumps trip, there is a second fall of the heat exchange between the hot and cold pools (from 1.6MW to 1.1MW). Then, the heat exchange remains constant at about 1.1 MW.

Heat removals by vessel cooling system and by the roof

Heat removals are boundary conditions for the calculation. At nominal condition, heat removal by the vessel cooling system and by the roof is much lower than heat removal through IHXs. But, in natural convection, it is important to take into account these heat sinks.

Heat removal by the vessel cooling is constant before the scram (around 0.32 MW) and after the scram slightly increasing (from 0.32MW to 0.39MW). Heat removal from the roof is constant during the transient (0.16 MW).

6.2.2.2. Long term (t = 1800s – 25000s)

Core inlet temperature

During phase 2 (natural convection on heat losses), CATHARE predicts correctly the slow increase of temperature. The phase 3 (natural convection with an efficient heat sink) begins at t=10 500s, but CATHARE code predicts the beginning of temperature decrease with some delay, due to the modeling and the over-estimation of the thermal inertia in the lower part of the cold pool. Then, the calculation is correct on the decrease of the pump inlet temperature.

Core outlet temperature

During phase 2 (natural convection on heat losses), the CATHARE prediction of the average core outlet temperature is consistent with Phenix data: the temperature decreases from 432°C to 425°C in nearly 3 hours, when Phenix data show a decrease from 435°C to 427°C.

During phase 3 (natural convection with an efficient heat sink), Phenix cooling is faster (-12°C/hour) and the code is consistent with the Phenix data.

Primary coolant temperature at IHX inlet

During phase 2, the CATHARE temperature is nearly constant around 425°C, as Phenix data show a small decrease from 430°C to 424°C.

During phase 3, the effect of opening the steam generator casing occurs later in CATHARE than in Phenix. Then, the cooling rate calculated by CATHARE is smaller than Phenix one. At t=24 000s, CATHARE predicts a temperature of 400°C when the Phenix data gives 387°C. This discrepancy could be linked to an inappropriate modeling of the thermal inertia of the hot pool by CATHARE code with a complex geometry and several hydraulics paths in natural convection.

Primary coolant temperature at IHX outlet

During phase 2, CATHARE calculates a slight decrease of the primary coolant IHX temperature (from 420°C at t=1000s to 403°C at t=5000s and 400°C at t=10000s). In Phenix, the evolution of the temperature is 410°C to 405°C from t=1000s to t=10 000s.

When phase 3 begins at t=10 500s, CATHARE predicts first a fall of the IHX outlet temperature (-20°C in 1500s) and after, a smoother cooling (-35°C in 10000s). In Phenix, the fall of temperature is lower (-12°C) and the long term cooling rate close to CATHARE cooling rate (-35°C in 10000s).

Secondary coolant temperature at IHX outlet

The secondary coolant flow rate in one IHX and temperature at IHX inlet temperature are inlet boundary conditions. During phases 2 and 3, Phenix data show that the secondary coolant temperature at IHX outlet follows the primary coolant at IHX inlet.

CATHARE also predicts such trend. As CATHARE over-estimates (about 10°C) the primary coolant temperature at IHX inlet, the secondary coolant temperature at IHX outlet is also over-estimated of about 10°C.

Hot pool, cold pool, reactor vessel cooling system levels

During phase 2, CATHARE predicts a slight increase of the hot pool level when Phenix data remains nearly constant (+1cm). For the cold pool and the reactor vessel cooling system levels, CATHARE predicts a higher increase compared to Phenix (+5cm and +8cm for CATHARE, +2cm and +4cm for Phenix).

During phase 3, all the levels decrease as the cooling of the reactor vessel is more efficient. For the hot pool level, due to the modeling of thermal inertia, the beginning of the level decrease occurs later (+1000s) in CATHARE than in Phenix. For the cold pool level, CATHARE predicts first a small increase of the level and then a constant decrease. Phenix data do not show the first increase (maybe because the sensor is located inside a primary pump cavity), then the agreement is good with CATHARE. For the reactor vessel cooling system level, CATHARE also predicts a first peak (+2cm for CATHARE, +0.5 cm in Phenix) and then a correct constant decrease. To sum up, CATHARE predicts rather well the different trends of the free levels.

Total core mass flow rate

During phase 2, CATHARE predicts an increase of the total core mass flow rate from 22 kg/s at t=1000s to nearly 40 kg/s at t=10 500s. During phase 3, with higher heat sink, CATHARE predicts an increase of the total core mass flow rate from 40 kg/s to 65 kg/s.

Mass flow rates in CATHARE fissile and fertile zones

In the fissile zone, CATHARE predicts an increase of the mass flow rate: from 30 kg/s to 40 kg/s during phase 2 and up to 60 kg/s during phase 3.

Outside fissile zone, predicts a small reverse flow during phase 2 and an increase of flow up to 5 kg/s during phase 3.

Reactor vessel cooling flow rate

In the CATHARE calculation, the reactor vessel cooling flow rate remains reversed during phases 2 and 3 at about 6 kg/s.

IHX heat removal

The heat removal per IHX estimated by CATHARE code is very low (around 0.2MW) during phase 2. But during phase 3, the code predicts a more significant heat removal per IHX (1.1 MW).

Hot/cold pools heat exchange

During phases 2 and 3, CATHARE predicts a decrease of heat exchange between hot and cold pools, as the temperature difference is decreasing. At the end of the test, the heat exchange is nearly zero.

Heat removal by vessel cooling system and by the roof

CATHARE predicts a nearly constant heat removal by the vessel cooling system (0.4 MW) and by the roof (0.16 MW).

6.2.2.3. Summary on CATHARE blind calculations

CATHARE code can predict the different phases of the Phenix natural convection test:

— Phase 1 (steam generator dry-out): this phase leads to an increase of the temperature in the lower part of the reactor vessel. Due to neutronics counter-effects, the core power falls drastically (fall of 60%). This phase finishes with a scram (cold shock at the core outlet) and the primary pumps trip (hot shock at the core outlet). CATHARE code shows its ability to predict the heating up of the lower part of the reactor vessel, even if due to the modeling choice, the thermal inertia is slightly over-estimated. The neutronics counter-effects are sightly over-predicted by the code;

— Phase 2 (natural convection on secondary loop heat losses): at the establishment of natural convection, the increase of the core outlet temperature is delayed in the calculation but the maximum value is correctly predicted. The core mass flow rate is relatively low and CATHARE calculates a reverse flow outside the fissile fuel assemblies. As the heat sink is low during this phase, the temperature in the vessel remains quasi-constant as CATHARE predicts a slow increase of temperature in the hot pool and a slow decrease of temperature in the cold pool;

— Phase 3 (natural convection with an efficient heat sink): the cooling function by the IHX is restored, and the stratification between upper and lower part of the reactor vessel increases. CATHARE code is in good agreement with Phenix measurements, with a delay on the core inlet temperature decrease due to assumptions on the cold pool thermal inertia.VI.2.c. IGCAR .

6.2.3. IGCAR

6.2.3.1. 3D calculation

The STAR-CD code predictions are compared with Phenix data for the following parameters:

— Pump inlet temperature;

— Average core outlet temperature;

— Primary coolant temperature at IHX inlet;

— Primary coolant temperature at IHX outlet;

— Secondary coolant temperature at IHX outlet;

— The other parameters - not measured in Phenix reactor;

— Total core mass flow rate;

— Mass flow rates in the different regions of the core.

6.2.3.2. Short term (t = 0s – 1800s)

Pump inlet temperature

The initial steady state pump inlet temperature predicted by STAR-CD code is comparing well with the measured value. Following loss of heat sink in steam generator, the cold pool temperature and hence pump inlet temperature increases. The code predicts the increase in temperature. The predicted rate of increase in temperature is in reasonable agreement with the measured value. The predicted maximum temperature is about 12°C less than the measured value. This may be due to higher thermal inertia considered for the cold pool. However, beyond 1200s, the predicted temperature is comparing well with the measured value.

Core outlet temperature

The initial core outlet average temperature predicted by STAR-CD code is about 8°C lower than the measured value. The cold shock induced by the decrease of the core power after the steam generator dry-out is over-predicted. The predicted temperature before scram is about 20°C lower than the measured value. The cold shock induced by the scram is well predicted. The predicted drop in temperature is 24°C as compared to the measured value of 22°C. Then, the primary pump trip and the onset of natural convection increase the outlet temperature to a maximum value. The predicted temperature oscillates and the average value is about 25°C more than the measured value. The reason for the higher predicted value may be the delayed participation of thermal capacity of core structural material in the CFD model during the fast transient. In the CFD model, the structural material for each zone is modeled as a separate solid volume and the heat transfer surface area between solid and fluid is much less compared to the real value. This delays the sharing of thermal load by the structural material. It is clear from the results that with time, the deviation in predicted values is reducing and beyond 1800 s, the predicted temperatures are comparing well with the measured values.

Primary coolant temperature at IHX inlet

The initial steady state IHX primary inlet temperature calculated by STAR-CD code is about 5°C lower than the predicted value. This could be linked to the initial under-estimation of the core outlet average temperature. The cold shock induced by the decrease of the core power after the steam generator dry-out is over-predicted, as for the core outlet average temperature.

Primary coolant temperature at IHX outlet

The initial steady state IHX primary outlet temperature predicted by STAR-CD code is in agreement with the measured value. The rapid increase of temperature due to the steam generator dry out is well predicted, with a small under-estimation of the maximum temperature (~8°C). The cold shock produced by the scram is well predicted. The predicted decrease in temperature is 15°C as compared to the measure value of 18°C. The stabilized temperature is also estimated correctly by the code.

Secondary coolant temperature at IHX outlet

The secondary coolant flow rate in one IHX and temperature at IHX inlet are boundary conditions for the calculation. The initial steady state IHX secondary sodium outlet temperature is predicted well by the STAR-CD code. Before the scram, the decrease of temperature is overestimated by the code (-15°C). When the natural convection is well established (t>900s), the STAR-CD results are quite good.

Total core flow rate

The primary coolant flow rate predicted by STAR-CD code follows the trend of the primary pump speed: nearly a constant value before the scram and a drastic fall after the primary pump trip with a minimum value of 8.5 kg/s. Then, with the development of natural convection, the core flow rate increases gradually to 43 kg/s at 1800s. Since the flow is not measured, these values cannot be compared.

Mass flow rates in fissile and fertile zones

In the fissile zone, STAR-CD predicts upward flow throughout the transient. In the fertile and blanket zones, STAR-CD code predicts a reverse flow during the onset of the natural convection (until t=1100s) and subsequently the flow becomes upward.

Reactor vessel cooling flow rate

At nominal condition, the reactor cooling vessel flow rate is 140 kg/s. When the primary pumps are stopped, the flow decreases and reverses. The maximum reverse flow rate is -12 kg/s. The flow remains negative throughout the transient and stabilizes at -5 kg/s

IHX heat removal

During initial steady state, the heat transferred through IHX is predicted as 28.8 MW per IHX. Due to the steam generator dry-out, the secondary IHX coolant inlet temperature increases. Therefore, the IHX heat removal decreases to nearly zero. Following scram and pump trip, the heat removal is negligible. In fact, there is a small amount of reverse heat transfer i.e., from secondary sodium to primary sodium for about 1000s.

6.2.3.3. Summary on STAR-CD code blind calculations

STAR-CD code can predict the different phases of the Phenix natural convection test:

— Phase 1 (steam generator dry-out): this phase leads to an increase in the cold pool temperature. Star-CD code shows its ability to predict the heating up of the cold pool. But the reduction in core outlet temperature during this period is slightly over predicted. Reactor scram results in cold shock and the predicted magnitude of the shock is comparing well with the measured value;

— Phase 2: (primary pumps trip and development of natural convection): The pump trip results in increase of core outlet temperatures. The hot shock at the core outlet has been over predicted by about 25°C. This is attributed to the delayed participation of thermal capacity of core structural material of the CFD model. The natural convection core flow is estimated as 43 kg/s at 1800s. In the fissile zone, the STAR-CD code calculates an upward flow during the whole transient. In the fertile and blanket zones, the code predicts a reverse flow during the onset of the natural convection, until t=1100s, after which the flow becomes upward.

6.2.4. IPPE

GRIF code predictions were compared with the Phenix data for the following parameters:

— Pump inlet temperature;

— Average core outlet temperature;

— Primary coolant temperature at IHX inlet;

— Primary coolant temperature at IHX outlet;

— Secondary coolant temperature at IHX outlet;

and with the results of calculations of other participants for the following parameters (not measured in Phenix reactor):

— Total core mass flow rate;

— Mass flow rates in the different regions of the core;

— Reactor cooling vessel flow rate;

— IHX heat removal;

— Pump head;

— Core pressure difference;

— IHX pressure difference.

Hot pool, cold pool, reactor vessel cooling system levels were not calculated in GRIF code. Hot/cold pools heat exchanges and heat removals by vessel cooling system and by the roof were not included in code output during blind stage of calculations.

6.2.4.1. Short term (t = 0s – 1800s)

Pump inlet temperature

The GRIF code predicts the increase of temperature due to the loss of heat sink with time delay 100-150 seconds refer to experiment. The maximum temperature is 10°C lower than in Phenix.

Core outlet temperature

The initial core outlet average temperature calculated by GRIF goes down after the loss of heat sink much faster than in experiment and reaches its local minimum value - 410°C. The corresponding Phenix core average temperature is higher - 435°C. After SCRAM calculated core outlet average temperature reaches its next minimum - 388°C which is 23°C less than experimental value.

Primary coolant temperature at IHX inlet

The initial IHX primary inlet temperature calculated by GRIF is equal to the reactor one. Then IHX primary inlet temperature follows the variation of core outlet temperature with some delay. Overcooling of the core during initial stage results in overcooling of sodium in the upper plenum.

Primary coolant temperature at IHX outlet

The initial IHX primary outlet temperature calculated by GRIF is a 17°C degrees lower than the reactor one. But the further transient behavior of that temperature is close to experimental data.

Secondary coolant temperature at IHX outlet

The secondary coolant temperature at IHX outlet is not very well predicted by GRIF for initial stage of transient. The reason of too large temperature drop after loss of heat sink and scram that is predicted by GRIF is overcooling of sodium in the core and upper plenum.

Total core flow rate

Due to misprinting of this value the sum of two flow rates –'core +vessel cooling flows'- is presented in the figure. If to subtract vessel cooling flow rate then the initial value will be close to the results of other participants.

The primary coolant flow rate rundown after scram is reproduced by GRIF coherently with results of other participants. The flow rate due to the development of natural convection is approximately equal to 20 kg/s, which is less than predictions of other participants.

IHX heat removal

IHX heat removal is an integral parameter and it is well predicted by GRIF and by all other codes.

6.2.4.2. Long term (t = 1800s – 25000s)

For long term (natural convection on heat losses), GRIF calculations of temperature are in better agreement with Phenix data than for short term. Code correctly predicts the tendency of parameters

variations. The deviation of calculated temperature from experiment for final stage (after opening of SG containments) normally doesn't exceed 5°C.

6.2.4.3. Summary on GRIF blind calculations

Comparison of blind GRIF calculations with experimental data and results of other participants show that GRIF code reasonably reproduces the transient behavior of most parameters.

- For initial stage the most pronounced deviation of GRIF calculation from experimental data is time delay in the increase of sodium temperature at core inlet. This delay leads to overcooling of the core and upper plenum and the differences between calculated and measured temperatures for some time instants can reach a 30-35°C. One of possible explanations of such divergence could be the underestimation of initial average sodium temperature in cold plenum. This possibility was investigated during the sensitivity study that was performed before final round of calculation of NC-test;
- For long term agreement of GRIF calculations with experiment could be classified as acceptable

6.2.5. IRSN

This part presents the CATHARE blind calculations results from IRSN.

A key parameter for any test in natural circulation is the mass flow rate evolution. However, no measurement was available for the primary circuit. The instrumentation used for nominal regimes is actually not adapted for low flow rate regimes. With CATHARE, the total core mass flow rate drops from 1284 to 85 kg/s after the primary pumps trip and then stabilizes at 95 kg/s. This value is not consistent with a quick estimation based on the balance between friction and buoyancy forces for a loop in natural circulation. A value of about 50 kg/s is indeed found with this method. This difference was later explained by an error in the IHX length and inlet location. A length of 5365 mm was used for the blind calculation (representing the total heat transfer length given in the data package) instead of 4795 mm (according to the Phénix schematic). This correction was taken into account for the post-test calculations.

Sodium levels measurements are available for the hot pool, the cold pool and the reactor vessel cooling system. However, the cooling circuit level was not modeled with CATHARE as not enough information was given in the data package concerning this zone. A common sodium level was then used for both the cold pool and the cooling circuit. No specific tuning was done for reproducing the levels evolution.

The CATHARE results can be compared with the following temperature measurements in the short (0 – 2000 s) and the long term (2000 – 24000 s):

- Core inlet temperature;
- Core outlet temperature;
- IHX primary inlet temperature;
- IHX primary outlet temperature;
- IHX secondary outlet temperature.

Core inlet temperature

The temperature increase at the core inlet resulting from the steam generator dry-out is well predicted with CATHARE. The effect of the steam generators air cooling at 10320 s appears with some delay (2500 seconds) with CATHARE.

Core outlet temperature

The temperature measurement provided for the core outlet comes from the core temperature treatment system. Thermocouples are located at the outlet of all the fuel assemblies and some fertile assemblies. A simple arithmetical average is then used (sodium flow rates in each assemblies is not taken into account). Comparison with calculation results should be regarded with caution as different definitions can be used for the core outlet temperature. For blind calculations, IRSN chose to plot the average temperature at the assemblies outlet weighted with mass flow rates. The cold shock following the decrease of the core power after the steam generator dry-out is over-predicted by CATHARE. As a result, the core outlet temperature after the scram is about 10°C lower than the experimental value. The dynamics after the scram is well reproduced. On the long term, the temperature decrease is overestimated by 10°C.

Primary coolant temperature at IHX inlet

The initial temperature at IHX inlet is underestimated (~5°C), and the cold shock following the power decrease is overestimated (~5°C). With the CATHARE model, the cold shock occurring at the core outlet propagates to the IHX inlet, which is not the case during the test according to the measurement available. However, the temperature provided for the primary IHX inlet should be taken with caution. The thermocouple is located in the upper part of the IHX window, where flow rate and temperature heterogeneities appears. As a consequence, this measurement is not necessarily representative of the average temperature at IHX inlet.

On the long term (after 15000 s), the temperature decrease is well predicted overall. The effect of the steam generators air cooling at 10320 s appears also with some delay (2500 seconds) with CATHARE.

Primary coolant temperature at IHX outlet

The cold shock following the scram (458 s) is underestimated. However, the measurement may not be representative of the average temperature at IHX outlet owing to large temperature gradients in the window area.

Secondary coolant temperature at IHX outlet

The temperature decrease occurring before the scram (458 s) is overestimated by 10°C. After the primary pumps trip (466 s), the secondary sodium temperature at IHX outlet gets lower than the secondary sodium temperature at IHX inlet, which means that the primary sodium is cooling the secondary sodium for a while.

6.2.6. KAERI

One of the most important parameters in this test is the natural circulation flow rate after the trip of primary pumps. However, the core flow rate has not been measured directly in the test. Therefore, the predictability of the MARS-LMR code can be evaluated through the comparison of the measured data and the calculated values of the following parameters:

— Pump inlet temperature;

— Average core outlet temperature;

— Primary coolant temperature at IHX inlet;

— Primary coolant temperature at IHX outlet;

— Secondary coolant temperature at IHX outlet;

— Hot pool, cold pool, reactor vessel cooling system levels.

Some other parameters, which have not been measured in the test but useful to understand the real phenomena, are predicted by the MARS-LMR code and compared with the results obtained from other participants. These parameters are as follows:

— Reactor cooling vessel flow rate;

— IHX heat removal;

— Core pressure drop;

— Hot/cold pools heat exchanges;

— Heat removals by vessel cooling system and by the roof.

6.2.6.1. Short term (t = 0s – 1800s)

Total core flow rate

In the MARS-LMR calculation, the primary coolant flow rate before the pump trip is calculated by the intrinsic pump model with a given pump speed. And the primary flow rate after the pump trip is described by the pump speed measured in the Phenix test. It is evaluated that the total primary flow before the pump trip calculated by the MARS-LMR is nearly identical to the design flow. The core flow rate after the pump trip is determined by the balance between the flow resistance at core and the resistance through the vessel cooling flow path. The core flow rate after the pump trip falls to the minimum of about 20 kg/s at 600 seconds after the initiation of the transient. After that, as the natural circulation becomes active, the core flow rate increases slowly to 40 kg/s at about 1400s. The calculations of core flow rate by other participants show similar behavior. The asymptotic value of core flow rate in other calculations spreads between 20 kg/s to 60 kg/s.

Pump inlet temperature

The pump inlet temperature measured in Phenix test is compared with the MARS-LMR prediction. The test data shows an abrupt increase at the initial stage of the test due to the imbalance between the heat generation at core and the heat removal through the IHXs. MARS-LMR over-predicts the initial peak temperature by about 10°C. After the scram, the predicted pump inlet temperature remains 20°C higher than the measured data. The reason of this discrepancy can be found from the nodalization effect, heat structure modeling and others

Average core outlet temperature

In the MARS-LMR prediction of core outlet temperature, the thermal inertia is slightly under-estimated. Therefore, the prediction shows a large decrease and increase before the reactor scram when it is compared to the measured data, which is not revealed in the real test. The temperature decrease caused by the reactor scram is well predicted with the code. However, the temperature increase after the scram due to the pump trip and the formation of natural circulation is slightly over-estimated. The measured data of core outlet temperature shows a steep increase until it reaches a stable temperature plateau at 700s after the initiation of the transient. However, the average temperature at core out region predicted by the MARS shows a mild increase, which is mainly due to nodalization effect

Primary coolant temperature at IHX inlet

The sodium temperature at IHX inlet in hot pool region predicted by the MARS-LMR is lower than the measured one. The reason of this over-estimated temperature decrease can be found from the inaccuracy in the modeling of heat structure distribution and the increased mixing in the hot pool due to the one-dimensional nodalization. The trend of temperature decrease after 1000s is well predicted by the MARS-LMR code with the underestimation about 5°C

Primary coolant temperature at IHX outlet

The MARS-LMR prediction includes initially underestimated primary IHX outlet temperature. This underestimation is maintained during the early stage of temperature increase before the reactor scram. The trend of temperature increase is accurately represented by the MARS-LMR. However, the drastic temperature decrease after the scram followed by the primary pump trip is not described in the MARS prediction. This discrepancy can be understood if one considers that the temperature is measured at one point at IHX outlet and the prediction is for a large volume of cold pool near the IHX out region. The mild temperature decrease after that is well predicted by the MARS-LMR.

Secondary coolant temperature at IHX outlet

The initial decrease of secondary temperature at IHX outlet before the reactor scram is also overestimated as the primary coolant temperature at core outlet and IHX inlet. The temperature trend after the reactor scram is dependent on the primary IHX inlet temperature and the primary flow rate through the IHXs as the natural circulation builds up. The temperature decrease after 1000s is also governed by the secondary mass flow rate which has been imposed as a boundary condition in the calculation. The accuracy of the prediction is maintained within 10°C of error band.

Hot pool, cold pool levels

With the MARS-LMR modeling of Phenix system, the hot pool and cold pool levels can be calculated. The general trend of the MARS-LMR prediction of pool levels is consistent with the test data. The initial pool levels and the level increase before the scram are predicted very accurately by the MARS-LMR. After the reactor scram and the primary pump trip, the level difference between the hot pool and the cold pool decreases due to the loss of pump head, which causes the decrease of hot pool level and the increase of cold pool level. The level decrease in the hot pool is underestimated in the MARS-LMR prediction by about 5cm and the increase of cold pool level is also underestimated by about 5cm.

Reactor vessel cooling flow rate

At the steady state of 120 MW reactor power, the reactor vessel cooling flow rate is predicted to be 6% of the primary flow rate. With the primary pump trip, the vessel cooling flow rate also decreases abruptly and reaches a reverse flow regime.

IHX heat removal

At the reactor power of 120 MW, the heat transfer from one IHX is about 30 MW. As the steam generators become dry-out, the secondary IHX inlet temperature increases and the heat removal rate from the IHXs decreases continuously. The IHX heat removal rate finally reaches to negative value at the time of reactor trip and primary pump trip. Then, the heat removal rate is recovered slightly with the development of natural circulation in the primary system.

Hot/cold pools heat exchange

The heat exchange between the hot and cold pools at initial condition is estimated to be about 0.5 MW. During the steam generator dry-out, the heat exchange between the two pools shows a sudden decrease and increase following the temperature change at core outlet region. After the reactor trip and the primary pump trip, the heat exchange drops again and then it reaches a plateau of 0.4 MW.

6.2.6.2. Long term (t = 1800s – 25000s)

Total core mass flow rate

In this phase of transient, the total core flow rate predicted by the MARS-LMR increases from 40 kg/s at 1800s to 50 kg/s at about 3500s. Then, it decreases to about 40 kg/s and increases again up to 50 kg/s with a more active heat removal to the secondary side through the IHXs.

Pump inlet temperature

The temperature difference between the measured data and the predicted by the MARS-LMR is about 20°C at 1800s. After that, the MARS-LMR prediction shows different trend with the test data. The reason of this discrepancy is presumed to be caused from the nodalization effect, heat structure modeling. In the later phase after 10000s, the MARS-LMR predicts the general trend of the temperature change.

Average core outlet temperature

The MARS-LMR over-predicts the core outlet temperature by 30°C at 1800s. During the time period from 1800s to 10000s, the core outlet temperature predicted by the MARS-LMR is still higher than the test data even though the over-prediction decreases with the time elapse. This means there is some distortion in the preliminary MARS-LMR modeling of flow paths and heat transfer paths, which should be assessed in more detail. The prediction by the MARS-LMR is consistent with the Phenix data in the later phase after 10000s.

Primary coolant temperature at IHX inlet

The MARS-LMR predicts the test data of IHX inlet temperature reasonably within the error band of 10°C before 10000s. The oscillations are mainly due to the oscillations in the secondary mass flow rate in IHXs which has been imposed as a boundary condition in the simulation. The cooling rate after 10000s is over-predicted by the MARS-LMR, which is also due to the higher secondary flow rate and a distortion in the modeling of thermal inertia of hot pool.

Primary coolant temperature at IHX outlet

The long term behavior of the IHX outlet temperature is predicted successfully by the MARS-LMR. The cooling rate in the MARS calculation just after 10000s is a little bit higher than the Phenix data. However, the cooling rate after 15000s is close to the test data.

Secondary coolant temperature at IHX outlet

The secondary coolant temperature at IHX outlet is a function of the secondary flow rate through the IHXs and the heat transfer from the primary side to the secondary side. In the MARS-LMR calculation, the heat removal through the IHXs is over-predicted. Thus, the temperature at IHX outlet is 10°C higher than the test data before the time of 10000s. The over-prediction diminishes in the later phase.

Hot pool, cold pool levels

The general trend of the level in hot pool is well predicted with the MARS-LMR code all through the transient. The initial increase in cold pool level up to 5000s is also reproduced correctly in the simulation. At the time of opening of steam generator casing (t=10500s), MARS-LMR gives an abrupt increase of cold pool level followed by a mild decrease. In the later phase, the rate of level decrease in test data is larger than the MARS-LMR prediction. This discrepancy could be caused by the unrealistic modeling of the upper part of the reactor vessel cooling system. The maximum deviation of the calculated levels from the measured data is less than 5cm.

Reactor vessel cooling flow rate

In the MARS-LMR calculation, the reverse flow through the vessel cooling path is decreased continuously and becomes positive in the later phase after 15000s.

IHX heat removal

The average heat removal per IHX predicted by the MARS-LMR is about 0.6MW before the opening of steam generator. After the opening, it increases to 1.0MW.

Hot/cold pools heat exchange

In the MARS-LMR calculation, the heat transfer from hot pool to cold pool decreases continuously as the temperature difference between the two pools decreases. During the very later phase of the transient, it is predicted that there exists reverse heat transfer from cold pool to hot pool.

6.2.6.3. Summary on MARS-LMR blind calculations

The MARS-LMR predictions for the three different phases of the Phenix natural circulation test are summarized as follows:

— Early phase (0s ~ primary pump trip): In this phase, the heat removal through the IHXs is decreased drastically due to the dry-out of steam generators, which causes a sudden increase of core inlet temperature and IHX outlet temperature in primary side. This increase of coolant temperature in core region results in the decrease of core power due to temperature feedback effect. The MARS-LMR simulation is estimated to describe the heat-up process correctly even though it predicts a little bit higher core outlet temperature and a slightly smaller thermal inertia.

— Mid phase (primary pump trip ~ opening of SG casing): After the reactor trip and primary pump trip, the core outlet temperature experiences a sudden drop and increase. With the development of natural circulation in the primary side, the rate of temperature increase at core outlet decreases and finally the core cool-down begins to be effective. The MARS-LMR predicts correctly the initial drop and increase of core outlet temperature. However, MARS-LMR calculation shows a continued increase of core outlet temperature up to 30°C higher than the test data. This discrepancy suggests that there exist some distortion in the modeling of flow path and heat transfer path mainly come from the nodalization effect and heat structure modeling in MARS-LMR simulation.

— Later pase (after the opening of SG casing): The heat removal rate is increased by the opening of the SG casing. The general trends of MARS-LMR prediction are in good agreement with the Phenix data.

6.2.7. PSI

6.2.7.1. Steady-state results

As mentioned in the introduction, the different members participating in the CRP agreed to perform the necessary model adjustments (due to limited design specifications) on the basis of the nominal Phenix operating conditions, viz. corresponding to 350 MW(th). The model has been used as such to simulate the Natural Convection test, starting from the reduced power at 120 MW(th).

This section presents the different adjustments of the TRACE model, performed for zero power at 400°C and for 350 MW(th), together with the comparison of the computed steady-state results with the test data at both nominal and reduced power.

6.2.7.2. Cold conditions: 400°C

In order to ensure that the circuit elevations were accurately modeled, a simulation at zero-power, zero-flow was performed at 400°C (initialization temperature for all components). The results showed that no flow was numerically generated, and that the pool levels remained at the initial value of 1783 mm. This demonstrated that the relative elevations of the different components were correctly represented.

6.2.7.3.. Nominal power: 350 MW(th)

The next step in the validation of the model has been performed for nominal operating conditions, viz. at 350 MW(th), the pump rotational speed being set at 56.6 rad/s and the intermediate inlet temperature and flow rate at 320°C and 1380 kg/s, respectively.

At this stage, the losses in the diagrid were adjusted to reproduce the core and vessel cooling flow rates. It has been seen that the flow area of the diagrid mainly influenced the total pump flow, while the hydraulic diameter and friction factor in the lower part of the diagrid affected the flow distribution between the core and the vessel cooling system. The latter was adjusted to correspond to about 10% of the core flow rate. Due to a lack of detail in the design specifications, the diagrid flow area was adjusted to simulate the specified total flow with the specified pump head and rated values.

The inlet plenum friction losses were adjusted in order to reproduce the correct hot pool free surface elevation, which is determined by the diagrid and core friction losses. Then, the IHX geometry (mainly hydraulic diameter) was adjusted to reproduce the correct cold pool free surface elevation. The following tables present the comparison of the calculated flow distributions, pool elevations and temperatures with the test data.

TABLE 12. PSI MODEL - MASS FLOW RATE IN CORE CHANNELS AT 350 MW(th)

	Mass flow (kg/s)						
	Core	Inner core	Outer core	Fertile core	Storage	CR	Reflector
Phenix	1988	861	779	226	46	14	62
TRACE	1988.1	849.1	779.8	236.3	46.7	14.0	62.3
Δ	0.1	-11.9	0.8	10.3	0.7	0.0	0.3
ε (%)	0.0	1.4	0.1	4.4	1.5	0.0	0.5

TABLE 13. PSI MODEL - INLET AND OUTLET TEMPERATURES IN CORE CHANNELS AT 350 MW(th)

	Temperature (K)						Elevation (mm)		
	Inlet core	Outlet core	Inlet IHX 1	Outlet IHX 1	Inlet IHX 2	Outlet IHX 2	Hot pool	Cold pool	**Δ**
Phenix	658	798	798	658	593	798	2061	1325	736
TRACE	657.1	796.3	795.2	656.4	593	791.2	2175	1460	715
Δ	-0.9	-1.7	-2.8	-1.6	0.	-6.8	114	135	-21
ε (%)	0.1	0.2	0.4	0.2	0.0	0.9	5.2	9.2	2.9

It can be seen that the computed results agree very well with the experiment, with less than 5% differences on the mass flow rates and 1% on the temperatures. The highest discrepancies are seen on the values of the pool elevations, predicted with up to 13.5 cm absolute error. Overall, the computed results satisfactorily reproduce the Phenix measurements.

6.2.7.4. Reduced power: 120 MW(th)

As mentioned previously, the NC test was initiated from a reactor steady-state corresponding to the reduced power of 120 MW(th). The model described formerly was used as such, changing only the

following boundary conditions: power of 120 MW, pump rotational speed of 36.6 rad/s, secondary-side IHX inlet temperature of 308°C and flow rate of 760 kg/s. The table below gives the main results corresponding to this steady-state.

TABLE 14. PSI MODEL - MASS FLOW RATE IN CORE CHANNELS AT 120 MW(th)

	Mass flow (kg/s)						
	Core	Inner core	Outer core	Fertile core	Storage	CR	Reflector
Phenix	1284	1055		149	30	9	41
TRACE	1283.5	546.3	501.7	154.8	30.7	9.2	40.9
Δ	-0.5	-7.0		5.8	0.7	0.2	-0.1
ε (%)	0.04	0.7		3.9	2.3	2.2	0.2

TABLE 15. PSI MODEL - INLET AND OUTLET TEMPERATURES IN CORE CHANNELS AT 120 MW(th)

	Temperature (K)						Elevation (mm)		
	Inlet core	Outlet core	Inlet IHX 1	Outlet IHX 1	Inlet IHX 2	Outlet IHX 2	Hot pool	Cold pool	Δ
Phenix	631	705	705	633	581	705	1876	1569	307
TRACE	630.9	703.6	702.9	630.2	581	702.8	1922	1579	343
Δ	-0.1	-1.4	-2.1	-2.8	0	-2.2	46	10	36
ε (%)	0.02	0.2	0.3	0.4	0	0.3	2.4	0.6	10.5

The comparison of TRACE-computed results with the test data shows good agreement, thus demonstrating the validity of the model at an operating point different from that used for the model adjustments.

6.2.7.5. Transient results

The comparison of the TRACE pre-test results with the experimental data is presented in Fig. 60 – 61.

The first figure shows the evolution of the core temperatures calculated by TRACE and compared to the experimental data. The experimental inlet core temperature is only displayed up to the pump trip since this measurement is only relevant in forced convection (due to the position of the sensor).

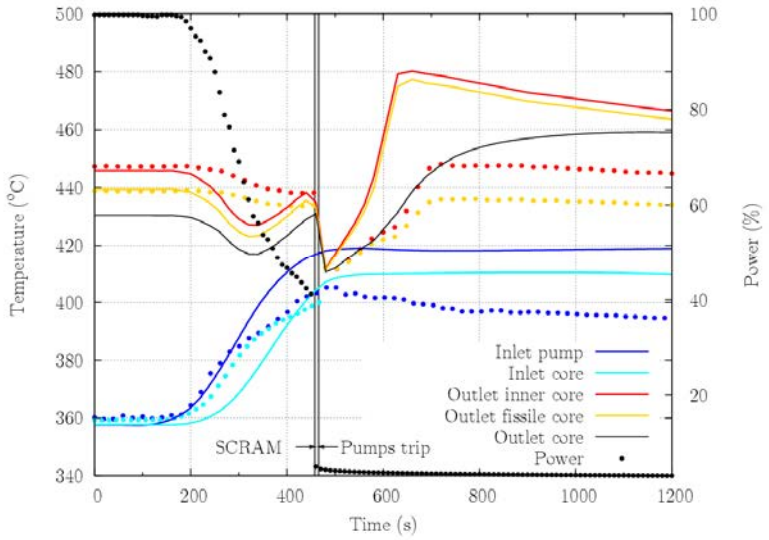

FIG. 60. PSI blind results: early phase of the transient (exp.: points, TRACE: solid lines).

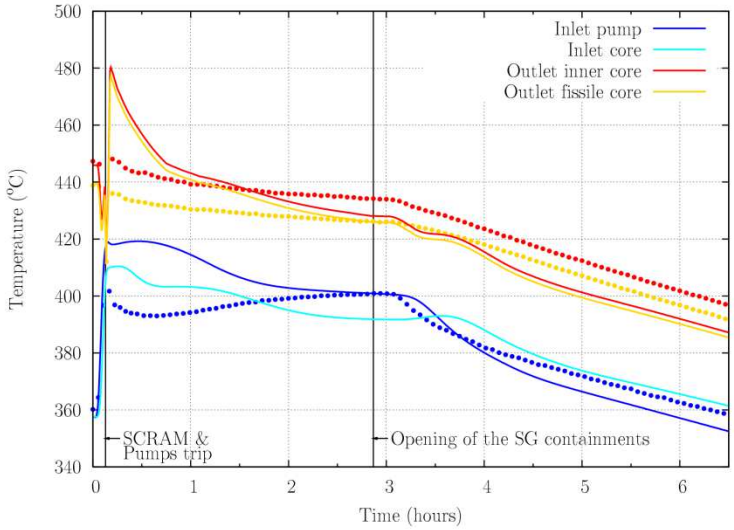

FIG. 61. PSI blind results: complete transient evolution of the core power and temperatures during the NC transient. (exp.: points, TRACE: solid lines).

At the beginning of the transient, the inlet pump and core temperatures increase. The short-term figure shows that TRACE predicts a constant rise rate, which results in an overestimation of the pump inlet temperature after ~300 s since the experimental increase rate starts to slow down at that time. This may be attributed to the formation of a convective flow in the lower part of the cold pool, which would be initiated by the increasing temperature difference and which would mix the cold sodium from the pool bottom with the hotter fluid coming from the IHX. This is not represented with the TRACE 1D model but might be improved using a 3D representation of the cold pool.

The predicted core inlet temperature follows the evolution of the pump inlet temperature with a time delay due to the thermal inertia of the diagrid structure. The comparison with the experiments, where

the two temperatures stay very close (within ~10°C), indicates that the pump and diagrid heat-transfer areas have been over-estimated in the present model and should be reduced in a post-test analysis.

The experimental inner-core and average fissile-core outlet temperatures are available for comparison with the calculated results. The sharp decrease in the reactor power only results in a small decrease (~10°C) of the experimental core outlet temperature due to the increase of the core inlet temperature and constant flow rate. It can be seen that TRACE predicts a sharper drop – due to an under-estimation of the inlet core temperature caused by the diagrid thermal inertia – succeeded by a slight increase, the rate of which is comparable to that of the inlet core temperature.

Thus, the predicted trends in the outlet core temperature can be understood from the evolution of the core inlet temperature, and a better prediction of the core inlet temperature should enable one to improve the calculated outlet temperature. It can be mentioned that a simplified core model presented in the frame of a point-kinetics analysis showed that TRACE satisfactorily predicted the outlet temperature when the experimental inlet core temperature was used as boundary condition.

After the reactor and pump trips, TRACE satisfactorily predicts the sharp drop measured in the core outlet temperature but largely over-predicts the following increase in temperature caused by the reduction of the flow rate. The post-test study has shown that the simulation of the core structures (mainly the SA wrappers) delayed the increase by 50 s, thus better reproducing the shape of the experimental data. However, the amplitude predicted by TRACE remains ~40°C too high, and the account of the over-predicted inlet core temperature would only explain ~20°C of the difference. The rest might be due to a change in either the flow rate or power distribution between the fissile core and the other core regions that are not reproduced in the model.

Also, it should be recalled that the temperature sensors are located 10 cm above the top of the SAs. Previous Phenix tests have shown that the SA outlet core temperatures are under-estimated by up to 30°C during the first minutes of natural convection, due to a chimney effect forming at the core outlet and the low coolant flow rate, especially during the establishment of natural convection, when the sodium in the hot pool is colder than at the core outlet. Therefore, one should be careful when comparing the test data with 1D-results, and a 3D representation of the hot pool could help to improve the computed results.

The long-term results for the core temperature evolutions are presented in Fig. 64. It appears that the pump inlet temperature is over-estimated during the first two hours of the transient. The differences between the computed pump and core inlet temperatures is related to the pump and diagrid thermal inertia. The error on the pump inlet temperature seems to pass on to the core outlet temperature, which is first largely over-estimated during the first hour and then under-estimated by ~15°C after 3 hours and towards the end of the transient.

Additionally, the figure below shows the evolution of the primary temperatures at the IHX inlet and outlet, along with the experimental data. At the beginning of the transient, the computed IHX outlet temperature is too low by 10 to 20°C, but the prediction is still satisfactory when one considers the high stratification of temperatures at the IHX outlet window – as much as 80°C variation at nominal power. However, TRACE does not predict the temperature drop measured at about 500 s, which coincides with the secondary flow rate reduction. After the secondary pump trips, the primary outlet IHX sodium temperature drops down to that of the secondary-side at the IHX inlet. This might come from the surrounding sodium in the cold pool, which would cool down the sodium in the IHX by conduction after the loss of flow.

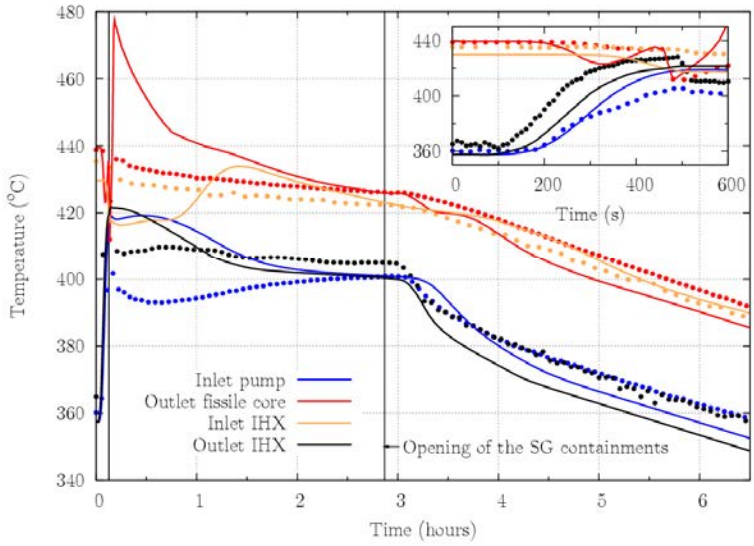

FIG. 62. PSI blind results: Evolution of the primary pool temperature during the NC transient (exp.: points, TRACE: solid lines).

In the TRACE results, the primary outlet IHX temperature follows the evolution of the secondary inlet IHX, which is used as boundary condition. An additional heat structure representing the IHX outer shell and its immersion in the cold pool could enable one to better reproduce the experimental results.

However, the actual model gives quite satisfactory results beyond the first hour after which, despite an under-estimation of the IHX outlet and core outlet temperatures by ~10°C, the evolutionary trend of the primary temperatures is well reproduced.

The analysis of the core flow rate distribution, presented below, shows that, after the pump trip, a reverse flow is predicted in the coldest channels. This illustrates the ealier mentioned modification of the hydraulic path at the core outlet, through the formation of a chimney effect in the hottest channels of the fissile core and a reverse flow in the lateral, cold part of the core.

A more detailed analysis revealed that the lower and colder part of the cold pool slowly heats up. The resulting homogenization of the temperatures decreases the natural convection flow rate after about the first hour, as can be seen from the figure below. The opening of the steam generator containments (after ~3 hours) enhances the cooling efficiency through air circulation. This improves the cooling of the reactor vessel and results in further stratification of the cold pool. The NC mass flow rate is thereby increased, and stabilizes at about 5% of the initial flow rate.

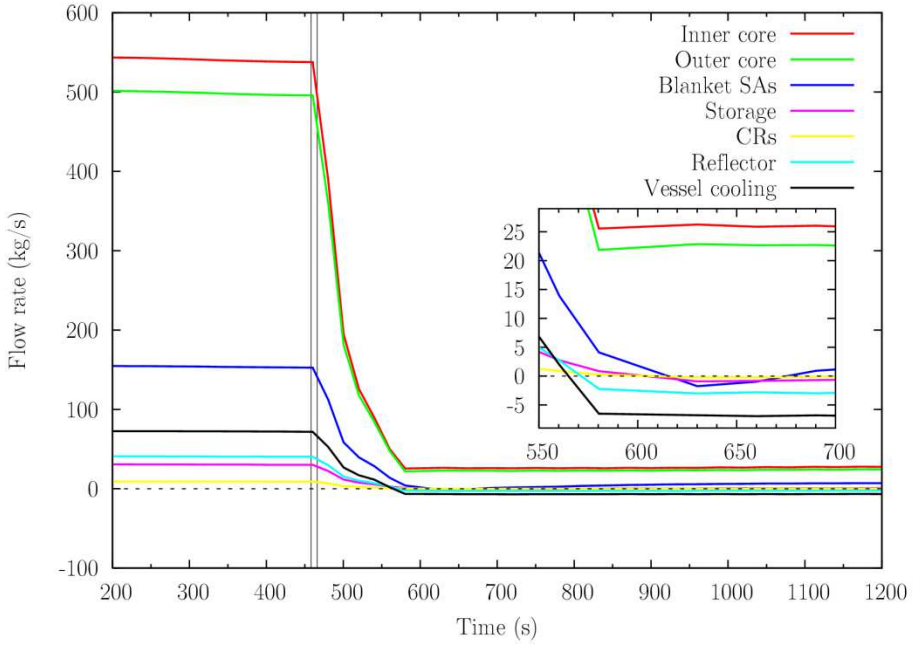

FIG. 63. PSI blind results : details of the core flow rate distribution in the early phase of the transient.

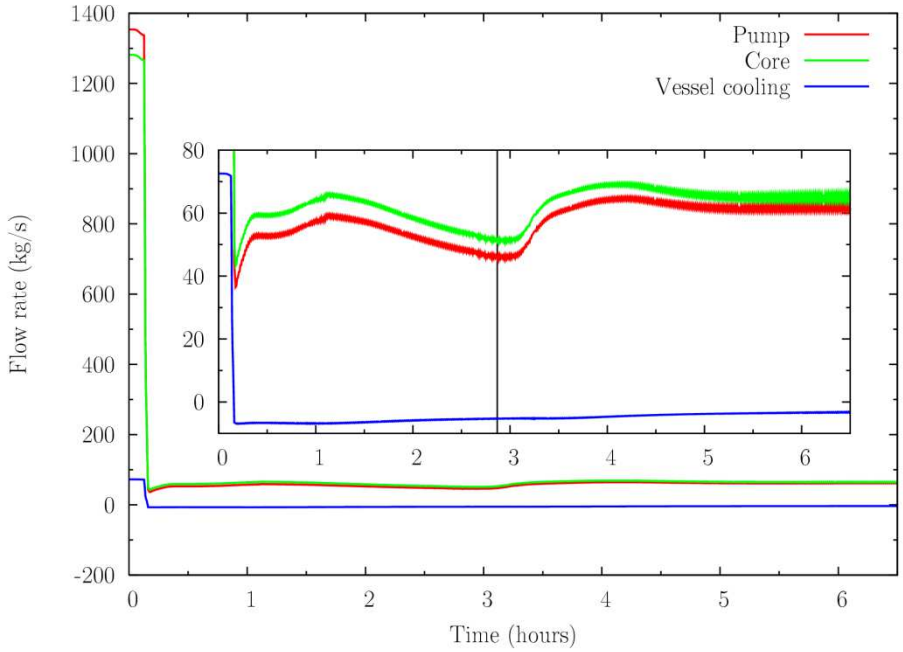

FIG. 64. PSI blind results: distribution of the flow rate in the primary vessel. Evolution of the flow rates during the NC transient.

The following figure presents the calculated and measured pool levels. The prediction of the steady-state is quite satisfactory, though over-estimated by almost 50 mm. After the pump trips, the elevation difference between the hot and cold pools decreases sharply and even reverses. It is seen that TRACE is able to predict the sharp drop, although this is of smaller amplitude and is not able to reproduce the corresponding inversion in pool elevation. The TRACE error on the cold pool level is almost 20 cm. Still, the evolutionary trend of the difference in elevation is quite well reproduced. The discrepancies with respect to the measurements might be due to differences in the computed temperatures as

function of pool height, which result in errors in the sodium density. The pool levels thus represent a good practical measure for checking the average pool temperatures in a post-test calculation.

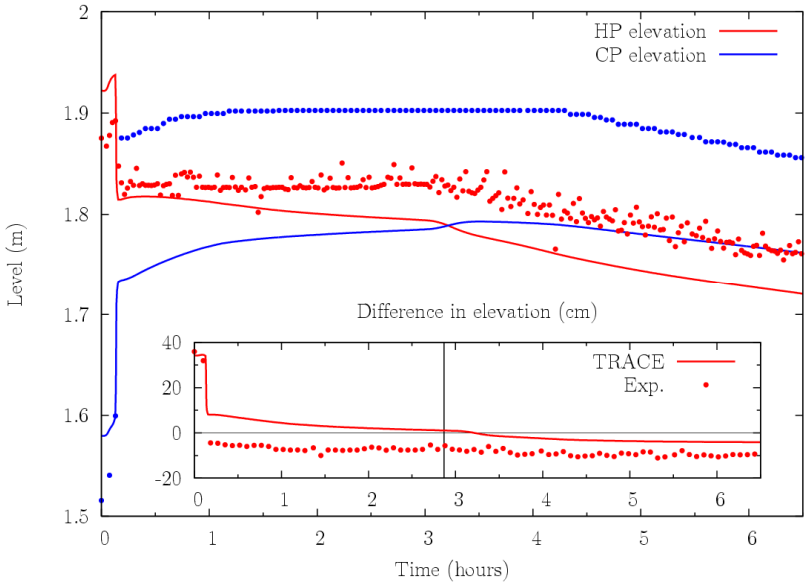

FIG. 65. PSI blind results: Evolution of the pool levels during the NC transient.

6.2.8. Results compilation and discussion

6.2.8.1. Figures for short term t=0 => 1800s

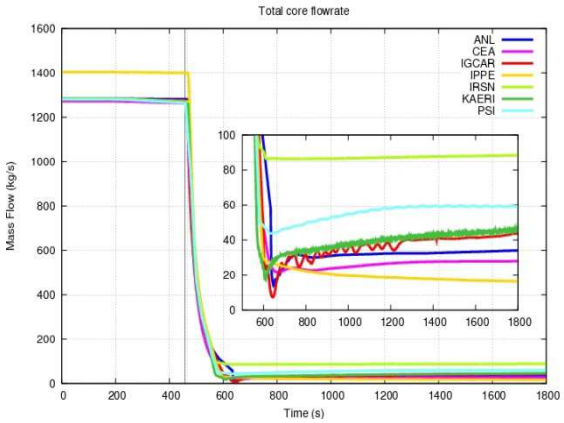

FIG. 66. blind calculations - Total core flow rate (short term).

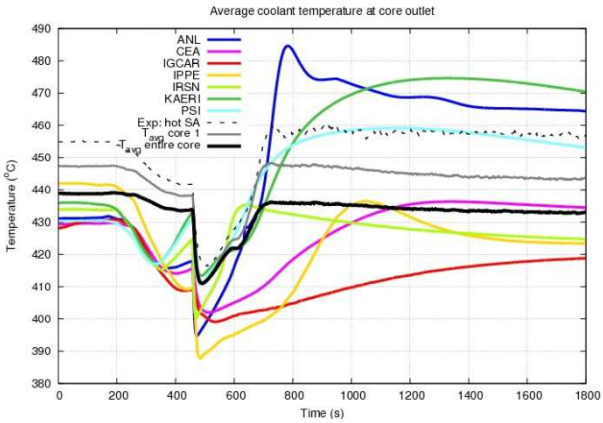

FIG. 67. blind calculations - Average coolant temperature at core outlet (short term).

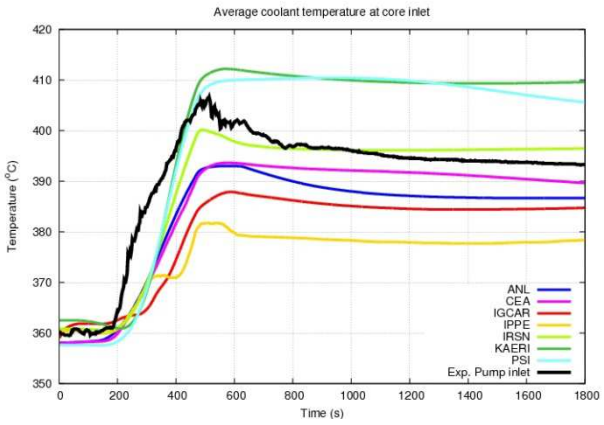

FIG 68. blind calculations - Average coolant temperature at core inlet (short term).

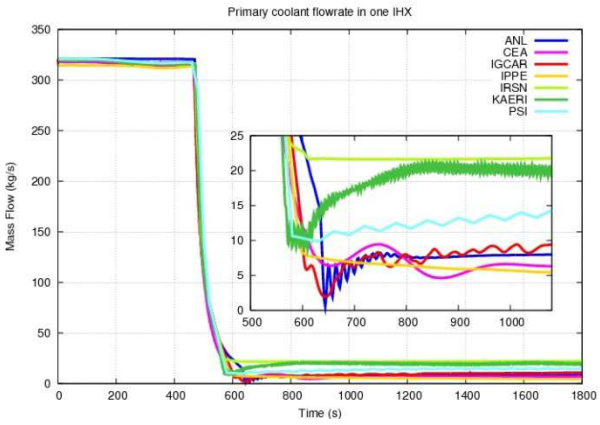

FIG 69. blind calculations - Primary coolant flow in one IHX.

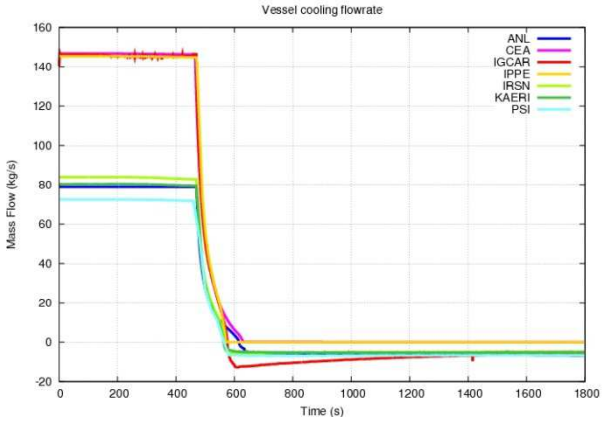

FIG. 70. blind calculations - Vessel cooling flow rate (short term.)

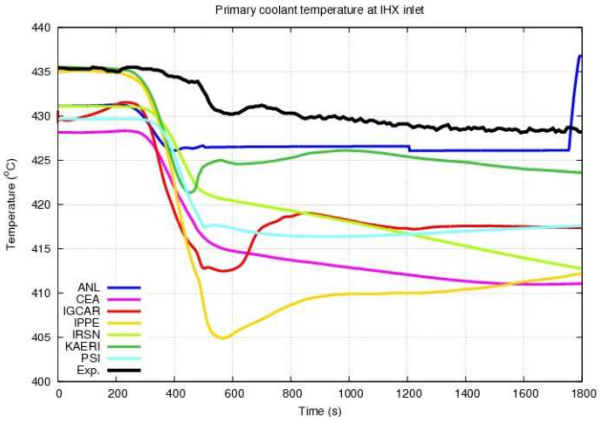

FIG. 71. blind calculations - Primary coolant at IHX inlet (short term).

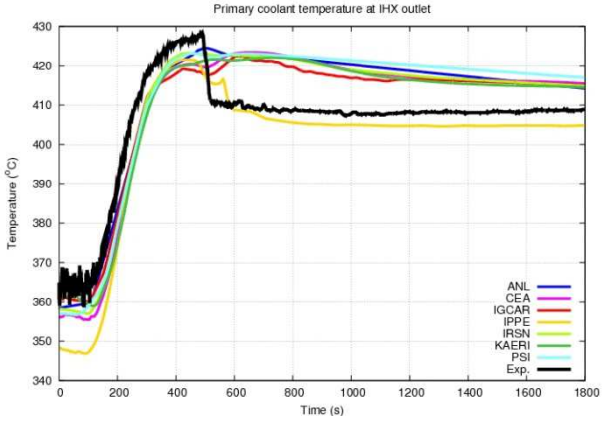

FIG 72. blind calculations - Primary coolant temperature at IHX outlet (short term).

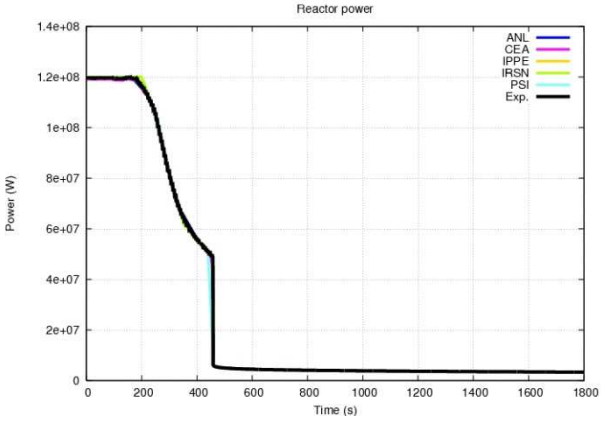

FIG. 73. blind calculations - Reactor power (short term).

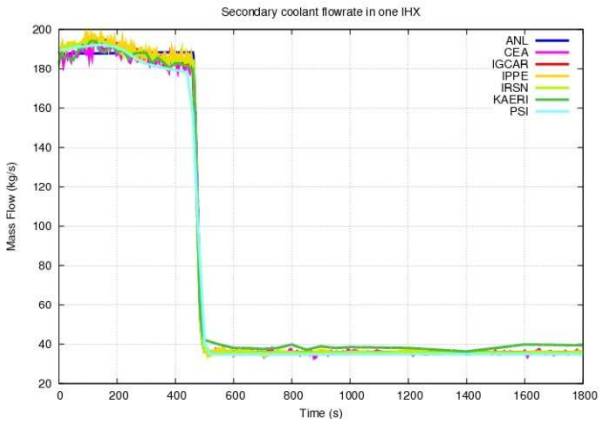

FIG 74. blind calculations - Secondary mass flow rate in one IHX (short term).

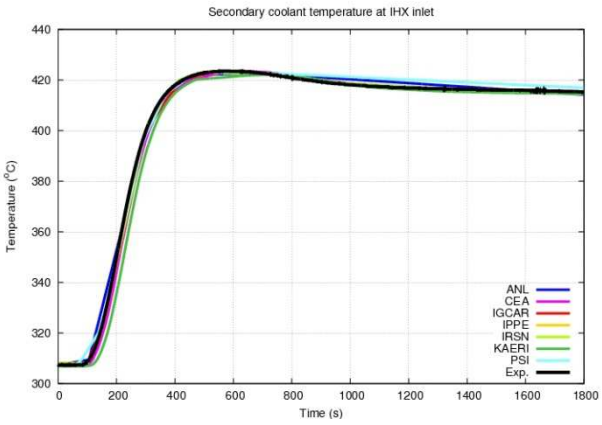

FIG 75. blind calculations - Secondary coolant temperature at IHX inlet (short term).

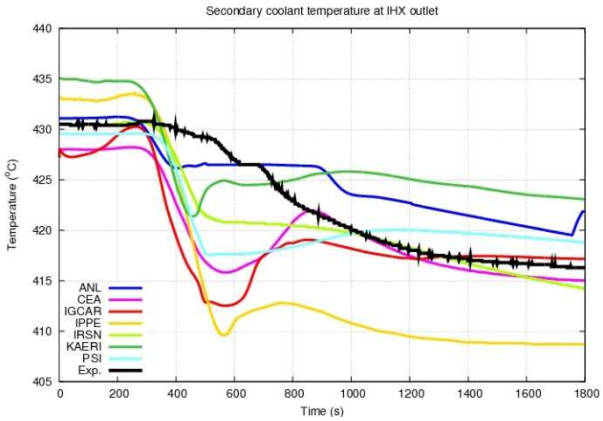

FIG 76. blind calculations - Secondary coolant temperature at IHX outlet (short term).

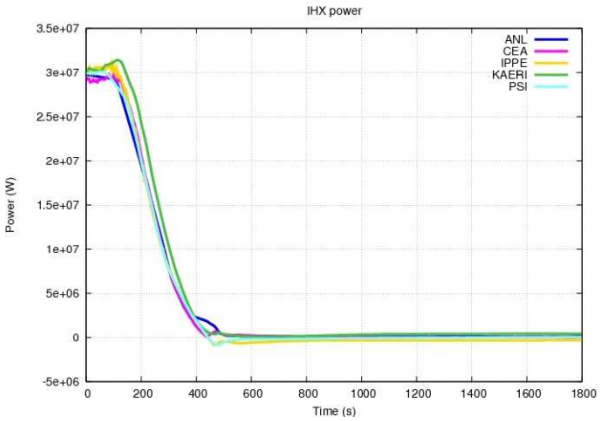

FIG 77. blind calculations - Heat removal from IHX (short term).

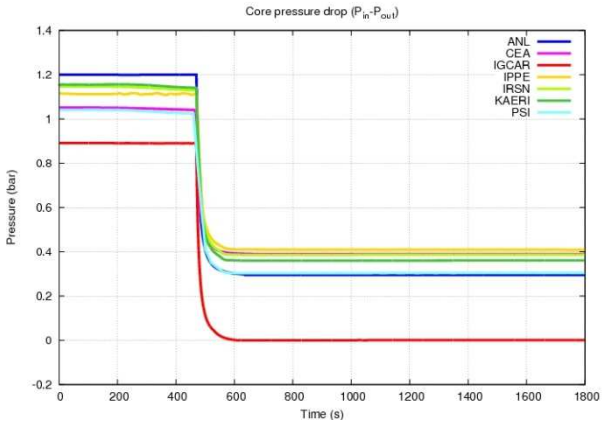

FIG 78. blind calculations - Core pressure difference (short term).

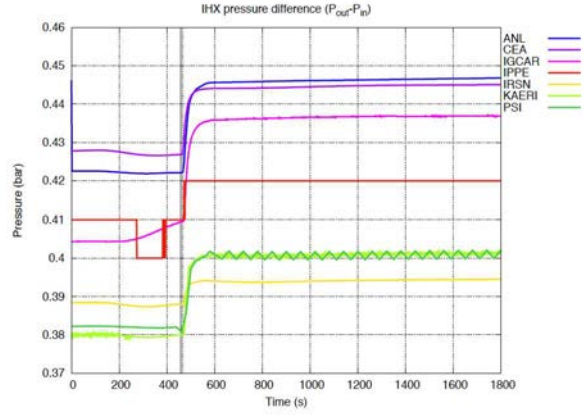

FIG 79. blind calculations - IHX pressure difference (short term).

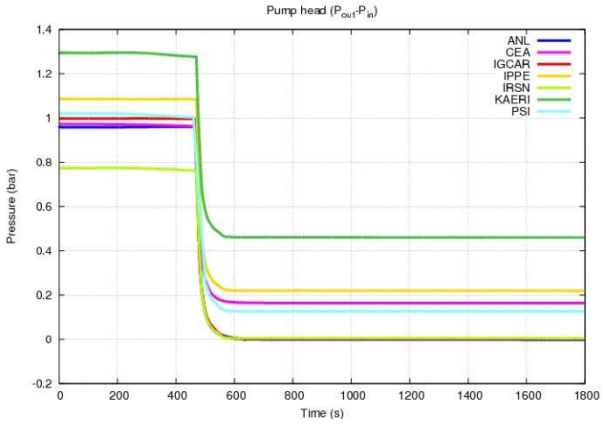

FIG. 80. blind calculations - Pump head (short term).

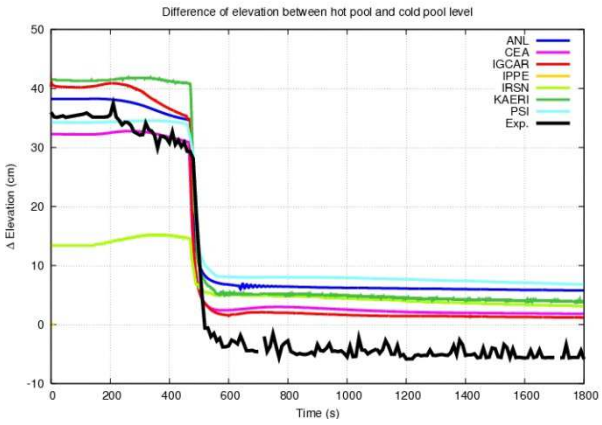

FIG. 81. blind calculations - Difference of elevation between hot and cold pools.

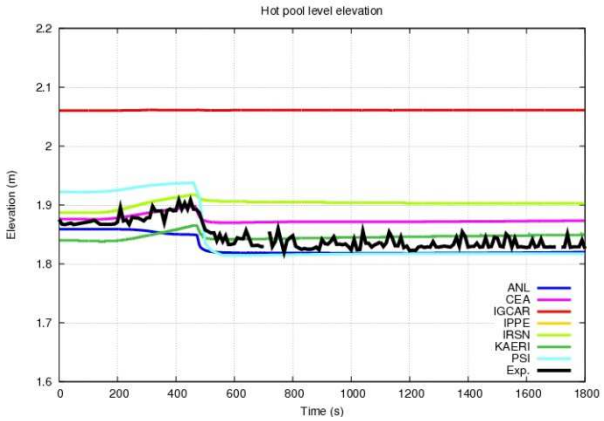

FIG. 82. blind calculations - Hot pool level (short term).

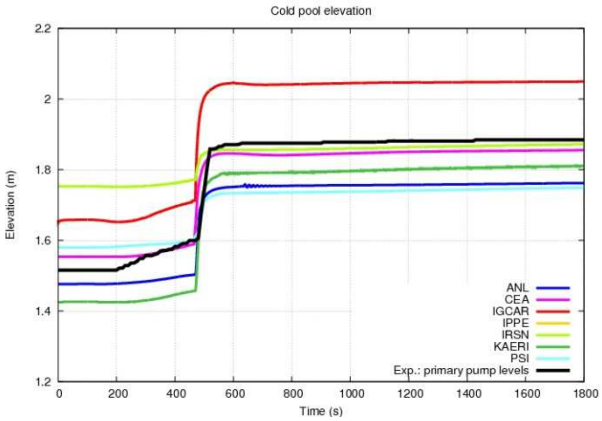

FIG. 83. blind calculations - Cold pool level (short term).

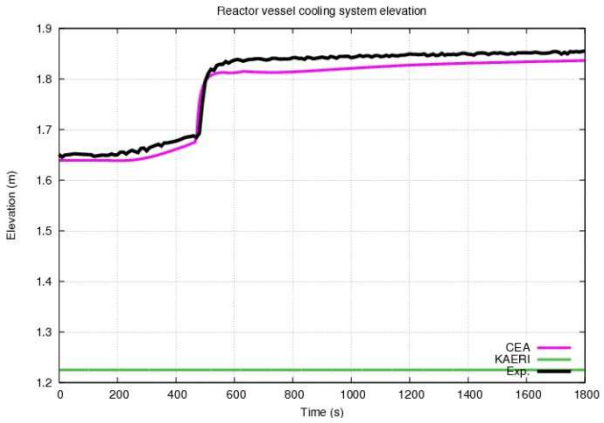

FIG .84. blind calculations - Reactor Cooling system level (short term).

6.2.8.2. Figures for long term (t=1000s to 24 000s)

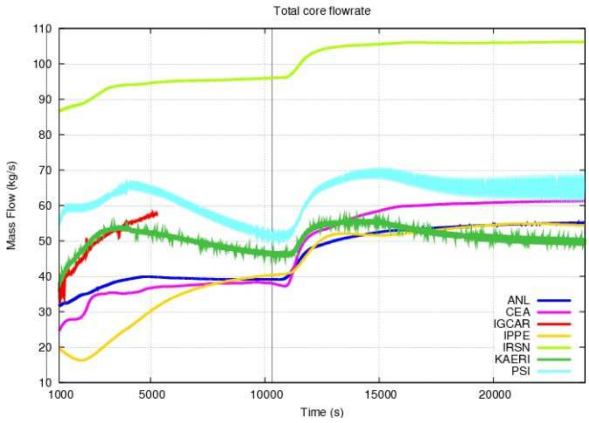

FIG. 85. blind calculations - Total core flow rate (long term).

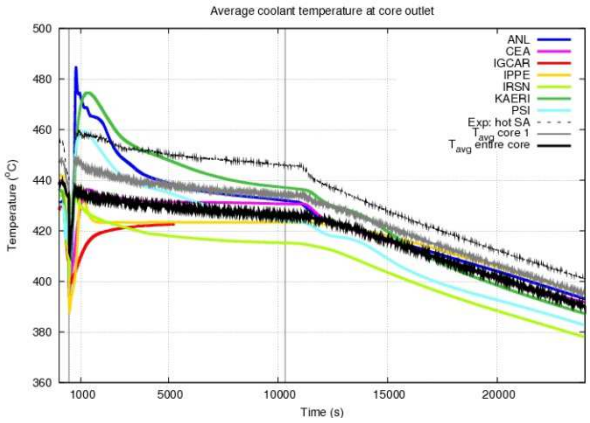

FIG. 86. blind calculations - Average coolant temperature at core outlet (long term).

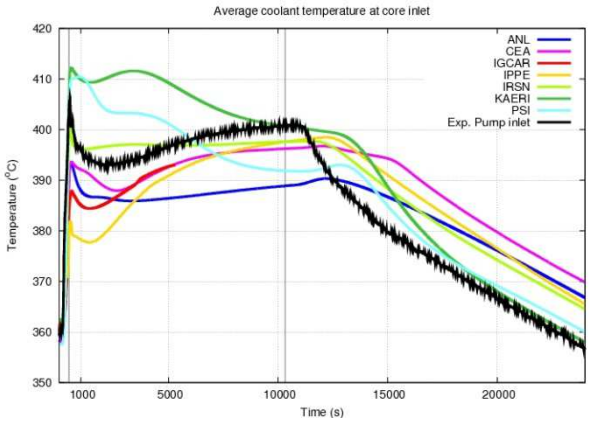

FIG 87. blind calculations - Average coolant temperature at core inlet (long term).

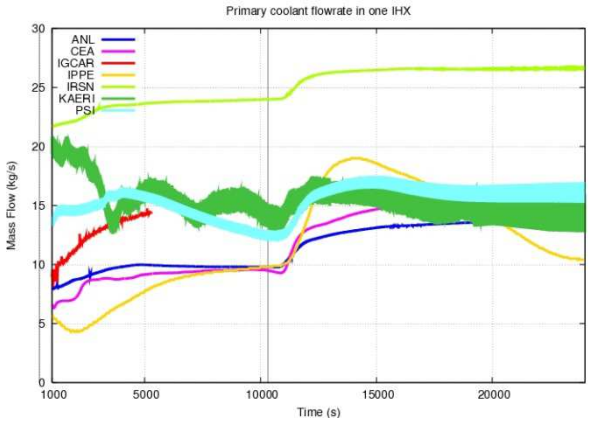

FIG. 88. blind calculations - Primary coolant flow in one IHX (long term).

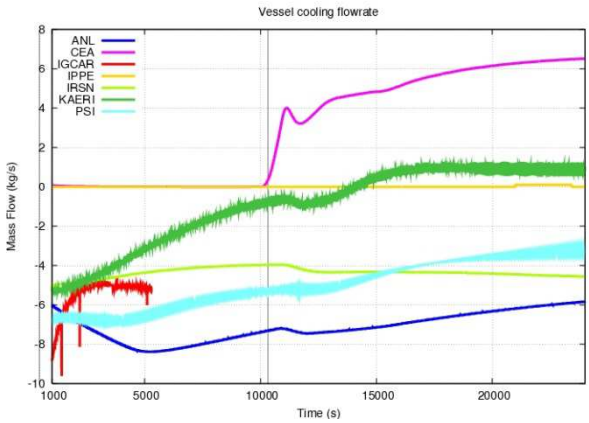

FIG. 89. blind calculations - Vessel cooling flow rate (long term).

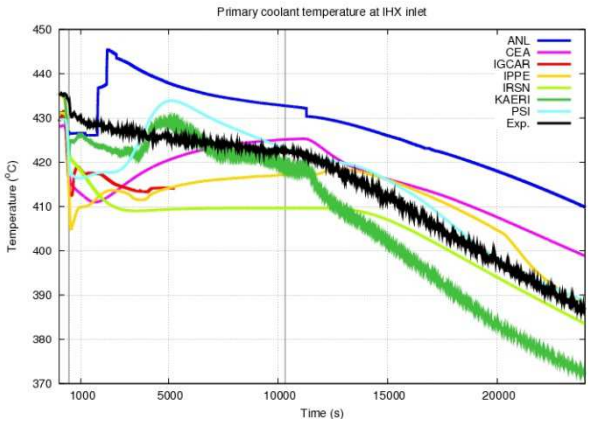

FIG. 90. blind calculations - Primary coolant at IHX inlet (long term).

.

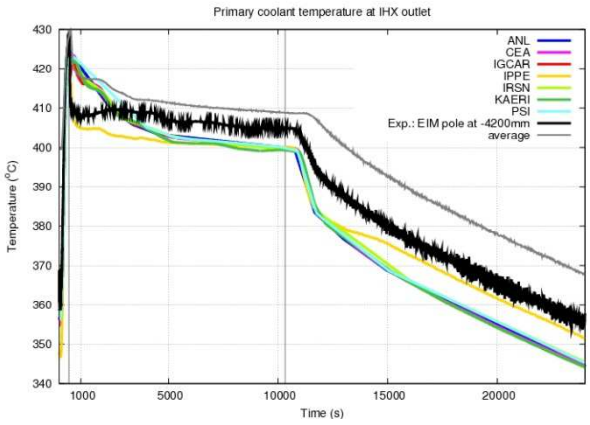

FIG. 91. blind calculations - Primary coolant temperature at IHX outlet (long term).

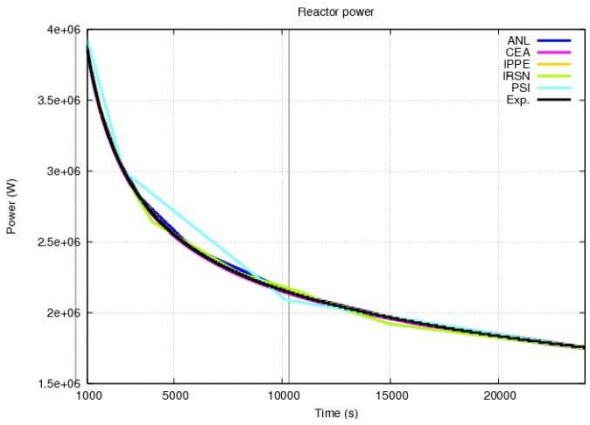

FIG. 92. blind calculations - Reactor power (long term).

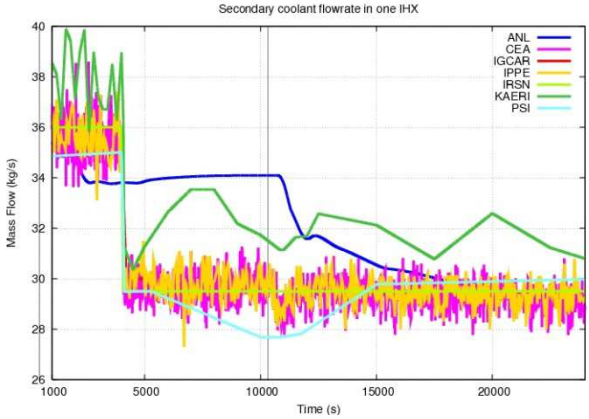

FIG. 93. blind calculations - Secondary mass flow rate in one IHX (long term).

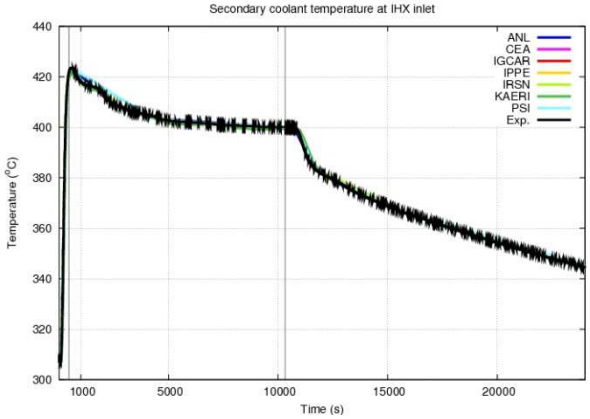

FIG. 94. blind calculations - Secondary coolant temperature at IHX inlet (long term).

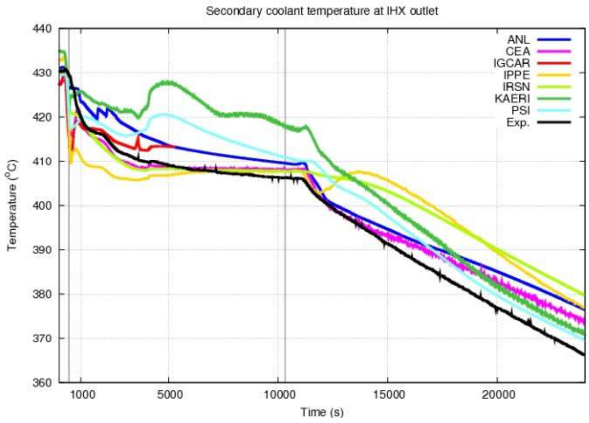

FIG. 95. blind calculations - Secondary coolant temperature at IHX outlet (long term).

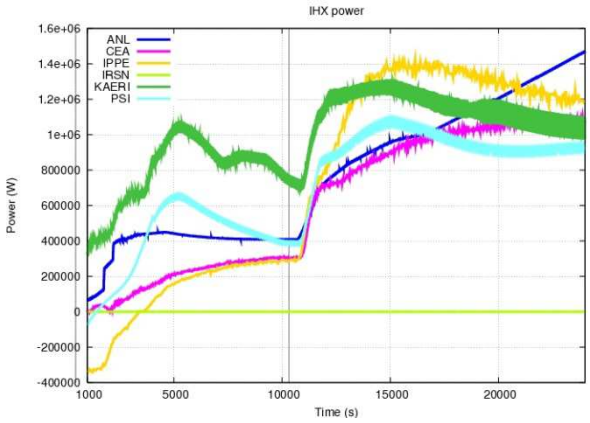

FIG. 96. blind calculations - Heat removal from IHX (long term).

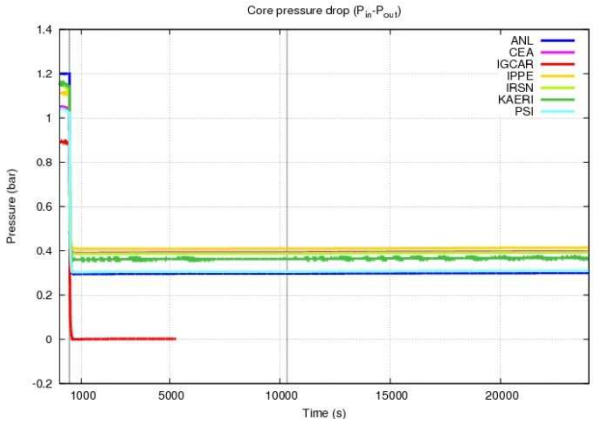

FIG. 97. blind calculations - Core pressure difference (long term).

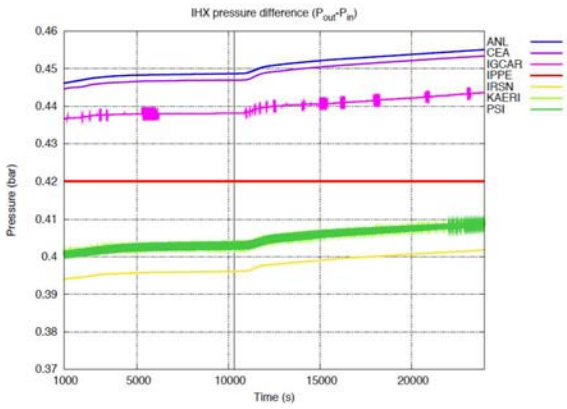

FIG. 98. blind calculations - IHX pressure difference (long term).

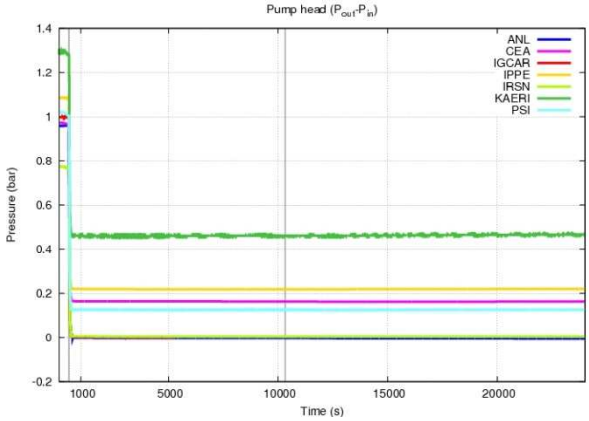

FIG. 99. blind calculations - Pump head (long term).

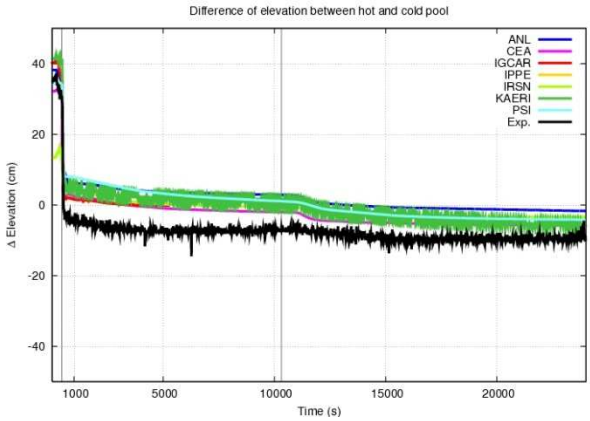

FIG. 100. blind calculations - Difference of elevation between hot and cold pools.

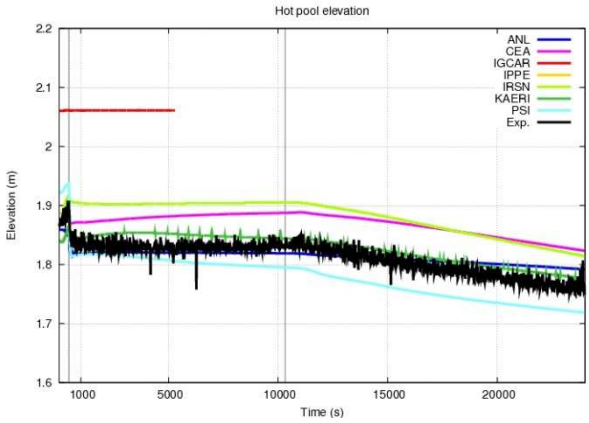

FIG. 101. blind calculations - Hot pool level (long term).

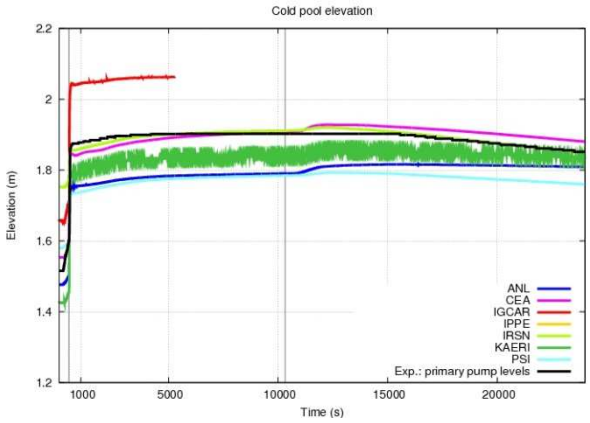

FIG. 102. blind calculations - Cold pool level (long term).

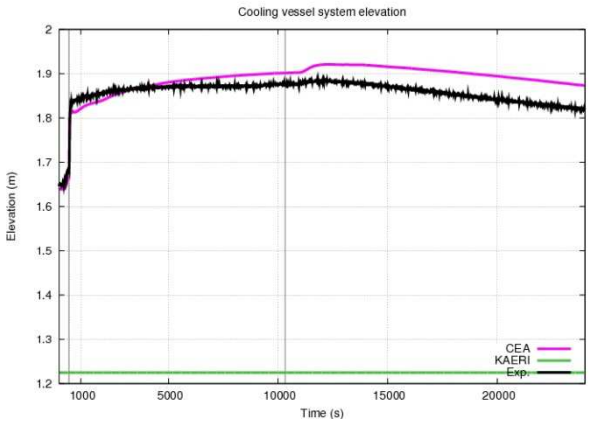

FIG. 103. blind calculations - Reactor Cooling system level (long term).

6.2.8.3. General discussion on blind calculations

— The discussion focuses on following items:

— Use of the input data. Code and participants have different constrains on input data. Therefore, it seems useful to point out these differences.

— Comparison of code predictions and Phenix data for pump inlet temperature, IHX outlet temperature, average core outlet temperature, IHX outlet secondary temperature, hot and cold pools levels

— Prediction of the total core mass flow rate. Unfortunately, there is no Phenix data to compare to code predictions. Nevertheless, it seems really interesting to compare the codes on this parameter, which is essential in natural convection regime.

Use of input data

It seems that some system codes cannot use directly the tables of input data provided by CEA (core power, primary pump speed, secondary IHX inlet mass flow rate and temperature for each loop at a frequency of 1 Hz), therefore regressions have been done: depending on the code, the number of points for these regressions is between 10 to 100. This can lead to a user effect on the input data. The influence of such a user effect on the code prediction has not been quantified.

Core mass flow rate

(a) Short term

For all the participants, the initial total core mass flow rate is between 1240 kg/s and 1400 kg/s. During the first step, as long as the primary pump speeds are constant, this total core mass flow rate remains constant. At t=1800s, when natural convection is established, the range of total core mass flow rate predictions is roughly between 20 kg/s and 40 kg/s, except for PSI at 60 kg/s and IRSN at about 90 kg/s. So, the discrepancy is rather large on this important parameter. This can be due to the different core pressure drop correlations used at low flow rate condition.

(b) Long term

From t=1000s to 10500s, two participants (KAERI and PSI) predict an increase and then a decrease of the total core mass flow rate, whereas the others participants (except IPPE) predict a core mass flow rate roughly stable after t=5000s. The previous discrepancy on IRSN value is maintained during this period.

After t=10500s (opening of the steam generators casing), all the codes predicts an increase of the core mass flow rate:

— For KAERI and PSI, the maximal flow rate has the same order of magnitude as in the second step;

— FOR IRSN, the increase is only about 10%;

— For the others participants, the increase is about 30 to 40%;

We can point out that there are some oscillations in IGCAR, KAERI and PSI calculations.

Average temperature at core outlet

(a) Short term

The initial average core temperature is within a range of 430°C to 442°C. All the predictions lead to a decrease of temperature between t=200s and t=350s, which is consistent with the Phenix data. But, we can notice that the temperature decrease in Phenix is much smaller than the code predictions. Later, all the codes predict an increase of temperature from t=350s to t=460s (before the scram). This increase of temperature is from few Celsius to almost 15°C (for KAERI and PSI), but no increase of temperature occurs in Phenix.

The manual scram and the primary pump trip lead to the cold and hot shocks, which are predicted by all the participants:

— The minimal temperature is between 389°C and 412°C, compared to 410°C in the reactor;

— The maximal temperature is between 420°C and 485°C, with an occurring time for the maximal temperature from t=600s to t=5000s (for IGCAR), compared to 435°C at 700s in the reactor.

The comparison of code predictions versus Phenix data is not easy because Phenix data are related to local outlet sub-assembly temperatures (hottest sub-assembly, average inner fissile sub-assemblies and average entire core) and for some codes (mainly 1D codes), there is just an average outlet module with a full mixing hypothesis. Such assumption cannot represent the radial difference of temperature encountered in the Phenix reactor. Moreover, according to the Phenix feedback, when the primary pump are stopped, the sub-assembly outlet temperature could be significantly influenced by the inter-wrapper flow which contributes to cool the subassemblies.

(b) Long term

From t=1000s to t=10500s in Phenix, all the core outlet temperatures decrease slightly:

— For the average entire core, from t=435°C to 427°C;

— For the average inner fissile core, from 445°C to 435°C;

— For the hottest fuel sub-assembly, from 457°C to 447°C.

After t=10500s, due to the efficient heat sink recovering, the core cooling is accelerated and the cooling rate of the different core regions are nearly the same.

Except IPPE and IGCAR which predict a constant temperature between t=2000s to t=10 500s, the others participants predict a slow decrease of the temperature which is consistent with the Phenix data.

After t=10 500s, all the codes predict rather well the efficient core cooling.

Average temperature at core inlet (pump inlet)

(a) Short term

All the code predictions are consistent with Phenix data and the associated uncertainty. Nevertheless, due to different topologic modeling choices, , the range of code prediction is from 380°C to 410°C at core inlet when the scram occurs, whereas reactor value is 405°C.

After the scram, all the participants predict a rather stable temperature as in the reactor, but the dispersion is between 380°C and 410°C compared to 390°C in the reactor at t=1800s.

(b) Long term

After t=1500s, the Phenix data increases slightly from 392°C to 400°C at t=10500s. We observe different kinds of prediction:

— IGCAR, CEA and IPPE predictions follow rather well this trend;

— For ANL and IRSN, the temperature remains roughly stable ;

— KAERI and PSI calculations show a global decrease of temperature.

After t=10500s, the Phenix temperature decreases due to the recovering of the efficient heat sink. All the codes predict rather correctly the slope of temperature decrease, with a dispersion of about 10°C.

Temperature at IHX primary inlet

(a) Short term

All the participants predict a significant decrease of temperature at IHX primary inlet before the scram, as the core average temperature is also decreasing in the computations. This is not recorded in the reactor where the average core outlet temperature remains nearly constant and the IHX primary inlet as well.

Due to the scram, the decrease of temperature at IHX primary inlet is well predicted by all the computations, sometimes a bit over-estimated. Then, the slight decrease of temperature is correctly estimated by most of the participants.

(b) Long term

During the second phase, the evolution of the temperature at IHX primary inlet is quite stable: from 430°C at t=1800s to 425°C at t=10 500s. During the third step, recovering a heat sink leads to a significant decrease of the IHX primary inlet temperature.

All the codes have difficulties to predict properly the stagnant phase during the second phase. These discrepancies could be explained by inappropriate modeling of the thermal inertia, local buoyancy effects and thermal stratification in the hot pool which cannot be correctly estimated by system codes. When the third step begins, the temperature at IHX inlet decreases from 425°C at t=10 500s to 387°C at t=24 000s. All the codes predict this global trend, with some differences in the slope of temperature decrease.

Temperature at IHX secondary outlet

(a) Short term

The initial temperature predictions are in a range of 425°C to 435°C, for a Phenix measurement of 430°C. During the first step, the temperature is constant. Most of the participants predict a decrease of temperature starting at about 300s, due to the computed decrease of temperature at IHX primary inlet. After the scram and the pump trip, the codes predict a fall of temperature as Phenix temperature decrease is delayed, maybe due to an under-estimation of the IHX thermal inertia.

From t=600s to 1800s, the Phenix temperature decrease slowly, whereas some participants (ANL, IGCAR, CEA and IRSN) predict rather well this trend and other participants (IPPE, KAERI and PSI) predict an increase followed by a decrease of temperature.

(b) Long term

The Phenix data show the two phases:

— second step, slight decrease and after t=5000s, nearly constant temperature

— third step, efficient cooling with first a fast cooling rate (t=11 000s to 12 500s) and then a slightly slower cooling rate.

For the second phase:

— ANL, CEA and IRSN predict nearly the same results with rather low discrepancies compared to Phenix data

— KAERI and PSI predict successively a decrease, an increase and a decrease of temperature

— IPPE and IGCAR predict a nearly constant temperature during this phase (420°C for IGCAR, 408°C for IPPE).

For the third phase:

— all the code predict the higher cooling rate

— PSI and KAERI are very closed to Phenix data

— ANL, IRSN and CEA seem to under-estimate the cooling rate after t=12500s

— IPPE prediction shows first an increase of the temperature (a maxima is reached at t=14 500s) and then a correct decrease.

Temperature at IHX primary outlet

(a) Short term

The initial predictions of all the participants are close to 360°C (except IPPE with a lower temperature of 350°C). We can observe that there are oscillations within a range of +/- 5°C in Phenix data, suggesting that the measurement is located in a mixing region. The increase of the IHX primary outlet temperature due the steam generator dry out is correctly predicted by all the participants. The maximum temperature reached is around 427°C in Phenix, whereas code predictions are in the range of 418°C to 425°C.

At t=460s, just after the scram and the primary pump trip, Phenix data show a fall of temperature of nearly 20°C:

— None of 1D system code captures this phenomenon;

— IPPE, with a 3D model, seems to predict such a trend but with a lower magnitude and some delay.

Additional analysis suggests that cold sodium maybe produced along the bottom of the IHX by heat exchange with the secondary sodium in the IHX. Such colder sodium could influence the IHX primary outlet measurement. New investigations, including coupling system and CFD codes, could bring 3D information to strengthen this assumption.

After the fall of temperature, the Phenix data tends to be constant (as the IPPE prediction), whereas the others codes predict a slight decrease of temperature.

(b) Long term

Phenix temperature at IHX primary outlet is nearly constant during the second phase. Then, during the third step, there is first a rather fast cooling (from t=11 000s to 12 500s) and then a slower cooling.

Except IPPE prediction which is quite correct during phase two, the other participants predict a slight decrease of temperature between t=1000s to t=5000s, followed by a nearly constant value.

During the third phase, all the participants slightly over-estimate the fast cooling rate and then predict correctly the slower cooling rate. The final temperature for all the participants is 345°C, except IPPE with 350°C, whereas Phenix final temperature is 355°C.

Hot pool level

(a) Short term

The initial hot pool level is estimated between 1.86m and 1.92m depending on the participants (except IGCAR with a constant level of 2.06m) whereas Phenix measurement is 1.87m. During the first phase, due to the heating of the lowest part of the reactor vessel and the density effect, the Phenix hot pool level increases:

— Some codes predict this level increase (CEA, KAERI IRSN and PSI);

— Others predict a slight decrease of the level (ANL and IGCAR).

At the primary pump trip, the pressure drop in the IHX shrinks. Therefore, the cold pool level and the hot pool level tend to become equal (the remaining difference is due to the difference of density between the hot and cold pools, and the low flow rate). This decrease of the hot pool level occurs in the Phenix data (-0.07m): all the code predicts this trend but with a range of magnitude from 0.05m for IRSN to 0.12m for PSI. The differences in level variations can be explained by the modeling choices for the pools.

The Phenix data shows a difference between hot and cold pool becoming negative after the scram and the primary pump trips (value around -5cm) but this value is closed to the level sensors uncertainties (+/- 5cm).

(b) Long term

During the second phase (from t=1000s to 10 500s):

— Phenix hot pool level is constant;

— ANL and IRSN predict a constant level;

— CEA predicts a slight increase of the level;

— KAERI and PSI an increase and after a decrease;

— During the third phase:

— With the efficient heat sink recovering, there is a global cooling of the reactor vessel. Due to the density effect, the level decreases slightly;

— All the code predicts such behavior;

— Note: according to the model hypothesis, there is no level computation by IPPE.

Cold pool level

(a) Short term

Remarks: in the Phenix plant, there is no cold pool sensor. The level given to follow the cold pool level is the average level in the primary pumps cavity. When the primary pumps are stopped, this level is closed to the real cold pool level.

At the initial state, the range of cold pool level for the participants is from 1.42m (KAERI) to 1.75m (IRSN). When the primary pumps are stopped, the level in the primary pump increase to reach a stable and asymptotic value of 1.87m in the reactor. All the participants predict the increase of the level, with an asymptotic value from 1.75m (ANL, PSI) to 2.05m (IGCAR).

(b) Long term

The Phenix data show the two phases:

— Second phase, from t=1000s to t=10 500s, heating of the cold pool with a slight increase of the level

— Third phase, from t=10 500s to 24 000s, efficient cooling with a slight decrease of the level.

— For the second phase:

— all the participants predict the slight increase of the cold pool level

— For ANL, CEA, KAERI, IRSN and PSI, after t=5000s, the increase of the level is slower than before t=5000s.

For the third phase:

— In long term all the codes predict the slight decrease of the level

— But, CEA, IGCAR; IRSN, PSI and KAERI predict first an increase (about 0.02m) and then a decrease starting at about t=12000s.

— ANL also predicts such trend with a lower decrease.

6.3. POST-TEST CALCULATIONS USING PHENIX TEST CONDITIONS

6.3.1. ANL

6.3.1.1. Boundary conditions

Tabulated measured data was provided to determine the boundary conditions that evolve with time, including the core power, steam generator outlet temperature, secondary circuit flow rate, and primary pump impeller speed. The core power evolution was derived from both measured data prior to scram and a decay heat model afterwards. The data from the two secondary circuits were integrated so that only one secondary circuit is required. Similarly, the pump speed data for the three primary pumps were averaged onto one representative pump. Without restarting the simulation, SAS4A/SASSYS-1 limits the number of entries in the power table to 20, the steam generator temperature table to 14, and the pump speed table to 20. For simplicity, the data in these tables were reduced; approximating the detailed tabulations with a few carefully selected points. The maximum error in the data reduction was estimated to be 4% for the power data and 7°C for the steam generator temperature data.

6.3.1.2. Results of Code Predictions

Early in the transient, the SAS4A/SASSYS-1 model under-predicts the pump inlet and IHX primary-side inlet temperatures. Near the time where the pump stops, the discrepancy is near 10°C in both cases. The temperature variation within the pool is represented by three discrete stratified layers of varying thickness. This relatively coarse discretization causes the apparent step-changes in the predictions of the IHX inlet temperature.

Overall, the predictions of the hot pool sodium elevation agree reasonably well with the measured data. The measured data shows strong oscillations, which is presumed to be noise in the measurements. The exception occurs at the beginning of the transient prior to the pump shutoff, where the measured data shows a rise in sodium level that is not predicted by the SAS4A/SASSYS-1 model. Note that the model tends to under-predict the hot pool sodium elevation over the course of the transient. This may be caused by hydraulic effects corresponding to a difference in the predicted IHX pressure drop during the transient.

The predictions for the IHX outlet temperature agree well with the measured data up to the peak value near the time of the scram. The measurements exhibit a sudden drop of about 20°C, which is not predicted by the SAS4A/SASSYS-1 model. This drop appears significantly sharper than the drop in the IHX inlet and pump inlet temperatures, which is counter to the expectation that the hot pool would mitigate the temperature drop to the IHX inlet.

The discrepancy in the IHX outlet temperature predictions could be partly explained by the absence of the bypass flow through the upper core structure in the model. According to the specifications, at nominal conditions about 1.5% of the core outlet flow bypasses the hot pool and passes through the upper core structure and into the IHX. This alternate flow path is not included in the current SAS4A/SASSYS-1 model. Another likely contributor to the discrepancy is the uncertainty in the measured data associated with thermal stratification at the IHX outlet window. The thermocouple selected for comparisons is located near the bottom of the IHX window, which may not suitably represent the mean temperature of coolant exiting the IHX.

Several modeling needs have been identified in order to obtain more accurate comparisons with the measured data:

— The tabulated specified boundary conditions (e.g. primary pump speed, power, secondary-side temperature and flow) were reduced from thousands of points in time to 15 – 20 points in time, and the influence of this on the predictions should be evaluated;

— The orifice coefficients in the hydraulic circuit should be adjusted to match the better-known conditions at normal operation, rather than the information provided about the test conditions;

— The model of the vessel-cooling network should be augmented to include the free surface in the small partition of the cold pool;

— A flow path should be added that permits coolant to pass from the core outlet directly to the IHX without first mixing in the IHX;

6.3.2. CEA

6.3.2.1. Boundary conditions

The boundary conditions, given by CEA, are:

— The core power;

— Issued from sensor data before the scram;

— Issued from calculation after the scram.

— The IHX secondary inlet temperature and coolant mass flow rate for loop 1 and 3;

— The primary pump velocities.

The CATHARE post calculations are the same as the CATHARE blind calculations: no modification in the modeling neither in the boundary conditions. So, we will just present in this section the additional computed data defined by the CRP group for the comparison of post calculations.

6.3.2.2. Additional computed parameters for code to code comparison

In this section, additional CATHARE computed parameters are discussed for code to code comparison, as defined by the CRP group:

— Peak inner wall cladding temperature at the inner and outer core zone;

— Peak inner wall cladding temperature at the blanket core zone;

— Primary coolant flow rate in one IHX;

— Core pressure difference;

— IHX pressure difference;

— Pump head;

— Difference of elevation between hot pool and cold pool.

Peak inner-wall cladding temperature at the inner and outer core zone

For short term and long term, the predictions of CATHARE code for both parameters follow the trend of the average coolant temperature at core outlet, with higher amplitudes.

Peak inner-wall cladding temperature at the blanket core zone

After the primary pumps trip, CATHARE code predicts an increase of the maximal peak inner-wall temperature in the blanket zone. This is due to the temporary inversion of the flow direction in the blanket zone.

After one hour, the peak inner-wall cladding temperature predicted by CATHARE code at the blanket core zone is closed to the temperature at core inlet. Then, this parameter follows the cooling of the reactor and decreases with the same cooling rate as the other temperatures.

Primary coolant flow rate in one IHX

The IHX primary mass flow rate follows the core mass flow rate behaviour:

— Constant value when the primary pumps are in operation;

— Sharp decrease due to the primary pump cast down;

— Slight increase during the second phase;

— Higher increase when the heat sink is more efficient.

Core pressure difference

When the pumps are in operation, the core pressure difference predicted by CATHARE code is around 1 bar. When the primary pumps are tripped, the difference of pressure decreases and reaches a stable value of 0.4 bars.

IHX pressure difference

During phase 1, the IHX pressure difference predicted by CATHARE code is due to the friction head loss and the gravity head. When the primary pumps are tripped, as long as the velocity becomes very low, the friction head loss is no more significant and the main term is the gravity. During phase 2, the IHX pressure difference predicted by CATHARE is nearly constant. During phase 3, due to the more efficient heat sink, the gravity term increases and the IHX pressure difference increases as well.

Pump head

The pump head is calculated as the pressure difference between pump inlet and outlet in the CATHARE calculation. When the pump is in operation, the pump head predicted by CATHARE code is around 1 bar. When the primary pumps are stopped, due to the design of the primary pump (primary inlet at a higher elevation than the primary pump outlet), the pump head remains positive due to the gravity.

During phase 2 and phase 3, the pump head predicted by CATHARE code is nearly constant.

Difference of elevation between hot pool and cold pool levels

At the beginning of the transient, the hot pool level is higher than the cold pool level, therefore the difference is positive. Due to a faster heating of the lower part of the reactor vessel (cold pool below the IHX primary outlet window elevation), the difference decreases slightly. When the primary pumps are stopped, the difference decreases rapidly. We can notice that all the codes (including CATHARE) predict a positive difference of level, whereas the Phenix difference of elevation is negative. This negative difference seems not physical because we expect that the hot pool level remains higher than

the cold pool level. Moreover, as long as this difference is about 5cm, it is closed to the level sensors uncertainty given by CEA (about 5cm); so, it is difficult to conclude on this point.

6.3.2.3.. Sensitivity calculations

The following sensitivity calculations have been performed:

- Modification of the friction correlation in the fuel pin of the sub-assemblies (use of Rehme's correlation instead of Pontier's correlation) : there are no major impacts on the total core mass flow rate predictions during the transient;
- Modification of the heat exchange between hot pool and cold pool produces an effect during phase 2 where the heat sink is low. If the heat exchange is increased, the CATHARE code predicts a decrease of the total core mass flow rate;
- Modification of the mass flow ratio through the Upper Core structure at nominal state has no major impact;
- Use of neutronics parameters issued from the data-package to simulate the whole transient:.

Before the scram: over-estimation of core power (60 MW instead of 48 MW when the scram occurs)

- After the scram: at short term (t<800s), over-estimation of core power; at longer term (t>800s), under-estimation of core power (-30% compared to core power input data). The initial over-estimation of core power by CATHARE code could be explained, at least partially, by the short time at full power in Phenix plant, before the beginning of the natural convection test.

6.3.2.4. Global analysis

Globally, CATHARE code shows it capability to calculate the different steps of the Phenix natural convection test. It is not yet fully clear if the discrepancies between CATHARE code prediction and Phenix data are coming from the simplified assumptions of the different CATHARE modules, from inappropriate modeling choices in the CATHARE calculation or from complex hydraulic paths in large pools. Future work and especially coupling CATHARE code with CFD code (Trio-U) will bring more information to solve these challenging technical questions.

6.3.3. IGCAR

The 3D post calculations are the same as the blind calculations. Because of the following reasons, post calculations have not been carried out using three dimensional code.

- There is no change in the boundary conditions
- Results of blind calculation are comparing reasonably well with experimental data
- Difficulty in carrying out parametric studies with 3D code due to large computational requirements
- Availability of in-house developed one dimensional code.

Post calculations have been carried out with the one dimensional system dynamics code DYANA-P.

6.3.3.1. Boundary conditions

The following boundary conditions obtained from CEA have been used for the calculation without any modifications.

— Power evolution in the core during the transient;

— The IHX secondary inlet temperature and secondary coolant flow rate

6.3.3.2. Results

The following parameters predicted by DYANA-P have been compared against experimental data.

— Pump inlet temperature;

— Average core outlet temperature;

— Primary coolant temperature at IHX inlet;

— Primary coolant temperature at IHX outlet;

— Secondary coolant temperature at IHX outlet;

— Hot pool level.

Apart from the above parameters, in order to understand the physical phenomena and to facilitate code to code comparison the following predicted parameters are also discussed.

— Core flow

— Primary coolant flow rate through IHX;

— Core pressure difference;

— IHX pressure difference;

— Pump pressure difference;

— Level difference between hot and cold pool.

6.3.3.3. Short term (t = 0s – 1800s)

Pump inlet temperature

Because of the increase in secondary inlet temperature to IHX there is reduction in heat removal through IHX. This results in increase in the IHX primary outlet temperature and hence the cold pool temperature rises. Evolution of sodium temperature at the pump inlet is comparing well up to 250 s. Subsequently, the predicted temperature becomes higher compared to the experimental data. Hence, the participating thermal inertia of cold pool (multi-dimensional flow pattern) considered in the calculation appears to be more than the actual. Maximum difference between predicted and experimental data at the end of 1800 s is 8°C. The cold shock effect observed in the experiment after scram is not predicted by the code.

Core outlet temperature

The initial core outlet temperature predicted by DYANA-P is 5 °C lower than the experimental data. This may be due to averaged core zone modeled in the code. During the SG dry-out period, the predicted core outlet temperature reduces more than the experimental data. At the time when scram is initiated there is a difference of 10°C between predicted and experimental values. This shows that the hydraulic and thermal inertia of core simulated is little less than the actual. Subsequent trip of primary pump causes the core outlet temperature to increase. The predicted outlet temperature during this period is more than the experimental value with a maximum deviation of 20 °C. Time of appearance of cold shock is closer to experimental data. However, the hot shock predicted is delayed. Maximum temperature reached in the calculation is at 750 s, whereas it is reached at 700s in Phenix. Subsequent slow reduction of the temperature is similar to that in the experiment. There is a difference of 15 °C between prediction and experimental data at 1800 s.

Primary coolant temperature at IHX inlet

The initial value of primary sodium temperature at IHX inlet calculated by DYANA-P is about 3°C lower than the experimental value. This is due to the initial under-estimation of the core outlet temperature. When the reactor power reduces, this temperature reduces similar to that observed in the experiment. However, when the primary sodium flow reduces to natural convective flow, primary sodium temperature at the IHX inlet increases faster than that observed in the experiment. This may be due to higher natural convective flow predicted or due to stratification effects which changes the flow pattern in the hot pool at low flow conditions.

Primary coolant temperature at IHX outlet

The initial value of IHX primary outlet temperature calculated by DYANA-P is 5°C lower than the experimental value. The sharp increase in this temperature due to the increase in secondary sodium inlet temperature, which is well predicted by the code. The maximum value reached is also comparable with experimental data. The cold shock caused due to primary pump coast down is under-estimated in the calculation. This could be due to the large temperature gradient at the IHX outlet window whereas the DYANA-P calculates average outlet temperature only.

Secondary coolant temperature at IHX outlet

The secondary coolant flow rate through IHX and its temperature at IHX inlet are boundary conditions for the calculation. The initial value of secondary coolant temperature at IHX outlet predicted by DYANA-P is 2 °C above the experimental data. Initial reduction in this temperature due to the reduction in primary sodium inlet temperature is well predicted by the code. Subsequently under natural convection conditions, the difference between code prediction and experimental data is widened (5 °C). This is due to deviated prediction of primary inlet temperature.

Hot pool level

Initial level of hot pool predicted by DYANA-P is close to the experimental data. Increase in hot pool level observed in the experiment before pump coast down is not predicted by the code. Level increase is reflected in the cold pool during this period due to rise in its temperature. But, hot pool level reduces due to reduction in its temperature. This is due to uncertainty in the thermal capacity modeling of pools. Subsequently, when the primary pump trip occurs, hot pool level reduces similar to that observed in the experiment.

Total core flow rate

In the DYANA-P calculation, the primary coolant flow rate follows the trend of the primary pump speed. It remains nearly constant before pump coast down is started. A drastic fall in the flow rate can be observed after primary pump trip with a minimum value of 20 kg/s and then picks up due to development of natural convection. Core flow rate increases slowly up to 53 kg/s at 1800s.

6.3.3.4. Long term (t = 1800s – 25000s)

Pump inlet temperature

During phase 2 (natural convection before SG trap door opening), DYANA-P predicts the slow increase and subsequent reduction in pump inlet temperature. The phase 3 (natural convection with an efficient heat sink) begins at t=10,500s and pool temperature reduces faster. There is a difference of 10 °C between the predicted and experimental evolutions showing that the total thermal capacity of cold pool is under estimated.

Core outlet temperature

During phase 2 (natural convection before SG trap door opening), the DYANA-P prediction of the average core outlet temperature is consistent with Phenix data: During phase 3 (natural convection

with an efficient heat sink), DYANA-P prediction of core cooling is faster compared to Phenix data. This may be due to over prediction of natural convective flow in this case.

Primary coolant temperature at IHX inlet

During phase 2, the DYANA-P predicted temperature is nearly constant at around 430°C, whereas Phenix data show a small decrease from 430°C to 424°C. During phase 3, the effect of opening the Steam Generator casing occurs little later in DYANA-P calculation than in Phenix. The cooling rate predicted is similar to that observed in the experiment. However, DYANA-P predicted temperature is higher than experimental data by 10 °C. This discrepancy could be linked to stratification effects in hot pool.

Primary coolant temperature at IHX outlet

Trend of reduction of this temperature is predicted accurately by the code. Code prediction is lower than that observed in the experiment. The deviation is attributed to temperature profile existing along the height of outlet window. The experimental data corresponds to temperature at particular location whereas the predicted value is average.

Secondary coolant temperature at IHX outlet

During phases 2 and 3, Phenix data show that the secondary coolant temperature at IHX outlet follows the primary coolant temperature at IHX inlet. DYANA-P also predicts this trend. Since, DYANA-P predicted temperature of hot pool is higher than experimental data by 10 °C, the same difference is observed in the evolution of secondary coolant temperature at IHX outlet also.

Hot pool, level

During phase 2, DYANA-P predicted evolution of hot pool level is very close to the experimental data. During phase 3, DYANA-P predicted level is higher than the experimental data. This is in line with higher temperature of hot pool predicted by the code compared to experimental data.

Total core flow rate

During phase 2, DYANA-P predicts a slight increase in total core flow rate from 53 kg/s to nearly 65 kg/s. During phase 3, with higher heat sink, this flow increases to ~ 80 kg/s.

IHX heat removal

The predicted initial heat exchange through each IHX is 29.65 MW per IHX. Due to the Steam Generator dry-out, the secondary IHX coolant inlet temperature increases. Therefore, the IHX heat removal decreases to 0.13 MW. During phase 2, the heat removal increases to 0.68 MW after the natural convection is established. During phase 3 this further increases to 1.4 MW.

6.3.3.5.. Additional computed parameters for code to code comparison

Primary coolant flow rate in one IHX

The IHX primary flow follows core flow evolution.

— Remains constant when the primary pumps are in operation;

— Sharp reduction during primary pump cast down;

— Slight increase during the second phase when natural convection is established;

— Further increase after the SG trap doors are opened.

Core pressure difference

When the pumps are in operation, the core pressure difference predicted DYANA-P code is around 1.165 bars. When the primary pumps are tripped, the difference of pressure decreases and reaches a stable value of 0.3 bars.

IHX pressure difference

During the phase 1, the IHX pressure difference predicted by DYANA-P code is due to the friction head loss and the gravity head. When the primary pumps are tripped, friction loss becomes very less and elevation difference between inlet and outlet governs the pressure difference. During phase 2, the IHX pressure difference predicted by DYANA-P is nearly constant. During phase 3, due to the faster cool down of sodium pools, hydrostatic head difference between inlet and outlet increases.

Pump head

The pump head is calculated as the pressure difference between pump inlet and outlet in the DYANA-P calculation. When the pump is in operation, the pump head predicted by the code is around 0.925 bars. When the primary pumps are stopped, the pressure difference drops close to zero. Pump inlet and outlet are considered to be at the same elevation in DYANA-P.

Difference of elevation between hot pool and cold pool

At the beginning of the transient, the hot pool sodium level is 0.4 m above the cold pool sodium level. When the primary pumps are stopped, the level difference reduces sharply. During phase 2, the level difference reduces gradually to zero. During phase 3, cold pool level increases higher than the hot pool level (maximum of 1.6 cm) due to increased natural convective flow. This is due to the increased pressure drop suffered by sodium flow in the core. This behavior is observed in the experimental results also.

6.3.3.6. Summary on DYANA-P calculations

DYANA-P predictions are close to experimental data during the initial period. However, deviation is found to increase during long term. Weighted nodal balance scheme adopted for IHX has been found to function well without any numerical instability even at low flow conditions. Closer prediction of core outlet temperature during the initial period (deviation less than 20 °C) indicates that development of natural convection flow through the core is well predicted. Trends of temperature evolutions of various parts of the plant during phase 2 and phase 3 of the transient are predicted reasonably well by the code. Sodium pools are modeled through single volume approximation. In order to facilitate accurate prediction of temperature evolution of pools during short term, sodium volume is only considered for the estimation of thermal inertia. This approximation causes large deviation between prediction and experiment in the long term. Multi-zone modeling of pools with accurate treatment of all the thermal capacities involved can reduce this discrepancy. Another reason for the deviations could be the non-consideration of stratification effects in the pools. Multi-dimensional modeling for pools can reduce this deficiency.

6.3.4. IPPE

6.3.4.1. Correction of GRIF code input data set

In-depth comparative analysis of 'blind stage' results revealed some discrepancies between GRIF predictions and experimental data and also some mistakes in the interpretation of input data. Therefore the revision of input data set was carried out. The following characteristics were corrected:

— In the blind calculations the reversed flow through vessel cooling path was artificially blocked. Now this blockage was cancelled;

— Heat capacities of different part of reactors were checked and recalculated;

— Primary pump head was corrected and flow distribution in the core for initial state was readjusted;

— Position of lower edge of primary pump skirt was wrongly specified. It was corrected;

— The position of the thermocouple at the pump outlet and IHX outlet were defined more precisely;

— Correlations responsible for heat transfer between hot and cold pools were modified.

6.3.4.2. Sensitivity calculations

One of the main targets of sensitivity study was to explain calculated by GRIF code overcooling of sodium at core inlet during the first stage of transient. The following sensitive calculations have been performed:

— Variation of fuel-clad contact resistance in the core pins (it was assumed that probably the thermal energy accumulated in the core is underestimated and as a result calculated transient temperature at core outlet becomes lower). Results of parametric calculations indicated that effect is insignificant;

— Variation of heat capacities of inlet header and cold pool also has no major impact;

— Modification of heat exchange between hot pool and cold pool. It was revealed during this parametric analysis that the important factor that strongly influences on the transient behavior of sodium temperature at core inlet and outlet is average temperature of sodium in the cold pool at the initial state. Calculations show that temperature distributions in the cold pool are significantly non-uniform in axial and azimuthal directions. The temperature in the upper part of cold plenum is relatively high and as a result average temperature in the cold pool could be much higher than sodium temperature at IHX outlet. After beginning of the transient this relatively hot sodium is washed out from the upper part of cold pool and temperature at core inlet increases more rapidly;

— Introduction of sodium leakage from hot to cold pool (it was assumed that leakage of hot sodium in the cold pool will lead to increase of sodium temperature in it). Parametric calculation for leakage value equal 1% of total core flow does not reveal the significant effect.

As it was mentioned above correlations responsible for heat transfer between hot and cold pools were improved on the base of results of sensitivity calculations.

Pump inlet temperature, core outlet temperature, primary coolant temperature at IHX inlet and outlet

Code predictions for coolant temperatures in primary loop became much close to experimental date after corrections of input data and first of all due to more correct simulation of heat exchange between cold and hot pools. Deviation from measurement mainly doesn't exceed 5 – 10 ºC with one exception: calculated primary coolant temperature at IHX inlet is 15 – 17 ºC lower then experimental value for selected instants of early transient. Possible explanation could be the following. The flow and temperature gradients in IHX inlet windows are rather high. GRIF code calculates local temperature at the point where the thermocouple is located but 3D-modelling of IHX and hot plenum is relatively rough due to lack of necessary information and limited code ability. As a result, the error in calculation of local temperatures could be significant

Secondary coolant temperature at IHX outlet

Prediction of GRIF code for secondary coolant temperature at IHX outlet was considerably improved. For blind calculations the deviation from experiment reached 40ºC but in the post test calculations it doesn't exceed 5ºC.

Total core flow rate, mass flow rates fissile and fertile zones, reactor vessel cooling flow rate

In the GRIF calculation, the coolant flow rates in the inner and outer zones decreases after pumps shut down almost to zero. Flow reversal during short time period is observed for the flow through the blanket zone and as a result for total core flow. Flow through vessel cooling path changes its direction at 55 second of transient and then stays negative. GRIF results for flow are close to predictions of other participants

IHX heat removal, heat removals by vessel cooling system and by the roof

For all these integral parameters GRIF code predicts smooth behavior that are in a good agreement with calculated results of the most part of participants.

6.3.4.3. Additional computed parameters for code to code comparison

Peak inner-wall cladding temperature at the inner and outer core zone and at the blanket core zone

The agreements of GRIF calculations of peak inner-wall cladding temperature at the inner and outer core zones with predictions of other codes are rather good particularly for long-term results. But as for the blanket zone GRIF predicts peak inner-wall temperature that is 30ºC less than other codes calculate. One can assume that overcooling of blanket zone observed in GRIF calculation caused by non-uniformity of sodium temperature distribution in hot plenum. As a result relatively cold sodium that was accumulated on the periphery of hot plenum gradually enters into the blanket zone and cools it down.

Core pressure difference, IHX pressure difference, pump head

The core gives the main contribution to primary friction losses. This contribution calculated by GRIF code agrees with results of other participants. For IHX underestimates the pressure drop if to compare with results calculated by other codes. Probably it can be explained by different friction correlations used by different participants.

6.3.4.4. Global analysis

The following conclusions could be made on the base of above performed analysis:

— The main stages of the NC test are predicted by GRIF code with reasonable accuracy. For temperatures the deviation from measurement mainly doesn't exceed 5 – 10 ºC;

— The correct simulation of sodium temperature distribution in the cold plenum at the initial state is rather important for adequate prediction of variation of temperatures in the reactor during the early stage of transient. Correct calculations of temperature distributions in the cold and hot reactor plenums are also necessary for more correct predictions of local values of temperatures in the thermocouple positions. GRIF calculations predict significant temperature non-uniformity in the cold and hot plenums This non-uniformity could effect on variations of temperature in the reactor especially during the early stage of NC-test. Therefore we consider that the extension of the benchmark to 3D calculations can be useful and interesting. Of course, for more reliable 3D calculations the some additional information concerning the reactor design is necessary.

6.3.5. IRSN

A few modeling adjustments were done for the CATHARE post-test calculations:

— The wall friction law used for fuel pins is the Pontier correlation. A correction for low Reynolds number was issued by the CATHARE team and lead to a flow inversion in the fertile and the steel reflector zone during the natural convection establishment.

— An abnormal temperature increase of about 15°C was observed at the pump inlet from 1000 to 5000 seconds. Sensitivity calculations showed that the steel mass defined inside the cold pool and along the primary pumps pipes had a lot of influence on this temperature. Better results were found by adjusting the steel distribution.

Short term results

The first stage of the transient is driven by three events: the dry-out of the steam generators (0 s), the scram (458 s) and the primary pumps trip (466 s).

The temperature increase at the pump inlet resulting from the steam generator dry-out is rather well predicted with CATHARE.

The cold shock induced by the decrease of the core power after the steam generator dry-out is over-estimated with CATHARE. The core outlet temperature before the scram is about 20°C lower than the experimental value. As this stronger cold shock propagates, similar discrepancies are observed at the IHX primary inlet and the IHX secondary outlet.

The scram and the primary pumps trip (8 seconds later) create successively a cold shock and a hot shock at the core outlet. The comparison of CATHARE results with experimental data is, as mentioned before, somehow tricky to analyze. If we consider the temperature at the core outlet region, i.e. the first layer of the hot pool, we observe that the dynamics of both thermal shocks is too slow. The thermal inertia of this zone appears to be too important. If we consider the temperature at the inner core outlet, the dynamics is better reproduced. However, the hot shock is overestimated by almost 50°C. Sensitivity calculations showed that a larger amount of steel along the channel (representing structures) do not improve sufficiently the results. Another explanation is a possible lack of reliability of the measurement during the natural convection establishment. During this stage, the sodium mass flow rate at the assemblies outlet is very low and recirculations occurring in the hot pool can bring cold sodium towards the thermocouples (see Fi. 104). As a result, the temperature measured at the inner core outlet can be underestimated.

The cold shock observed at the primary IHX outlet is not reproduced with CATHARE. However, as mentioned before, the measurement may not be representative of the average temperature at IHX outlet owing to large temperature gradients in the window area.

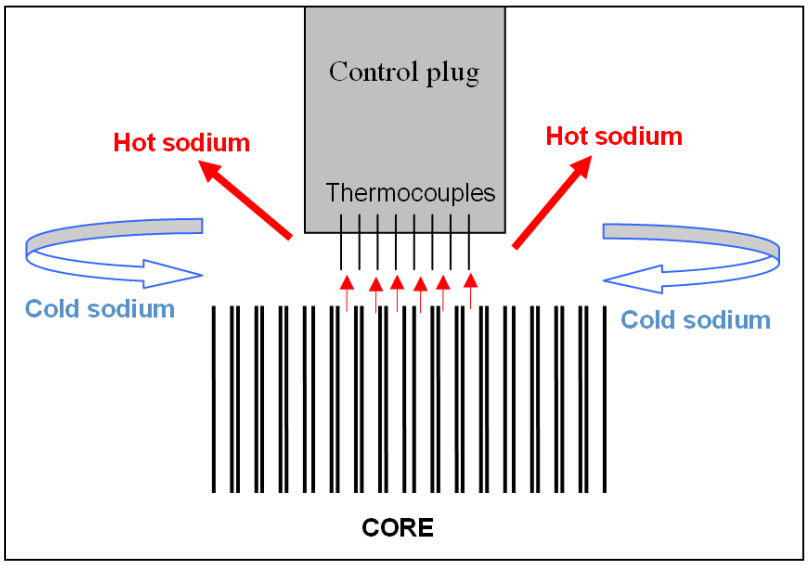

FIG. 104. IRSN calculations: sodium flow in the core zone outlet during the natural convection establishment

Long term results (2000 – 24000 s)

The second stage of the transient is driven by the steam generators air cooling at 10320 s (~3 h). The effect of this improved cooling appears with some delay with CATHARE. On the long term, the temperature decrease is well predicted overall. Sensitivity calculations showed that heat exchanges between the hot and cold pools can improve the results.

Conclusion

The CATHARE long term results are in good agreement with measurements overall. Discrepancies are mainly observed on the short term, when natural convection is establishing and local phenomena are significant. However, the comparison is sometimes limited by the lack of reliability and relevance of some measurements during the natural convection regime. It would have been interesting to have access to additional measurements for further analysis and modeling adjustments, especially in the hot pool and the cold pool. Indeed, no information was available concerning the thermal-hydraulics behavior of these two large volumes of sodium during the natural convection test.

6.3.6. University of Fukui

The natural convection test conducted at the Phenix plant was calculated by a model without heat transfer between the hot pool and the cold pool at first. Calculated inlet temperature of the IHX overestimates the measured result after the scram. This is caused by non-heat transfer between two pools and the inferior mixing in the hot pool. Therefore, two heat exchange units are provide between two pools taking into account the equivalent heat transfer area and flow area. The single tube side corresponds to the hot-pool, and the shell side corresponds to the cold pool. Since the main parameters of the Phenix reactor were described under the rated power of 350 MW in the IAEA document, all the plant parameters such as local loss coefficients were adjusted at first.

6.3.6.1. Boundary conditions

Since the natural convection test was conducted after decreasing the reactor power to 120 MW(th), the steady state calculation was conducted based on the adjusted loss coefficients. After the steady state for 20,000 seconds is calculated by the time marching method and confirmed the steady state, the natural convection transient is calculated by the code. The reactor power transient is given to the code based on the given curve by the document. Since there were small differences of temperatures and flow rates between the loop-1 and loop-2 in the secondary heat transport system, two different input data are given to the code for each loop.

6.3.6.2. Short term (t = 0s – 1800s)

Pump inlet temperature

Temperature at the primary pump inlet shows the similar trend as the measured result after the dry-out of the steam generator. The predicted peak temperature is quite same as the measured result. However, the temperature is overestimated a bit after the reactor is scrammed.

Primary coolant temperature at IHX inlet

The initial IHX primary inlet temperature calculated by NETFLOW++ is about 5°C lower than the measured result. The temperature decrease transient due to the scram is simulated in the same manner as the reactor response, and the temperature approaches to the measured result at the final stage of the short term. Because of the heat transfer between the hot-pool and cold-pool, this result could be obtained.

Primary coolant temperature at IHX outlet

The initial IHX primary outlet temperature calculated by NETFLOW++ is a few degrees lower than the measured result. The rapid increase of temperature due to the steam generator dry out is well predicted. However, the sharp temperature drop due to the scram is not traced correctly. The calculated temperature shows the slow decrease after the reactor scram.

Secondary coolant temperature at IHX outlet

The initial secondary coolant temperature at IHX outlet is well predicted by NETFLOW++. After the reactor scram, the temperature is underestimated by the code for a while. And then the temperature is overestimated by approximately 6 °C after 800 seconds.

Core outlet temperature

The initial inner core outlet average temperature calculated by NETFLOW++ is approximately 4°C lower than the measured result. The temperature decrease induced by the power decrease after the dry-out of steam generator is well predicted by the code. However, temperature increase before the establishment of the natural convection is overestimated greatly. The temperature transient for the outer core outlet shows the similar trend as the inner core. Regarding the calculated average coolant temperature at the core outlet shows the similar trend before the hot shock, and the calculated temperature approaches to the measured result before and after the reactor scram.

Total core flow rate

The primary coolant flow rate is almost constant value before the scram. However, the flow rate is influenced a bit by the pump inlet temperature change. The flow rate decreases along the coast-down characteristics. The core flow rate during the natural convection is estimated at approximately 45 kg/s.

Reactor vessel cooling flow rate

The vessel cooling flow rate is indicated as 10% of the primary flow rate when the reactor power is 350 MW(th). The loss coefficient of the vessel cooling system is trimmed in order to achieve this characteristic. When the primary pumps are tripped, NETLOW++ predicts a reverse flow in the reactor vessel cooling system because the outer vessel is cooled by the water pipes and the inner vessel is cooled by the radiative heat transfer. This reversal flow rate is almost constant at approximately -5 kg/s during the short term transient.

IHX heat removal

At the initial condition, the one IHX heat exchange rating is approximately 29 MW. After the steam generator dry-out, the IHX heat removal decreases to nearly zero due to the decrease of flow rate and the secondary temperature increase. When the scram and the primary pump trip occur, the heat removal remains very low level at 0.23 MW. This situation continues for long period.

Hot/cold pools heat exchange

The heat exchange between the hot and cold pools is calculated by NETFLOW++ code. Since a special option is required to output the rating, the heat removal rating is unclear at present.

Heat removals by vessel cooling system

Heat removals are calculated by NETFLOW++ code using a vessel cooling model for Phenix. The rating is approximately 0.34 MW at the initial. The removal rating increases as the inlet temperature increases. After the pump trip, the removal rating decreases to approximately 55 kW.

6.3.6.3.. Long term (t = 1800s – 25000s)

Pump inlet temperature

Temperature at the pump inlet underestimates the measured result during the period of 1h to 3.5h after the good agreement during the short term transient. After the SG is cooled by the air, the calculated trend follows the measured result.

Primary coolant temperature at IHX inlet

The primary coolant temperature at the IHX inlet shows a small amount of peaks that may be caused by the delay of mixing in the hot pool. The temperature is overestimated a bit over the term. However, the calculated temperature is close to the measured result. The maximum discrepancy is approximately 10°C.

Primary coolant temperature at IHX outlet

The overall trend of the predicted temperature shows the similar trend as the measured one. However, the calculated temperature underestimates the measured result after 1h from the start of the transient. This trend is very much dependent on the secondary side inlet temperature because of small heat removal from IHX.

Secondary coolant temperature at IHX outlet

The overall secondary coolant temperature at IHX outlet is well predicted by NETFLOW++. A discrepancy between the calculation and measurement is approximately 5 °C over the transient term.

Core outlet temperature

The inner core outlet average temperature for long term is well predicted by NETFLOW++. After the temperature peak occurred within 1h, calculation traces the measured result within 5°C. The calculated average coolant temperature at the core outlet traces the measured result without a large peak. The large peak appeared at the outlet of the subassemblies are suppressed due to the mixing in the hot pool.

Total core flow rate

The primary coolant flow rate during the natural convection is in the range from 44 to 47 kg/s. When the SGs are cooled by air, the flow rate increases to approximately 55 kg/s and keeps this situation during the cool-down process.

Reactor vessel cooling flow rate

After the reversal of the reactor cooling vessel flow rate, the flow rate is in the range of -5 to -7 kg/s. This reversal flow rate is almost constant during the whole transient.

IHX heat removal

The IHX heat removal remains very low level at 0.23 MW for a while after the pump trip. The rating increases up to 0.45 MW after 1h. When the SGs are cooled by air, the rating increases to 0.97 MW.

Hot/cold pools heat exchange

The heat exchange between the hot and cold pools is calculated by NETFLOW++ code. Since a special option is required to output the rating, the heat removal rating is unclear at present.

Heat removals by vessel cooling system

The heat removal rating decreases after the pump trip and keeps the low rating conditions at nearly zero for approximately 1 hour. Then after, the rating of heat removal increases gradually to approximately 350kW.

6.3.7. KAERI

For the post-test calculation with the MARS-LMR code, the KAERI has reinforced the modeling for the following components:

— Heat structures in hot pool;

— Heat structures in cold pool;

— Steel structures in core;

— Heat loss from roof and vessel;

— Core outlet region flow path.

The secondary coolant flow rate through the IHXs, which is one of the boundary conditions, has also been corrected. The effect of these modeling changes on the MARS-LMR simulation of the Phenix natural circulation test is detailed below.

6.3.7.1. Short term (t = 0s – 1800s)

Total core flow rate

Compared to the blind post-test analysis, the core flow rate decreases to a much smaller value of 7 kg/s at 610s. This change is caused by the reinforced modeling of heat structures around the core region. Then, a natural circulation flow is developed in the primary system, which gives the core flow rate of 29 kg/s at 700s after the initiation of the transient. After that, the total core flow increases steadily and it reaches 41 kg/s at 1800s.

Pump inlet temperature

The pump inlet temperature predicted in the post-test analysis shows an enhanced result compared to the blind analysis. The trend of the test data is well simulated in the post-test analysis with 10°C over-estimation.

Average core outlet temperature

In the MARS-LMR post-test analysis, the under-estimation of thermal inertia is reduced, thus, the amplitude of temperature decrease and increase before the reactor scram is reduced. The temperature decrease caused by the reactor scram is well predicted with the code. However, the amplitude of increase of core outlet temperature just after pump trip is less than the measured data. Then the average temperature at core out region predicted by the MARS shows a mild increase. The maximum deviation from test data is about 40°C.

Primary coolant temperature at IHX inlet

A sudden drop of IHX inlet temperature is still predicted in the post-test analysis, which suggests that the temperature distribution in the hot pool includes some distortion. However, the trend of the MARS-LMR simulation is consistent with the Phenix test data with the maximum under-estimation of 6°C at 1800s.

Primary coolant temperature at IHX outlet

The MARS-LMR under-predicts the temperature at primary IHX outlet before the pump trip. This underestimation is related to the lower IHX inlet temperature. However, the drastic temperature decrease after the scram followed by the primary pump trip is not described in the MARS prediction. This discrepancy can be understood if one considers that the temperature is measured at one point at IHX outlet and the prediction is for a large volume of cold pool near the IHX out region. After the pump trip, MARS-LMR simulates the test data quite accurately.

Secondary coolant temperature at IHX outlet

The initial decrease of secondary temperature at IHX outlet before the reactor scram is overestimated as the primary coolant temperature at core outlet and IHX inlet. The temperature trend after the reactor scram is dependent on the primary IHX inlet temperature and the primary flow rate through the IHXs as the natural circulation builds up. The predicted temperature decrease after 1000s is consistent with the Phenix test data with 5°C over-estimation.

Hot pool, cold pool levels

The general trend of the MARS-LMR prediction of pool levels is consistent with the test data. The initial pool levels and the level increase before the scram are predicted very accurately by the MARS-LMR. After the reactor scram and the primary pump trip, the level difference between the hot pool and the cold pool decreases due to the loss of pump head, which causes the decrease of hot pool level and the increase of cold pool level. The predicted level difference after the pump trip is 4 cm higher than the measured level difference.

Reactor vessel cooling flow rate

Before the primary pump trip, the reactor vessel cooling flow rate is predicted to be 6% of the primary flow rate. After the primary pump trip, the vessel cooling flow rate decreases abruptly to a negative flow and it is maintained in a reverse flow regime.

IHX heat removal

The behavior of heat removal rate through IHXs in post-test analysis is similar to the prediction in blind analysis. As the steam generators become dry-out, the secondary IHX inlet temperature increases and the heat removal rate from the IHXs decreases continuously. The IHX heat removal rate finally reaches to negative value at the time of reactor trip and primary pump trip. Then, the heat removal rate is recovered slightly with the development of natural circulation in the primary system.

Hot/cold pools heat exchange

The heat exchange between the hot and cold pools at initial condition is estimated to be about 0.5 MW. A sudden drop of hot pool-to-cold pool heat transfer before the reactor scram is not observed in post-test analysis. At the time of pump trip, there occurs a drastic increase of heat transfer between two pools then it reaches a constant value of 0.2 MW.

6.3.7.2. Long term (t = 1800s – 25000s)

Total core mass flow rate

In this phase of transient, the total core flow rate predicted by the MARS-LMR increases from 40 kg/s at 1800s to 50 kg/s at 1hour after the initiation of the transient. Then, it decreases continuously before the opening steam generator casing. After opening it increases abruptly and reaches a constant value of flow rate.

Pump inlet temperature

As a result of the over-prediction in pump inlet temperature during the early stage of the transient, the pump inlet temperature predicted by the MARS-LMR shows a continuous decrease until the time of SG opening. The Phenix data shows a different trend, a decrease followed by an increase. The MARS-LMR predicts the test data accurately after the opening of SG casing.

Average core outlet temperature

The MARS-LMR over-predicts the core outlet temperature during the mid-phase of the transient before the opening of the SG casing. This suggests that there still exists some distortion in the

modeling with one-dimensional approach. The cooling rate predicted by the MARS-LMR is consistent with the Phenix data in the later phase after the SG opening.

Primary coolant temperature at IHX inlet

The MARS-LMR predicts the test data of IHX inlet temperature reasonably even though there are some oscillations caused by the secondary mass flow rate imposed as a boundary condition in the simulation. The cooling rate after the SG opening predicted by the MARS-LMR is consistent with the Phenix test data.

Primary coolant temperature at IHX outlet

The MARS-LMR predicts successfully the long term behavior of the IHX outlet temperature. The maximum deviation of the prediction from the test data does not exceed 5°C.

Secondary coolant temperature at IHX outlet

It seems that there is a systematic distortion in the modeling of heat transfer through IHXs in MARS-LMR simulation. Therefore, higher IHX outlet temperatures in the secondary side are predicted through the simulation period. It is predicted that the heat removal rate after the SG opening is consistent with the Phenix data.

Hot pool, cold pool levels

The long term trend of hot pool level is well simulated with the MARS-LMR. The change of cold pool level is also reproduced correctly in the simulation. The maximum deviation of the calculated levels from the measured data is less than 4cm.

Reactor vessel cooling flow rate

In the MARS-LMR calculation, the reverse flow through the vessel cooling path is predicted through whole transient after the primary pump trip.

IHX heat removal

The average heat removal per IHX predicted by the MARS-LMR is about 0.7 MW before the opening of steam generator. After the opening, it increases to 1.0 MW.

Hot/cold pools heat exchange

In the MARS-LMR calculation, the heat transfer from hot pool to cold pool decreases continuously in the later phase of the transient as the temperature difference between the two pools decreases.

6.3.7.3. Summary on MARS-LMR post-calculations

The post-test analysis with the MARS-LMR code for the three different phases of the Phenix natural circulation test are summarized as follows:

— Early phase (0s ~ primary pump trip): The distortion in the prediction of core outlet temperature has been improved by the enhancement in the modeling of steel structures in the core and pool regions. Therefore, the MARS-LMR simulation is estimated to describe the heat-up process correctly;

— Mid phase (primary pump trip ~ opening of SG casing): After the reactor trip and primary pump trip, the core outlet temperature experiences a sudden drop and increase. The MARS-LMR reproduces the drop of core outlet temperature successfully. However, the core outlet temperature during the first part of the mid phase is still overestimated considerably. This implies there is some distortion in the modeling of natural circulation mainly due to the limitation of one-dimensional approach for the description of multi-dimensional effect in the pool region. The

temperatures for other locations and the overall cooling rate are predicted consistently with the Phenix data.;

— Later phase (after the opening of SG casing): The heat removal rate is increased by the opening of the SG opening. The general trends of the Phenix data are well predicted with the MARS-LMR code in this phase.;

6.3.8. PSI

PSI results

After comparison with the experimental data, the major sources of error during the early transient seem to be related to the simulation of the reactor structures. A finer modeling, including the core SA wrappers and the description of the IHX as integrated into the reactor pools, has been performed in a post-test analysis. The results are presented in Figs 108 – 105.

It can be seen that:

— The core inlet temperature, through the reduction of the pump and diagrid heat-transfer area, thus decreasing the corresponding thermal inertia;

— The core outlet temperature, due to the improved core inlet temperature and the better representation of the core structures (mainly SA wrappers), which enabled one to improve the results during the 200 s following the SCRAM;

— The IHX outlet temperature, through the representation of the IHX outer shell and its integration into the cold pool, which results in a global improvement of the temperatures;

— Reduction of the core natural convection flow rate by 10%, now representing 4.5% of the initial core flow rate;

— The evolutions of the pool levels which, despite the remaining error on the predicted absolute levels, are now very well reproduced.

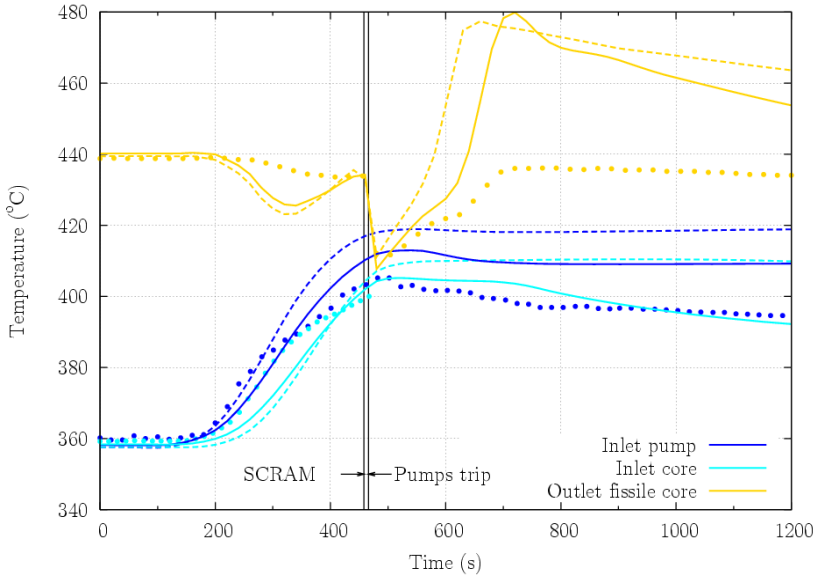

FIG. 105. PSI post-calculations: Evolution of the core power and temperatures during the early phase of the transient. (exp.: points, TRACE blind results: dashed lines, TRACE post results: plain lines).

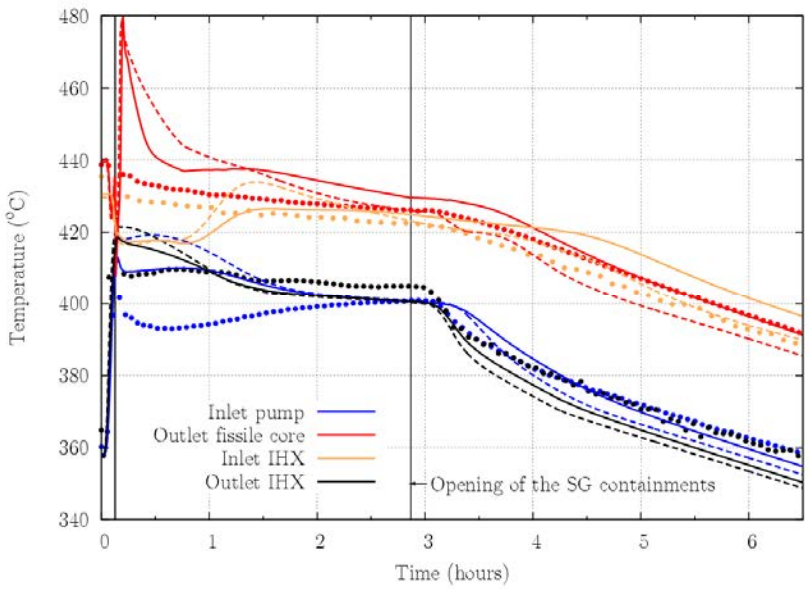

FIG. 106. PSI post-calculations: Evolution of the primary pool temperature during the complete transient. (exp.: points, TRACE blind results: dashed lines, TRACE post results: plain lines).

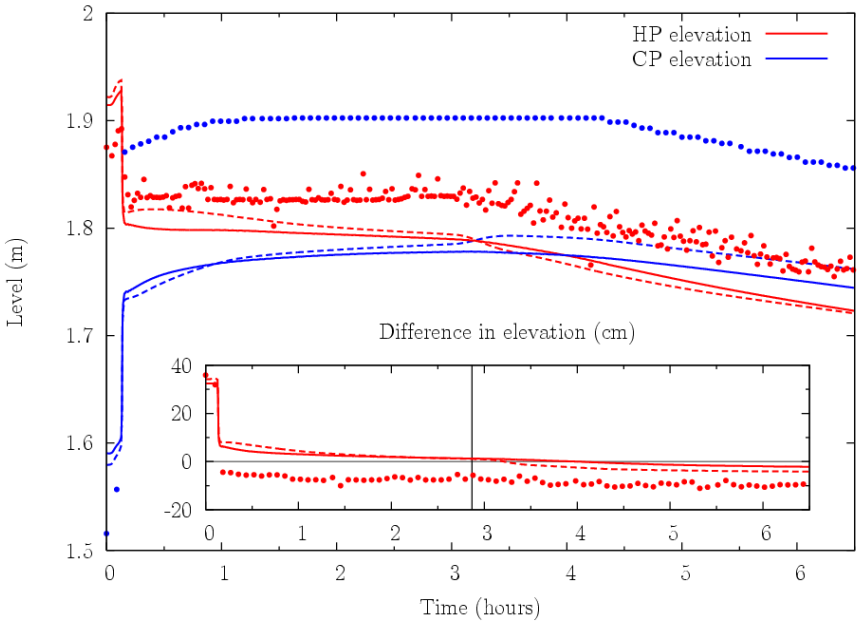

FIG. 107. PSI post-calculations: Evolution of the pool levels during the complete transient. (exp.: points, TRACE blind results: dashed lines, TRACE post results: plain lines).

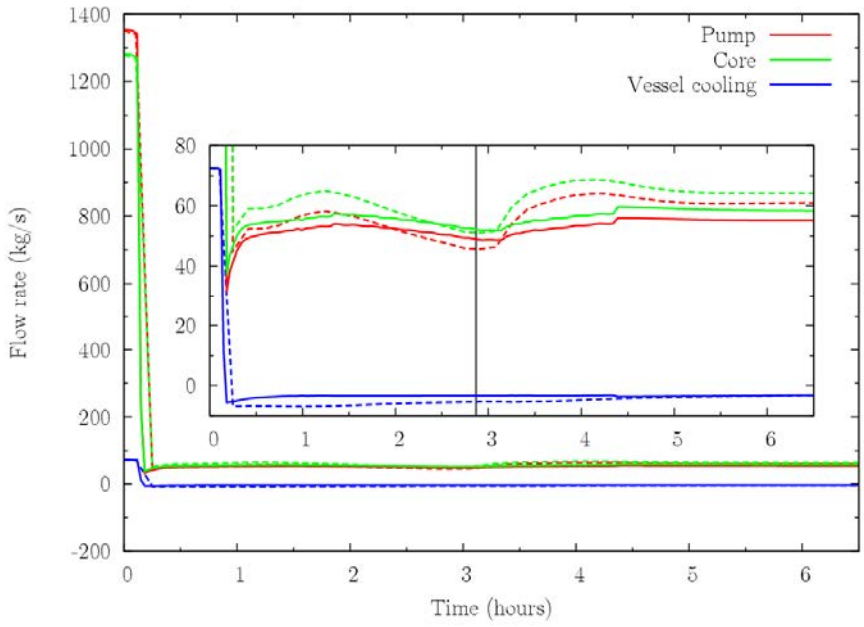

Figure 108. PSI post-calculations: Evolution of the primary vessel flow rates during the complete transient. (TRACE blind results: dashed lines, TRACE post results: plain lines).

6.3.9. Results compilation, summary and discussion

6.3.9.1. Figures

The figures include:

- Boundary conditions;
- Comparisons to Experimental Results;
- Important code to code comparisons;
- Complementary code to code comparisons.

Short Term Results (t < 1800 sec) Long Term Results (t < 24,000 sec)

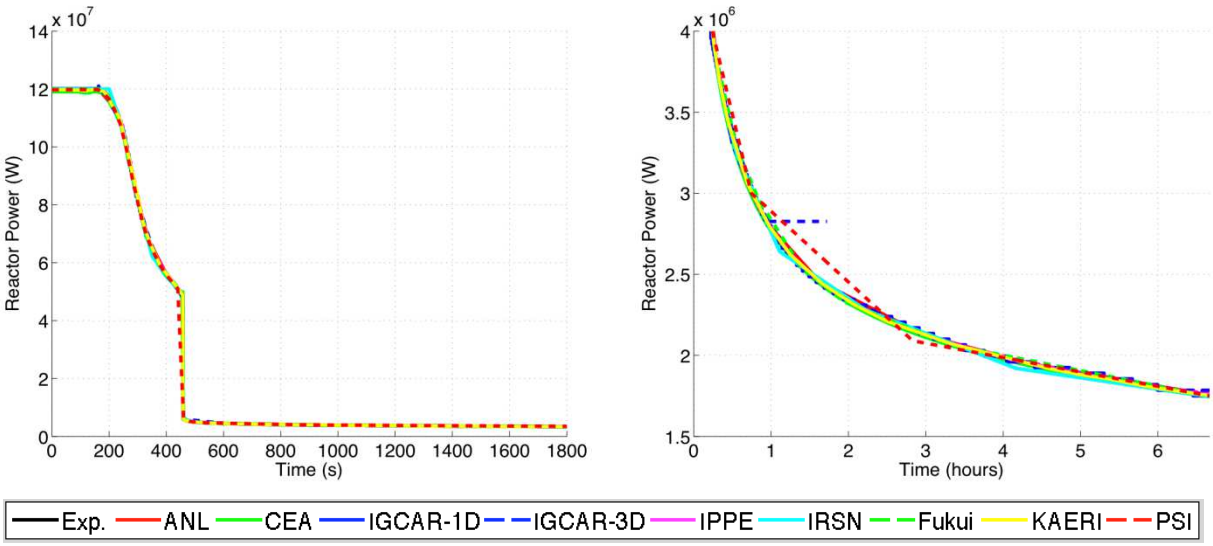

(a) Reactor Power

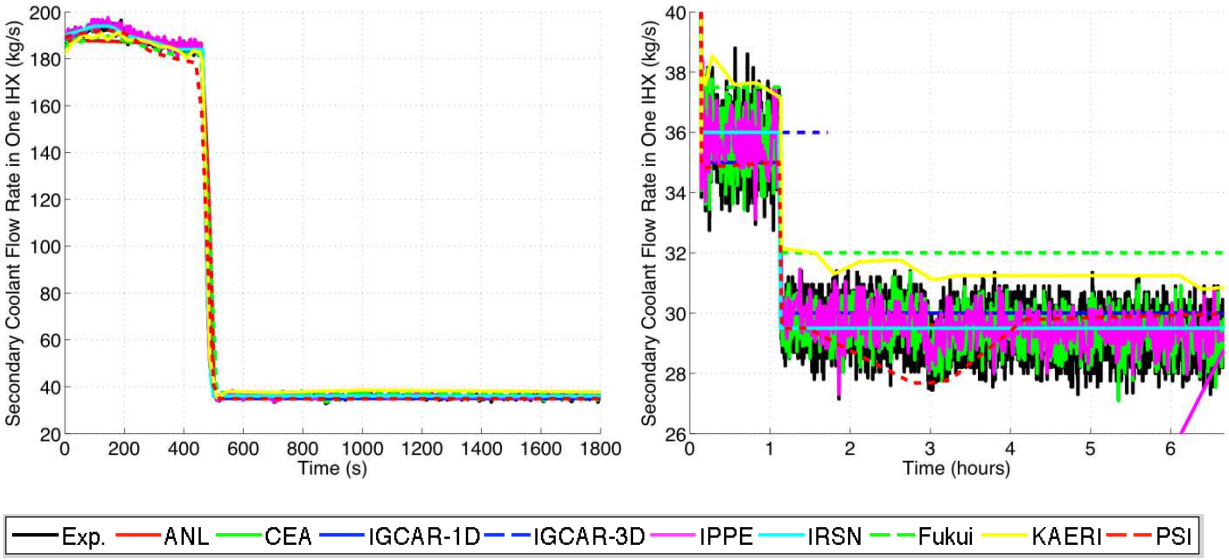

(b) Secondary Coolant Flow Rate Through One IHX

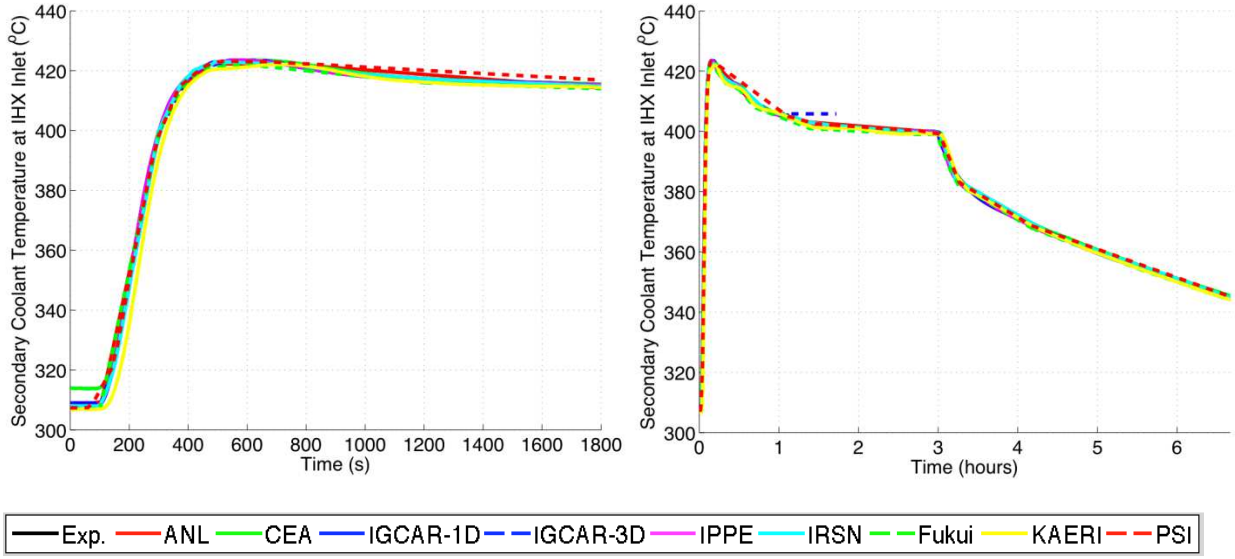

(c) Secondary Coolant Temperature at IHX Inlet

FIG. 109. post-calculations – Boundary conditions provided by CEA and boundary conditions of each participant.

Short Term Results (t < 1800 sec) Long Term Results (t < 24,000 sec)

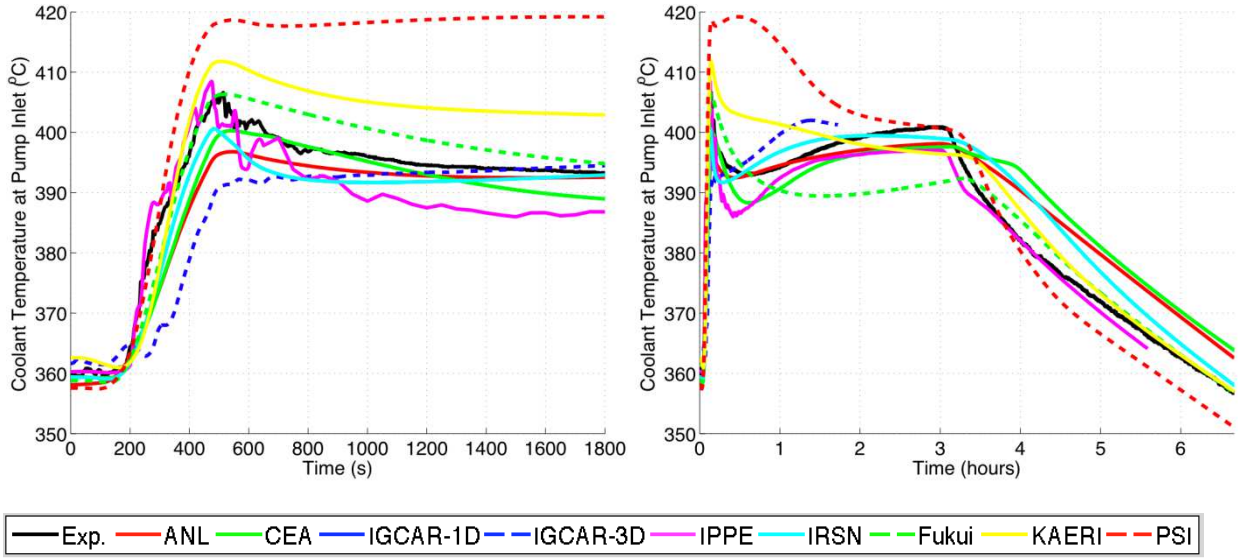

(a) Coolant Temperature at the Primary Pump Inlet (in lieu of Core Inlet).

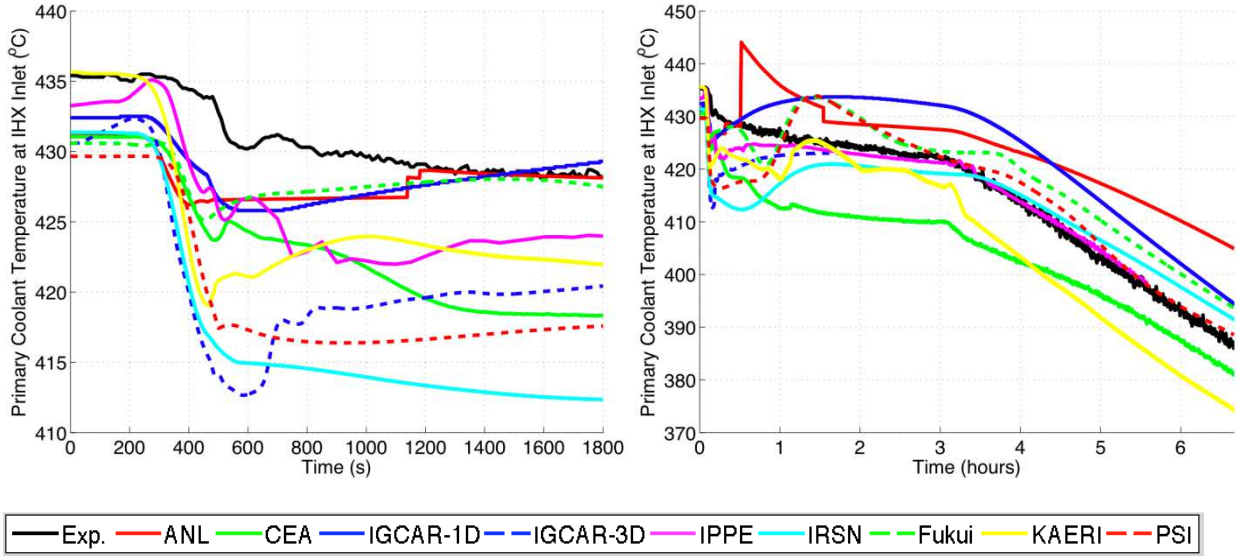

(b) Primary Coolant Temperature at the IHX Inlet.

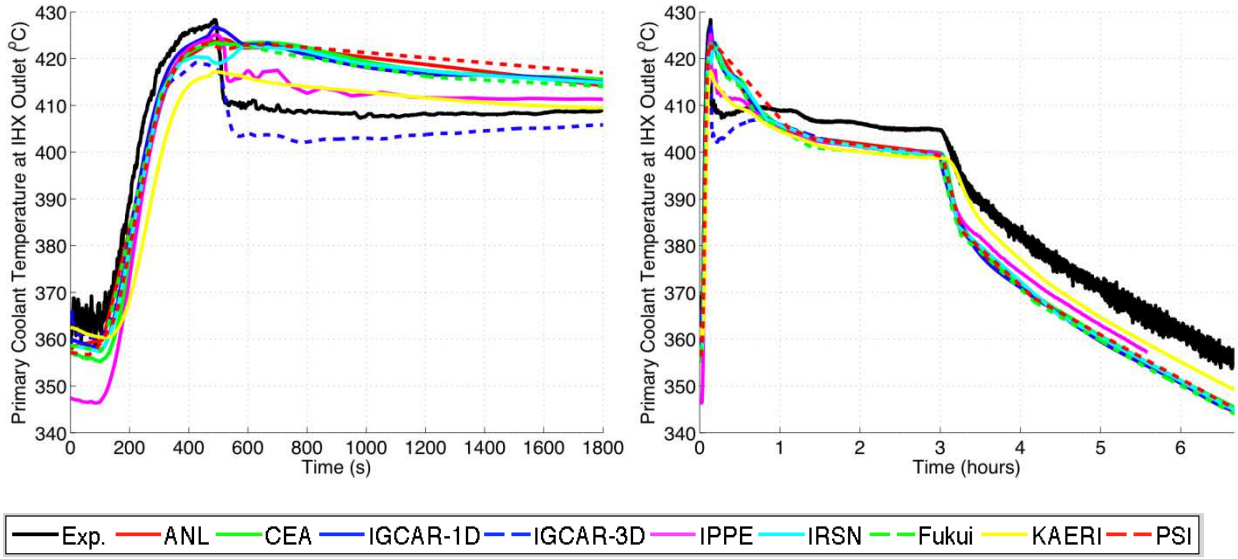

(c) Primary Coolant Temperature at the IHX Outlet.

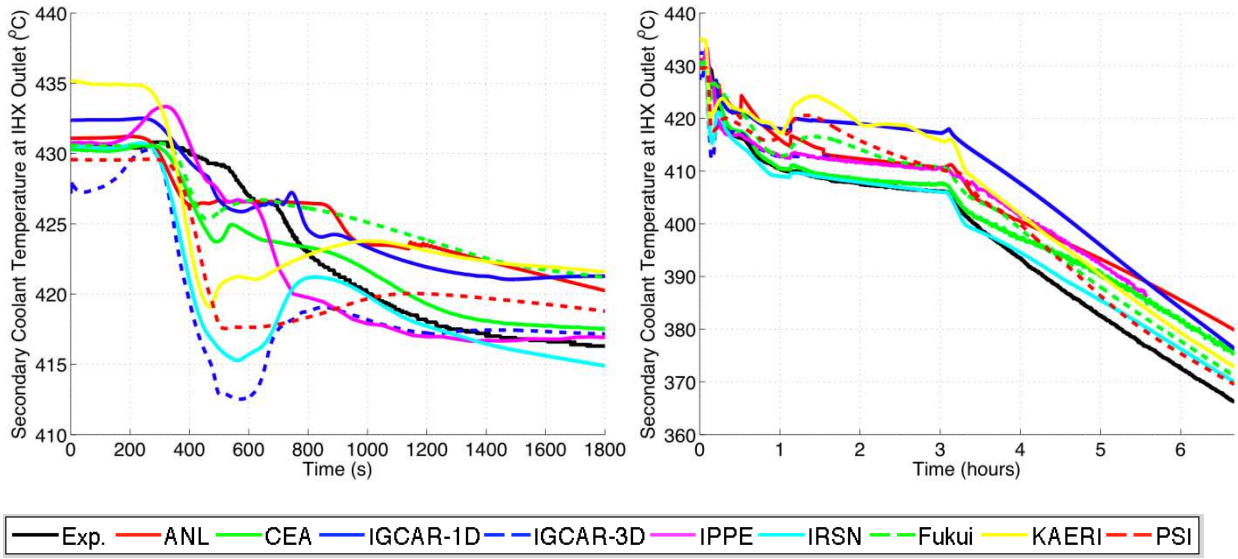

(d) Secondary Coolant Temperature at the IHX Outlet.

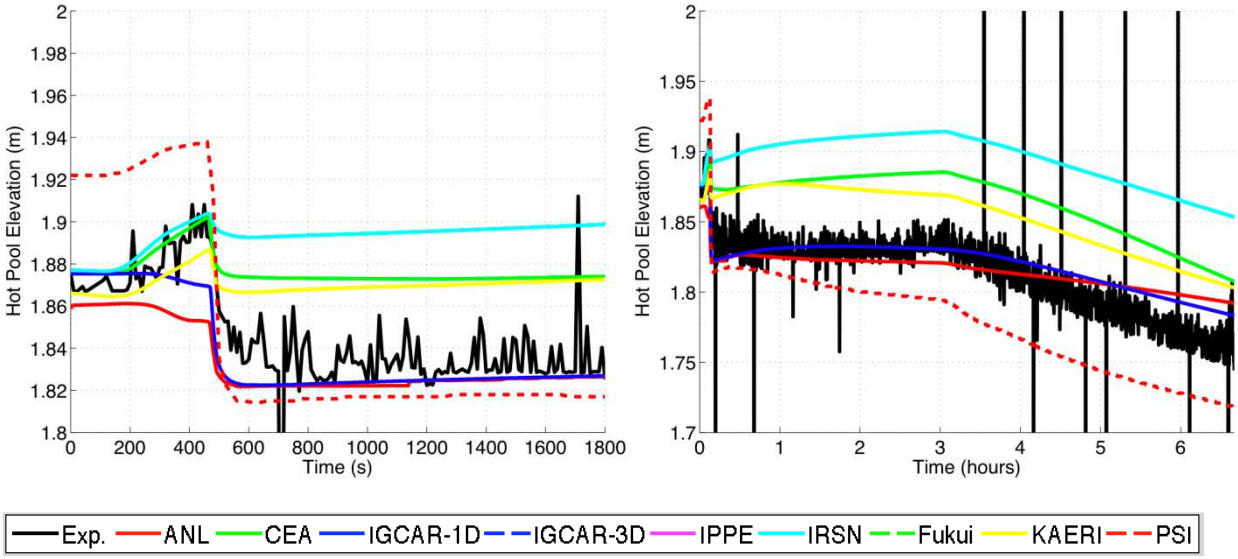

(e) Sodium/Gas Interface Elevation in the Hot Pool.

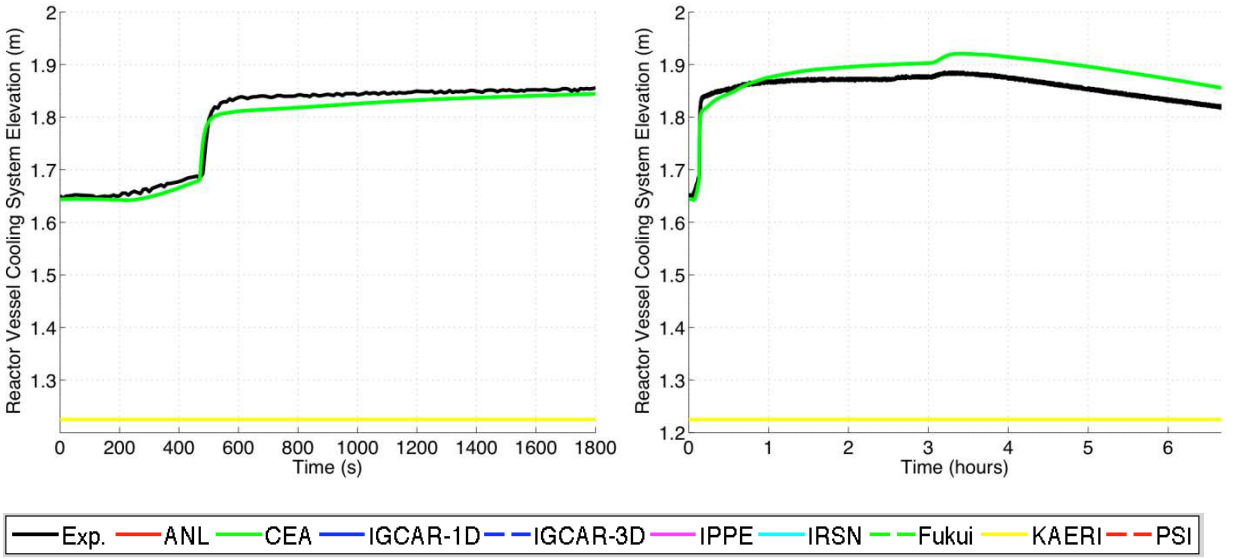

(f) Sodium/Gas Interface Elevation in the Reactor Vessel Cooling System.

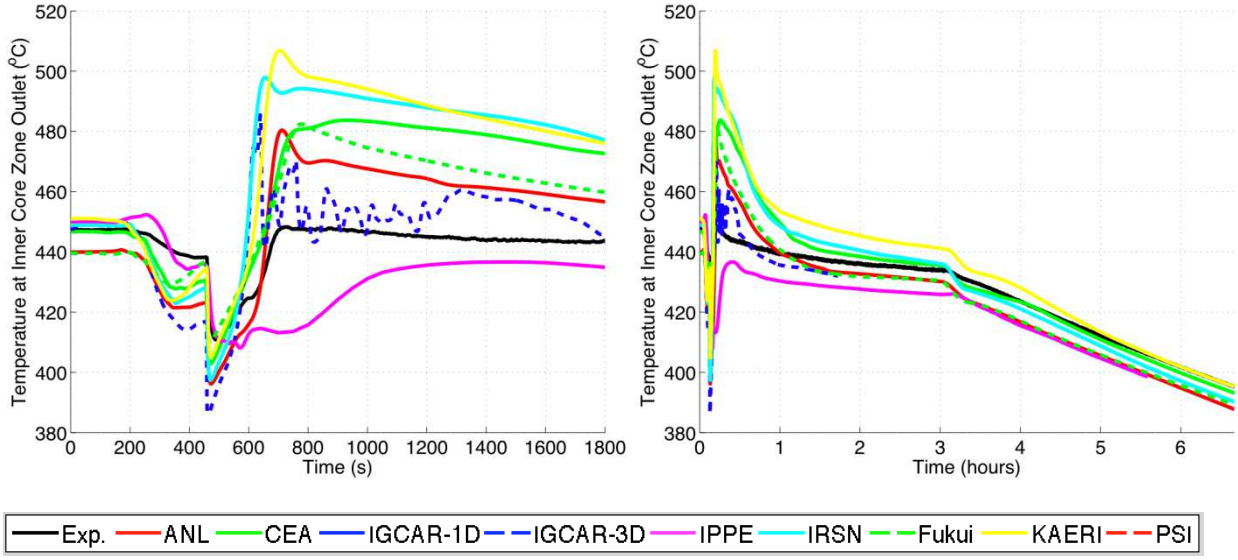

(g) Average Coolant Temperature at the Outlet of the Inner Core Zone.

FIG. 110. post-calculations – Comparison of measured results to the predictions of each participant

Short Term Results (t < 1800 sec) Long Term Results (t < 24,000 sec)

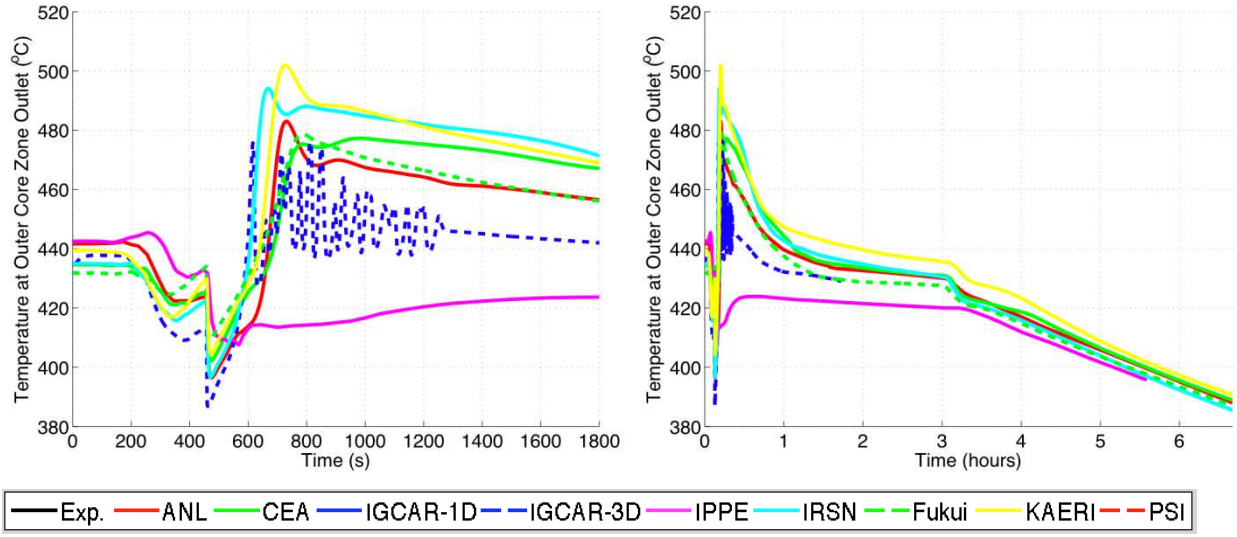

(a) Average Coolant Temperature at the Outlet of the Outer Core Zone.

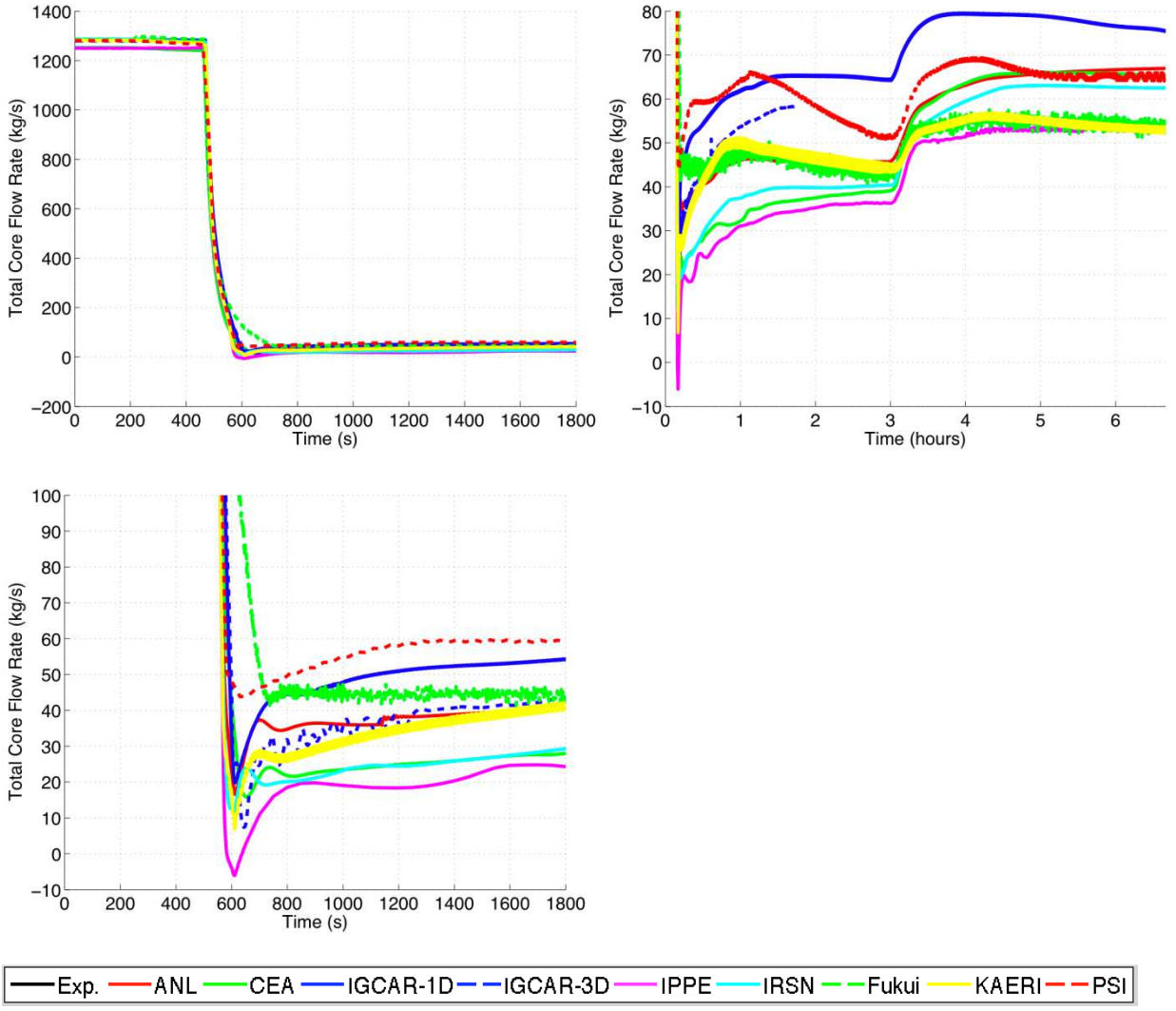

(b) Total Core Flow Rate.

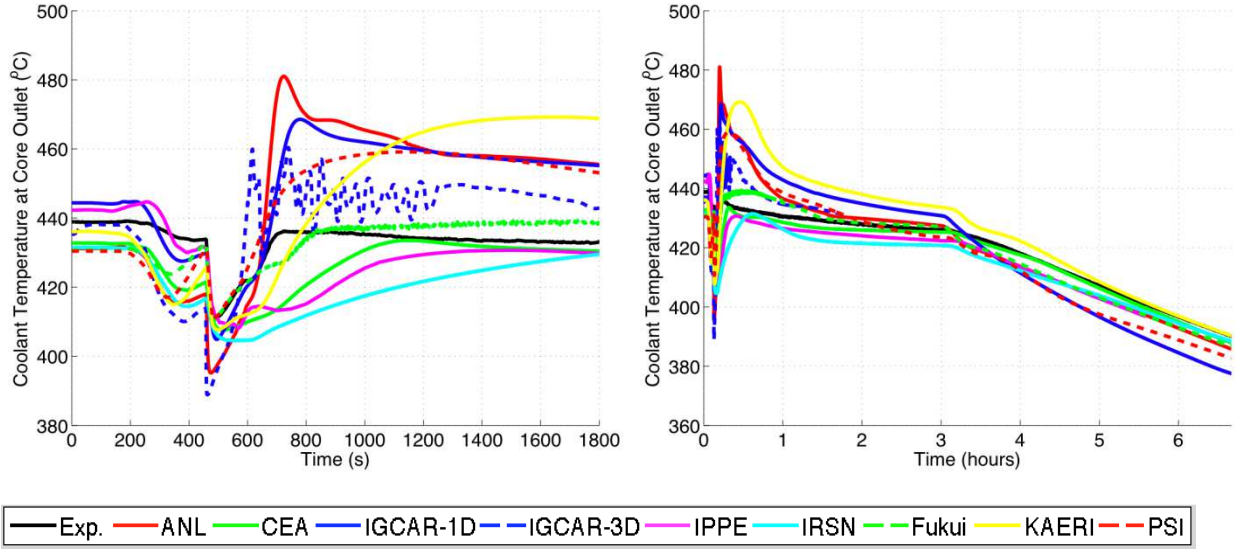

(c) Average Coolant Temperature at Core Outlet.

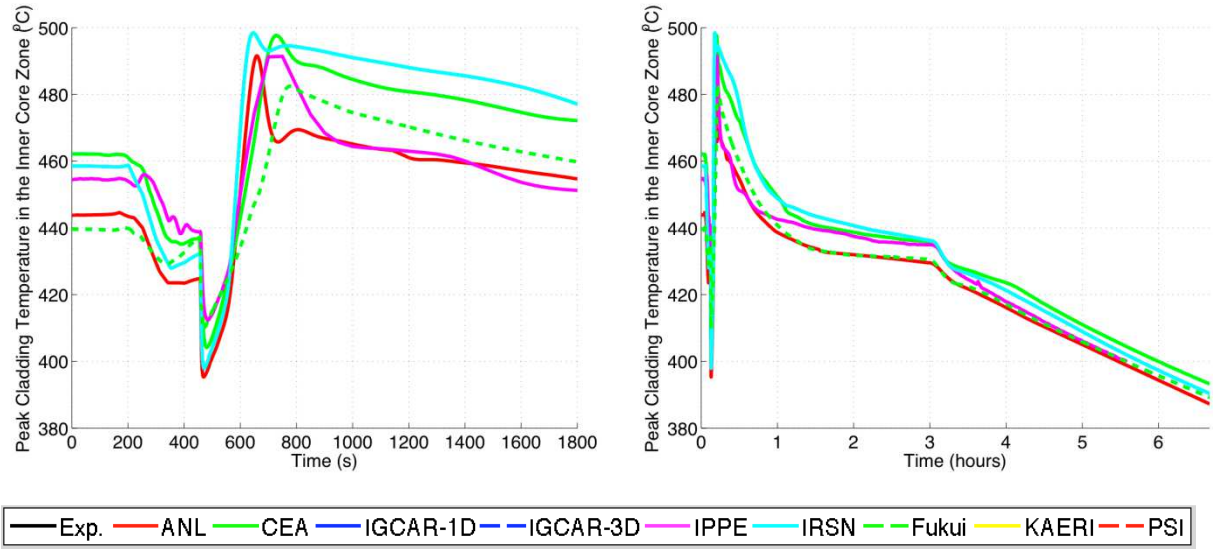

(d) Peak Inner Wall Cladding Temperature in the Inner Core Zone.

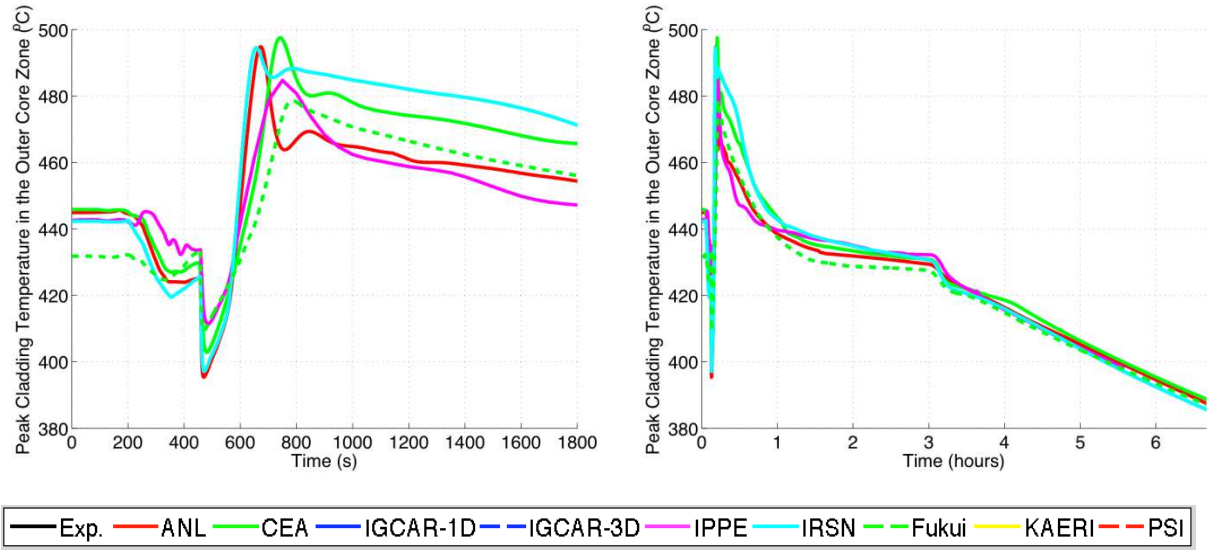

(e) Peak Inner Wall Cladding Temperature in the Outer Core Zone.

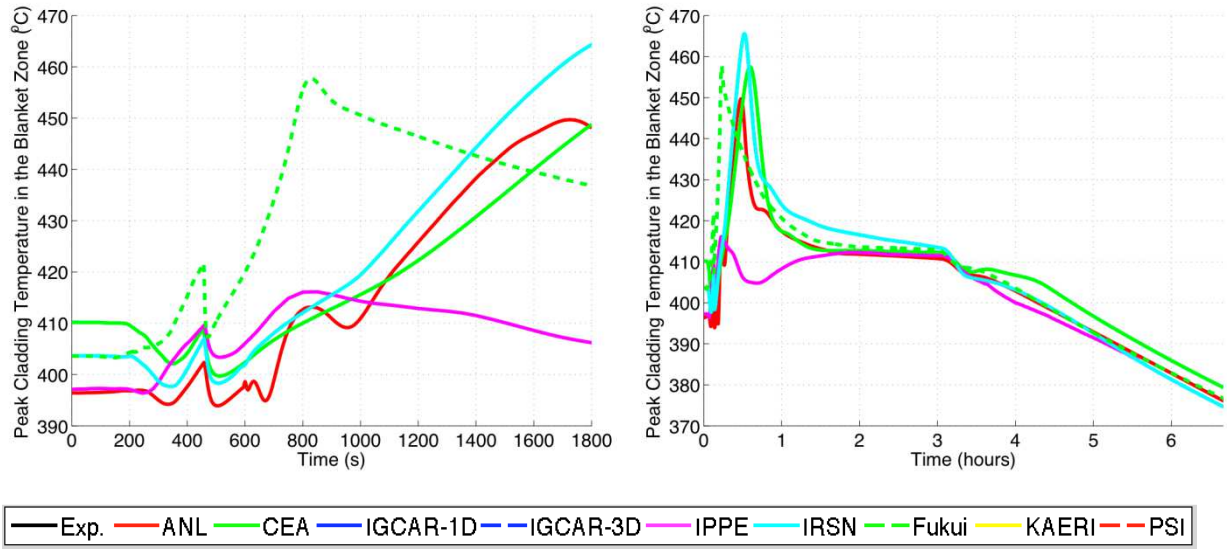

(f) Peak Inner Wall Cladding Temperature in the Blanket Core Zone.

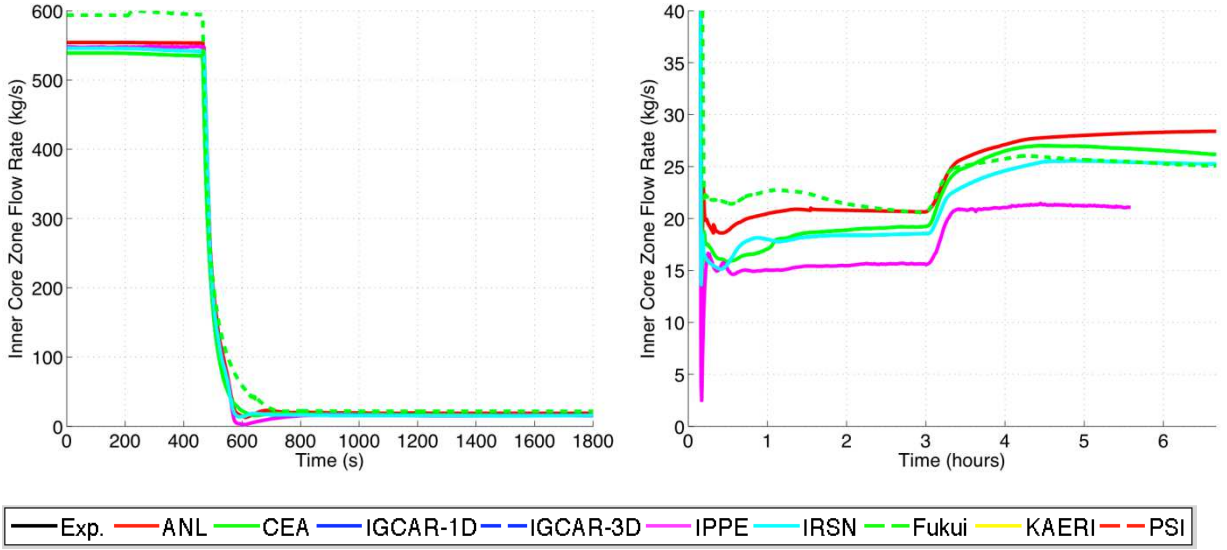

(g) Flow Rate in the Inner Core Zone.

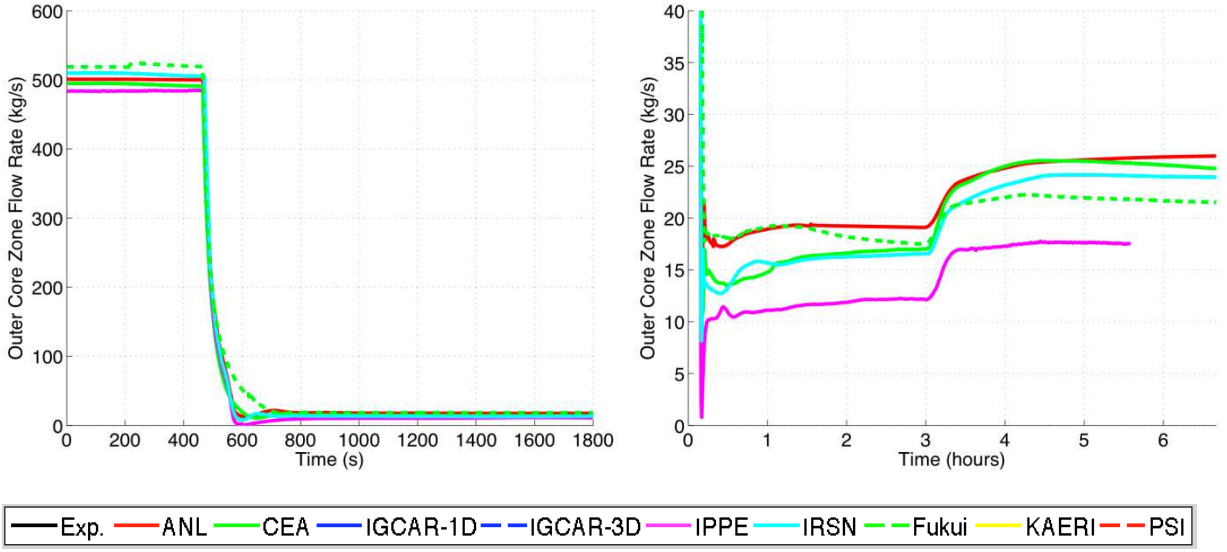

(h) Flow Rate in the Outer Core Zone.

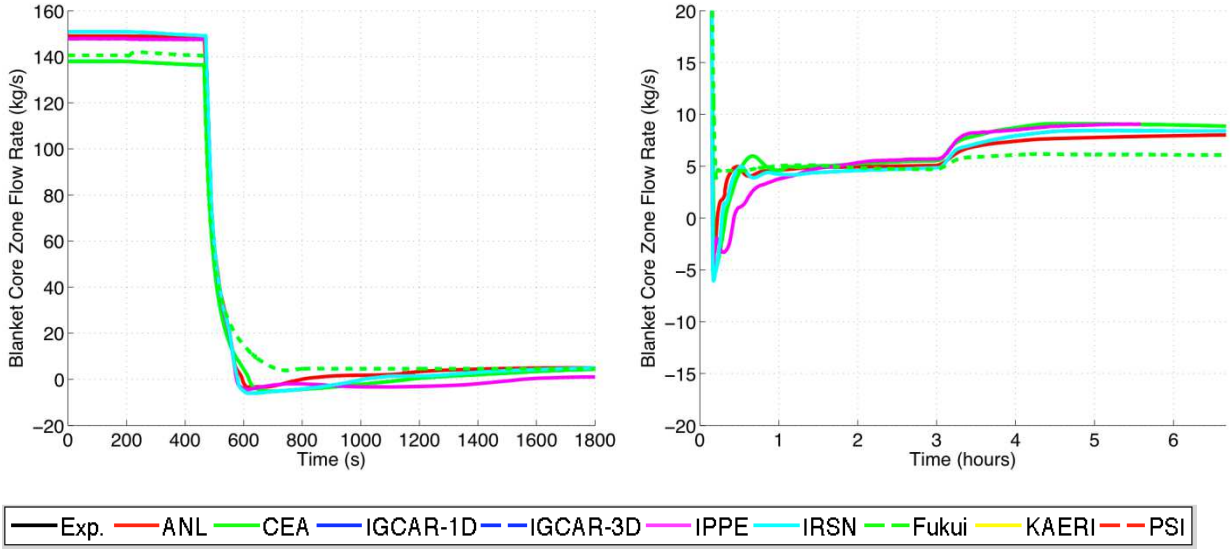

(i) Flow Rate in the Blanket Core Zone.

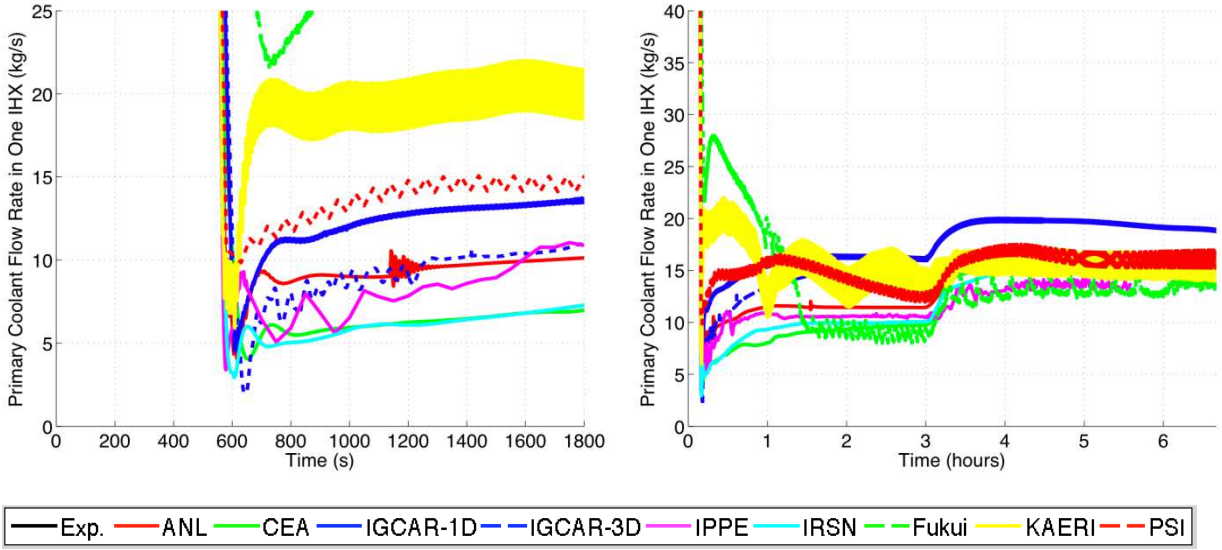

(j) Primary Coolant Flow Rate in One IHX.

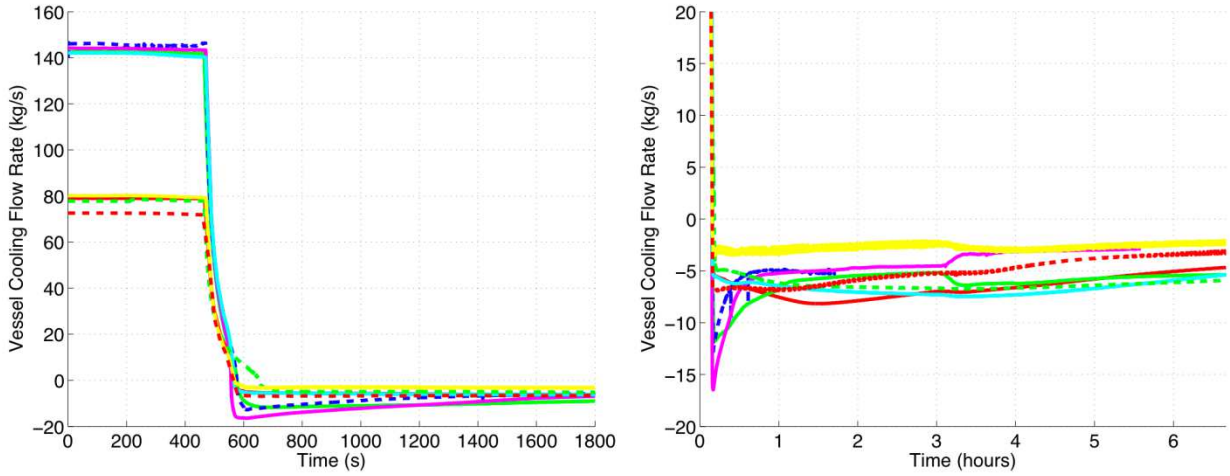

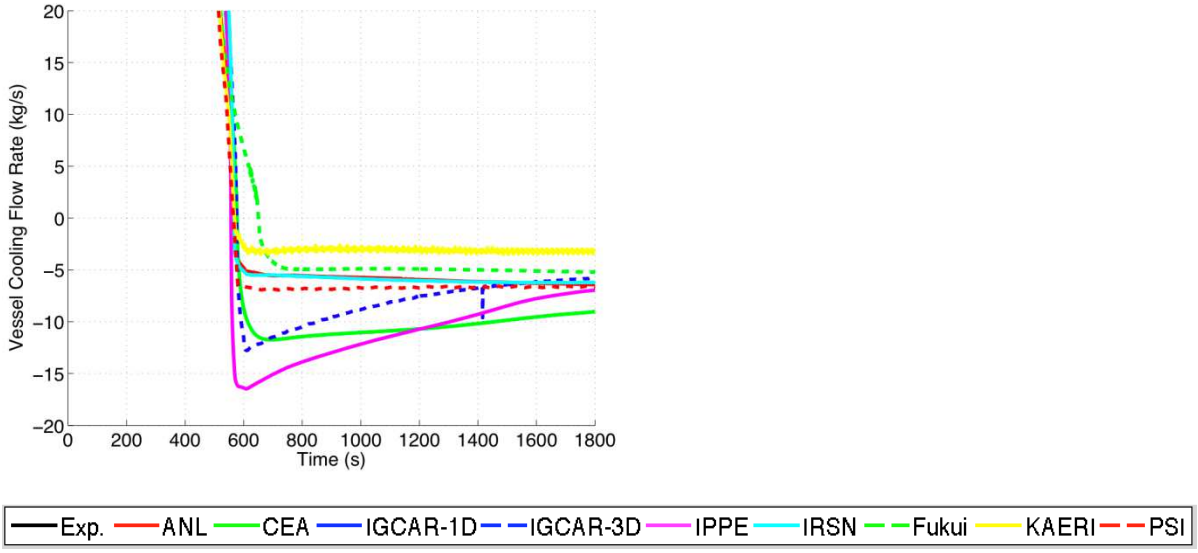

(k) Flow Rate Through Vessel Cooling System.

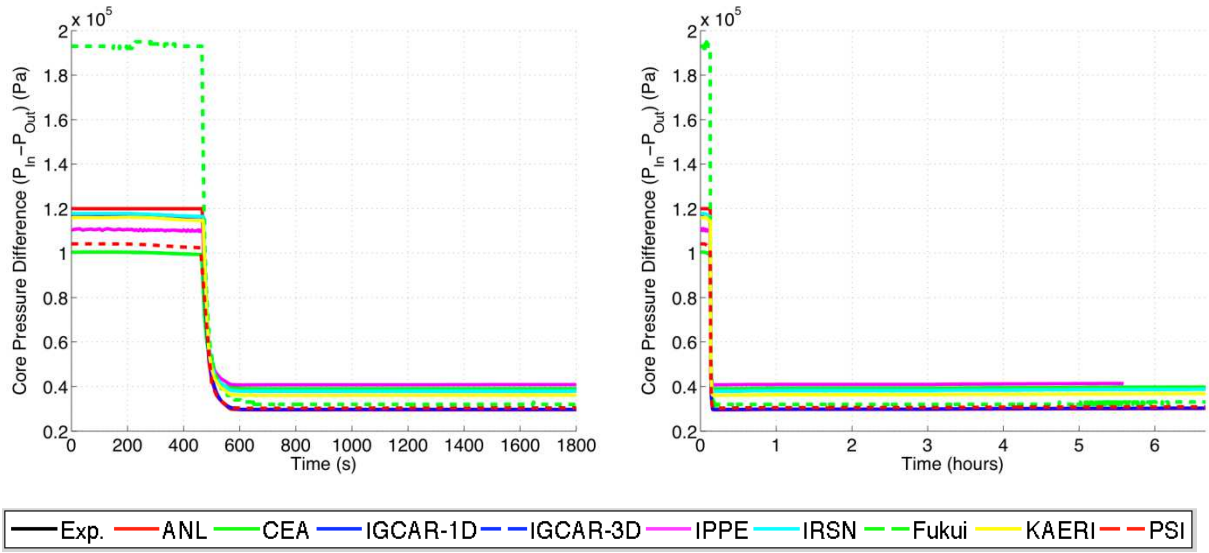

(l) Core Pressure Difference.

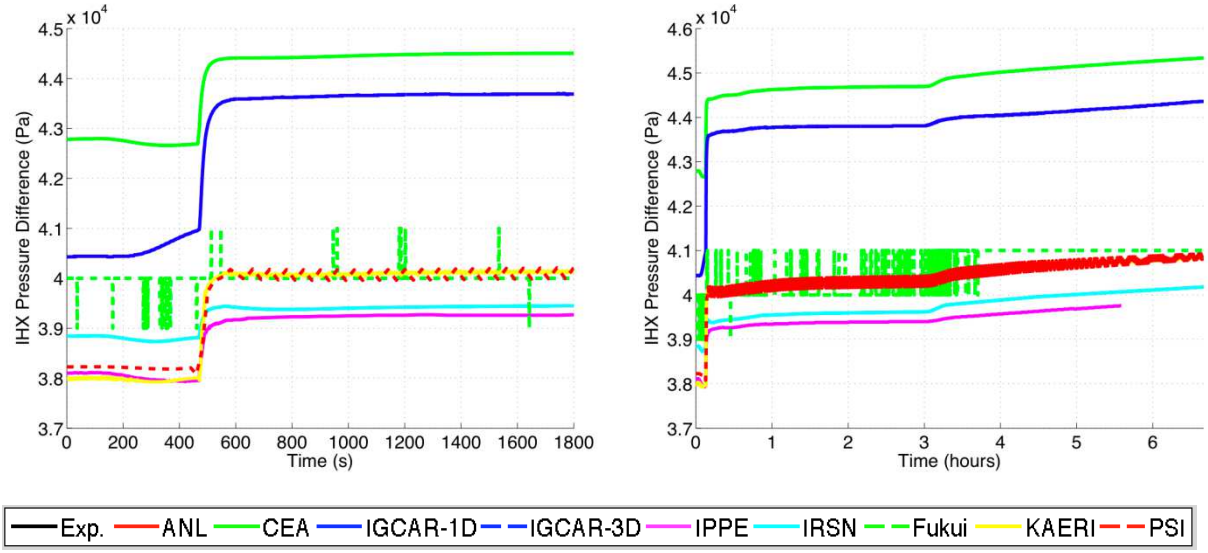

(m) IHX Pressure Difference.

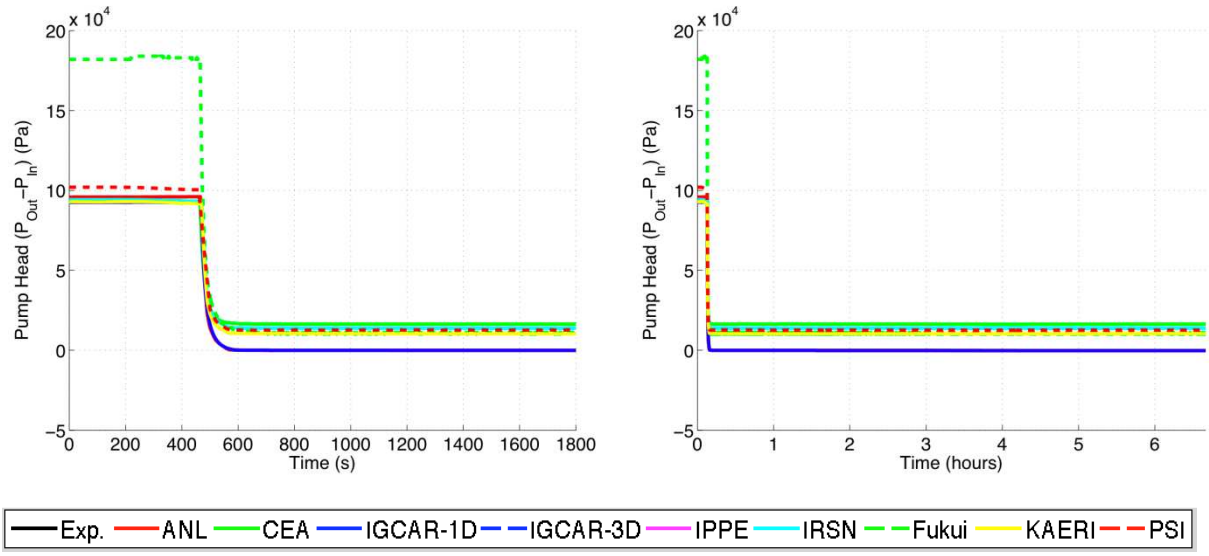

(n) Primary Pump Head.

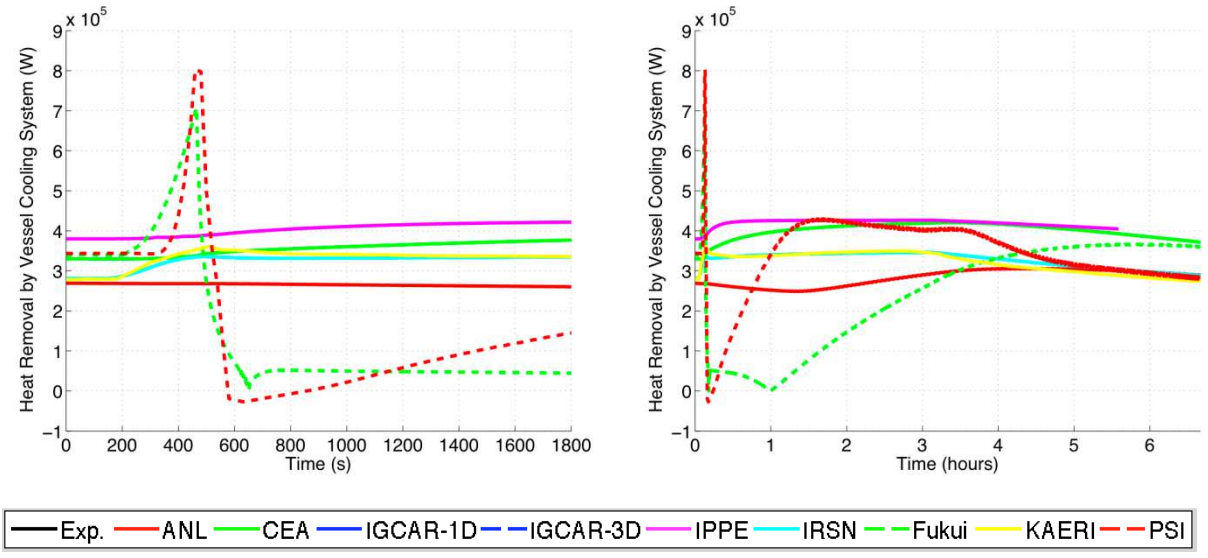

(o) Heat Removal by Vessel Cooling System.

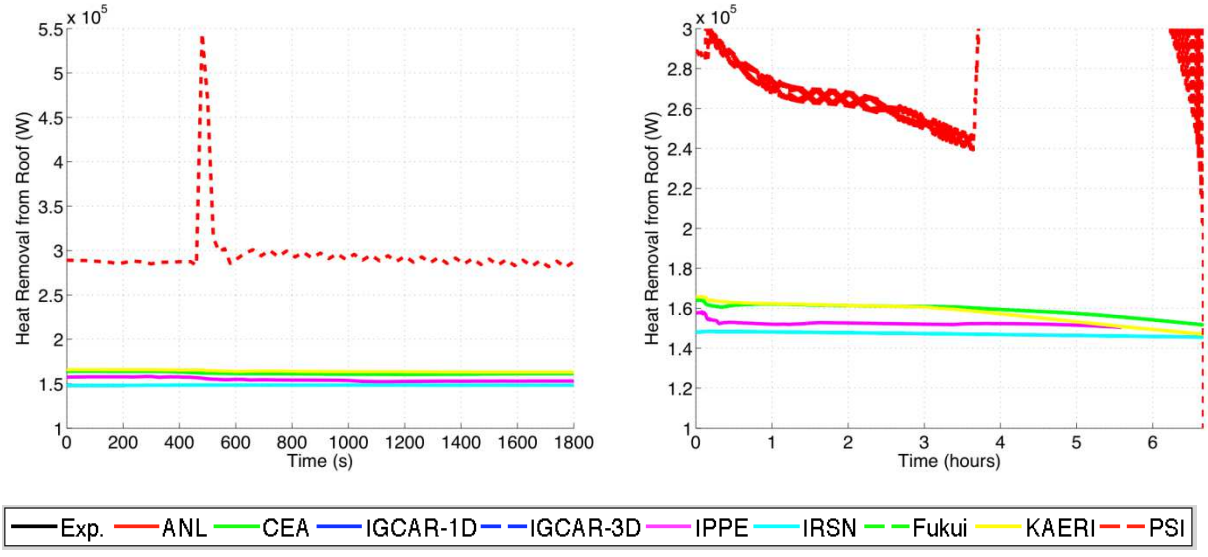

(p) Heat Removal from Roof.

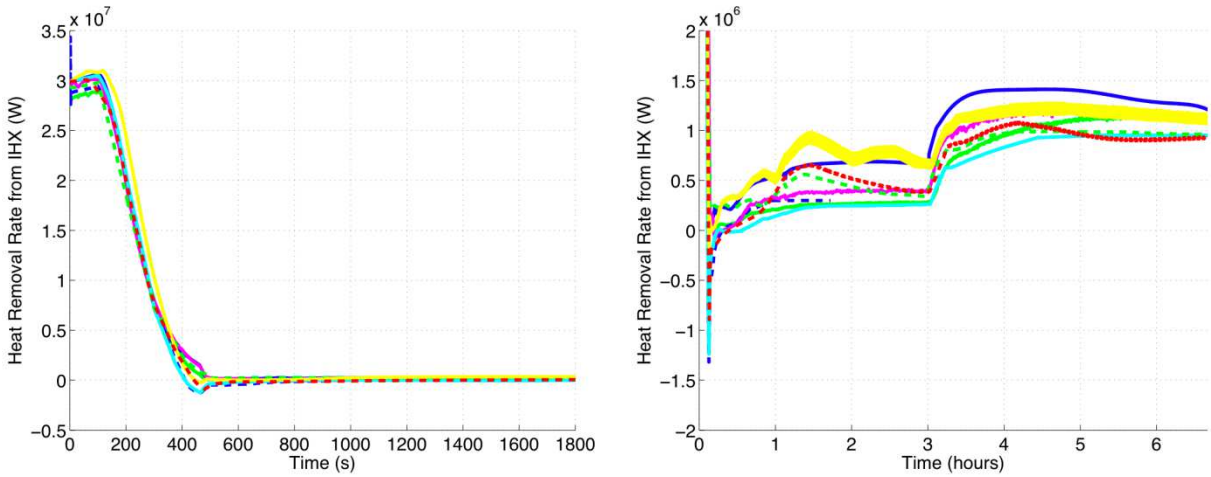

(q) Heat Removal from One IHX.

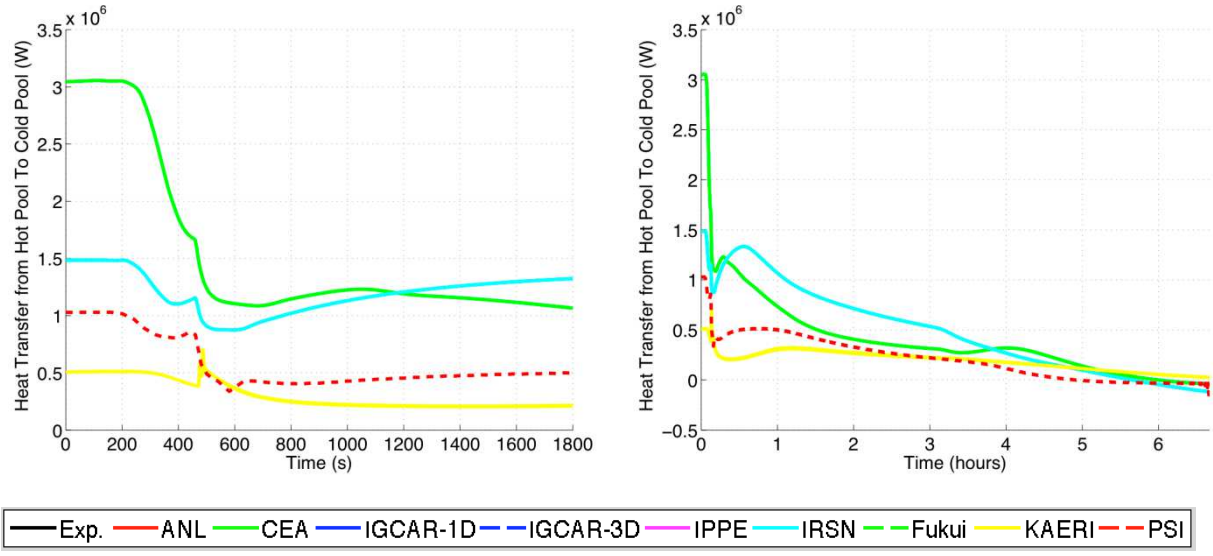

(r) Heat Transfer from the Hot Pool to the Cold Pool.

FIG. 111. post-calculations – Comparison of the code predictions from each participants (No experimental data are available for these quantities)

6.3.9.2. General discussion on post-test calculations

Note: IGCAR has performed a 3D calculation called IGCAR-3D for only 5000s, due to the CPU time and the cost of such computation. We can also note that for IGCAR-3D, all the input data (core power, secondary IHX inlet mass flow rate and secondary IHX inlet temperature) are constant.

The discussion treats the following items:

— Comparison to experimental results;

— Important points on code to code comparison ;

— Supplementary code to code comparisons.

6.3.9.2.1 Comparison to experimental results.

Coolant temperature at the primary pump inlet

(a) Short term (before the scram)

All the participants predict the pump inlet heating due to the steam generators dry out:

— PSI and KAERI over-estimates the peak of temperature (Tmax=420°C for PSI and Tmax=412°C for KAERI instead of 405°C in Phenix;

— IPPE and Fukui University predictions are closed to the Phenix data at scram;

— ANL, CEA and IRSN slightly under-estimate the peak of temperature (between 395°C to 400°C);

— IGCAR 3D gives the lowest prediction for the peak of temperature (392°C).

(b) Long term

After the scram, we can see that there are three kinds of prediction during the second phase:

— PSI predicts a nearly stable temperature around t=420°C until t=40mn, then the temperature decrease (high cooling rate between t=40mn to t=1h40mn, and lower cooling rate later). Before the beginning of the third phase, the pump inlet temperature is closed to the Phenix data, i.e. 400°C;

— KAERI predicts a continuous decrease of temperature after the scram until the beginning of phase 3;

— IPPE, ANL, CEA and IRSN predict a decrease of temperature after the scram followed by an increase of temperature until the beginning of phase 3. This trend is the most consistent with the experimental data;

— Fukui prediction leads to a delay in the first cooling followed by a slight increase of temperature before the beginning of phase 3;

— IGCAR 3D prediction leads to a slight increase of temperature between the scram and t=1h40mn.

Considering the third phase, all the codes predict rather well the efficient cooling of the reactor vessel:

— In Phenix, the cooling rate is first around -10°C/h until t=3.5 hours, and then around -5°C/h;

— CEA predicts the beginning of temperature decrease with some delay, due to the modelling and the over-estimation of the thermal inertia in the lower part of the cold pool;

— IPPE predicts rather well the Phenix trend with the two different cooling rates;

— ANL, PSI, IRSN, KAERI and Fukui predict a nearly constant cooling rate during this last phase;

Primary coolant temperature at the IHX inlet

(a) Short term

Before the scram, all the codes predict the decrease of temperature too early compared to Phenix data:

— KAERI, Fukui, PSI, IRSN, IGCAR-1D, ANL and CEA predict first a stable temperature, which seems consistent with the Phenix data and then a decrease of the temperature around t=350s (which can be linked to the decrease of the core power before the scram);

— IPPE and IGCAR-3D predict first a slight increase and then the decrease;

— The decrease of temperature is over-estimated by all the codes: the order of magnitude of this decrease is from 7°C to 20°C, whereas for Phenix it is closed to 5°C.

After the scram and the primary pump stop:

— CEA, IRSN and IPPE predict a slow decrease of temperature which leads to an equilibrium value depending on the order of magnitude of the cold shock ;

— ANL prediction is linked to the model of layer in the hot plenum (refer to ANL analysis);

— IGCAR-1D, IGCAR-3D, KAERI, Fukui and PSI predict a slight increase of the temperature, with a value at t= 1800s depending on the order of magnitude of the cold shock.

(b) Long term

For the second phase:

— In Phenix, the decrease of temperature is very slow: less than 10°C in nearly 3 hours. The temperature is 422°C at t=3.5 hours;

— ANL prediction remains linked to the multi-layers model (refer to ANL analysis);

— IGCAR-1D, IGCAR-3D, IRSN and IPPE predict an increase of the temperature followed by a stabilization;

— Fukui, PSI and KAERI predict an increase followed by a decrease;

— CEA predicts a slight decrease of temperature.;

For the third phase, all the codes predict rather well the efficient cooling;

— KAERI, Fukui, IPPE and PSI predict a cooling rate consistent with the Phenix data;

— ANL and CEA slightly under-estimate the cooling rate during this phase.

Primary coolant temperature at the IHX outlet

(a) Short term

All the codes predict correctly the increase of temperature due to the steam generators dry out. Just after the scram and the pump trip, only IPPE and IGCAR-3D predict properly the good trend for the drastic fall of temperature as seen in the reactor, whereas all the other participants show a slight decrease of the temperature. So, it is seen that the 3D modeling is recommended to predict the thermal stratification at the IHX outlet window. At t=1800s, the range of temperature at IHX outlet is from 409°C for KAERI to 417°C for PSI, whereas Phenix data is 410°C.

(b) Long term

During the second phase, Phenix data shows a nearly stable temperature of 405°C before the beginning of the third phase. All the codes follow the same trend and converge to a stable value around 400°C.

During the third phase, as long as the efficient heat sink is recovered, the IHX outlet temperature decrease with two cooling rate (a high one from t=3h to t=3h30mn and a lower one after t=3h30mn). All the codes predict correctly the two different cooling rates.

Secondary coolant temperature at the IHX outlet

(a) Short term

Until t=360s, Phenix data shows a constant value of 431°C. Then, there is a continuous decrease until t=1200s and a stabilization.

ANL, IRSN, IGCAR-1D, Fukui, PSI, CEA and KAERI predict the constant temperature before t=360s, but IPPE and IGCAR-3D predict an increase of the temperature. After t=360s, all the codes predict the decrease of the temperature:

— CEA, IGCAR-1D and ANL follow the same trend as Phenix data; KAERI, IGCAR-3D, PSI predict a more important fall of temperature followed by a slight increase.

(b) Long term

In the second phase, the temperature is nearly stable in Phenix (407°C). As for the calculations:

— CEA and IRSN predict a stable temperature closed to the Phenix one;

— IPPE and ANL show a little higher temperature;

— KAREI, PSI and Fukui have more variation during this phase;

— IGCAR-1D over-predicts by nearly 10°C the stabilized temperature.

In the third phase, the Phenix temperature decreases with the two cooling rates (already mentioned). All the participants predict the good behaviour with a discrepancy from 2°C for PSI to 12°C for ANL.

Average coolant temperature at core outlet

(a) Short term

In Phenix, until t=200s, the temperature is constant. Then, before the scram and primary pumps trip at t=460s, due to the core power decreases, the temperature decreases slightly (-5°C). Due to the scram, there is a cold shock (-25°C) and due to the primary pumps trip, there is a hot shock (+25°C).

PSI, ANL, CEA, IRSN, KAERI, IGCAR-3D and Fukui predict an initial value slightly lower than the Phenix data, whereas IPPE and IGCAR-1D give a slightly higher initial value. All the participants predict a significant decrease of temperature before t=460s. After the scram, the participants predict a cold shock of –about 15°C. For the hot shock, depending on the modeling choice, the peak of temperature is reached sooner (ANL, IGCAR-3D) or later (other participants). The maximum temperature is higher than the Phenix data for ANL, IGCAR-3D, PSI, KAERI, and lower for the other participants. IGCAR-3D predicts oscillations between t=600s to 1200s, at the onset of the natural convection.

(b) Long term

In Phenix during the second phase, the temperature is nearly stable: from 435°C to 430°C before the beginning of the third phase. During the third phase, the temperature decreases with a relative constant cooling rate.

During the second phase, all the participants predict a temperature which converges to a stable value:

— KAERI and IGCAR-1D over-estimate the temperature of about 10°C;

— IRSN and IPPE under-estimate the temperature of about –5°C.

During the third phase, the cooling rate is predicted by all the participants.

Comments:

— The average Phenix core outlet temperature is just an arithmetic average value issued from the fuel outlet sub-assemblies thermocouples (it does not take into account the mass flow distribution because there is no flow rate measurement). Moreover, there is a notable gradient at the core outlet, between inner core, outer core, blanket and external zones);

— Several 1D codes use a full mixing hypothesis at the core outlet (mixing between the different core outlet zones). With such an hypothesis, it is not possible to predict the radial gradient of temperature.

Sodium/gas interface elevation in the hot pool

(a) Short term

Due to the heating of the lower part of the cold pool, before t=460s, the level in the hot pool increases in Phenix. Then, with the primary pump trip, the level decrease is about -6cm.

The discrepancies between Phenix data and code results are due to the initial state tuning by each participant. Before t=460s, all the participants predict a slight increase of the hot pool level, except ANL, IGCAR-1D and IGCAR-3D who predict a slight decrease.

With the primary pump trip, all the participants predict the level decrease in a range between -0.5cm to -12 cm.

(b) Long term

After the scram and during the second phase, the Phenix level is stable with some oscillations:

— For IRSN and CEA, there is a slight increase of the level;

— For KAERI and IGCAR-1D, the level first increases and then decreases;

— For ANL the level remains constant;

— For PSI, there is a continuous decrease of the level.

During the third phase, the Phenix level decreases, due to the effective cooling of the reactor vessel:

— All the participants predict the decrease of the level during this phase;

— IRSN, KAERI, CEA and PSI show a good slope of decrease;

— IGCAR-1D and ANL slightly under-estimate the slope of decrease.

Sodium/gas interface elevation in the reactor cooling system

Before t=460s, the Phenix level increases slightly, due to the heating of the lower part of the cold pool. At t=460s, just after the primary pumps trip, there is an equilibrium of the different columns of fluid in the reactor vessel (reactor cooling vessel level, cold pool level and hot pool level). Due to the difference of area between the different zones, the reactor cooling vessel increases a lot (+12cm against -6cm for the hot pool level). During the second phase, the Phenix level is stable. During the third phase, the level decreases due to the efficient cooling of the reactor vessel.

Only CEA has computed the evolution of the reactor cooling vessel level. CEA prediction agrees with the reactor data until t=460s. During the second phase, CEA prediction seems to over-estimates slightly the increase of the level. During the third phase, the slope of level decrease predicted by CEA is consistent with the Phenix data.

Average coolant temperature at the outlet of the inner core zone

(a) Short term

In Phenix, until t=200s the temperature is constant. Then, before the scram, the temperature decreases slightly due to the core power decrease. Due to the scram, there is first a cold shock (-30°C) and just after due to the primary pumps trip, there is a hot shock (+40°C).

CEA, KAERI, IPPE, IRSN and Fukui provide this parameter from computations. All the code predicts the first decrease of temperature, even if the amplitude of the variation seems higher than in the reactor. Then, all the codes predict the cold shock and the hot shock:

— KAERI and IRSN predict the hottest temperature (about 500°C versus 450°C in Phenix);

— CEA and Fukui predict a high temperature (480°C);

— IPPE predicts the lowest temperature (438°C);

— IGCAR predicts some oscillations between t=600s to 1200s, at the onset of natural convection. After, the temperature follows the global trend in a smoother way.

Due to the influence of heat exchange with the inter-wrapper zone after the primary pumps trip, the peak of temperature in the inner core could be under-estimated by the outlet thermocouples (previous measurements showed that the order of magnitude of this under-estimation could be between 20°C to 30°C).

(b) Long term

In Phenix during the second phase, the temperature decreases slightly. In the third phase, the cooling is more efficient and the temperature decreases significantly.

The predictions of the participants during the second and third phases are consistent with the Phenix data: stabilization during the second phase and efficient cooling rate during the third phase.

6.3.9.2.2 Important additional parameters for code to code comparisons

Average coolant temperature at the outlet of the outer core zone

All the participants compute an initial temperature about 10°C lower than at the outlet of the inner core zone. Then, the decrease of temperature before and after the scram is nearly similar for each participant to the inner core behavior estimation. The hot shock due to the pumps trip is also nearly similar for each computation. During the second phase, the temperature stabilizes for each computation at a slightly lower value compared to the outlet temperature of the inner zone (IGCAR predicts again some oscillations at the beginning of phase 2, from t=600s to 1200s). In the third phase, the temperature decreases according to the mean cooling rate of the reactor vessel.

Total core flow rate

Before the scram, all the codes are consistent with the CEA data package. After the scram and the primary pumps trip, the primary pumps completely stop at roughly t=600s, and the minimal mass flow rate is reached:

— For IPPE, there is a small reverse flow of about -7kg/s;

— For the other participants, the total core mass flow rate remains positive, within a range from 5 kg/s for KAERI and IGCAR-3D to 45 kg/s for PSI;

— During the onset of natural convection in the primary vessel;

— IGCAR-1D, IRSN, IPPE and CEA predict an increase of the core mass flow rate until t=1hour and then a nearly stable value from 35 kg/s for IPPE to 65 kg/s for IGCAR-1D;

— ANL, KAERI, PSI and Fukui predictions are more complex: first a sharp increase, a peak (between t=1h and t=1h30mn) and then a slight decrease;

During the third phase, all the codes predict an increase of the total core mass flow rate, followed by a stabilization. The differences in the final core flow rate predictions roughly correspond to the differences at the beginning of the third phase.

Peak inner wall cladding temperature in the inner core zone

CEA, IPPE, IRSN and Fukui provide this parameter. All the code predictions show the same trend and they are quantitatively consistent, with a maximum temperature in the range from 480°C to 500°C. Fukui initial temperature is about 10°C lower than others and the amplitude of variation is smaller. In longer term, all the code predictions show the same trend and are again quantitatively consistent.

Peak inner wall cladding temperature in the outer core zone

Same comments as for the previous parameter.

Peak inner wall cladding temperature in the blanket core zone

The initial value is 397°C for IPPE, 403°C for Fukui and IRSN and 410°C for CEA.

After t=200s, there are two kinds of prediction:

— Due to the core power decrease before the scram, the temperature computed by CEA and IRSN first decreases; then, due to the heating of the core inlet temperature, the temperature increases;

— Fukui and IPPE predict only a heating before the scram.

After the scram, for Fukui and IPPE, as long as the mass flow rate remains positive the peak of temperature is reached at about t=800s (with a much higher value for Fukui 455°C than for IPPE 415°C). For CEA and IRSN, as long as they compute a reverse flow, the heating is slower and the maximum temperature is much higher (465°C for IRSN and 458°C for CEA at about t=40mn).

During the second phase:

— For CEA and IRSN, the mass flow rate is down top again: the temperature decrease quickly to reach a nearly stable value of 412°C at about t=1h30mn, (Fukui follows as similar trend);

— For IPPE, the temperature decreases from 415°C to 405°C, and then increases to the same value of 412°C;

For the third phase, the global trend of all the codes is consistent, with the efficient cooling of the reactor vessel.

Flow rates in the inner core zone / outer core zone and blanket zone

Inner core

The initial mass flow rate for the inner core is slightly higher for Fukui than for IPPE, IRSN and CEA. During the primary pumps trip, the Fukui mass flow rate remains a bit higher than for the other participants. The IPPE prediction seems to reach 0. at t=600s before increasing with the onset of natural convection. For the other participants, there is no decrease to zero and always a positive (upwards) mass flow rate. At t=800s, the natural convection is effective and the mass flow rate is stable during the second phase. After the beginning of the third phase, the mass flow rate in the inner core increases a little.

Outer core

Same analysis as for the previous parameter.

Blanket zone

Before t=460s, the mass flow rate in the blanket zone is nearly constant for all the participants. During the primary pump trip, the Fukui prediction remains positive. Whereas IPPE, IRSN and CEA predict a reverse flow during a while:

— IRSN reverse flow between t=550s and 1000s;

— CEA reverse flow between t=620s and t=1000s;

— IPPE reverse flow between t=550s and 1600s.

After 1600s, all the codes predict a positive flow with a nearly stable value. During the third phase, the mass flow increases (it seems that it increases a bit more for IPPE, IRSN, CEA than for Fukui).

Primary coolant flow rate in one IHX

The initial primary coolant mass flow rate in one IHX is from 290 kg/s for Fukui to 310 kg/s for the others participants (ANL, CEA, IGCAR-1D, IGCAR-3D, IPPE, IRSN, KAERI and PSI). After the scram and the primary pumps trip, the flow rate in the IHX decreases:

— Fukui predicts a lowest flow rate of 22 kg/s;

— All the other participants predict a flow rate between 2kg/s to 6 kg/s.

After t=800s, the flow rate is increasing slowly for all the participants. In long term during the second phase, the mass flow rate is quiet constant (we can notice for KAERI and PSI the evolution of mass flow rate connected to the evolution of the total core mass flow rate). With the third phase, the mass flow rate increases, except for KAERI and PSI where the mass flow rate remains nearly constant.

Flow rate through vessel cooling system

The initial flow rate through the vessel cooling system is 80 kg/s for PSI, Fukui and KAERI and 140 kg/s for the others participants (ANL, CEA, IGCAR-3D, IRSN and IPPE). When the primary pumps are stopped, the flow rate falls down. Due to the fact that the density of the hydraulic column in the cooling vessel system is higher than the average density in the (lower plenum-core-hot pool), there is a reverse flow in the vessel cooling system: the fluid is flowing downwards.

The order of magnitude of the downward flow is from -17kg/s for IPPE to -3 kg/s for KAERI. Then, the flow rate through the vessel cooling system remains downwards with a nearly constant value for all the codes during the second phase.

During the third phase, all the participants except CEA predict a slight decrease of this reverse mass flow rate, which remain negative for all the participants until the end of the transient.

Core pressure difference

When the primary pumps are in operation, the core pressure difference computed by each participant is:

— 1.95 bars for Fukui;

— About 1.2 bars for ANL, IRSN, KAERI, IGCAR-1D;

— 1.1 bars for IPPE;

— 1.0 bar for PSI and CEA.

At the primary pumps trip, the core pressure difference shrinks. After t=600s, the core pressure difference reaches a stable value:

— 0.4 bars for IPPE, CEA, IRSN and KAERI;

— 0.3 bars for Fukui, IGCAR-1D and PSI.

Due to the low evolution of density during the whole transient, the core pressure difference predicted by the participants remains constant.

IHX pressure difference

At the initial state, the IHX pressure difference is nearly the same for all participants:

— 0.38 bars for PSI, IPPE and KAERI;

— 0.39 bars for IRSN;

— 0.40 bars for Fukui (with fluctuations) and IGCAR-1D;

— 0.43 bars for CEA.

All the participants predict a qualitatively same trend of evolution for the IHX pressure difference, except Fukui who predicts a nearly constant IHX pressure difference. For the others:

— When the primary pump trips, there is a increase of the IHX pressure difference (with IGCAR-1D having the highest increase +0.025 bars and IRSN the lowest increase +0.005 bars);

— During the second phase, this parameter remains nearly constant;

— During the third phase, all the participants (except Fukui) predict a slight increase of this parameter. This could be connected to the increase of the stratification in the reactor vessel, leading to an increase of IHX difference of pressure due to density effect.

The IHX pressure difference is linked to the hot and cold pool level difference. If the IHX pressure difference is low, the hot and cold pool difference is low. We can also notice that, when the primary pump stops, as long as the velocity in the IHX shell shrinks, the friction losses also shrink and the only significant term in the IHX pressure difference is the gradient of density.

Primary pump head

The nominal value of the primary pump head is linked to the nominal value of the core pressure difference: as long as Fukui predicts the highest core pressure difference, Fukui also predicts the highest primary pump head.

When the primary pumps are tripped, the primary pump head shrinks:

— For IGCAR-1D, the value falls to 0;

— For others, there is still a residual level, around 0.1 bars, due to the gravity term, as the primary pump outlet is located at a higher elevation than the primary pump inlet.

Heat removal from roof

The initial power is 0.15 MW for CEA, IPPE, IRSN, KAERI and 0.29 MW for PSI. For CEA, IPPE, IRSN and KAERI this value remains constant during all the transient.

For PSI:

— there is a first peak at the scram (0.55 MW);

— at the transition between second and third phase, there is an increase (0.57 MW at t=4h20mn) and a decrease. After t=6h10mn, there are oscillations (from 0.1 MW to 0.82 MW).

Heat removal from vessel cooling system

The order of magnitude of the heat removal from vessel cooling system is 0.28 MW for ANL, IRSN, KAERI, 0.33 MW for CEA, Fukui, PSI and 0.39 MW for IPPE.

For Fukui and PSI, there is an increase of this parameter (after t=200s for Fukui and after t=360s for PSI). At the time of the manual actions, (scram and primary pump trips), Fukui and PSI predict a maxima (0.8 MW). After this maximum, the level decreases to reach a minimum (negative value for PSI and closed to zero for Fukui). The PSI data reaches a stable value at t=1h and decrease slightly during the third phase. The Fukui data increases from 0 MW at t=1h to 0.35 MW at t=4hours.

For the other participants, the heat removal from vessel cooling system increases very slowly during the second phase; then, the evolution is rather weak.

Heat removal from one IHX

Due to the steam generators dry out, the IHX power decreases from t=100s to 400s. It seems that some participants predict a reverse heat transfer between primary and secondary circuit: the secondary circuit heats the primary circuit (KAERI, PSI, IGCAR-3D, others?). For others, the heat removal seems always positive: the secondary circuit remains colder than the primary circuit. For all the participants, after t=1000s, the heat removal from IHX is closed to zero. There is nearly no heat transfer through the IHX.

With the third phase, heat transfer through IHX increases slightly as long as the SG casings are open. There is a direct link between the total core mass flow rate prediction and the heat removal from IHX prediction.

Heat transfer from hot pool to cold pool

The initial heat transfer from hot pool to cold pool is between 3 MW for CEA and 0.5 MW for KAERI. For CEA with the scram, this value decreases to about 1.2 MW until t=1800s. For IRSN, the initial value is 1.5 MW, there is a slight decrease with the scram and the primary pump stop and an increase until t=1800s. For KAERI, the initial value is 0.5 MW, and it decreases slowly to 0.2 MW at t=1800s. For PSI, the initial value is 1.0MW, and it decreases to 0.9 MW at t=1800s.

During the second phase, as long as the stratification becomes smaller in all the calculations, the heat exchange between the pools decreases: the reactor vessel is becoming rather homogeneous. During the third phase, the heat exchange is even becoming is closed to zero.

7. CONCLUSION

The overall objective of the CRP was to improve the Member States' analytical capabilities in the field of sodium cooled fast reactor thermal hydraulic simulation for passive decay heat removal issues. A required condition towards achieving this objective is a wide international effort on the validation of codes currently employed in this field. The CRP has contributed towards achieving the stated objective with the help of benchmark exercises focusing on the experimental results obtained during the Phenix End-of-Life (EOL) tests in 2009.

The specific objectives of the CRP on natural convection test in Phenix reactor are:

— to study the onset of sodium natural circulation in the primary circuit, as well as to determine the efficiency of natural convection in passively removing decay heat after a scram;

— to validate the various modelling choices and to qualify the numerical codes used to simulate natural convection in the primary circuit in classical 1D approach, as well as in coupled 1D/3D approach.

The CRP has been implemented in several stages. The first stage consisted in preparatory studies and modelling in view of the Phenix EOL test. In the second stage, the CRP participants have performed blind calculations based on the Phenix test conditions. In the third stage, the CRP participants have performed post-tests calculations with an open information on the Phenix results. Several CRP meetings and constant exchange of information between the participants have produced a significant common improvement in the validation of modelling choices and codes.

Among the informations produced by the natural convection test in Phenix, we can point out the following ones:

— The increase of the core inlet temperature (from 360°C to 400°C) after the steam generators dry out produces an important core power decrease (from 120 MW(th) to 50 MW(th) before the scram; this negative reactivity feedback is mainly due to the expansion of the diagrid and the relative insertion of control rods by expansion;

— The onset of natural convection after the scram and the primary pumps trip is rapid and efficient, as the core outlet temperature reaches a limited maximum value within 5 minutes and then starts decreasing;

— The thermal inertia of the reactor and the natural heat losses (without any significant heat sink) are sufficient to stabilize the core outlet temperature and even to reduce it slowly during at least 3 hours (and probably more if no action had been decided after 3 hours);

— The natural convection of air in the steam generators casing is very efficient to cool the secondary circuits (secondary pumps still operating at lower speed) and to reduce the core inlet and vessel temperatures;

— The temperature information given by a thermocouple can be suitable in forced convection but inadequate for natural convection situations depending on the local flow behavior influenced by buoyancy.

With the blind calculations, the CRP participants could look at the discrepancy in the various numerical results and analyze the reasons for such dispersion: choice in modeling, meshing, pressure drop and heat transfer correlation and so on. The discrepancies on some parameters between blind calculations and Phenix data are of course of great interest to improve future calculations.

Concerning the dispersion between numerical results and the discrepancies with Phenix data, we can point out the following ones:

— The increase of temperature at the core inlet after the steam generators dry out is slightly under-estimated by most participants and slightly over-estimated by two participants;

— The decrease of temperature at the core outlet due to the negative reactivity feedback after the steam generators dry out is not correctly predicted by most participants; improvements in the neutronic model and the relative expansion evaluation are required;

— The slight increase of temperature at the core inlet during the first natural convection phase without heat sink is predicted by most participants;

— The decrease of temperature at the core inlet during the second natural convection phase with heat sink is well predicted by all the participants;

— The short term evolution of the core outlet temperature after the scram is different for each calculation and relatively far from the reactor data; but, one has to keep in mind that the reactor average core outlet temperature is not easy to define as we have no direct information on the flow radial distribution in the core during natural convection;

— The decrease of temperature at the core outlet during the second natural convection phase with heat sink is well predicted by all the participants;

— A large dispersion appears on the core flow rate predicted by the participants in natural convection (first phase and second phase); unfortunately, there is no measurement of the natural convection core flow rate in the reactor to be compared with the computations;

— The heat exchanger inlet temperature is not well predicted by most participants as thermal stratification occurs in the hot pool, which is rather difficult to calculate with system codes;

— The sodium level in hot and cold pools are not very well predicted by several participants at the initial steady-state condition, so that discrepancies remain during the transient;

— The inversion of the flow in the vessel cooling system during natural convection is predicted by most participants, but some dispersion exists on the quantitative value and there is no reactor measurement.

With the post-test calculations, the participants could take into account the experience gained from the blind calculations. Most participants introduced modifications in the modeling choices and performed sensitivity computations to see the influence of several parameters on the prediction.

Many interesting results were obtained with the post-test calculations and they are described in the report. In the present conclusion, we just recall and point out some important outcomes on the parameters which were not well predicted during the blind calculations:

— The increase of temperature at the core inlet after the steam generators dry out is better estimated by most participants, thanks to a better modeling of the stratification in the hot and cold pools;

— The computed evolution of temperature at the core outlet remains difficult to compare with the reactor, as we have no direct information on the flow radial distribution in the core during natural convection; the discrepancy in the computed results remains rather large during the first phase of the test, mainly due to modeling choices; then, the agreement is better when natural convection is established;

— The discrepancy in the core flow rate predicted by the participants in natural convection (first phase and second phase) remains important, although some participants have improved their results; unfortunately, there is no measurement of the natural convection core flow rate in the reactor to be compared with the computations;

— The evolution of temperature at the heat exchanger inlet is better estimated by some participants, thanks to a better modeling of the stratification in the hot pool; however, several computed results remain rather far from reactor data, maybe due to discrepancies on the core flow rate and the core outlet temperature;

— The evolution of temperature at the heat exchanger outlet is better estimated by 3D models which can take into account the thermal stratification at the outlet window.

Based on the various lessons summarized just above, participants can propose some general recommendations. Sodium cooled fast reactors have a real capability of passively removing decay heat through natural convection. But, modeling natural convection in a reactor is a real challenge as the thermal hydraulic behaviour can be very complicated. So, the first recommendation is the necessity of developing a complete validation process of numerical codes used for the prediction of natural convection decay heat removal. The validation must concern the modeling (1D and/or 3D), the meshing, the pressure drop and heat transfer correlations and so on. Sensitivity analysis is useful to detect the most important parameters which have an influence on the main issues as the cladding temperature and the core outlet temperature. Based on this sensitivity analysis, the need of experimental data can be defined. Analytical tests will give information on correlations to be used in natural convection for the various components involved in the circuit. Moreover, reduced scale water models can be developed to qualify the code on more global representative geometries. Anyway, reactor data are needed to verify the adequacy of the codes to compute real reactor conditions. The natural convection test in Phenix reactor has been used as one common support in this process, in the frame of the present CRP.

APPENDIX I: MODEL DESCRIPTION FOR THE ANALYSIS OF PHENIX NATURAL CONVECTION TEST

This gives an overview of the main model choices for each participant, through tables.

TABLE 16. HYDRODYNAMIC VOLUME (LIQUID VOLUME AT 350 MW)

Volume (m^3)	ANL	CEA	IGCAR-3D	IGCAR-1D	IRSN	IPPE	KAERI	PSI	Remarks
Primary side									
Pump discharge pipe	1.69	1.57	1.6	1.69	10.3 including pump inlet	2.0	0.7625	4.6 From +173mm to diagrid	P/p outlet to diagrid inlet For 1 pump
Inlet plenum	9.0	17.0	39	23.0	35.8	?	31.91	/	
Hot pool	313.21	276.0	238 (excluding UCS, IHX and Pump)	319.3		316.	252.03	309.0	
IHX primary side	2.3	4.3	5.2	3.03	3.5	3.14	2.7814	2.86 For 1 IHX	Including inlet and outlet windows
Cold pool	394.28	401.0	348	406.2	500.9	580.	388.6	648.0	
Pump inlet	8.69	1.57	11.8	2	included in pump discharge pipe	0.4	11.403	4.23	Annulus between p/p shroud and discharge pipe for 1 pump
Lower diagrid	220.12	13.6	30	-	59.2	9.3	113.8	12.6 Including inlet plenum	Between elevation -8155~-7305 [1)]
Vessel cooling system – Part I	0.	114.0	37	-	22.4	29.0	11.612	126.0 Part I and II	Below elevation -5297 [1)]
Vessel cooling system – Part II	47.28	29.3	28.7	-	28.0	117.0	19.7439	/	Above elevation -5297 [1)]
Secondary side									
IHX inlet	0.00	2.0	0	-	/	/	0.4015	/	For 1 IHX
IHX tube side	7.42	1.37	1.38	1.38	1.64	3.1	1.3576	4.9	For 1 IHX
IHX outlet	0.00	1.02	0	-	/	/	0.4015	/	For 1 IHX

TABLE 17. VOLUME LENGTH (OCCUPIED BY LIQUID)

Length (m)	ANL	CEA	IGCAR-3D	IGCAR-1D	IRSN	IPPE	KAERI	PSI	Remarks
Primary side									
Pump discharge pipe	7.40	7.37	5	7.4	9.137	10.0	3.330	6.8	P/p out to inlet diagrid
Inlet plenum	N/A	0.85	1.08	-	1	?	1.065	/	
Hot pool	N/A*	4.76	4.7	Volume model	4.41	8.0	4.540	4.91	
IHX primary side	5.365	6.28	5.27	5.365	5.465	5.365	5.27	4.89	including inlet and outlet windows
Cold pool	N/A*	9.48	9.73	Volume model	9.361	8.0	9.146	10.34	
Pump inlet	5.651	5.47	5	5.5	6.395	2.8	5.472	5.47	Annulus between p/p shroud and discharge pipe
Lower diagrid	N/A*	1.06	0.85	-	1.65	1.5	1.57	1.9 Including inlet plenum	Between elevation -8155~-7305 [1)]
Vessel cooling system – Part I	0	3.50	4.7	-	3.59	7.0	3.31	20.0 Part I and II	Below elevation -5297 [1)]
Vessel cooling system – Part II	6.90	3.75	11.4	-	10.04	9.0	6.974	/	Above elevation -5297 [1)]
Secondary side									
IHX inlet	0	14.6	0	-	/	/	0.664	/	For 1 IHX
IHX tube side	5.365	5.365	5.27	5.365	5.365	5.365	5.27	4.8	For 1 IHX
IHX outlet	0	6.40	0	-	/	/	0.664	/	For 1 IHX

TABLE 18. CORE CHANNELS:

Parameters	ANL	CEA	IGCAR-3D	IGCAR-1D	IRSN	IPPE	KAERI	PSI	Remarks
# of Subassemblies (SAs)									
Inner core	54	54	54	54	110	54SA+7CR	54	54	
Outer core	48	56	56	56		56	56	56	
Ferfile SA	86	86	86	86	86	86	86	86	
Reflector SA	212	1274	212	212	212	212	14	212	
Shielding SA	1062		765	-	X	765B4C+ 297SSA	765	/	
Others	40		304	-	X	90Storage	7	30 storage 7 CR + SR	
Flow area for each SA zones (m^2) – estimated for the fuel pin region									
Inner core	0.2319	4.297e-3	0.26	0.004297	0.454	0.293	0.2320	4.297e-3	
Outer core	0.2061	4.297e-3	0.27	0.004297		0.231	0.2405	4.297e-3	
Ferfile SA	0.2732	3.176e-3	0.42	0.003176	0.258	0.432	0.2731	3.176e-3	
Reflector SA	1.210	1.1309E-2	1.036	0.003176	0.778	1.037	0.0536	7.94e-3	
Shielding SA	7.714		3.74	-	X	/	2.9804	/	
Others	1.718		0.24	-	X	0.37	0.0455	4.297e-3	
Hydraulic diameter (m) – estimated for the fuel pin region									
Inner core	3.038e-3	3.e-3	-	0.00304	0.373	0.00304	3.035e-3	3.04e-3	
Outer core	3.083e-3	3.e-3	-	0.00304		0.00304	3.035e-3	3.04e-3	
Ferfile SA	3.996e-3	4.e-3		0.003995	0.348	0.00438	3.988e-3	4.0e-3	
Reflector SA	5.707e-3	12e-3	-	0.003965	2.513	0.01	1.010e-2	5.e-3	
Shielding SA	9.616e-2		-	-	X	0.01	1.260e-2	/	
Others	3.083e-3		-	-	X	0.00304	2.465e-2	3.04e-3	

TABLE 19. PRESSURE DROP:

Pressure Drop (Pa)	ANL	CEA	IGCAR-3D	IGCAR-1D	IRSN	IPPE	KAERI	PSI	Remarks
Primary side									
Pump head	95800	1.9352E5	2.0913E5	2.0913E5	388.4	209010.	2.01724E+05	2.224e5	At power of 350 MW(th)
Pump discharge pipe	3320	0.08E5	0.0494E5	0.0494E5	4592	3300	9.2690E+02	0.24e5 From P/P to core	P/p out to inlet diagrid
Inlet plenum	0	0.057E5	0.0304E5	0.0304E5	/	Included in Pump discharge pipe	4.4593E+04	/	
Core dP	83900	2.04E5	1.955E5	1.955E5	1.947e5	195500.	1.3892E+05	2.0e5	including inlet orifice and outlet nozzle
IHX primary side	2360	0.32E5	0.0565E5	0.0565E5	1831	3000.	7.3936E+03	0.345e5	including inlet and outlet windows
Lower diagrid	N/A	0.079E5	-	-	1.752e5	Included in Pump discharge pipe	1.0284E+04	2.0e5	At elevation -7305 [1)]
Vessel cooling system – Part I	0	0.059E5	-	-	/	169000.	~10	Included in lower diagrid	Below elevation -5297 [1)]
Vessel cooling system – Part II	92500	0.936E5	-	-	5.04e3	0	4.8568E+04 + 1.3162E+05	Included in lower diagrid	Above elevation -5297 [1)]
Secondary side									
IHX inlet	-	0.11e5	-	-	/	/	4.4020E+03	/	For 1 IHX
IHX tube side	180	0.55e5	-	-	/	/	1.7236E+04	0.48e5	For 1 IHX
IHX outlet	-	0.56e5	-	-	/	/	1.5260E+03	/	For 1 IHX

TABLE 20. PRESSURE DISTRIBUTION:

Pressure (Pa)	ANL	CEA	IGCAR-3D (Hydrostatic pressure-858*9.81*height of sodium column)	IGCAR-1D	IRSN	IPPE	KAERI	PSI	Remarks
Primary side				At 120 MW(th)					
Cover gas	1.2e5	1.2E5	0	1.2E5	1.2e5	12000	1.17131E+05	1.2e5	
Pump inlet	2.251e5	1.650E5	-2920 (in cold pool near pump inlet) -4805 at impeller inlet	1.3086E5	1.76e5	15700.	3.55226E+05	1.76e5	
Pump outlet	3.209e5	3.290E5	84200	2.2336E5	3.75e5		3.60517E+05	3.97e5	Just after the pump impeller
Inlet plenum	2.776e5	3.602E5	88000	2.76658E5	3.75e5	38800.	3.10316E+05	3.85e5	
Core bottom	1.578e5	3.336E5	1700	2.7539E5	3.6e5	38800.	1.45949E+05	3.61e5	Above the inlet orifices
Core top	1.258e5	1.362E5	-90	1.5889E5	1.6e5	15500.	1.13672E+05	1.60e5	Before the out nozzle
IHX inlet	1.258e5	1.279E5	-200	1.27020E5	1.21e5	12000	1.48027E+05	1.31e5	including inlet and outlet windows
IHX outlet	1.681e5	1.678E5	-3000	1.6745E5	1.62e5	16600.	3.61339E+05	1.66e5	Before the IHX out window
Vessel cooling system – Bottom	3.00e5	1.938E5	-2800	-	1.87e5	38800.	2.57865E+05	2.16e5	At the bottom of RV
Vessel cooling system – Return point	1.52e5	1.508E5	-3150	-	1.21e5	11700.	1.17131E+05	1.21e5	Just before to cold pool
Secondary side									

IHX inlet	5.006e5	5.657e5	-	-	/		2.70989E+05	1.68e5	
IHX tube side-mid point	-	5.390e5	-	-	/		2.35329E+05	1.45e5	
IHX outlet	4.557e5	5.120e5	-	-	/		1.99836E+05	1.2e5	

TABLE 21. IHX:

Parameters	ANL	CEA	IGCAR-3D	IGCAR-1D	IRSN	IPPE	KAERI	PSI	Remarks
Primary side									
Heated length (m)	5.365	5.365	5.27	5.365	5,365	5.365	5.27	4.795	For one tube
Heat transfer area (m^2)	538	537.8	530	537.8	450	460.9	452.78	480.0	For 1 IHX
Heat transfer coefficient (W/m^2 K)	2.86e4	21.23	38000	38000		25000.-38000.	34942	3.45e4	At power of 350 MW(th) At the mid- elevation of IHX
Heat transfer correlation		Borowhanski $6+0.006.Pe^{1.0}$	Graber and Reiger $Nu = 9.1+0.0387\ Pe^{0.76}$	Graber and Reiger $Nu = 9.1+0.0387\ Pe^{0.76}$	6+0,006.Pe	Kirilov For pin bundle		Mikityuk $0.047(1-e^{-3.8(P/D-1)})(Pe^{0.77}+250)$	
Secondary side									
Heat transfer area (m^2)	461	460.9	461	460.9	450	460.9	528.24	412.0	For 1 IHX
Heat transfer coefficient (W/m^2 K)	1.47e4	20.87	38000	38000		24400.	55354	7.0e4	At power of 350 MW(th) At the mid- elevation of IHX
Heat transfer correlation		Spukinski $4.82+0.0185.\ Pe^{0,827}$	Subbotin et. al $Nu=5+0.025\ Pe^{0.8}$	Subbotin et. al $Nu=5+0.025\ Pe^{0.8}$	$4,82+0,0185\ .Pe^{0,827}$	Kirilov 7.5+0.005*Pe		Mikityuk	

TABLE 22. HEAT STRUCTURES:

Parameters	ANL	CEA	IGCAR-3D	IGCAR-1D	IRSN	IPPE	KAERI	PSI	Remarks
Heat Transfer Area (m^2) – primary side			Wall functions are used						
Hot pool - Cold pool	0	143	-	-	42.474	/	200.77	300	
Cold pool – Vessel cooling system	433	450	-	-	452	/	98.10	452	
Others structures (inside the vessel)		149	-	-	91.39 (diagrid) 120 (Pumps) 16 (core plug) 5,2 (transfer arm)	/	N/A		IHX shroud, Pump shroud, etc.
Heat Transfer Area (m^2) – Secondary side			-						
IHX downcomer pipe (m^2)	0	6.4	-	Capacity model	450	/	N/A	412.0	For 1 IHX
Solid mass (kg) – primary side			-			/			
Hot pool - Cold pool	1.3e5	Primary vessel: 47t Hydraulic wrapper: 44.5t Control plug+transfer arm: 20 t	-	Primary vessel – 47 t Conical shell – 21 t Control plug – 10t Transfer arm and ramp – 11 t	0	/	Later	Primary vessel: 46.1 t	

		IHX and DOT: 115.4t		Diagrid – 74.6 t PSP – 82.5 t Main vessel – 65.5 t					
Cold pool - Vessel cooling system	2.52e5	Main vessel : 65.5t Strongback+ diagrid : 100t	-	-	0	/	Later	Main vessel: 65.3 t	
Others structures (inside the vessel)	3.05e5	Conical shell: 26t Primary pump: 82.5t Control plug+transfer arm+handlong ramp: 20 t	-	-	74600 (diagrid) 75000 (Pumps) 10000 (core plug) 6000 (transfer arm)	/	N/A	Diagrid: Pumps: 82.4t Roof: 73.1t	IHX shroud, Pump shroud, etc.

REFERENCES

[1] REVUE GENERALE NUCLEAIRE, The Phenix Reactor – Assessment of 35 Years' Operation, RGN No.1 (2009).

[2] VASILE, A., FONTAINE, B., VANIER, M., GAUTHE, P., PASCAL, V., PRULHIERE, G., JAECKI, P., TENCHINE, D., MARTIN L., SAUVAGE, J.F., DUPRAZ R., WOAYE-HUNE A., "The PHENIX final tests", Proc. of ENC2010, Barcelona, Spain, 30 May–2 June 2010.

[3] DUNN, F.E., PROHAMMER, F.G., WEBER, D. P., VILLIM, R.R., "The SASSYS-1 LMFBR systems analysis code", Proc. of Intl. Topl. Mtg. Fast Reactor Safety, Knoxville, Tennessee, 1985, pp. 999–1008.

[4] GEFFRAYE, G., FARVACQUE, M., KADRI, D., LAVIALLE, G., RUBY, A., RAMEAU, B., ANTONI, O., "CATHARE 2 V2.5_2: a single version for various applications", Proc. of NURETH-13, Kanazawa City, Ishikawa Prefecture, Japan, 27 September–2 October 2009.

[5] PIALLA, D., et al., "Natural convection test in Phenix reactor and associated CATHARE calculation", Proceeding of the 14th International Topical Meeting on Nuclear Reactor Thermalhydraulics (NURETH-14), Toronto, Canada, 25–29 September, 2011.

[6] TENCHINE, D., et al., Status of CATHARE code for sodium cooled fast reactors, Nuclear Engineering and Design, **245** (2012), pp. 140–152.

[7] CD-ADAPCO, Star CD code Version 3.26, Computational Dynamics Limited, New York, USA, 2005.

[8] NATESAN, K; KASINATHAN, N., VELUSAMY, K., SELVARAJ, P., CHELLAPANDI P., CHETAL S.C., Dynamic simulation of accidental closure of intermediate heat exchanger isolation valve in a pool type LMFBR, Annals of Nuclear Energy, Vol. **38** (2011), pp. 748–756.

[9] CHVETSOV, I., VOLKOV, A., "3-D thermal hydraulic analysis of transient heat removal from fast reactor core using immersion coolers", IAEA Technical Committee Meeting on Methods and Codes for Calculations of Thermal hydraulic Parameters for Fuel, Absorber Pins and Assemblies of LMBFR with Traditional and Burner Cores, Obninsk, Russian Federation, 27–31 July 1998.

[10] MOCHIZUKI, H., Verification of NETFLOW Code using Plant Data of Sodium Cooled Reactor and Facility, Nuclear Engineering and Design, **237** (2007), Issue 1, pp.87–93.

[11] MOCHIZUKI, H., Development of the plant dynamics analysis code NETFLOW++, Nuclear Engineering and Design, **240** (2010), pp. 577–587.

[12] HA, K.S., et al., "Development of MARS-LMR and Steady state Calculation for KALIMER-600", Technical Report No. KAERI/TR-3418/2007, Korea Atomic Energy Research Institute, Rep. of Korea, 2007.

[13] MIKITUK, K., PELLONI, S., CODDINGTON, P., BUBELIS E., CHAWLA, R., FAST: an advanced code system for fast reactor transient analysis, Ann. Nucl. Energy, **32** (2005), pp. 1613–1631.

[14] SPORE J. W., et al., TRAC M FORTRAN 90 (Version 3.0) theory Manual, Division of Systems Analysis and Regulatory Effectiveness, Office of Nuclear Regulatory Research, U.S. Nuclear Regulatory Commission, Washington DC (2001).

[15] CHENU, A; MIKITYUK K., CHAWLA, R., TRACE simulation of sodium boiling in pin bundle experiments under loss-of-flow conditions, Nucl. Eng. Des., **269** (2009), pp. 2417–2429.

[16] CHENU, A., MIKITYUK K., CHAWLA, R., Pressure drop modeling and comparisons with experiments for single- and two-phase sodium flow, Nucl. Eng. Des., **241** (2011), pp. 3898–3909.

CONTRIBUTORS TO DRAFTING AND REVIEW

Chang, W.	Korea Atomic Energy Research Institute (KAERI), Republic of Korea
Chellapandi, P.	Indira Gandhi Centre for Atomic Research (IGCAR), India
Cochemé, F.	Institut de Radioprotection et de Sûreté Nucléaire (IRSN), France
Fanning, T. H.	Argonne National Laboratory (ANL), USA
Gauthe, P.	Commissariat à l'énergie atomique et aux énergies alternatives (CEA), France
Ha, K.	Korea Atomic Energy Research Institute (KAERI), Republic of Korea
Jeong, H. Y.	Korea Atomic Energy Research Institute (KAERI), Republic of Korea
Kikuchi, N.	University of Fukui, Japan
Li, S.	Institut national des sciences et techniques nucléaires (INSTN), France
Maas, L.	Institut de Radioprotection et de Sûreté Nucléaire (IRSN), France
Mikityuk, K.	Paul Scherrer Institute (PSI), Switzerland
Mochizuki, H.	University of Fukui, Japan
Monti, S.	International Atomic Energy Agency
Natesan, K.	Indira Gandhi Centre for Atomic Research (IGCAR), India
Partha, Sarathy U.	Indira Gandhi Centre for Atomic Research (IGCAR), India
Pialla, D.	Commissariat à l'énergie atomique et aux énergies alternatives (CEA), France
Shvetsov, I.	Institute of Physics and Power Engineering (IPPE), Russian Federation
Sofu, T.	Argonne National Laboratory (ANL), USA
Stanculescu, A.	International Atomic Energy Agency
Tenchine, D.	Commissariat à l'énergie atomique et aux énergies alternatives (CEA), France
Thomas, Justin W.	Argonne National Laboratory (ANL), USA
Toti, A.	International Atomic Energy Agency
Vasile, A.	Commissariat à l'énergie atomique et aux énergies alternatives (CEA), France
Velusamy K.	Indira Gandhi Centre for Atomic Research (IGCAR), India

IAEA
International Atomic Energy Agency

Where to order IAEA publications

In the following countries IAEA publications may be purchased from the sources listed below, or from major local booksellers. Payment may be made in local currency or with UNESCO coupons.

AUSTRALIA
DA Information Services, 648 Whitehorse Road, MITCHAM 3132
Telephone: +61 3 9210 7777 • Fax: +61 3 9210 7788
Email: service@dadirect.com.au • Web site: http://www.dadirect.com.au

BELGIUM
Jean de Lannoy, avenue du Roi 202, B-1190 Brussels
Telephone: +32 2 538 43 08 • Fax: +32 2 538 08 41
Email: jean.de.lannoy@infoboard.be • Web site: http://www.jean-de-lannoy.be

CANADA
Bernan Associates, 4501 Forbes Blvd, Suite 200, Lanham, MD 20706-4346, USA
Telephone: 1-800-865-3457 • Fax: 1-800-865-3450
Email: customercare@bernan.com • Web site: http://www.bernan.com

Renouf Publishing Company Ltd., 1-5369 Canotek Rd., Ottawa, Ontario, K1J 9J3
Telephone: +613 745 2665 • Fax: +613 745 7660
Email: order.dept@renoufbooks.com • Web site: http://www.renoufbooks.com

CHINA
IAEA Publications in Chinese: China Nuclear Energy Industry Corporation, Translation Section, P.O. Box 2103, Beijing

CZECH REPUBLIC
Suweco CZ, S.R.O., Klecakova 347, 180 21 Praha 9
Telephone: +420 26603 5364 • Fax: +420 28482 1646
Email: nakup@suweco.cz • Web site: http://www.suweco.cz

FINLAND
Akateeminen Kirjakauppa, PO BOX 128 (Keskuskatu 1), FIN-00101 Helsinki
Telephone: +358 9 121 41 • Fax: +358 9 121 4450
Email: akatilaus@akateeminen.com • Web site: http://www.akateeminen.com

FRANCE
Form-Edit, 5, rue Janssen, P.O. Box 25, F-75921 Paris Cedex 19
Telephone: +33 1 42 01 49 49 • Fax: +33 1 42 01 90 90
Email: formedit@formedit.fr • Web site: http://www. formedit.fr

Lavoisier SAS, 145 rue de Provigny, 94236 Cachan Cedex
Telephone: + 33 1 47 40 67 02 • Fax +33 1 47 40 67 02
Email: romuald.verrier@lavoisier.fr • Web site: http://www.lavoisier.fr

GERMANY
UNO-Verlag, Vertriebs- und Verlags GmbH, Am Hofgarten 10, D-53113 Bonn
Telephone: + 49 228 94 90 20 • Fax: +49 228 94 90 20 or +49 228 94 90 222
Email: bestellung@uno-verlag.de • Web site: http://www.uno-verlag.de

HUNGARY
Librotrade Ltd., Book Import, P.O. Box 126, H-1656 Budapest
Telephone: +36 1 257 7777 • Fax: +36 1 257 7472 • Email: books@librotrade.hu

INDIA
Allied Publishers Group, 1st Floor, Dubash House, 15, J. N. Heredia Marg, Ballard Estate, Mumbai 400 001,
Telephone: +91 22 22617926/27 • Fax: +91 22 22617928
Email: alliedpl@vsnl.com • Web site: http://www.alliedpublishers.com

Bookwell, 2/72, Nirankari Colony, Delhi 110009
Telephone: +91 11 23268786, +91 11 23257264 • Fax: +91 11 23281315
Email: bookwell@vsnl.net

ITALY
Libreria Scientifica Dott. Lucio di Biasio “AEIOU”, Via Coronelli 6, I-20146 Milan
Telephone: +39 02 48 95 45 52 or 48 95 45 62 • Fax: +39 02 48 95 45 48
Email: info@libreriaaeiou.eu • Website: www.libreriaaeiou.eu

JAPAN
Maruzen Company Ltd, 1-9-18, Kaigan, Minato-ku, Tokyo, 105-0022
Telephone: +81 3 6367 6079 • Fax: +81 3 6367 6207
Email: journal@maruzen.co.jp • Web site: http://www.maruzen.co.jp

REPUBLIC OF KOREA
KINS Inc., Information Business Dept. Samho Bldg. 2nd Floor, 275-1 Yang Jae-dong SeoCho-G, Seoul 137-130
Telephone: +02 589 1740 • Fax: +02 589 1746 • Web site: http://www.kins.re.kr

NETHERLANDS
De Lindeboom Internationale Publicaties B.V., M.A. de Ruyterstraat 20A, NL-7482 BZ Haaksbergen
Telephone: +31 (0) 53 5740004 • Fax: +31 (0) 53 5729296
Email: books@delindeboom.com • Web site: http://www.delindeboom.com

Martinus Nijhoff International, Koraalrood 50, P.O. Box 1853, 2700 CZ Zoetermeer
Telephone: +31 793 684 400 • Fax: +31 793 615 698
Email: info@nijhoff.nl • Web site: http://www.nijhoff.nl

Swets and Zeitlinger b.v., P.O. Box 830, 2160 SZ Lisse
Telephone: +31 252 435 111 • Fax: +31 252 415 888
Email: infoho@swets.nl • Web site: http://www.swets.nl

NEW ZEALAND
DA Information Services, 648 Whitehorse Road, MITCHAM 3132, Australia
Telephone: +61 3 9210 7777 • Fax: +61 3 9210 7788
Email: service@dadirect.com.au • Web site: http://www.dadirect.com.au

SLOVENIA
Cankarjeva Zalozba d.d., Kopitarjeva 2, SI-1512 Ljubljana
Telephone: +386 1 432 31 44 • Fax: +386 1 230 14 35
Email: import.books@cankarjeva-z.si • Web site: http://www.cankarjeva-z.si/uvoz

SPAIN
Díaz de Santos, S.A., c/ Juan Bravo, 3A, E-28006 Madrid
Telephone: +34 91 781 94 80 • Fax: +34 91 575 55 63
Email: compras@diazdesantos.es, carmela@diazdesantos.es, barcelona@diazdesantos.es, julio@diazdesantos.es
Web site: http://www.diazdesantos.es

UNITED KINGDOM
The Stationery Office Ltd, International Sales Agency, PO Box 29, Norwich, NR3 1 GN
Telephone (orders): +44 870 600 5552 • (enquiries): +44 207 873 8372 • Fax: +44 207 873 8203
Email (orders): book.orders@tso.co.uk • (enquiries): book.enquiries@tso.co.uk • Web site: http://www.tso.co.uk

On-line orders
DELTA Int. Book Wholesalers Ltd., 39 Alexandra Road, Addlestone, Surrey, KT15 2PQ
Email: info@profbooks.com • Web site: http://www.profbooks.com

Books on the Environment
Earthprint Ltd., P.O. Box 119, Stevenage SG1 4TP
Telephone: +44 1438748111 • Fax: +44 1438748844
Email: orders@earthprint.com • Web site: http://www.earthprint.com

UNITED NATIONS
Dept. I004, Room DC2-0853, First Avenue at 46th Street, New York, N.Y. 10017, USA
(UN) Telephone: +800 253-9646 or +212 963-8302 • Fax: +212 963-3489
Email: publications@un.org • Web site: http://www.un.org

UNITED STATES OF AMERICA
Bernan Associates, 4501 Forbes Blvd., Suite 200, Lanham, MD 20706-4346
Telephone: 1-800-865-3457 • Fax: 1-800-865-3450
Email: customercare@bernan.com · Web site: http://www.bernan.com

Renouf Publishing Company Ltd., 812 Proctor Ave., Ogdensburg, NY, 13669
Telephone: +888 551 7470 (toll-free) • Fax: +888 568 8546 (toll-free)
Email: order.dept@renoufbooks.com • Web site: http://www.renoufbooks.com

Orders and requests for information may also be addressed directly to:

Marketing and Sales Unit, International Atomic Energy Agency
Vienna International Centre, PO Box 100, 1400 Vienna, Austria
Telephone: +43 1 2600 22529 (or 22530) • Fax: +43 1 2600 29302
Email: sales.publications@iaea.org • Web site: http://www.iaea.org/books

International Atomic Energy Agency
Vienna
ISBN 978–92–0–139610–5
ISSN 1011–4289